| N° of Dissertation | |
|---|---|

# A DISSERTATION

Submitted to the Doctoral Research Programme on Climate Change and Energy

University Abdou Moumouni of Niamey, Niger

In Fulfilment of the Requirements For PhD

**DOCTORAL SCHOOL OF EXACTS AND TECHNICS SCIENCES**

**Domain: Sciences and Technologies**

**Mention: Physics**

**Specialty: Climate Change and Energy**

by


## MAHAMADOU DJIBRILLA ALIO SANDA


# PHOTOVOLTAIC COOLING GREENHOUSE ADAPTED FOR HORTICULTURE IN THE SAHEL

| | |
|---|---|
| **M. BOUKAR Makinta**<br>Professeur Titulaire, Université Abdou Moumouni, Niamey-Niger | **Président** |
| **M. Nana Sarfo Agyemang Derkyi**<br>Professeur Titulaire, University of Energy and Natural Ressources, Sunyani-Ghana | **Rapporteur** |
| **M. MOUNKAILA SALEY Moussa**<br>Maître de Conférences, Université Abdou Moumouni, Niamey-Niger | **Rapporteur** |
| **M. ADOUNKPE Julien**<br>Professeur Titulaire, Université Abomey Calavi, Cotonou-Bénin | **Examinateur** |
| **Mme. DRAME YAYE Aissetou**<br>Professeur Titulaire, Université Abdou Moumouni, Niamey-Niger | **Co-Directrice de thèse** |
| **M. ADAMOU Rabani**<br>Professeur Titulaire, Université Abdou Moumouni, Niamey-Niger | **Directeur de thèse** |


SPONSORED BY THE
Federal Ministry of Education and Research

**Acknowledgements**

First of all, I am very grateful to the Almighty for His mercy and grace upon my life before and during my study.

My sincere appreciation goes to the Federal Ministry of Education and Research (BMBF) and the West African Science Service Centre on Climate Change and Adapted Land Use (WASCAL) for providing the scholarship and financial support for this programme.

Warm thanks are to be given to AUF (Agence Universitaire de la Francophonie) for providing financial support to this initiative.

I would like to thank the Vice Chancellor of the UNIVERSITE ABDOU MOUMOUNI (UAM), Prof. Rabani ADAMOU, the Dean of the School of Doctorate studies section exact science and technique, Prof. Dungal LAOUALI and the Dean of the Faculty of Science and Technique, Prof. Bisso SALEY, for their collaboration and support during the program.

I say thanks to the Director of DRP-CCE, Prof. Rabani ADAMOU for all he has done for us.

My thanks go also for the Coordinator, Prof. INOUSSA Maman Maarouhi as well as to WASCAL Niger administration team.

I thank my main supervisor Prof. Rabani ADAMOU, University Abdou Moumouni, Niger, for his helpful assistance, instructions, criticism, comments, advice and for his kindness before and during the project.

I thank my co-supervisor, Prof. Aissetou DRAME YAYE University Abdou Moumouni, Niger, for her useful instructions, comments, and criticism. She is always available and has made available the research area, as the research was conducted in her farm.

I thank the other members of my scientific committee members: Dr. ATTO HALADOU Abdoulkader of the Department of Physics, Faculty of Science and Technique and Dr. KARIMOUN MASSALATCHI Illyassou of the Department of Chemistry, Ecole Normale Supérieure.

I say thanks to the Head of the Department of Soil science of the Faculty of Agriculture, UAM, Prof. Didier ALOU and his department laboratory team for their assistance in sample analysis.

My thanks go to Mr. Djika Hachimou, department of animal productivity of the Faculty of Agriculture, UAM for his assistance in sample analysis.

I say thanks to the team of the department of Chemistry and Physics of the University Abdou Moumouni (UAM) for their help, collaboration and assistance of all sorts and to the Member of the Jury for the valuable contributions to improve the scientific quality of this work.

**Abstract**

Photovoltaic greenhouse is a breakthrough technology that creates a synergy between agriculture and energy sectors worldwide. In harsh Sahelian environment, conventional greenhouse generates a microclimate that gets saturated and heats up, becoming unbearable for crops. This work aims to develop an effective and affordable cooling photovoltaic greenhouse for year-round horticulture in the Sahel. The study investigated tomatoes production under the microclimate conditions inside a greenhouse in which 20% of the roof area was replaced by photovoltaic panels and the remaining part covered by a green semi-transparent ligno-cellulosic material in order to reduce the intense local solar irradiance. A cellulosic evaporative cooling pads system powered by poly-crystalline modules of 1.56kWp was used to decrease indoor heat. The greenhouse's microclimate parameters such as temperature, relative humidity and solar irradiance were recorded with the aid of a weather station, thermo-hygrometer sensors installed inside and outside the greenhouse, and the whole greenhouse system thermodynamic behaviour was simulated through computational fluid dynamic (CFD) software (ANSYS). The carbon dioxide ($CO_{2)}$ contents and grown tomatoes physical parameters inside and outside the greenhouse were also regularly measured. While the outside temperature was around 34.2 – 41.6$^{o}$C with an average relative humidity of 46.13%, the temperature within the greenhouse was around 29 - 32.8$^{o}$C with an average relative humidity of 72.24%, causing respectively a temperature drop of 5.2 - 8.8$^{o}$C for an average relative humidity improvement of more than 26%. The thermal heat distribution and flow patterns showed a well-distributed heat around crop's coverage area in the greenhouse when analysed under CFD. The CFD analysis allowed to notice that when exposed to the highest solar irradiation event (1355.6 w/m$^2$, 34.3$^{o}$C and 71% relative humidity), the greenhouse cooling system could create a drop of 4.9 $^{o}$C and an increase of 15% relative humidity. The lowest temperature attained in the greenhouse was 15.7 $^{o}$C (at night) whereas the highest temperature (in the afternoon) was 37.8$^{o}$C against 40.8$^{o}$C outside. The measured $CO_2$ contents (700 - 920 ppm) and solar irradiance (120 - 220 Wm$^{-2}$) inside the greenhouse are suitable for plant growth and main horticulture crops production under very sunny Sahelian conditions. A simultaneous tomato crop cultivation (Variety Mongal) inside and outside the greenhouse showed that plants inside the greenhouse could reach 190 cm height with leaves size of Length x Width (LxW) = 10x5cm against 70 cm high and LxW = 6x2.5 cm for outside plants' physical parameters. This situation resulted from the plant photosynthesis improvement due to sufficient carbon dioxide availability under adequate sun irradiance. Tomato fruits inside greenhouse turned from green to deep red at harvesting stage whereas under ambient conditions tomatoes colours turned green, light yellow then red or light red due to extreme conditions. Energy production for cooling averaged around 4199.016 Wh/day despite the observation of 7620.792 Wh/day of energy loss due to full battery state. Optimization is necessary for cost effectiveness of the greenhouse cooling system.

**Keywords**: direct evaporative cooling, greenhouse, cellulosic pad materials, horticulture, Computational Fluid Dynamic, green energy, heat transfer.

**Résumé**

La serre photovoltaïque est une technologie révolutionnaire qui crée une synergie entre les secteurs de l'agriculture et de l'énergie dans le monde entier. Dans un environnement Sahélien difficile, la serre conventionnelle génère un microclimat qui se sature et se réchauffe, devenant insupportable pour les cultures. Ce travail vise à développer une serre photovoltaïque de refroidissement efficace et abordable pour une horticulture au Sahel tout au long de l'année. L'étude a enquêté sur la production de tomates dans les conditions microclimatiques situées à l'intérieur d'une serre dans laquelle 20% de la surface du toit a été remplacée par des panneaux solaires photovoltaïques et la partie restante couverte par un matériau ligno-cellulosique vert semi-transparent afin de réduire l'intensité de l'irradiation solaire. Un système de refroidissement évaporatif cellulosique alimenté par des modules poly-cristallins de 1,56 kWp a été utilisé pour réduire la chaleur interne. Les paramètres microclimatiques de la serre tels que la température, l'humidité relative et l'irradiance solaire ont été enregistrés à l'aide d'une station météorologique, des capteurs thermo-hygromètres installés à l'intérieur et à l'extérieur de la serre, et le comportement thermodynamique du système de la serre en entier a été simulé grâce au logiciel (ANSYS) de la Mécanique des Fluides Numériques (MFN). Le contenu en dioxyde de carbone ($CO_2$) et les paramètres physiques des tomates cultivées à l'intérieur et à l'extérieur de la serre ont également été mesurés régulièrement. Alors que la température extérieure était d'environ 34,2 à 41,6 ° C avec une humidité relative moyenne de 46,13%, la température de la serre était d'environ 29 à 32,8 ° C avec une humidité relative moyenne de 72,24%, causant respectivement une chute de température de 5,2 à 8,8 ° C pour une amélioration moyenne de l'humidité relative de plus de 26%. La distribution de la chaleur thermique et de l'allure des flux ont montré une chaleur bien répartie autour de la zone de culture dans la serre lorsqu'elles sont analysées sous MFN. L'analyse de la MFN a permis de noter que lorsqu'exposé à l'événement d'irradiation solaire le plus élevé (1355,6 W / $m^2$, 34,3 ° C et 71% d'humidité relative), le système de refroidissement de la serre pourrait créer une baisse de 4,9 ° C et une augmentation de 15% d'humidité relative. La température la plus basse atteinte dans la serre était de 15,7 ° C (la nuit) alors que la température la plus élevée (dans l'après-midi) était de 37,8 ° C contre 40.8 $^{O}$ C à l'extérieur. Le contenu en $CO_2$ mesuré (700 à 920 ppm) et l'irradiance solaire (120 à 220 $Wm^{-2}$) à l'intérieur de la serre conviennent à la croissance des plantes et à la production principale des cultures horticoles dans des conditions Sahéliennes très ensoleillées. Une culture simultanée de la tomate (variété Mongal) à l'intérieur et à l'extérieur de la serre a montré que les plantes à l'intérieur de la serre pouvaient atteindre une hauteur de 190 cm avec une taille de feuilles de longueur x largeur (Lxl) = 10x5cm contre 70 cm de hauteur et Lxl = 6x2,5 cm comme paramètres physiques des plantes à l'extérieur. Cette situation résulte de l'amélioration de la photosynthèse en raison de la disponibilité suffisante de dioxyde de carbone sous une irradiance du soleil adéquate. Les fruits de tomates à l'intérieur de la serre se sont tournés du vert au rouge foncé au stade de la récolte, tandis que dans des conditions ambiantes, les couleurs de tomates ont varié du vert au jaune clair puis rouge ou rouge clair en raison des conditions extrêmes. La production d'énergie pour le refroidissement a moyenné autour de 4199,016 Wh / jour malgré l'observation de 7620,792 Wh / jour de perte d'énergie due à l'état de la batterie remplie. L'optimisation est nécessaire pour la rentabilité du système de refroidissement de la serre

**Mots-clés**: refroidissement évaporatif direct, serre, matériaux cellulosiques pour pad, horticulture, Dynamique de la mécanique des fluides, énergie verte, transfère de chaleur.

## Table of Contents

**List of Tables**

**List of Figures**

**List of Symbols**

| | | | |
|---|---|---|---|
| Greenhouse with local coolers | Dji Greenhouse | Hyphaene thebaica fibers pad | HF-pad |
| Greenhouse imported coolers | CN Greenhouse | Celdek pad | C-pad |
| Photovoltaic | PV | Discrete Ordinate | DO |
| Greenhouse | GnH | Reynolds Average Navier-Stokes | RANS |
| Computational Fluid Dynamic | CFD | Second Order Upwind | SOU |
| Vapor Pressure Deficit | VPD | Carbon Dioxide | $CO_2$ |
| Actual Vapor Pressure | AVP | Watt hour | Wh |
| Saturated Vapor Pressure | SVP | Fourier Transform Infrared spectroscopy | FTIR |
| Relative Humidity | RH | Thin Layer Chromatography | TLC |
| Dry bulb temperature | Tdb | Frontal ratio | Rf |
| Wet bulb temperature | Twb | Ultraviolet | UV |
| Evaporative saturation efficiency | eff | Photosynthetically active radiation | PAR |
| Cooling capacity of the pad | q and $q_{pad}$ | Coefficient of performance | COP |
| Air mass flow rate | ma | Cost-to-efficiency ratio | CER |
| Mass flow rate of water vapor | mv | Coefficient of permeability | K |
| Humidity ratio | W = | Pressure drop across the pad | $\Delta Pv$ |
| Inlet and outlet enthalpy of air | $ha_1$, $ha_2$ | Vapor pressures at outlet and inlet temperature respectively | $Pv_2$, $Pv_1$ |
| Enthalpy of water | hw | Saturated vapor pressures at outlet and inlet temperature | $Ps_2$, $Ps_1$ |
| Heat loss by the pads | q | Log mean mass density difference of water vapor | $\Delta\rho v$ |
| Relative humidity | RH | Mass density of water vapor at inlet, outlet and wet bulb conditions | $\rho v1$, $\rho v2$ and $\rho vwb$ |
| Frontal/inlet velocity | v | Actual density of water vapor from saturated water table | $\rho vw$ |
| Outlet velocity | vout | Power of fan and pump | $P_{fan}$, $P_{pump}$ |
| Mass of water evaporated | me | Fan and motor efficiencies | $\eta_{fan}$ and $\eta_{motor}$ |
| Humidity ratio | W | Total wetted surface area of the pad | s |
| Heat transfer coefficient | $h_H$ | Amount of water evaporated | Er |
| Mass transfer coefficient | $h_M$ | Analysis of Agro Ecosystem | AAES |

# CHAPTER ONE - INTRODUCTION

## 1.1 Background

Greenhouse technology is a revolutionary technology in the agricultural sector that allows the production of a crop sensitive to climatic conditions while considering the advantages of the market and the quality system. Greenhouses protect crops from harsh weather conditions like high temperatures, heavy rain or very low humidity, as well as from pests such as insects or animals (Kumar et al., 2009).

In tropical dry and sub-Saharan regions such as the Sahelian and Sudanese, the sudden change in temperature and humidity between morning and evening, accompanied by the late arrival and stabilization of the rainy season, result in the loss of seeds and the drying of plants leading to poor agricultural yields (Manuwa & Odey, 2012). Therefore, in such a region, it is necessary to grow greenhouse crops under controlled conditions. Unlike conventional greenhouses designed to provide heat, in the sub-Saharan region, especially in desert areas, greenhouses must have the function of providing cool and humid environment (Manuwa & Odey, 2012).

In order to guarantee optimal plant production conditions in dry sub-Saharan and tropical regions, cooling system becomes an essential basic requirement for the production of greenhouse crops (Kumar et al., 2009). Developing such a system around unfavorable ambient conditions is a difficult task, knowing that the ambient temperature can reach almost 50 $^{o}$C and vary by more than ten degrees Celsius (10 ° C) between the morning and the evening, with a relative humidity lower than twenty percent (20%) (Kumar et al., 2009). In addition, the design of an appropriate cooling system depends on the crop targeted, maintenance, fabrication and economic viability. For an efficient greenhouse, it is important to have, first, the climatic characteristics of the area or zone in which it will be operated, to understand the related physical processes (geothermal and thermal) as well as the greenhouse modelling or its analysis according to the size, the shape and outdoor weather conditions (Kumar et al., 2009). Evaluating the microclimate in different designs of the greenhouse and establishing physical, chemical and physiological relationships between crops and the environment are necessary for the designing greenhouse in order to improve the cooling system adapted to crop optimized growth (Kumar et al., 2009).

The developed on greenhouse cooling systems showed that the obtained prototypes are not sufficiently satisfactory or effective for the sub-Saharan environmental conditions. Greenhouse technologies imported from overseas to be applied in the Sahel suffered of adaptation issue as they consume a lot of energy for cooling (mostly using air conditioners), they are expensive rendering profitability difficult and above all, they are inadequate since their environment saturates when outside heat is very high (Kumar et al., 2009; Wang et al., 2021). In addition, little documentation is available on cooling greenhouses in sub-Saharan regions and its functional characteristics influencing the created microclimate. Therefore, it is imperative to develop better cooling systems for greenhouse technology for the Sahel harsh environmental

conditions taking into account all the construction parameters such as the shape, dimension and configuration of the roof, construction materials associated with building techniques and proper ventilation and cooling systems.

The greenhouse cooling system uses traditionally electricity issued from the grid or generators obtained from unsustain energy sources like fossil fuels (oil, gas and charcoal). With the introduction of smart agriculture policies, farmers are more interested to effective and sustainable technology to improve yields, even if their activity remains seasonal and highly dependent on weather conditions (Bakker et al., 2006). Thus, introduction of photovoltaic technology in agriculture will not only help to secure energy for agricultural activity, but it will also ensure access to energy in remote areas (rural and decentralized areas) as well as the reduction of environmentally harmful greenhouse gas emission. Moreover, greenhouses fueled by photovoltaics can be a mini-plant capable of injecting its excess energy into the grid if big greenhouse size is considered. This will provide external income to the farmer.

## 1.2 Problem statement

The unfavorable weather conditions in the Sahel region accompanied by a change in the usual cycle of the rainy seasons due to climate change makes agricultural crops difficult and almost impossible to carry out throughout the year. In fact, rainfall deficit in the year 2021has caused a decrease of 11% in crop production in the Sahelian countries during agricultural season affecting livelihood and food production in Niger, northern Mauritania and north-eastern Mali (Kandji et al., 2006).Moreover, recurring drought with varying degree of severity occurring two out of five years' time makes harvest of major food and cash crops very uncertain. Therefore, climate variability poses a big obstacle to achieving food security and reducing poverty in the Sahel region (OECD, 2022). On the other hand, greenhouse technology is considered to be the most viable option for sustainable agricultural production, especially in regions with adverse climatic conditions (Kumar et al., 2009). This technology allows agricultural production in a controlled manner for a long time. In harsh temperate conditions, greenhouse is developed to create an adequate microclimate to allow many crops to grow year-round. Unfortunately, the conventional greenhouses largely used have some limits under sub-Saharan area (SSA) whereby their microclimate saturates, heats up and becomes unbearable for crops, especially when exposed to extremely dry and prolonged hot weather seasons. In some cases, air conditioners are used to cool the system (Bakker et al., 2006); But this temporary solution makes culture very expensive and inappropriate for large scale application. Other more affordable cooling technics for greenhouses have been developed among which the evaporative cooling pad system emerged to be the one with the best cost-efficiency ratio in dry and hot regions of the world (Chijioke, 2017). This method based on the thermodynamics of water can provide comfort for crops in the greenhouse but requires some energy to function. As an energy source for the cooling system, the photovoltaic solar system would be one of the best alternatives since these regions are mostly characterized by long sunny days ( Kumar et al., 2009; Chijioke, 2017). In Niger, particularly, the daily insolation ranges between 5 to 7 kWh/$m^2$/day showing the high solar potential in the

region (Dajuma et al., 2016). Taking advantage of this energy source and considering the cost-effectiveness of the technology, it is imperative to develop a greenhouse technology that could provide conducive environment allowing crop cultivation towards the achievement of sustainable agriculture irrespective of outside weather variability obstacle.

## 1.3 Aim of the study

The aim of this research is to contribute to the reduction of food insecurity (Sustainable Development Goal n°2 = Zero Hunger) by promoting clean technology that can allow agricultural work throughout the year in a cost-effective and environmentally friendly manners in the Sahel.

## 1.4 Objectives of the study

### 1.4.1 Main objective:

The main objective of this study is to develop an energetically independent cooling greenhouse allowing cultivating vegetables in the Sahelian region (case of Niger) throughout the year.

### 1.4.2 Specific objectives:

To reach the study main objective, some specific objectives that give stepwise directions, have been assigned.

i. To design a photovoltaic greenhouse with cooling function that is adapted to Niger extreme climate conditions
ii. To analyze the greenhouse system thermodynamic, the energy balance and heat exchange between the greenhouse microclimate and the surrounding weather while optimizing the benefit of involved climatic factors.
iii. To evaluate vegetables production, under controlled cooling photovoltaic greenhouse and compare findings with those of culture under ambient conditions.

## 1.5 Research questions

i. What materials do we need to build an efficient environmentally friendly cooling greenhouse?
ii. What are the energy balance and heat exchange involved in a photovoltaic Greenhouse?
iii. How do crop productivity differ from PV-cooling greenhouse to traditional practice under ambient Sahel weather?

## 1.6 Research hypothesis

i. Locally available steel materials, local cellulosic plant materials, solar photovoltaic modules coupled to an evaporative water system approach can all help to develop a cooling greenhouse adapted for the Sahel.
ii. The greenhouse microclimate internal temperature, pressure and relative humidity can be optimized through microclimate system thermodynamic, energy and heat balance investigations for more plant growth and yield compared to ambient conditions.

# CHAPTER TWO - LITERATURE REVIEW

## 2.1 Greenhouse design and functional characteristics

### 2.1.1 Concept and Choice of greenhouse type

The first criterion for choosing the type of greenhouse is the cost of the investment envisaged, followed in second place by the technical aspects linked to the type of production, the technology available and many other aspects (Hassanien et al., 2016). It should be taken into account: protection against rain and invaders, control of the greenhouse microclimate, resistance to winds and landslides, the dimensions of the framework (Hassanien et al., 2016).

### 2.1.2 Design of greenhouses

The performance of a greenhouse is regulated by creating a microclimate suitable to a certain culture. Some of the parameters influencing the microclimate within a greenhouse are: temperature, humidity, light / solar irradiation, ventilation, wind speed and structural materials (Hassanien et al., 2016; Kumar et al., 2009).

When comparing the building materials, it was found that the galvanized steel tunnel structures are much more resistant than the wooden structures as they can withstand tornadoes (Elsner et al., 2000). In order to allow a certain amount of light for the photosynthesis of plants, plastic films are mostly used on the side and on the top of the structure with a film change method (Elsner et al., 2000). To ensure air exchange in humid tropical regions, Elsner et al. (2000) suggests that the greenhouse ventilation system maintains a high ratio between ventilation and floor area. Since then, many of these designs have been developed. Campen (2005) have applied the technique of digital fluid dynamics (CFD) to the development of a new greenhouse system adapted to tropical regions such as Indonesian weather conditions. He has examined the distribution of indoor temperature; the size and location of the ventilation opening and came out with a greenhouse with a large opening area for ventilation (40.4% of the greenhouse's area) (Campen, 2005). In another experiment, the Greenhouse Process Model (KASPRO) was tested for data collection. The results showed that for a cucumber crop in summer, an average air change rate of 26 volume changes per hour was required. In Hemming et al. (2006), a greenhouse model adapted to tropical lowlands has been developed. This design, tested in Indonesian climatic conditions, was carried out using the CFD technique. The design was equipped with a very large ventilation capacity covered with a combination of nets and a special polyethylene film which blocks near infrared radiation. In the same Indonesian climatic conditions, a greenhouse with a large ventilation opening at the ridge and sides with a cover reflecting the NIR (near infrared) is more suitable for growing tomatoes (Hemming et al., 2006; Impron et al., 2007).

#### 2.1.2.1 Orientation and Shape

The orientation of a greenhouse is highly dependent on the type of greenhouse as to whether it is a simple type or a photovoltaic type. For a simple greenhouse, there is a need to consider the

climatic data on about the zone in which it is going to be implemented. For the photovoltaic greenhouse, in addition to the previous conditions, there is a need to consider the solar irradiation orientation as part of the design parameter.

A comparative performance of different configuration of the greenhouse with equal floor area and central height was studied by Gupta and Chandra (2002) and Jain and Tiwari (2002) on Indian climatic conditions. They were able to improve the design's performance for cooling and heating purpose through the modified IARI (Indian Agricultural Research Institute) design (Gupta & Chandra, 2002; Jain & Tiwari, 2002). Under the same Indian climate conditions, Manuwa and Odey (2012) deduced that the uneven span shape greenhouse, with east-west orientation, was much more illuminated over the year on all latitudes tested. The greenhouse inside air temperature varies with its shape whereby a rise of 3.5-4.6°C (average-maximum) at 31°N latitude was reached (Manuwa & Odey, 2012).

#### 2.1.2.2 Height

Usually, the height of the greenhouse determines its volume which in turn has a direct effect on the greenhouse microclimate heat exchange with the outside environment. The bigger the greenhouse volume is, the lower the exchange rate with the outside environment (Elsner et al., 2000). The trend in greenhouse height is between 2.5-4.5 m in contrast to the traditional height of 1.5-2 m. A high greenhouse is more favorable for crop growth in high temperature regions. A high greenhouse is more favorable to the growth of crops in regions with high temperatures. The optimal height of a greenhouse is 4 m. This calculation results from a compromise between four constraints:

i. Obtain quality fruit: In the case of tomatoes, the plant measures on average 2.5 m between the apex and the first harvestable fruits. Therefore, the culture wire which supports the trellising strings, must be at least 3 m above the ground
ii. Promote the development and setting of the apices: The apices should not be too close to the hot area located in the upper part of the greenhouse
iii. Facilitate the management of the greenhouse climate: A large space above the plants promotes and improves ventilation.
iv. Minimize the cyclonic risk: An optimal height and techniques to improve the resistance of the frame will minimize the cyclonic risk (Simon, 2009).

#### 2.1.2.3 Covering materials

Plastic films are mostly used to allow light to penetrate into the greenhouse. A special plastic film having the properties of near infrared reflection during the day and far infrared reflection during the night was reported to maintain a cool microclimate for plant growth in tropical zones (Elsner et al., 2000). Studying covering materials using tomatoes crops, Elsner (2000) noticed that an insect proof net as covering material maintained a favorable temperature compared to a polyethylene film and a photo-selective red colored film. Furthermore, Shen and Yu (2002) in Kumar (2009) indicated that the best cooling method in tropical regions is a fan-aided ventilated

greenhouse covered with a material reflecting near infrared sun rays (Kumar et al., 2009). While studying the production of eggplants with varying films, Bilal et al (2006) in Kumar (2009) discovered that a double layer polyethylene cover film gave a better yield with faster plant growth compared to single layer polyethylene film, ultraviolet stabilized film and infrared absorbed film. The ultraviolet stabilized gave an intermediate result whereas the infrared gave the lowest (Elsner et al., 2000).

#### 2.1.2.4 Ventilation area

Some parameters are to be considered in assuring favorable greenhouse ventilation in tropical zones: vent opening angle, wind velocity, wind angle, air exchange rate and temperature variation (Elsner et al., 2000). Another important parameter is the volume-to-floor which is said to help maintain a favorable microclimate if set high in case of low wind velocity. To assure cool temperature, an opening area of 20% of the floor area is to be kept in a case of a naturally ventilated greenhouse. This helps to regulate extreme temperature rise (Elsner et al., 2000; Simon, 2009). Better microclimate conditions were obtained when the side wall opening was 33% of the floor area. However, the optimum microclimate allowing tomatoes greenhouse production throughout the year, was obtain when a ventilation area of 60% was reached under natural wind velocity in humid tropics (Elsner et al., 2000; Simon, 2009).

#### 2.1.2.5 Protection against crop invaders

It is also important to protect your crops from all harmful animals and insects even when growing in a greenhouse. The means of protection are largely physical and can be summarized as:

i. Choice of operating location: choosing a location less susceptible to invasions is an asset
ii. Windbreak installation
iii. Weeding around and inside the greenhouses: considerably reduces the shelter of invaders
iv. Installation of anti-insect net: a very interesting multifunctional device
v. Disinfection of plastic mulches
vi. Soil protection (Simon, 2009)

##### 2.1.2.5.1 Insect-proof net

The insect –proof net contributes at the same time to the protection of the plantation against enemies and helps regulate the air exchange rate (Campen, 2005). In some designs, the insect-proof net replaces completely the greenhouse side covering materials and still gives a favorable microclimate inside the greenhouse. With decrease in the net pore size, the temperature within the greenhouse increases. Studies showed slight temperature variations with the use of nets in the case of natural ventilation (Campen, 2005; Kumar et al., 2009). However, there was significant temperature variation in the case where ventilators, configured differently, were used and covered with insect-proof nets compared to when they were not covered (Campen, 2005).

#### 2.1.2.5.2 Soil protection

The soil can be the reservoir of harmful organisms and pests such as nematodes, ground caterpillars, and certain vectors of diseases such as *Fusarium ssp*, *Verticillium ssp*, *Pythium ssp*, *Ralstonia solanacearum* etc (Simon, 2009). Faced with the risk of losing their crops, some farmers isolate their soil or engage in above-ground crops due to the costs involved in the frequent treatment of its infected soils. A few rules must be observed to protect crops:

i. Isolation of crops from the soil: the plants could be put in pots, bags or the substrate could be isolated from the soil of the place.
ii. Use of pest-free substrates
iii. Storage of substrates in a closed and safe place
iv. Protection of the entrance to the greenhouse: The entrance is often the place of introduction of harmful organisms. Several tips exist in particular:
    a. Gravel ground cover
    b. Imposition of shoe change at entry
    c. Consistent disinfection of entrances (Simon, 2009).

#### 2.1.2.5.3 Protection of use water

Sometimes harmful agents can be contained in irrigation water, runoff like that of cisterns and in storage tanks which constitute the main source of contamination by bacterial wilt (Simon, 2009). However, it is important to disinfect its waters. Based on the various analyses above, it can be deduced that there is no specific design for greenhouses. Models are set up to adapt the greenhouse to a specific climatic environment and to a given agricultural production (Simon, 2009).

## 2.2 Greenhouse cultivation

A greenhouse offers the advantage of being sheltered from the caprices of the weather, where one can control the temperature, humidity, irrigation, amount of nutrients, carbon dioxide and light intensity. It is also possible to control pollination, diseases and crop pests. For example, temperature control in tomato cultivation has an effect on the growth rate as well as the vegetative and reproductive balance of the plant (Iraqi et al., 1997; Ureña-sánchez et al., 2012). Since energy is needed to maintain these favorable conditions for plants, the greenhouse must have a reliable source of energy. In this regard, integrated systems creating synergy between agriculture and energy have pushed towards the development of energy-efficient greenhouses with renewable energy (photovoltaic). For an optimum cultivation in a greenhouse, one has to design and prepare it to suit crop’s demanding.

### 2.2.1 Preparation of the greenhouse

#### 2.2.1.1 Levelling and profiling

The levelling ensures a slight slope on the surface of the greenhouse in anticipation of the water drainage. In theory, the levelling of the greenhouse should have a slope of 0.5%. Therefore, one can take advantage of the topography of the terrain or create a slope in case of flat terrain. Profiling involves shaping the foundation of substrate containers, drainage channels and aisles (Simon, 2009).

#### 2.2.1.2 Support plan and drainage system

The support plan for organic substrates in bags and slag gutters is both:

i. Raised by 5 cm from the walkway
ii. Very slightly incline towards the drainage channel so that the drainage water flows without runoff towards the walkway
iii. The drainage channel has a regular slope over the entire length of the greenhouse in order to avoid stagnation of water (Simon, 2009).

#### 2.2.1.3 Layout of walkways and mulching

The aisles have a width of 80 to 100 cm to allow all handling with or without a cart and maintenance operations of the crop.

It is to note that the crop must be protected from any possible threat from the ground. For this, while respecting the profiling, a white-black two-sided polyethylene film on the interior surface of the greenhouse:

Black surface facing the ground to prevent the development of weeds
White surface above to reflect light and have good brightness in the greenhouse (Simon, 2009).

#### 2.2.1.4 Trellising wire

To grow varieties with indeterminate growth and to increase planting density, plants like those of tomatoes are trained. For each crop line, trellising consists of a solid culture wire (or trellising wire) made of wire with a minimum section of 3 $mm^2$, stretched throughout the greenhouse between 2.5 and 3 m height. To avoid sagging, the wire must be stretched sufficiently and reinforced with transverse supports distributed along the greenhouse (Simon, 2009).

#### 2.2.1.5 Irrigation system

The irrigation system should be installed at least a week before planting to allow the preparation of the substrates. An irrigation comb configuration consisting of secondary and tertiary pipes is installed for irrigation. The secondary pipes (Diameter = 32 mm) are placed along each line and the tertiary pipes (Diameter = 16-20 mm) are placed in the drainage channels and are fitted with drippers.

In greenhouse applications, potential evapotranspiration is variable depending on the geographic location and the type of greenhouse. Therefore, the amount of water to be supplied is evaluated according to the behavior of the plant, the percentage of drainage and the volume of the substrates. This quantity also varies according to the physiological stage of the plant (Ministère de l'Agriculture & PromAP, 2019; Simon, 2009; Ureña-sánchez et al., 2012).

#### 2.2.1.6 Crop density

A distance between plants of 30 cm is preferable in the planting line. The crop density can also vary according to the sunshine of 2.5 plants / $m^2$ in the cool season and to 3 plants / $m^2$ in the hot season (Ministère de l'Agriculture & PromAP, 2019; Simon, 2009).

#### 2.2.1.7 Organic cultivation & Fertilization of soil

Horticulture requires high number of fertilizers for good yield contributing to the release of contaminants in aquifers, rivers or lakes. Although the high cost of chemical fertilizers, the response of plants to such chemicals is sometimes uncontrollable (Del Amor, 2006). Organic farming stresses less soil and allows soil fertility recovery especially in areas with poor soil predominance. On the other hand, those areas are also encountering acute and recurring food insecurity due to under exploitation of this land's potential as well as climate change (Philippes et al., 2013). On the other hand, fertilizers prices are high and making them not accessible for most local farmers.

#### 2.2.1.8 Cases of some crops

##### 2.2.1.8.1 Sweet pepper

Organic farming on poor soils makes difficult for farmers to attain optimum yield with good quality. Many research have been done to determine optimum conditions for organic farming. Del Amor (2006) studied sweet pepper crop response under greenhouse environment managing the fertilization process through Nitrogen sources control under conventional, integrated and organic farming. Other researchers have been working on ways of improving crop yield by amending soils. In fact, Górecki and Górecki (2010) investigated on the yield of tomato, sweet pepper and eggplant yield cultivation after soil amendment with sheep waste wool. Their results showed an increase in yield, fruit number or both. Sheep wool is known to be a source of protein and keratin rich in nitrogen, sulphur and carbon essential for plant growth (Górecki & Górecki, 2010). Gravel et al (2012) studied the effect of organic fertilization on the development of sweet pepper plants. (Gravel et al, 2012) found that on fresh basis both organic and conventional method gave the same carbohydrate content. In fact, 5 weeks after plantation, plant height in conventional was higher as well as shoot weight with similarity in stem length. The same results were obtained 10 weeks later.

##### 2.2.1.8.2 Tomatoes

The actual conventional tomatoes cultivation requires a lot of pesticides for disease and pest control. However, this practice is not with no consequence on farmers' health and the

environment since it creates an intensive system because of heavy mineralization, and lack of adequate resistance in the cultivars. In searching for pesticide replacement, Modolon et al. (2012) prepared a homeopathic and high dilution. An increase in tomatoes yield under field condition was observed with the preparation of Arnica Montana 12 decimal Hahnemannian (DH) high dilution (Modolon et al., 2012). The use of natural fertilizer help overcome phyto-sanitarian issues while restoring the biological dynamic equilibrium (Modolon et al., 2012).

Pieper and Barrett (2009) have studied the effect of conventional and organic production technic on tomatoes quality and nutritional status. Given the growth period, physiological parameters differed. In fact, Organic production presented a lower red tomatoes and moisture content, higher percentage of attached stems, soluble and total solids. Conventional tomatoes reached maturity faster than organic ones which could have affected results even though at the end in both productions, tomatoes had similar primary nutritional parameters such as vitamin C, lycopene and rutin (Pieper and Barrett, 2009).

#### 2.2.1.8.3 Courgette or Zucchini

Organic cultivation of zucchini through cover crop termination was proven to be a technic that made nitrogen be more availability to crops (Montemurro et al., 2013). N fertilizations are recommended based on soil composition and crop's nutritional needs Montemurro et al. (2013).

### 2.2.2 Nutrient supply in greenhouse

#### 2.2.2.1 The essential nutrients for the tomato plant

The plant, nourishing itself through the roots, needs nutritional intake in an assimilated form by the root system of the plant. Some elements, called macro elements, occur in large quantities while others are in minimum quantities known as trace elements. Among the macro elements we have nitrogen (N), potassium (K), calcium (Ca), magnesium (Mg), sulfur (S) and silicon (Si). As trace elements, we can cite iron (Fe), zinc (Zn), manganese (Mn), boron (Bo), copper (Cu), molybdenum (Mo), chlorine (Cl), etc (Vallières, 2018).

### 2.2.3 Some parameters for controlling plant growth

Plant growth is influenced by many parameters such as the environment temperature, relative humidity, carbon dioxide content or even the Vapor Pressure Deficit. In tomato cultivation, especially, temperature control has an effect on the vigor of the plant, on the speed of growth and plays on the balance of the plant in other words, on the relationship between the reproductive and vegetative parts. It is possible to monitor crop growth over a 24-hour period by measuring the average temperature (Vallières, 2018).

#### 2.2.3.1 Average temperature over 24 hours

Measuring the average temperature over 24 hours helps manage the growth rate of a plant as well as its biological development. Thus, the higher this temperature, the more the plant believes through the more photosynthesis, transpiration and respiration provided that all the elements necessary for this growth are present (carbon dioxide, water, light and nutrients). On the other hand, a loss of vigor of the crop could be observed if the average temperature over 24 hours is very high and the food for plant growth is absent (Vallières, 2018).

#### 2.2.3.2 Temperature differential

Another important parameter in controlling the growth of a plant is the temperature differential. This is the difference between the average temperature during the day and the average temperature at night. A positive difference increases the length of the internodes while a negative difference shows a more compact plant. Furthermore, too high a night temperature would increase the respiration rate, which could only benefit from excessive plant cover (Vallières, 2018).

#### 2.2.3.3 Influence of carbon dioxide ($CO_2$) on plants

Naturally, $CO_2$ is essential for photosynthesis. A tomato plant, for example, has an assimilation rate of 1000 μmol / mol while the air contains on average 400 μmol / mol of $CO_2$. However, one can simply inject $CO_2$ by promoting the exchange of air between the inside and outside of the greenhouse or by using other more complex methods. However, a high concentration of $CO_2$ can cause necrosis on the leaves of tomato plants (Vallières, 2018). Thus, the source of $CO_2$ influences the profitability of greenhouse cultivation. In addition, there are several sources of $CO_2$ available:

i. From an industrial process,
ii. By direct combustion of hydrocarbons in the greenhouse such as natural gas (butane, propane),
iii. By condensing gas from a propane or natural gas kettle.

#### 2.2.3.4 Influence of vapor pressure deficit (VPD) on plants

The concept of Vapor Pressure Deficit gives information about how much moisture is being sucked out of the plant by the atmosphere. The way humans transpire through pores, plants release moisture through stomata with the difference that plants need transpiration process to pull in more liquids through their roots to fuel photosynthesis. Transpiration is essential for photosynthesis, nutrient uptake and plant cooling. VPD expresses how temperature and relative humidity affects plant's growth, stress and diseases. Therefore, VPD can help growers and farmers to control irrigation, heating/cooling and dehumidification within a greenhouse (Amitrano, et al. 2021; Lopez et al. 2021; Pettigrew, et al. 1990; Lu et al. 2015).

Vapor Pressure Deficit (VPD) is the difference between the Saturated Vapor Pressure (SVP) and the Actual Vapor Pressure (AVP); SVP being the maximum amount of moisture atmospheric air can hold and AVP being the current amount of moisture held by the atmospheric air.

Vapor pressure is the water vapor content of air measured as pressure. It appears as part of the total air pressure. The maximum amount of water vapor that can exist in the air at a given temperature is defined as saturated vapor pressure (SVP), and the actual water vapor pressure in the air at that same temperature by AVP. Even water vapor pressure corresponding to the percentage (%) of actual and current relative humidity.

VPD = AVP - SVP in kPa **Equation 2. 1**

% RH = ($AIR_{AVP}$ / $AIR_{SVP}$) x 100% **Equation 2. 2** (Iraqi et al., 1997; Vallières, 2018)

It should be noted that relative humidity alone does not establish a link with transpiration. In other words, the driving force causing water vapor to spread out of the leaves is the difference between the water vapor inside the leaves and that just outside the same leaf. The internal environment of the leaf is 100% RH.

VPD = $LEAF_{SVP}$ - ($AIR_{SVP}$ x AIR% RH) **Equation 2. 3** (Iraqi et al., 1997; Vallières, 2018)

Also $AIR_{SVP}$ = e ($C1 / T + C2 + C3T + C4T^2 + C5T^3 + C6 \ln T$) / 1000

Where T: temperature in K, RH: Relative humidity in%

And C1 = -5.80E + 03, C2 = 1.39E + 00, C3 = -4.86E-02, C4 = 4.18E-05, C5 = -1.45E-08, C6 = 6.55E + 00 (Vallières, 2018)

Global VPD has increased because of global increase in atmospheric temperature over recent decades. This situation is not with no effect on plants' physiology caused by increasing transpiration rate; hence, more water loss from leaves, soils (Grossiod et al. 2020). The currently earth global increase in atmospheric temperature is causing an increase in VPD. This change in VPD has a strong impact on variables capturing global water cycle (transpiration and stomatal conductance) and carbon fixation (photosynthesis and canopy growth) (López et al., 2021). It is confirmed that the increase in ambient air temperature along the day produces an increase in VPD (Pettigrew et al., 1990).

VPD can be used to control greenhouse environment. Many attempts were precisely targeting the prevention of leaf dehydration. Lu et al. (2015) showed that the application of fogging system significantly decreases VPD. Under experimental tomato cultivation under greenhouse condition during midday, VPD could reach 1.4 kPa under normal system against 0.8 kPa under fogging system (Lu et al. 2015) whereas stomatal density and conductance increased significantly under fogging. However, $CO_2$ concentration and air temperature were similar in both conditions (Lu et

al. 2015). In general, plants growth well at VPD interval of 0.5-0.8 kPa (Bakker et al., 2006; Lu et al., 2015).

Plant growth is influenced by environmental or atmospheric conditions especially by changes in vapor pressure deficit. Modulating VPD is one of the ways to optimize water consumption in a context of environment with freshwater scarcity caused by climate change (Amitrano, et al. 2021). Through the analysis of photosynthesis stomatal and hydraulic related traits of green and red butterhead lettuce (Lactuca sativa L.), Amitrano et al. (2021) demonstrated that lettuce grown under low VPD condition developed higher stomatal frequency as found in tomatoes and rose by reducing stress of transpiration, but allowing the production of smaller size of the pores (Amitrano et al., 2021).

Ray et al. (2002) worked under 33$^{o}$C room temperature on maize hybrids (hybrids 3165 and 3737) response to different VPD environment with dying soil conditions. It was found that the total water transpired ranged from 2472 g to 3746 g as VPD increased from 1.1 kPa to 3.6 kPa while the available soil water within experimental pots remained constant. However, there was a threshold for transpiration decrease which was found to occur at a VPD between 0.30-0.35 kPa (Ray et al., 2002). High VPD means that humidity is low. Thus, it implies that the atmospheric air is pulling out much and faster more water from the plant: evaporation of water exceeds water supply. This causes stomata to close leading to low or no more photosynthesis. To avoid injury and death of wilting, some plants curl their leaves of orient them downward in order to expose less leaves surface area to sun. High VPD can significantly reduce the growth rate and quality of crops. On the other hand, Low VPD means humidity is high. Plant is unable to evapotranspirate enough to allow nutrient uptake to cells. Some plants might extrude water in a form of drops called guttation. In a case of extremely low VPD, water may condense onto leaves creating development of fungal or mold and diseases (Monteith & Mike H. Unsworth, 2013). Leaf Vapor Pressure Deficit is a process through which evaporation occurs from the leaf's surface to the atmosphere. This process draws out heat from the leaf, hence cooling it. This will tell how well the plant grows leading to quality harvest.

Leaves via stomata, help plants to regulate transpiration (McAdam & Brodribb, 2015). Relative humidity expressed as vapor pressure deficit between the leaf and the atmospheric air has been the principal determinant in stomatal aperture (McAdam & Brodribb, 2015). Species exposed to a reversible sequence of VPD (0.7 to 1.5 to 0.7 kPa) showed a reduction in stomatal conductance during the increase to 1.5 kPa (McAdam & Brodribb, 2015). High humidity followed by condensation on the plant promotes the development of botrytis and mildew. Furthermore, Vallières (2018) has observed a reduction in plant growth, wilting of the leaves and even death in some cases of the apical part of the plant when the VPD is low (Vallières, 2018). In addition, an increase in the total fresh and dry mass of the aerial part of the tomato dishes was observed after six months of transplantation under conditions of high VPD (0.97 kPa over 24 hours) compared to the case of low VPD (0.4 kPa by day and 0.4 kPa by night). Thus, the yield of salable fruit was reduced by 32% and 41% respectively in plants subjected to a low rate of VPD (0.4 kPa

over 24h) compared to a high rate of VPD (0.97 kPa over 24h) (Iraqi et al., 1997; Vallières, 2018).

### 2.2.4 Favorable conditions for tomatoes cultivation

#### 2.2.4.1 Climatic conditions

Tomatoes crops can be grown almost throughout the year but with a varying yield due to weather conditions. The ideal conditions for normal growth are of a night temperature between 14 to 20$^{o}$C and a day temperature between 24 and 30$^{o}$C, especially during the period from planting to settling where the growth can be stopped by elevated night temperatures drained (Ministère de l'Agriculture & PromAP, 2019).

#### 2.2.4.2 Soil characteristics

Tomatoes plants prefer a soil that is not too heavy, but rather loose and deep and rich in well-decomposed organics matters and well-drained (Ministère de l'Agriculture & PromAP, 2019).

#### 2.2.4.3 Needs in water and nutrients

Water and nutrients are one of the key parameters for plants' growth in a greenhouse. As an efficient horticulture practice, nutrient and water are coupled and supplied to the plants respecting the crop's need. For greenhouses using water as cooling media, water recirculating and proper drainage systems are needed. Their proper management is synonymous of an optimum plant growth and yield (Kläring et al., 1997). The plant, nourishing itself through the roots, needs nutritional intake in a form that can be absorbed by the root system of the plant. Some elements, called macro elements, occur in large quantities while others are in minimum quantities known as trace elements. Among the macro elements we have nitrogen (N), potassium (K), calcium (Ca), magnesium (Mg), sulfur (S) and silicon (Si). As trace elements, we can cite iron (Fe), zinc (Zn), manganese (Mn), boron (Bo), copper (Cu), molybdenum (Mo), chlorine (Cl), etc (Vallières, 2018). From planting to flowering, a tomatoes plant requires 3 to 6 liters of water per square meter per day, and from that time to the harvesting, the need can reach 12 liters per square meter per day drained (Ministère de l'Agriculture & PromAP, 2019). Therefore, the main strategy in substrate systems is to supply nutrient solution via drip irrigation. The drip frequency is usually based on the solar radiation as it has a strong impact on the transpiration and water uptake by the plant. In general, nutrient to water ratio uptake is calculated for individual water uptake (Kläring et al., 1997).

## 2.3 Greenhouse cooling technologies

Greenhouses are used to maintain or create a warm microclimate for certain crops in some parts of the world, but in other regions where the climate is already very hot and dry, cooling is necessary; in other words, a greenhouse needs to create a moist, cool microclimate (Cuce et al., 2016; Elsner et al., 2000; Kumar et al., 2009).

### 2.3.1 Control of the greenhouse microclimate

The external climatic conditions in the dry tropical, Sahelian and desert zones are unfavorable for vegetable crops cultivation during a large portion of the year, in particular for tomatoes. However, controlling the climatic factors in a greenhouse presents a big step towards a sustainable market gardening. Parameters such as temperature, relative humidity, $CO_2$ content, internal irradiation must be under control. If there is no adequate control system (semi or automatic), the temperatures under the shelter can very quickly rise due to the greenhouse effect. From 28°C, the photosynthesis of the tomato decreases and the yield drops above 30°C. A series of high temperatures ranging from 35 to 40°C for a few days is enough to compromise production. It is therefore important to optimize all these parameters in order to ensure a productive, efficient, sustainable and profitable culture (Simon, 2009).

To lower the temperature in the greenhouse, several techniques exist which can be grouped into three main cooling techniques:

i. Aeration: It is the simplest and most economical way. This is the renewal of the warm indoor air by the fresh outdoor air. Aeration can be done through openings, natural ventilation as forced, dynamic as static or even coupled with cooling systems. In general, simple ventilation does not allow the indoor temperature to drop below the outdoor temperature (Simon, 2009).
ii. Cooling: It makes it possible to reduce the interior temperature below that of the exterior. Here, the principle is based on the exploitation of the thermodynamic properties of water during its passage from the liquid state to the gaseous state. This transformation cools the air which in turn lowers the temperature. Some techniques using this concept are promoted these days namely the mist system, misting, nebulization, the evaporative cooling buffer system, air conditioning, composite systems etc. (Simon, 2009).
iii. Anti-heat supplies / blankets: these are techniques that reduce the heating of the greenhouse by limiting the penetration of light rays. We can count among so many techniques:
    a. Adding paint to the film or bleaching: These additives applied to the outside of the cover limit the penetration of light energy. You can use lime (whitening) or products reflecting light and having good resistance to rain.
    b. Heat shields.
    c. Special films with improved properties reducing light rays (Simon, 2009).

### 2.3.2 Natural ventilation

Natural ventilation can be defined as the direct result of pressure differences created and maintained by wind or temperature gradients (Kumar et al., 2009). It is highly dependent on the crop's evaporative and transpiration process. Due to its low requirement in terms of energy and equipment, this cooling technique appears to be the cheapest of among the cooling methods.

Based on natural cooling, Soni et al. (2005) studied the effect of screen mesh on greenhouse microclimate in humid tropical zones. The highest temperature value of 5°C was obtained at the point near the roof which was higher than the values obtained at the points in vertical direction. In fact, at 60% of the height profile, 86- 92% of the maximum temperature was registered whereas up to 92-100% of the maximum value was registered at the upper 40% of the height profile. It is to note that, a decrease in mesh size increased the vertical gradients from 5 to 10% (Soni et al., 2005).

### 2.3.3 Evaporative cooling

Evaporative cooling is, to date, the most effective controlled cooling method in greenhouse technology. However, its design is highly dependent on the region of application.

#### 2.3.3.1 Fan-pad system

The experiment conducted by Gupta and Chandra (2002) on a 24 $m^2$ plastic covered greenhouse using negative pressure fan and pad system as cooling material (Gupta & Chandra, 2002). With the help of the Landsberg's model, a decrease in air temperature to range of 4 – 5°C was observed inside the greenhouse compared to outside. The same observation was done by Jain and Tiwari (2002) from which they added that some of the parameters to control in order to optimize the fan-pad cooling system is the length of the greenhouse and the height of the cooling pad (Jain & Tiwari, 2002). Fuchs et al. (2006) developed a procedure to evaluate the latent heat cooling by means crops transpiration and free water evaporation from wet fan and pad system. They also reported that they were able to maintain the temperature of the greenhouse for optimum growth of rose crop during summer using covering material with properties reducing solar radiation transmission by 30% at a ventilation rate of 30% volume exchanges per hour (Fuchs et al., 2006; Laknizi et al., 2018).

#### 2.3.3.2 Misting

Misting consists of a network of sprinklers installed above the plants which use low flow nozzles with a pressure of 3 to 4 bars to produce fine droplets (20-100 µm). This technique uses the concept of adiabatic cooling, which involves spraying fine water droplets into the air to cool the air. The evaporation of these droplets lowers the temperature of the greenhouse (Simon, 2009; Vallières, 2018). This technique transforms sensible heat into latent heat, the enthalpy of the air remains constant. The energy that is contained in the air is transmitted to water vapor, which increases the relative humidity of the air and lowers its temperature. The disadvantage of this technique is that it creates a fairly large deposit of water on the foliage, thus creating an

environment favorable for the development of certain diseases such as bacterial scabies with xanthomonas, botrytis, through this humid atmosphere (Simon, 2009; Vallières, 2018).

#### 2.3.3.3 Fog / Fog system

In this cooling system, water droplets (2 to 60 µm in diameter) are produced and sprayed into the greenhouse using high-pressure nozzles (30 to 70 bar) to cool the indoor environment. The droplets are so fine that they evaporate before reaching the plants, without wetting their leaves. Rather, the evaporation of the droplets cools the atmosphere. This method is very effective in increasing relative humidity (Simon, 2009).

The comparative test of Arbel et al. (1999) showed that the mist system was better than the fan cushion system because the variations in temperature and relative humidity were <5 ° C and 20% (Arbel et al., 1999). A combined system consisting of forced ventilation and a misting system was also tested by Arbel et al. (2003). High pressure nozzles were coupled to fans placed at both ends of the greenhouse to meet cooling demands. The results obtained showed that the air temperature and the relative humidity of 28°C and 80%, respectively, were maintained throughout the summer, at noon (Arbel et al., 2003; Laknizi et al., 2019)

#### 2.3.3.4 Roof evaporative cooling

This cooling method consists of sprinkling of water onto a surface of the roof so as to form a thin layer of the free water surface causing an increase in the evaporation rate and to fall to the wet bulb temperature of the closely surrounded air (Cuce et al., 2016; Kumar et al., 2009). By wetting the outer roof and inner crop soil surfaces where tomatoes are grown, the cooling method efficiency on the greenhouse microclimate was investigated. The results showed that wetting the roof has smaller effect than wetting the canopy in reducing air and canopy temperature. However, the combination of both wetting methods was able to reduce inside air temperature by about 5°C and canopy temperature by about 7°C below the ambient condition. The effect of flowing water over the roof on greenhouse air temperature was studied by several of researchers. With intermitted application of water over externally mounted shade net, a reduction of inside air temperature by 41% under wet cloth against 18% under dry cloth. Ghosal et al. (2004) developed a mathematical model using flowing water film on shade cloth stretched over the roof and south wall of an even span greenhouse at Delhi, India. The model was validated with experimental data giving good prediction and description of the reality, i.e. shade net with water flow, without water and even without shade (Ghosal et al., 2004; Harjunowibowo et al., 2018).

#### 2.3.3.5 Evaporative cooling pad or pads

This cooling system is very effective when the outside climate is hot and dry. It works through an adiabatic process of cooling the greenhouse air using warm, low-moisture outdoor air. By evaporating the water from the wet pad, the warm outside air becomes cold and high in water content. This contributes to lowering the ambient temperature of the greenhouse. The presence of impurities in the water can lower the efficiency of the system. It is therefore highly recommended to use this system with an incoming water filtration mechanism (Vallières, 2018).

#### 2.3.3.5.1 Direct evaporative cooling

Direct evaporative cooling is a cooling process by which the water stream is directly in contact with the air stream usually through a spray (misting technic) or a wetted media (cellulosic pad). Here, water absorbs heat from hot and dry air and evaporates. This process cools down the air and humidify it (Chijioke, 2017; Khobragade & Kongre, 2016). In evaporative cooling pad system, a fan with a controlled frontal velocity pulls air out of a permeable wetted pad. As air passes through this membrane, heat exchange occurs between water and air, then, air get filtered, cooled and humidified. The water feed is assured by a recirculating pumping system and excess water is drained and recovered in a sump (Khobragade & Kongre, 2016). In this system, the dry bulb temperature is reduced whereas the wet bulb temperature is kept constant (Khobragade & Kongre, 2016). The efficiency of direct coolers is highly dependent on the pad media. A rigid pad such as Celdek pad can reach an efficiency as high as 90% whereas a more loose pad such as Aspen wood fiber pad can provide up to 50-60% efficiency (Chijioke, 2017; Khobragade & Kongre, 2016).

#### 2.3.3.5.2 Effect of air velocity on evaporative cooling

Aziz et al. (2017) studied the effect of water temperature and air stream velocity on the performance of direct evaporative air cooler. He found that the cooling rate is affected by air velocity and water temperature. A low water temperature of 10$^{o}$C with a high air velocity of 4.57 m/s was able to drop the comfort zone temperature to 26$^{o}$C (Aziz et al., 2017). Similar trend was found by Laknizi et al. (2018) while studying the performance of an evaporative cooler pad under Morocco climatic conditions. In fact, the frontal air velocity was found to be proportional to the cooling capacity. The cooling capacity attained its maximum value at a frontal velocity of 3m/s with a pad thickness of 300 mm (Khobragade & Kongre, 2016).

Barzegar et al. (2012) tested the performance of Kraft and NSSC papers cooling pads. He obtained an efficiency as high as 92% with Kraft paper cooling pad at an air velocity of 1.8ms$^{-1}$. An increase in the air velocity caused less cooling effect because less evaporation rate was occurring as the air passes through the pad (Barzegar et al., 2012).

#### 2.3.3.5.3 Effect of heat and mass transfer on evaporative cooling

The mass transfer increases with increasing in water consumption rate, air flow, pad thickness and frontal velocity (Laknizi et al., 2018). In fact, cellulosic material of thickness 4 inch was reported to have given the highest saturation efficiency of about 92.8% (Khobragade & Kongre, 2016). Also, more available time is needed to allow heat and mass transfer between air and water for the cooling to be more efficient efficiency (Barzegar et al., 2012).

Using local plant materials, Khus-grass material gave a saturation efficiency of 40.13% at an air flow rate of 0.45 m$^3$/s and water flow rate of 80 cc/hr. (Khobragade & Kongre, 2016).

The degree of comfort created by an evaporative cooler can be checked through some parameters such as the operability and the coefficient of performance (COP). The experiment carried by

Laknizi et al. (2018) showed that the heat transfer increases with increasing pad thickness and air residence time, hence, decreasing frontal velocity (Laknizi et al., 2018). Also, the higher the wetted surface and thickness are, the higher the saturation efficiency. This outlet air temperature is found to vary between 24 $^{o}$C and 29 $^{o}$C (Laknizi et al., 2018).

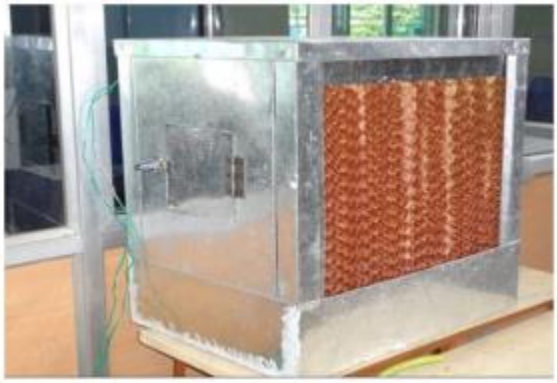

**Figure 2. 1** Photograph of a direct evaporative cooler (Khobragade & Kongre, 2016)

#### 2.3.3.5.4 Effect of Flute size and fiber size on the evaporative cooling pad

The cooling efficiency of the cooling pad was noticed to be affected by the flute size, the porosity and the water absorption capability of the pad. As tested by Barzegar et al. (2012), Kraft paper which has longer fiber (0.7mm) compared to NSSC paper (0.47) pad happen to absorb more water. Besides, the smaller flute size of Kraft paper (B: 2.5 mm) favors heat and mass transfer between air and water, hence, better cooling (Barzegar et al., 2012). Effect of water quality on efficiency were detailed by Bruno (2009) (Bruno, 2009).

#### 2.3.3.6 Indirect evaporative cooling

In indirect evaporative cooling system, air is cooled indirectly or via a heat exchanger which contains the cooling medium such as water (Chijioke, 2017; Khobragade & Kongre, 2016). In this system, both the dry and wet bulb temperatures are reduced and air conserves its humidity but is more costly than the direct cooling system with a lower efficiency (range of 60-70% efficiency) (Khobragade & Kongre, 2016).

#### 2.3.3.7 Two stage or Combined Direct-Indirect Evaporative Cooling

This cooling system combines both direct and indirect cooling technics. Air is pre-cooled by passing through a heat exchanger. This air is, then, let to pass through a water-soaked pad that cools it down again and humidify it. The final air is less humid than in direct cooling system since air affinity to moisture is related to temperature. Yet, this final air is cooler than in both direct and indirect single-stage systems separately (Chijioke, 2017; Khobragade & Kongre, 2016).

#### 2.3.3.8 Shading system

##### 2.3.3.8.1 Paint and Net Shading

Although light is important for photosynthesis, it is crucial to control it because certain radiations are necessary for plant's growth while others are harmful. Besides, excessive radiation can heat up greenhouse microclimate during summer. Shading is one of the parameters that can be used to control the amount and the intensity of light penetrating a greenhouse. At times, one used to use shading paints applied onto the greenhouse wall to selectively allow some radiations into the greenhouse. But, these paints get washed out during raining seasons. Practitioners turned towards shading nets which are nets of different mesh size to attain selective shading. The effect of reflective aluminized polyethylene shading net on the photosynthesis process of citrus plants was studied. It was observed that the net reduced the photo-synthetic active radiation (PAR) levels and leaf temperatures (Carlini et al., 2012).

##### 2.3.3.8.2 Photovoltaic shading

Carlini (2012) simulated a solar greenhouse performance under Italian climate conditions using TRNSYS 17 software together with Google SketchUp. The simulation showed that photovoltaic roof saves energy for cooling throughout the year. Besides, the solar radiation inside the solar greenhouse if half of that which is inside the glass greenhouse. That was deduced to have a potential effect on the photosynthetic efficiency of plants (Carlini et al., 2012).

Photovoltaic modules mounted on roofs of greenhouses have been reported not to have affected the marketability of tomatoes fruits, but rather caused a decrease in fruit size, hardness and color (Sanda et al., 2021; Ureña-sánchez et al., 2012).

In addition, the use of opaque solar panels on the roof will not have an impact on the irradiation in the greenhouse. Indeed, Cossu et al. (2014) studied the diffusion of solar irradiation inside a greenhouse throughout the year. Its results showed that PV greenhouses with 50% roof coverage decreased the yield of tomatoes compared to conventional greenhouses, but generated a large income from the energy produced. However, with the other data of the distribution of solar radiation obtained from the study, one can choose the most suitable crop to grow under such conditions of 50% coverage (Cossu et al., 2014).

#### 2.3.3.9 Composite system: Earth-to-air heat exchange system

The earth to air heat exchange system is a system that uses the cool temperature of the ground, which is mostly constant (26-28°C), as a means to cool the greenhouse. With a thermal model, Ghosal et al. (2004) investigated the potential of using stored thermal energy of the ground for greenhouse cooling with the help of earth-to-air heat exchangers (EAHEs). Similarly, to the experimental results, the temperature was found to be 5-6°C lower in the summer in greenhouse EAHEs than in greenhouse without EAHEs. Many research and development have been achieved on greenhouse cooling technology concerning tropical and subtropical zones with each their advantages and limits (Ghosal et al., 2004).

Greenhouse in tropical and subtropical climates should follow the orientation of East-West for single span and North-South for multi-span with gutter connected for maximum inception of light throughout the year. Fan and pad system are best suitable in areas with low humidity as a drop of inside temperature of 4-6°C can be observed if used alone and of 4-12°C if combined with shading. Fog/mist system is most suitable in peak summer in order to suddenly drop inside temperature by 3-8°C lower than outside condition (Ghosal et al., 2004).

## 2.4 Photochemical method for plant growth and light spectrum needs analysis through Thin Layer Chromatography

### 2.4.1 Principle

Thin layer chromatography is based on the different interactions between two phases: a fixed phase and a mobile phase. The fixed phase is the TLC plate, or silica that has numerous hydroxyl groups (-OH) on its surface and which will interact with the dissolved molecules of the mobile phase or liquid phase consisting of an eluent containing the different molecules of photosynthetic pigments to be separated. The more the molecule is polar and has oxygen atoms, the more it can bond with hydroxyl groups of the support and therefore the more difficult it will be carried away by the solvent (Nguyen, 2018).

### 2.4.2 Extraction

The extraction of leaf pigment is a practice giving details about photosynthetic pigments present. The distance run by the pigment on the chromatogram could be calculated and depend on the chromatographic medium, the solute solubility and the solvent used. The choice of the extracting solvent and the way of extracting are important. This extraction technique is based on the principle of solvent diffusion through the matrix of the targeted compound and solubilization of this compound (Strati and Oreopoulou, 2014). A good solvent extraction should release all the desired pigments in solution from the plant matrix without degrading them. This phase is important because it allows the separation photosynthetic pigments from other organic compounds in order to have an optimum filtrate quality leading to the best results.

The chromatography obtained from leaf extract using propanone-pet ether and combined pet ether-propanone-tricholroethane. After separation it could be observed five distinct lines representing Carotene α and β (orange yellow), pheophytin a breakdown product (grey), chlorophyll A (blue green), chlorophyll B (yellow green) and lutein a xanthophyll (deep yellow) (reference: Tomkins and Miller, 1991)

. Under UV light chlorophyll fluoresces red quite strongly while carotenoids do not.

**Table 2. 1** Identification of pigments after TLC test **(**Tomkins and Miller, 1991)

| Pigment colour | Pigment name | $R_f$ values for 2 different solvents | |
|---|---|---|---|
| | | Trichloroethane-propanone- pet ether | Propanone-pet ether |
| Orange yellow | Carotene α and β | 95 | 96 |
| Grey | Pheophytin (a breakdown product) | 80 | 82 |
| Blue green | Chlorophyll A | 60 | 72 |
| Yellow green | Chlorophyll B | 50 | 64 |
| Deep yellow | Lutein (a xanthophyll) | 35 | 59 |

In searching for components as antioxidants in sea grass (Enhalus acoroides) from its leaf's extracts, Pharmawati and Wrasiati (2020) run a TLC test on leaves extract and found the same photosynthetic pigments. They used pet ether, acetone and n-propanol (ratio 90:10:0.45)

**Table 2. 2** Identification of compounds based on Rf values and color from TLC profiling (Pharmawati and Wrasiati, 2020)

| **Fraction No.** | **Rf Value** | **Colour** | **Colour from Reference [26]** | **Identification** | **Maximum Spectra (nm)** |
|---|---|---|---|---|---|
| 1 | 0.11 | Bluish-green | Blue-green | Chlorophyll a | 655 |
| 2 | 0.21 | Dark green | Green | Chlorophyll b | 435 and 645 |
| 3 | 0.24 | Bluish-green | Blue-green | Ethyl-chlorophyllide a | 434 and 654 |
| 4 | 0.28 | Yellow | Yellow | Mg-free chlorophyll b | 654 |
| 5 | 0.33 | Light yellow | Yellow | Lutein | 649 |
| 6 | 0.39 | Yellowish-grey | Grey | Mg-free chlorophyll a | 630 and 656 |
| 7 | 0.53 | Grey | Grey | Pheophytin | 424 and 658 |
| 8 | 0.94 | Orange | Yellow-orange | β-carotene | 425 |

# CHAPTER THREE – MATERIALS AND METHODOLOGY

## 3.1 Greenhouse design and construction

This section consists of designing up the erection of the framework.

### 3.1.1 Study area and Criteria for design and construction

The area selected for the project is a plot of land of 150 $m^2$ in five hectares land owned by the company Sahel Agro. The area is located at Dalway in the department of Say (Niger) geographically at 13 ° 10.1969'N and 002 ° 19.0080'E.

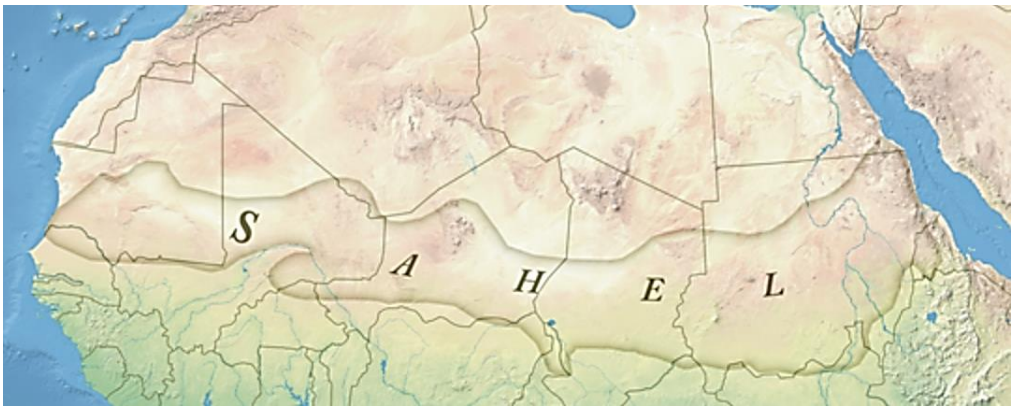


**Figure 3. 1** Map of Sahel region


**Figure 3. 2** Ground view and satellite view of the field


**Figure 3. 3** Crop cultivation area: From Left to right 1) Dji Greenhouse, 2) CN Greenhouse, 3) Outside and 4) Outside Bonus

Water recovery system 1 Water recovery system 2

**Figure 3. 4** Photograph of water recovery system

### 3.1.2 3D sketch of the structure

A 3D sketch of the structure was made using the software Sketch-up to have a view of all angles in space and have the possibility to make changes before going on the field.

**Dimension:**

Length: 15 m (from East to West) Height: 3 m ;

Width: 10 m Height of truss: 0.66 m

Tilt angle: 15°

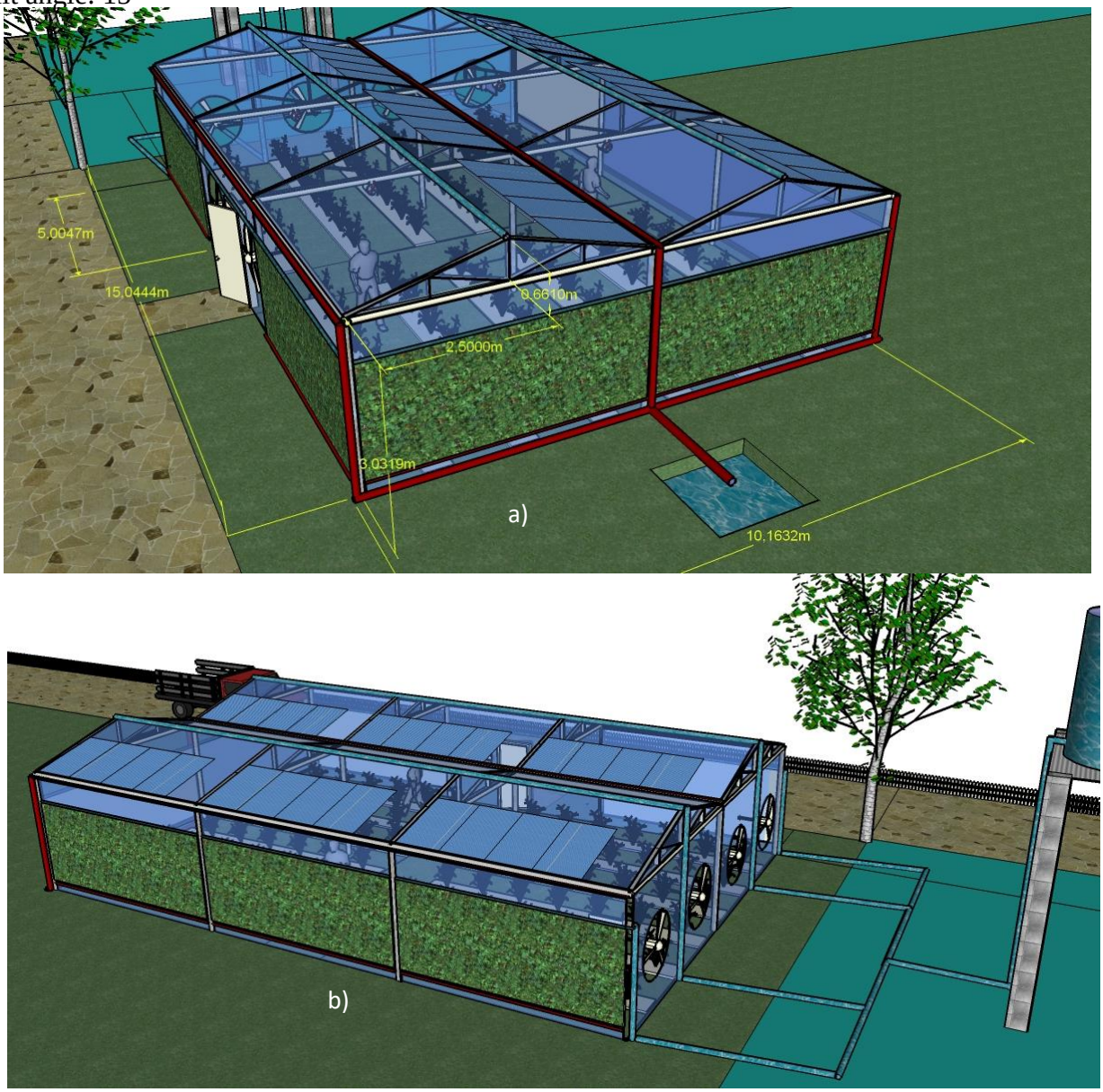


**Figure 3. 5** a) and b) Side view of the initially proposed greenhouse

### 3.1.3 Materials and mechanical studies

This section gives a clear detail on the type of materials best fitted for the framework of the greenhouse through studies using professional software such as Robot Structural Pro 2017. In fact, the software uses the load applied on the structure to derive the cross-sectional area upon selection of a range of materials' type. It studies the strength of the material and the total resistance of the structure based on the total load affecting it including the self-load of the structure, that of the wind pressure, the snow if there is, and of anything capable of stressing the framework.

#### 3.1.3.1 Materials for setting up the skeleton of the greenhouse

The selected materials are galvanized steel round tubes for all the structure with the roof that was in a bar. The round tubes are resistant to abrasion and corrosion, more resistant to the constraints of all kinds caused by external forces compared to other forms of tube section such as square tubes. They have low thermal conductivity compared to other metals and are accessible and available everywhere in the local market.

#### 3.1.3.2 Charges on the structure

The resistance of the overall metal structure faces to the external forces such as the wind and external charges has been studied to be convinced of the choice of materials. To do this, the structural robot software has been used to perform this task. A wind of 13.7 m / s (maximum wind speed in the study area (Department of Say) from the South (X-) and West (Y +), and a series of charges has been applied on all the areas concerned. The charges are constituted of the proper load of the structure, that of the photovoltaic solar modules of 250W and their frames (pz = -0.12 kN (kilo Newton)), from the maintenance (people on roof), the cooling pad and the water flowing in the structure (pz = -0.25 kN).

### 3.1.4 Arrangement of the intervention ground

A ground study was conducted to avoid any inconvenience and so that the structure foundation is better adapted to the field. Then, the ground was cleared for any culture using a tractor. In addition, a rapid poll of the ground was carried out using basic instruments such as a decameter and a steel mine to know the most stable layer of the soil, so the depth at which the foundation will be made. Finally, the foundation was done at a good depth conceding the sandy soil.

## 3.2 Development of greenhouse cooling technology

### 3.2.1 Prototype on cooling material testing

Different cooling materials based on local cellulosic materials were experimented. This is to develop potential replacement for the commercial evaporative cooling pads. In this part of the experiment, the thermodynamic of water was exploited by applying the evaporative cooling principle whereby the plant materials should be able to retain water molecules for enough time for the exchange between water and air to occur. Besides, the cellulosic material should be porous enough to allow this process.

#### 3.2.1.1 Experimental Method

The main purpose of this experiment is to develop cooling pad that can give an optimum thermal comfort. According to ASHRAE, a comfort zone for relative humidity is between 19.8% and 79.5% and 20 – 24 $^{o}$C with note on humidity ratio, air speed, clothing and metabolic rate (ASHRAE, 2013).

Seven different local materials from indigenous plants parts (*Ctenium elegoms* (Baata pad), *Antropogon gayanus* (Gamba pad), *Hyphaene thebaica* (leaves) (Kaba pad), *Pennisetum glaucum* (husk) (Kaikai pad), *Ceba pentandra* (fibers) (Kuriya pad), 'Red and white wood' (Wood shavings pad), *Hyphaene thebaica* (leaves stipulates) (Wood wool pad)) were tested as candidates for a new cost-effective evaporative cooling pad. The pads were characterized under two different inlet velocities with water being recycled and its temperature being measured. The saturation efficiency of each of them was derived as long as their cooling capacities (Djibrilla et al., 2021b).

Saturation efficiency is given by: $\mathbf{eff} = \frac{\mathbf{T_{db1} - T_{db2}}}{\mathbf{T_{db1} - T_{wb}}}$ **Equation 3. 1**

Cooling capacity is given by: $Q = \mathbf{m_a Cp_a (T_{db1} - T_{db2})}$ **Equation 3. 2**

Where eff = Evaporative saturation efficiency in %, Q = Cooling capacity in kW, $T_{db1}$ and $T_{db2}$ are inlet and outlet dry bulb temperatures in $^{o}$C, and $T_{wb}$ is wet bulb temperature in $^{o}$C measured with thermometer's probe covered by a wet cotton., $m_a$ and $Cp_a$ are mass flow rate and specific heat capacity of air respectively.

#### 3.2.1.2 Experimental setup

An experimental setup of 180 cm of length was fabricated in order to duct the characterization of natural locally made pads from local plant materials with a high precision (see figure 3.8 and 3.9). The setup was made up of a square duct made of aluminum sheet insulated by glass wool (4 cm thickness). At the inlet is found: (1) a fan blower, with a square screen creating a uniform wind flow, that forces ambient air inside the conduct, (2) a pad exchanging section with a slut at 100 cm away from the blower, and (3) measuring instrument slut at 40 cm before and after the

pad slut to record inlet and outlet data. The pad section has a hole through which a pipe passes to sprinkle water over the pad by means of a pump, and another hole for recycling water.

Cross sectional area or wetted area: $A = H \times L$ where H represents height and L is length

$$A = 0.47 \times 0.41$$

$A = 0.00193\ m^2$

Thickness of pads is constant: $\mathcal{E} = 5$ cm.

Pump power = 18W

Fan velocity = $v_{high}$ 5.522 m/s and $v_{low}$ = 5.110 m/s

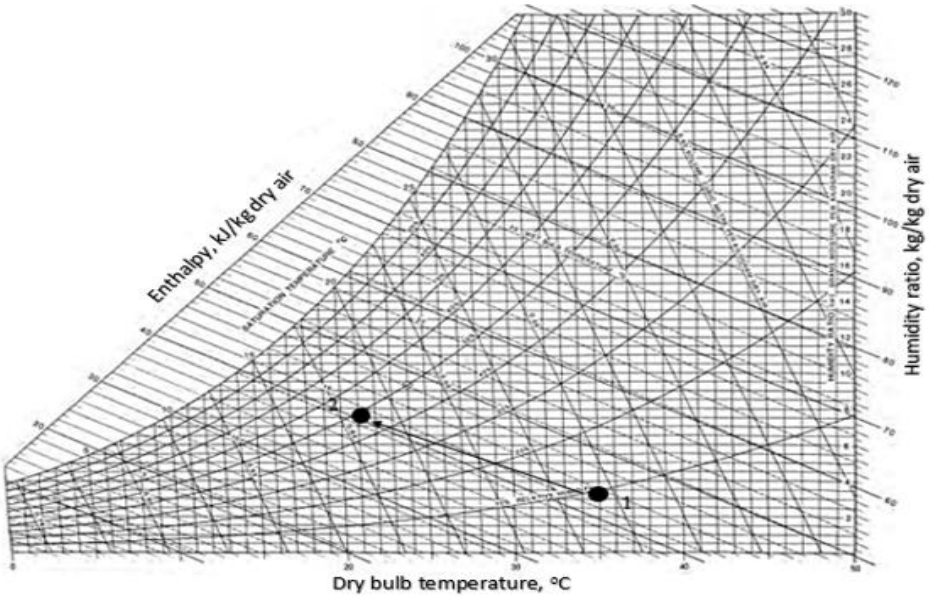


**Figure 3. 6** Cooling process on psychometric chart (ASHRAE, 1992)

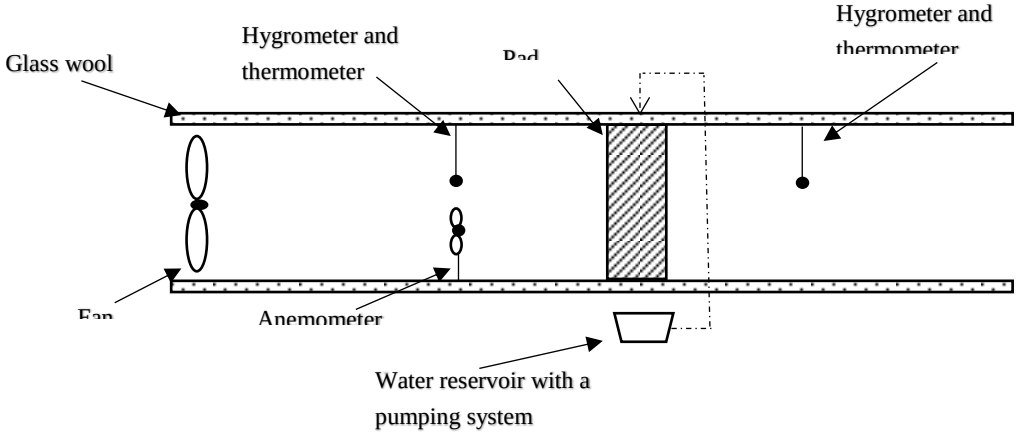


**Figure 3. 7** Schematic diagram of a cross sectional view of the experimental setup (Djibrilla et al., 2021b, 2021a)

Back

Front

Water storage

**Figure 3. 8** Experimental and characterization setup views

**Figure 3. 9** Side view of experimental and characterization setup

### 3.2.1.3 Measuring instruments

Thermodynamic parameters about inlet and outlet conditions were taken using digital instruments: Anemometer HoldPeak HP-856A for wind velocity and inlet dry bulb temperature; two digital multimeters HoldPeak HP-90EPC with a thermocouple probe. One of them is used for measuring outlet dry bulb temperature and the other had its probe covered with a wet cotton wool in order to measure wet bulb temperature. Two hygrometers (HTC 1) were used for relative humidity measurement and a TP101 thermometer was used for measuring water temperature.

### 3.2.1.4 Balance around the pads

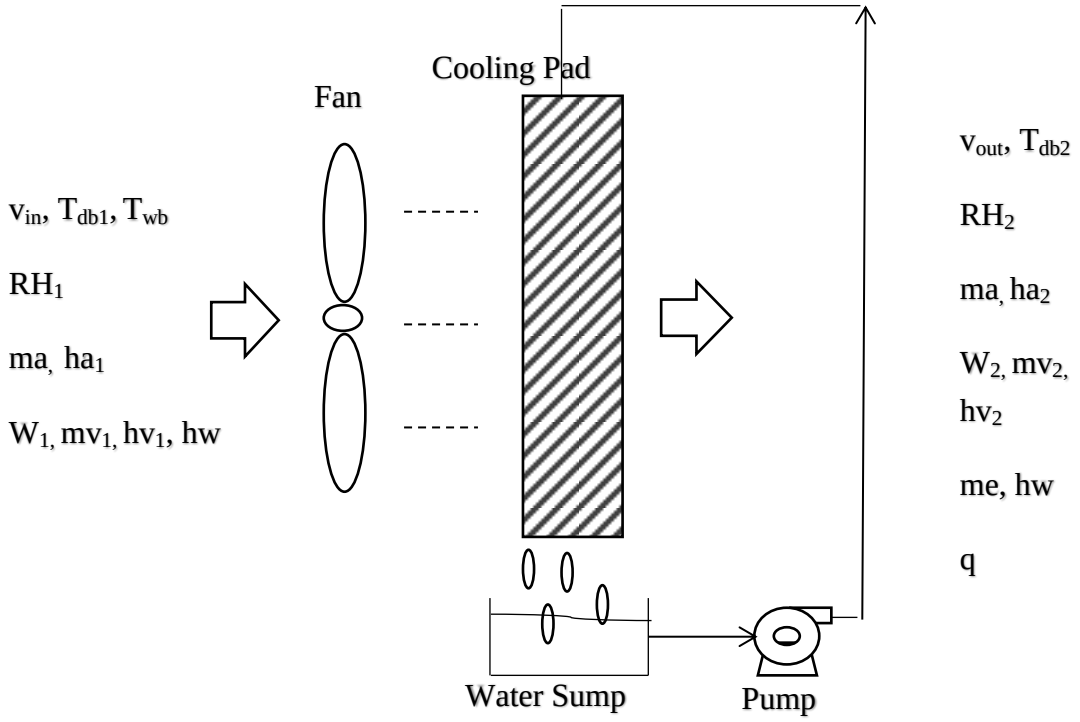


**Figure 3. 10** Diagram of a balance around the pad

Where the indices 1 and 2 indicate inlet and outlet parameter respectively

ha, hv, W, mv, RH, $T_{wb}$ and $T_{db}$ represent enthalpy of air, enthalpy of water vapor, humidity ratio, mass flow rate of water vapor, relative humidity, wet bulb temperature and dry bulb temperature respectively.

$v_{in}$ and $v_{out}$ are inlet and outlet velocities; ma is air mass flowrate; hw is enthalpy of water vapor q is heat loss and me is the mass of water evaporated or lost during the process.

**Assumptions:**

i. Steady state system
ii. Heat transfer to surrounding is zero, heat radiation is ignored
iii. Fluid flow at entry is uniformly distributed in the plane perpendicular to the flow
iv. Mass and heat transfer direction is normal to the flow
v. Complete surface wetting of the pads is assumed
vi. Resistance to heat transfer from water layer core to its surface is neglected

### 3.2.1.5 Mass balance

$$\mathbf{maW_1 + mv_1W_1 = maW_2 + mv_2W_2} \qquad \textbf{Equation 3. 3}$$

where the indices 1 and 2 indicate inlet and outlet parameter respectively,

ma = air mass flow rate, kg/s; mv = mass flow rate of water vapor, kg/s; and W = humidity ratio, kg of air/kg of water;

The contribution of the Water of the reservoir in and out cancelled out because it was recycled.

### 3.2.1.6 Energy balance

When thermal equilibrium is reached, the energy balance for air/water vapour mixture across the pads can be written as:

$$\mathbf{ma\ ha_1 + mv_1hv_1 + mv_1hw = m_aha_2 + mv_2hv_2 + mv_2hw} + q \qquad \textbf{Equation 3. 4}$$

where the indices 1 and 2 indicate inlet and outlet parameter respectively,

ma = air mass flow rate, kg/s; mv = mass flow rate of water vapor, kg/s;

ha = enthalpy of air, kJ/kg of dry air; hw = enthalpy of water, kJ/kg of dry air and;

q = heat loss by the pads, kJ/s; W = humidity ratio, kg of air/kg of water;

RH = relative humidity, %; v = frontal/inlet velocity, m/s;

$v_{out}$ = outlet velocity, m/s; $T_{db}$ = dry bulb temperature, $^oC$;

$T_{wb}$ = wet bulb temperature, $^oC$.

Let me = mass of water evaporated, me = $\mathbf{mv_2 - mv_1}$ **Equation 3. 5**

W = humidity ratio, W = mv/ma **Equation 3. 6**

q = heat loss, q = ma Cpa ($\mathbf{T_{db1} - T_{db2}}$) **Equation 3. 7**

Applying equation 2.5 into equation 2.4, we obtain:

$$\text{ma } (\mathbf{ha_1 - ha_2}) + \text{me } \mathbf{hw + mv_1hv_1 + mv_2hv_2} = q \qquad \textbf{Equation 3. 8}$$

Dividing equation 2.4 by ma, we get:

$$\mathbf{ha_1 + W_1hv_1 + W_1\ hw - ha_2 - W_2hv_2 - W_2\ hw} = \frac{\mathbf{q}}{\mathbf{ma}} \qquad \textbf{Equation 3. 9}$$

Applying equation 2.4 into 2.7, we obtain:

$$\mathbf{ha_1 - ha_2 + W_1 (hv_1 + hw) - W_2 (hv_2 - hw)} = \text{Cpa } (\mathbf{T_{db1} - T_{db2}}) \qquad \textbf{Equation 3. 10}$$

#### 3.2.1.6.1 Heat and mass transfer coefficients

The heat loss (q) is also known as the heat transferred which is carried by the cool air serving as a comfort. The heat transferred can also be expressed as:

$$q = h_H A_s \Delta T \qquad \textbf{Equation 3. 11}$$

And the mass of water evaporated (me) or mass transferred through the evaporative cooling process can be expressed as:

$$me = h_M A_s \Delta \rho_v \qquad \textbf{Equation 3. 12}$$

Where $h_H$, is the heat transfer coefficient, $h_M$ is the mass transfer coefficient, $A_s$ is the total wetted surface area of the pad used, $\Delta T$ is the log mean temperature difference and $\Delta \rho_v$ is the log mean mass density difference of water vapor.

$$\Delta \mathbf{T} = \frac{\mathbf{T_{db2} - T_{db1}}}{\mathbf{ln}((\mathbf{T_{db2} - T_{wb}})/(\mathbf{T_{db1} - T_{wb}}))} \qquad \textbf{Equation 3. 13}$$

$$\Delta \boldsymbol{\rho_v} = \frac{\boldsymbol{\rho_{v2} - \rho_{v1}}}{\mathbf{ln}((\boldsymbol{\rho_{v2} - \rho_{wb}})/(\boldsymbol{\rho_{v1} - \rho_{wb}}))} \qquad \textbf{Equation 3. 14}$$

Where the indices 1, 2 and wb are used to represent parameter taken at inlet, outlet and wet bulb conditions.

**Table 3. 1** Some formulae used in the work

| | Formula | Details |
|---|---|---|
| Increase in relative humidity | %inc = $\frac{RH_2 - RH_1}{RH_1}$ x 100% | $RH_1$ and $RH_2$ represent relative humidity or air stream at inlet and outlet respectively |
| Mass flow rate of air | ma = v x A x ρa | where v is the inlet velocity of air, A is the cross-sectional area and ρa is the air density obtained from air properties table (Alvarado & Klein, 1970). |
| Mass density of water vapour in the air stream | $\rho v = \frac{W}{SV}$ | Where W is humidity ratio and SV is specific volume. Both W and SV are obtained from psychometric table (ASHRAE, 1992). |
| Specific heat capacity of air or of moist air | Cpa = Cpaa + Wa x Cpv | Where Wa is humidity ratio of air at inlet temperature, Cpaa is specific heat capacity of dry air and Cpv is specific heat capacity of water vapour. |
| Mass of water vapour | mv = maW | Where W is humidity ratio and ma is mass flow rate of the air stream |

#### 3.2.1.6.2 Water evaporation rate

Water evaporation rate through the evaporative cooling process is calculated as:

$$Er = \frac{me}{\rho vw} \qquad \textbf{Equation 3. 15}$$

Where me is mass flow rate of water evaporated and ρvw is density of water vapour obtained from saturated water table (International Association for the Properties of Water and Steam (IAPWS), 1995).

#### 3.2.1.6.3 Pressure drop

Evaporative cooling process causes a Pressure drop across the pads which can be expressed as

$$\Delta Pv = Pv_2 - Pv_1 \qquad \textbf{Equation 3. 16}$$

Where $Pv_2$ and $Pv_1$ are vapor pressures at outlet and inlet temperature respectively.

$Pv_2 = Ps_2 \times RH_2$ ; $Pv_1 = Ps_1 \times RH_1$

Ps is the saturated vapor pressure obtained from air properties table while RH is relative humidity (Alvarado & Klein, 1970).

#### 3.2.1.6.4 Permeability of pads

Knowing the capacity of the pads to retain water for the mass and heat exchange long enough for a better efficiency is a good information in the design of an effective pad. This function is expressed in terms of the permeability coefficient, K as first proposed by Darcy through Darcy's law and restudied by Pal et al. (2006). The permeability of a porous media for single phase and multi-phase flow describes the kinetics of fluid flow though porous media in terms of driving force and permeability of the medium (Djibrilla et al., 2021a; Pal et al., 2006). It is expressed as:

$$q = \frac{K}{\eta} \frac{\Delta P}{\Delta L} A \qquad \textbf{Equation 3. 17}$$

where Q is volumetric flow rate ($m^3/s$), K is permeability coefficient ($m^2$), $\Delta P$ is pressure drop, $\Delta L$ flow length of thickness, A is cross section area to flow and $\eta$ is fluid viscosity.

This formula can be adapted for evaporative cooling pad as:

$$q = \frac{K}{\eta} \frac{\Delta Pv}{\varepsilon} As$$

$$K = \frac{\frac{me}{\Delta \rho v} \eta \times \varepsilon}{\Delta Pv \times As} \qquad \textbf{Equation 3. 18}$$

where me is mass flow rate of water evaporated, $\Delta\rho v$ is log mean mass density of water vapour, $\eta$ is dynamic viscosity obtained air properties table, $\varepsilon$ is thickness of the pad and $\Delta Pv$ pressure drop (Alvarado & Klein, 1970; Djibrilla et al., 2021b).

The greater the K value, the higher will be the rate of fluid flow through a material. K is dependent on the fluid and porous material used reference (Pal et al., 2006).

#### 3.2.1.6.5 Coefficient of performance (COP)

This parameter contributes in evaluating the energy efficiency aspect of the cooling pads. The higher the COP value, the more efficient is the cooling pad.

$$COP = \frac{q_{pad}}{P_{fan} + P_{pump}} \qquad \textbf{Equation 3. 19}$$

Where $q_{pad}$ is the cooling capacity of the pad, $P_{fan}$ and $P_{pump}$ represent power of fan or blower and pump respectively.

$P_{pump}$ = 18W given by the manufacturer.

$$Pfan = \frac{\mathbf{ma\ x\ \Delta Pv}}{\mathbf{\rho a\ x\ \eta_{fan}\ x\ \eta_{motor}}} \qquad \textbf{Equation 3. 20}$$

Where ma and ρa are mass flow rate and density of air respectively; ΔPv pressure drop; $\eta_{fan}$ and $\eta_{motor}$ are fan and motor efficiencies. $\eta_{fan} = \eta_{motor}$ = 80%

#### 3.2.1.6.6 Cost to efficiency ratio (CER)

This parameter helps to get the optimum material considering the cost of the pad using the plant cellulosic material and its efficiency when used. The higher the CER value, the better the material.

$$CER = \frac{\mathbf{Cost}}{\mathbf{eff}} \qquad \textbf{Equation 3. 21}$$

## 3.3 Crop cultivation under ambient conditions: a preliminary work for greenhouse cultivation preparation

### 3.3.1 Materials and chemicals

#### 3.3.1.1 Chemicals

Ethanol ($CH_3CH_3O$, 99.9%, AnalaR NORMAPUR) was used as a solvent in the extraction of photosynthetic pigments. Ethanol served as a reference for baseline for absorbance and transmittance measurements. Acetone ($C_3H_6O$, 99.5%, Analytical Reagent) and petroleum ether ($CH_3(CH_2)_n\ CH_3$, 0.01% aromatic hydrocarbon, AnalaR NORMAPUR) were used to prepare the eluent used for the migration of photosynthetic pigments.

#### 3.3.1.2 Measuring devices and Instruments

##### 3.3.1.2.1 For Laboratory analysis

Scissors and gloves were used during sampling. Pipettes (1 mL and 2 mL), beakers (50 mL and 100 mL), test tubes (50 mL and 100 mL) were used as well. An electronic scale PRECISA 2005 A was used for weighing the masses of plant matter. A mortar equipped with a pestle, fine sand (silica), a funnel and standard pleated filter paper (diameter 150 mm porosity 10-20 μm) were used in the photosynthetic pigments' extraction step.

Silica TLC plates 15 cm long and 2 cm wide with a support in aluminum and 20 cm long a wide with a glass stand, and capillary tubes were used for the chromatographic characterization of the extracted photosynthetic pigments.

The spectral analysis was carried out using a double UV-Visible spectrophotometer Evolution 300 bundles. Quartz cuvettes (Hellma 100B-QS) with an optical path $\ell = 1$ cm are associated with the spectrophotometer for measurement of absorbance and transmittance signal.

#### 3.3.1.2.2 For environmental parameters measurement

The environmental parameters were measured using specific devices. Soil temperature and pH were measured with a digital pH/temperature soil analyzer (KETOTEK). Leaf temperature was measured using a contactless infrared thermometer (KETOTEK). The relative humidity and temperature of air were measured using a thermo-hygrometer (Digital, Temperature from -20 to 60°C, Humidity from 5 to 95%). The intensity of the light is taken through the electronic luxmeter (Digital Luxmeter/photometer TASI-8721).

#### 3.3.1.2.3 For data analysis

Data analysis software are used to analyze the obtained laboratory and field data among which we have Origin 6.0 and Microsoft Excel software.

### 3.3.2 Experimental methods

#### 3.3.2.1 Study site

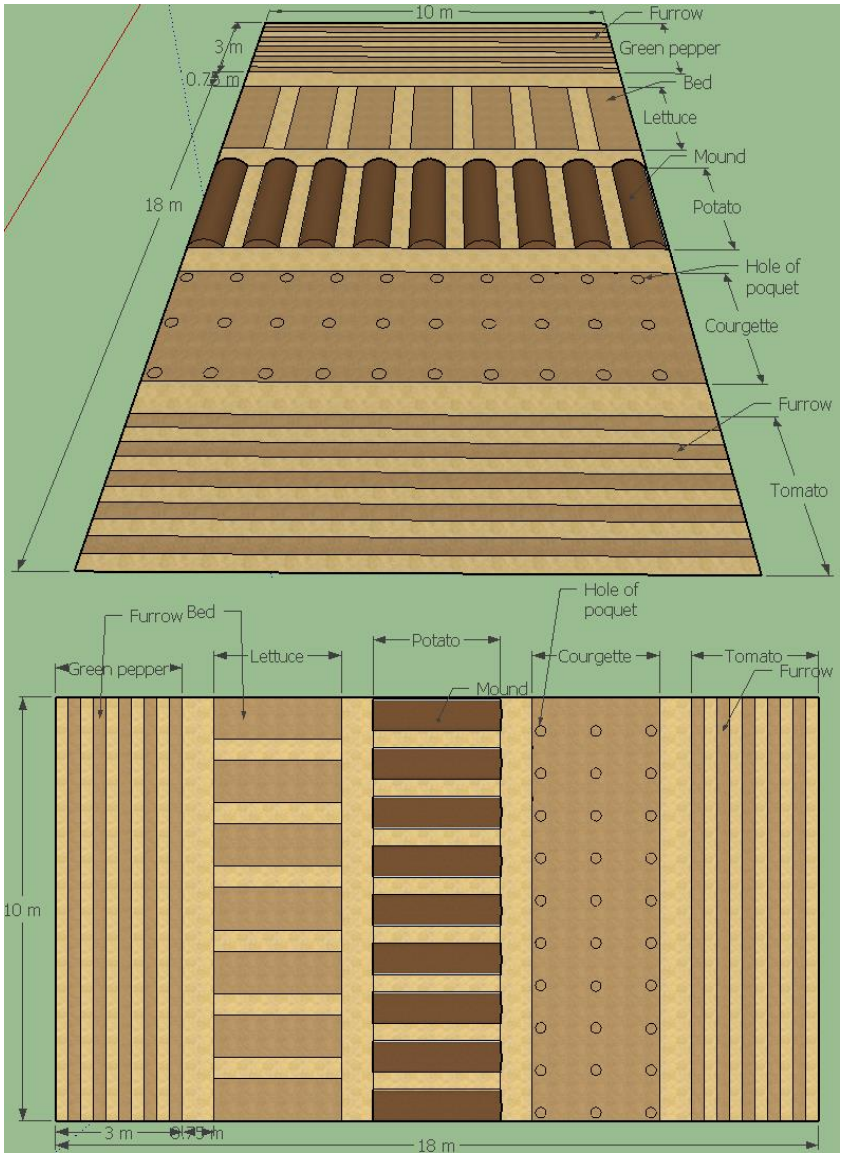


**Figure 3. 11** Arrangement of plots

The study was done on a 180 $m^2$ piece of land located in a 5 hectares farm.

#### 3.3.2.2 Soil sampling and characterization

The soil in which crop cultivation was done was analyzed before plantation. Soil samples were taken in systematic random manner before being sent for analysis at the Faculty of Agronomy, University Abdou Moumouni.

Two types of components were sought for: physical characterization and chemical composition. The granulometry of the cultivation soil through its composition of clay, silt and sand constituted

the physical characterization. The chemical composition characterizes the salinity of the soil. This salinity is revealed through the measurement of the following parameters: potential hydrogen (pH), electrical conductivity (EC), total phosphorus (Pt), organic matter (OM), carbon nitrogen ratio (C/N), exchangeable cations ($Ca^{2+}$, $Mg^{2+}$, $Na^{+,}$, $K^{+}$), cationic exchange capacity (CEC).

It is important to know the state of the soil before planting any crop on it; whereby rise the need to carry out a soil analysis before starting the cultivation. The following soil analysis procedures, described by the agronomic sciences laboratory of the Abdou-Moumouni University of Niamey served reference for soil analysis.

Thus, the particle size analysis was done by the Robinson pipette method which is based on the difference in sedimentation rate between the lighter and bigger particles. In this method a sample is pipetted at different times and at different suspension depths of the sample in a test tube. Organic matter is deleted beforehand because of its binding characteristics.

#### 3.3.2.2.1 Potential Hydrogen (pH)

The pH was measured respecting the ratio (m, v) 1/2.5 which consists of putting 20 g of sol in 50 mL of distilled water. The mixture is left to stand for two (2) hours. This stage is called saturation. Thus, the pH of the solution is measured using a pH meter.

#### 3.3.2.2.2 Electrical conductivity (EC)

Electrical conductivity (EC) is measured with a ratio (m, v) of 1/5. A solution containing 20 g of soil and 100 mL of distilled water is prepared. The latter is left to rest for two (2) hours. Electrical conductivity is measured using a conductivity meter.

#### 3.3.2.2.3 Total phosphorus (Pt)

Four (4) **s**teps determined the measurement of total phosphorus (Pt). It follows these steps: mineralization, extraction, color development and reading. Mineralization consists of heating for five (5) hours, a solution of 5 g of soil and 10 mL of nitric acid ($HNO_3$). The solution obtained is filtered using with a Wattman filter paper. Then, on five (5) mL of filtrate obtained from the extraction are added 10 mL of ammonium molybdate ($(NH_4)_2MoO_4$) and one (1) mL of sodium chloride cyanide $(NCCl)_3$. Finally, the reaction medium is topped up to 50 mL with distilled water. The solution obtained is blue in color. This solution is read using a spectro-chlorometer.

#### 3.3.2.2.4 Available phosphorus

The available phosphorus analysis has three phases. The first phase is extraction. It consists of homogenizing 5 g of soil and 35 mL of extraction solution. The solution obtained is filtered using Wattman filter paper. The second step is the color development and the third stage and reading. These last two steps are the same as those of total phosphorus.

#### 3.3.2.2.5 Carbon

Carbon is analyzed using the Walkley-Black method. This method involves heating for 30 min a solution containing 1 g of soil, 10 mL of potassium dichromate ($K_2Cr_2O_7$) and 10 mL of hydrochloric acid (HCl). The latter is dosed with the sulphate ferric ammonium ($NH_4Fe$ (SO4)).

#### 3.3.2.2.6 Nitrogen

Nitrogen is analyzed by the KJELDHAL method. This method consists of heating for 15 minutes a solution containing 5 g of soil and 10 mL of sulfuric acid ($H_2SO_4$) to which is added the KJELDHAL catalyst. Then, the heated solution is made alkaline by adding soda. This is distilled with a KJELDHAL distiller.

#### 3.3.2.2.7 Exchangeable bases

The exchangeable bases are extracted using the method called ammonium acetate extraction method ($C_2H_7NO_2$). The method consists of leaving for 16 hours a mixture containing 10 g of soil and 100 mL of ammonium acetate ($C_2H_7NO_2$) in a percolator. Then, 100 mL of the previous solution are recovered drop by drop. Finally, calcium and magnesium ions are measured by titrimetry and the sodium and potassium ions are measured using a flame spectrometer.

#### 3.3.2.2.8 Cation exchange capacity

The cation exchange capacity (CEC) was determined by extraction method with KCl. This method has three (3) steps. The first step is to prepare a solution containing 10 g of soil and 250 mL of KCl. The second step is the extraction. And the last step is titrimetric assay.

### 3.3.2.3 Environmental and climatic condition data sampling

While taking any sample, environmental conditions or climatic data such as air, soil and leaves temperatures, relative humidity and light intensity around each plant. These data were recorded between 11 am and 02 pm. Another data on the measurement of the height of the plant as well as seize and weight of the fruits was also taken alongside.

#### 3.3.2.3.1 Vapor pressure deficit

Low vapor pressure deficits (VPD) and availability of light are limiting factors in the productivity of sheltered crops since the absorption of nutrients from the growing medium is directly related to the flow of water through the plant. The flow of water in the plant is governed by transpiration, which is one of the two phases of evapotranspiration (soil-plant-atmosphere continuum) (Iraqi et al., 1997; Vallières, 2018). VPD is also the difference between the maximum amount of water vapor that can exist in the air (SVP) and the actual water vapor at a given temperature (AVP).

VPD = AVP - SVP in kPa **Equation 3. 22**

% RH = ($AIR_{AVP}$ / $AIR_{SVP}$) x 100% **Equation 3. 23**

VPD = $LEAF_{SVP}$ - ($AIR_{SVP}$ x AIR% RH) **Equation 3. 24**

#### 3.3.2.3.2 Plant parts' sampling

The various crops were followed and sampled throughout their growth stages. Seeds were planted in December 2020, and seedling were transplanted and followed later on. Sampling was done for four (4) months precisely from January 2021 to April 2021.

Samples of plant leaves were collected in a systematic random manner. A measuring tape/ruler was used for measuring plants height, a pair of scissors and plastic bags were used for sampling. Plant samples were put in an ice chest for transportation till the university Abdou Moumouni laboratory where analyses were conducted.

The plants studied were: Lettuce (*Lactuca sativa*) Eden variety, Courgette or Zucchini (*Curcubita pepo*) F1 color variety, Tomatoes (*Solanum lycopersicum*) F1 Mongal variety, Potatoes (*Solanum lycopersicum*) Pamela variety and Sweet pepper (*Capsicum annuum*) Jason variety.

**Figure 3. 12** Sampling technic

#### 3.3.2.3.3 Lettuce

The lettuce was sown on December 22$^{nd}$, 2020 and its transplanting followed twenty-six days (26) after sowing. Samples were collected at each stage of development. Three stages make up the development of lettuce. The three stages are respectively: the seedling stage (stage of two true leaves), the foliage growth stage (stage of ten leaves) and the bolting stage. The first sampling was carried out eleven (11) days after transplanting; the second sampling was twenty-eight (28) days after the two-true-leaves stage and the last sampling twenty-eight days after the ten-leaf stage.

#### 3.3.2.3.4 Potato

The potato was pre-germinated on December 22$^{nd}$, 2020. Its planting was performed on January 18$^{th}$, 2021, twenty-seven (27) days after pre-germination. The growth of the potato is made in three main stages.

The first sampling corresponding to the stage of lifting or vegetative stage was carried out ten (10) days after planting. In the second stage which is the tuber formation stage (tuber formation

and tuber enlargement), the collection of the sample was done twenty-eight (28) days after the first. During this stage, some of the plants may present flowers (white flower). The third sampling was carried twenty-seven (27) days after the enlargement of the tubers which corresponds to the stage of senescence.

#### 3.3.2.3.5 Courgette

The courgette or zucchini seeds were sown on December 22nd 2020 and its transplanting carried out twenty-three (23) days after sowing. The stage of advanced emergence, the stage of flowering and the stage of fruiting constitute successively the phases of development of the courgette. One sample is collected at each stage of development respectively at ten (10) days after transplanting, twenty-eight (28) days after advanced emergence, twelve (12) days after the flowering stage.

#### 3.3.2.3.6 Tomato

The tomato crop was sown on December 22nd, 2020 and its transplanting carried out forty (40) days after sowing. Tomato developed in three growth stages. The first sampling was carried out twelve (12) days after transplanting, which corresponds to the stage of advanced emergence. The second sampling was done at the flowering stage, seventeen (17) days after the advanced emergence stage. The third and final sampling was carried out twenty-eight (28) days after the flowering stage which corresponds to the fruiting stage.

#### 3.3.2.3.7 Green pepper

The pepper was sown on January 11th, 2021 and its transplanting was carried out on February 27th 2021. The first sampling was carried out two (2) days after the transplanting at advanced emergence stage. The second sampling followed by analysis at laboratory was carried out at the flowering stage forty-seven (47) days after the advanced lifting. The third and last sampling was done at the fruiting stage exactly twelve (12) days after the flowering stage.

### 3.3.2.4 Preparation of plant samples for extraction

Plant samples were prepared in a way to eliminate the waste which can be on the parts to be analyzed and to limit any contamination. The leaves of the selected vegetables were washed and rinsed with distilled water and, then, dried with paper towel. Next, a mass of 5 g of these leaves was weighed using an electronic balance, then, these leaves were finely divided using a pair of scissors.

### 3.3.2.5 Photosynthetic pigment extraction

Plant material prepared for extraction is then used in this step extraction. Ethanol, a polar organic solvent, is the most suitable solvent for the extraction of photosynthetic pigments.

Various plant matters were placed in a mortar and ground with 2.5 g of fine sand and 5 mL of absolute ethanol until the solvent takes on a marked green tint. Then, the crushed was filtered using a filter paper, and the filtrate obtained was of a limpid green. The collected filtrate is

divided in two parts, one part was subjected to a thin layer chromatographic characterization process and the other part was used for UV-Vis spectrophotometric reading.

### 3.3.3 Characterization

The characterization of photosynthetic pigments was carried out on one hand through thin layer chromatography and on the other hand via UV-Visible spectrophotometry.

#### 3.3.3.1 Thin Layer Chromatography (TLC) Analysis

Photosynthetic pigments are sought after at all growth stages of the plant from the first stage to the last. The frontal ratio (Rf) is also used for the identification of these pigments.

$$Rf = \frac{\text{distance travelled by pigment}}{\text{distance travelled by eluent}} \qquad \textbf{Equation 3. 25}$$

##### 3.3.3.1.1 Best eluent determination

To determine the best eluent, six compositions were previously prepared with petroleum ether and acetone in different proportions:

i. Eluent 1: 40% petroleum ether and 60% acetone,
ii. Eluent 2: 50% petroleum ether and 50% acetone,
iii. Eluent 3: 60% petroleum ether and 40% acetone,
iv. Eluent 4: 70% petroleum ether and 30% acetone,
v. Eluent 5: 75% petroleum ether and 25% acetone,
vi. Eluent 6: 80% petroleum ether and 20% acetone.

##### 3.3.3.1.2 TLC of individual plant samples

The TLC test was done, first, with a piece of the plate and was, then, applied over a full plate using three spots.

A TLC plate was labeled with a cross using a pencil 1 cm from the lower edge, taking care not to damage the silica layer. At this cross, using a capillary tube, a few drops (0.5 mL) of the extracted solution are placed, leaving one drop dried before dropping another. The slices are then gently deposited in test tubes graduated previously prepared. The test tube is placed in a dark place away from the light. When the eluent rises to within 1 cm away from the top edge of the plate, the plate was removed and the observation of the different photosynthetic pigments of interest was made. The same method was applied for all plant samples.

**Figure 3. 13** TLC tests showing pigments migration

#### 3.3.3.2 UV-Visible Spectrophotometric analysis

Absorption spectrophotometry is a physical method of chemical analysis. It measures the proportion of light absorbed by a colored species in solution. This is crucial in determining quantitatively and qualitatively the different photosynthetic pigments of interest.

#### 3.3.3.3 Analysis of raw samples

Using the UV-Visible Evolution 300 dual-beam spectrophotometer, the measurements of the absorbance (A) and the transmittance (T) of the extracts containing the photosynthetic pigments were performed against ethanol as a reference, scanning between 190 and 1100nm. This scan covered the three most important regions of the solar spectrum (Ultra-Violet, Visible light and Infra-Red) for the absorption of light by plants. At necessary, dilutions were carried out to make the spectra of the raw extracts.

##### 3.3.3.3.1 Analysis of separated samples

The clearly separated pigments with the best eluent were recovered by scraping each TLC plates. Dissolved into ethanol, separated samples or pigments were scanned through the spectrophotometer to obtain the characteristic peaks of each. Moreover, these spectra helped in estimating the necessary radiation each plant need at various growth stages.

## 3.4 Crop cultivation under greenhouses' microclimate against outside weather conditions

### 3.4.1 Description of experimental area and setup

Three plots of 50 $m^2$ (L x W = 10 x 5m) were used for these experiments: one was exposed to ambient climate conditions and two were under two greenhouses microclimate conditions. An additional plot was reserved for excess nursery and as a back-up.

Individual greenhouse called cooling photovoltaic greenhouse is an east-west oriented greenhouse that is composed of a metal frame/skeleton with a truss pointed towards the South at $15^o$ angle for maximum sunshine harvesting, on which multi crystalline (1640 x 990 x 40 mm / 260 W) solar panels are mounted covering a total area of 9.74 $m^2$, and which serves as energy source. A covering material (lignocellulosic material made from jute bags) and a slot for cooling systems/ devices are used to complete the structure, accompanied with watering and draining systems, and weather parameters control system. The cooling system is made up of cooling devices which are made from cellulosic cooling pads, fan or ventilators and extractors. Pipes are installed as well as drip irrigation system to allow proper watering and the used water is recovered via a recycling unit in order to be used for watering after filtering. The microclimate control system allows regulating water flow and fanning ventilation speed according to needed inlet temperature or relative humidity. It is made up of a weather station, temperature and humidity sensors controlled by a monitor and an application for phones allowing distance control.

All this greenhouse system work in harmony allowing agriculture work year-round while producing energy from a renewable source (solar photovoltaic), reducing water waste and optimizing its use for productivity, and assuring an optimum land use.

### 3.4.2 Cladding materials' analysis

Some covering materials were characterized to see their light reduction capacity. A 50W while IP66 LED projector was used for the test. Later , pieces of the materials were taken for further analysis under UV spectrophotometer. The spectral analysis was carried out by the double UV-Visible spectrophotometer Evolution 300 bundles. Quartz cuvettes (Hellma 100B-QS) with an optical path $\ell = 1$ cm are associated with the spectrophotometer for measurement of absorbance and transmittance signal.

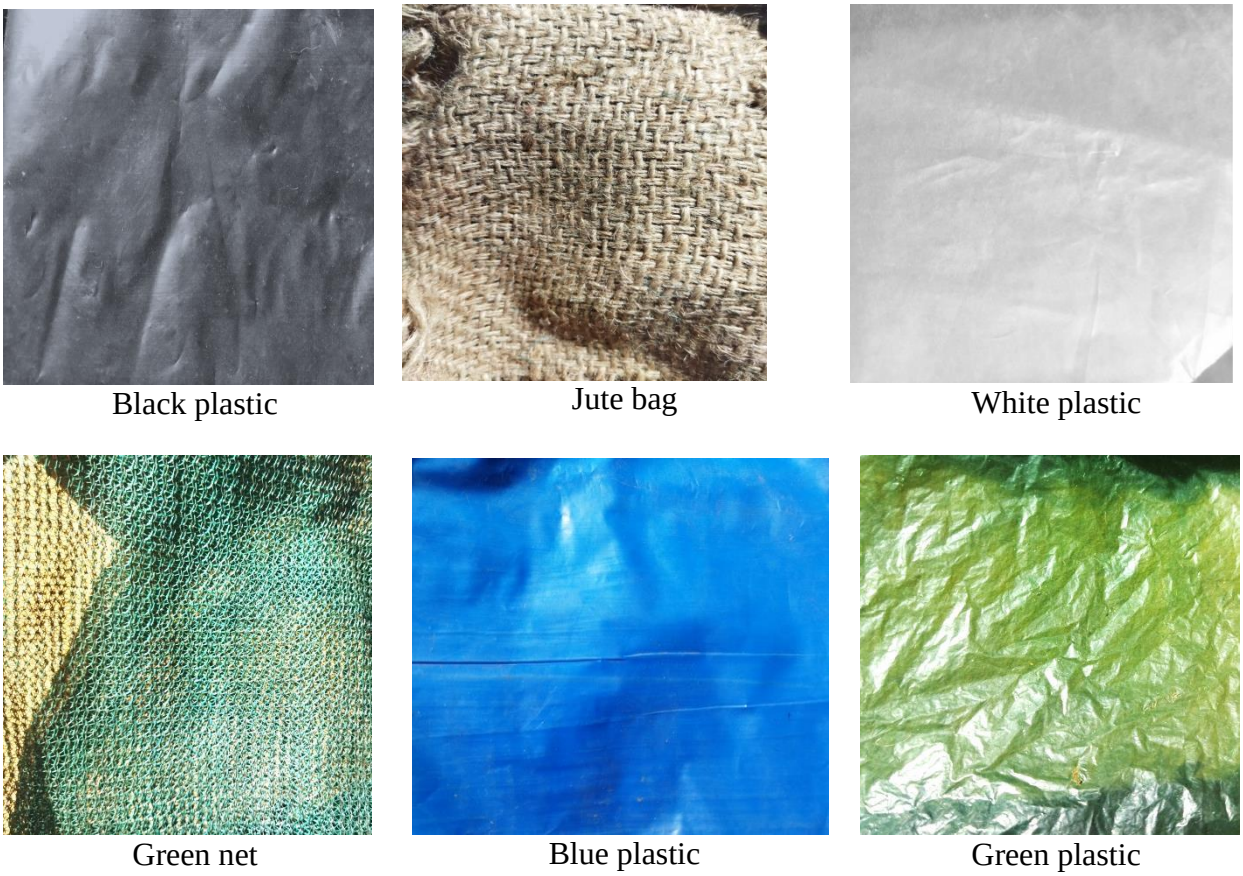


**Figure 3. 14** Locally available greenhouse of covering materials

The experimental set-up was composed of a lux meter (solar power meter TM-206 Tenmars) and a stand. Light intensity varied from 100 to 500 w/m$^2$.

A weather station (Ambient Weather WS-2902) placed at 3 m above the ground level at about 30 m away from the greenhouses was taking continuous data with some of its sensors placed inside the two greenhouses. Aside automatic data, manual data taking was conducted every Wednesday and Saturday from 1 pm to 5:30 pm in order to get afternoon harsh condition data. A $CO_2$ measuring device (Temtop M2000C) was used to collect $CO_2$ content in the atmosphere. Finally, digital thermometers (HoldPeak HP 90 - EPC) with wetted cotton attached to a thermocouple type K were used to measure wet bulb temperatures.

Temperatures measured with normal thermometer were named dry bulb temperature (Tdb) while temperatures measured with probes covered with wetted cotton were named wet bulb temperatures.

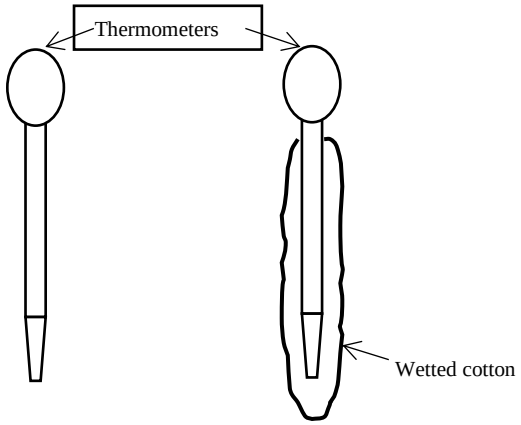


**Figure 3. 15** Thermometers probe state for dry and wet bulb temperatures

### 3.4.3 Physico-chemical characterization of the cultivation soil: particle size and salinity

Samples of soil and fertilizer used were taken for analysis to the laboratory of Faculty of Agronomy, Department of Soil Science. Sampling was done in a stratified random manner and stored in plastic bags before analysis.

### 3.4.4 Agricultural analysis

#### 3.4.4.1 Plant physical properties

The plants' physical data started 1 week after transplantation. With the aid of a measuring tape and a digital balance, plants' height and fruits weight were recorded twice a week on Wednesdays and Saturdays from 30/07/2022 to 29/10/2022 in other terms, till constant heights were observed during harvesting period.

### 3.4.5 Nutritional content analysis

Fruits, stems and leaves from tomatoes crop cultivated under the two greenhouses and under ambient conditions were analyzed in order to have their nutritional content. Most samples were dried before analysis.

**Figure 3. 16** Outside tomatoes (left) VS inside tomatoes (right) for analysis

#### 3.4.5.1 Dry Matter content test

##### 3.4.5.1.1 Wet sample basis

Beakers were washed, dried into an oven and weighed. Then, fresh tomatoes were weighed, cut into small pieces and put into an oven for 2 days till they dry off at 105 $^{o}$ C. The result is grinded into powder and weighed.

##### 3.4.5.1.2 Dry sample basis

Beakers were put into an oven to dry up for 15 minutes at 105 $^{o}$ C before being transferred into a desiccator for 15 minutes again to cool down. Beakers were removed and weighed immediately removed from desiccator. Beakers filled with samples were put into an oven for 24 hours at 105 $^{o}$ C. The whole was weighed as soon as brought out of the oven.

$$\% \text{ DM} = \frac{\mathbf{W_f - W_{emplty}}}{\mathbf{W_{sample}}} \times 100\% \qquad \textbf{Equation 3. 26}$$

$$\%RH = 100 - \%DM \qquad \textbf{Equation 3. 27}$$

**Figure 3.17** An Oven (left) and a desiccator (right)

### 3.4.5.2 Mineral matter content test

Empty pots were calcinated in an oven at T = 550-600 $^{o}$C to remove any humidity trace for 15 minutes, then, the oven was left to cool for another 15 minutes. Samples was placed into pot and weighed before bringing the whole back to the furnace (Heraeus model) for calcination for 2 hours. Cooling for 30 minutes or to room temperature was allowed.

$$\% \text{ IM} = \frac{\mathbf{W_f - W_{emplty}}}{\mathbf{W_{sample}}} \times 100\% \qquad \textbf{Equation 3. 28}$$

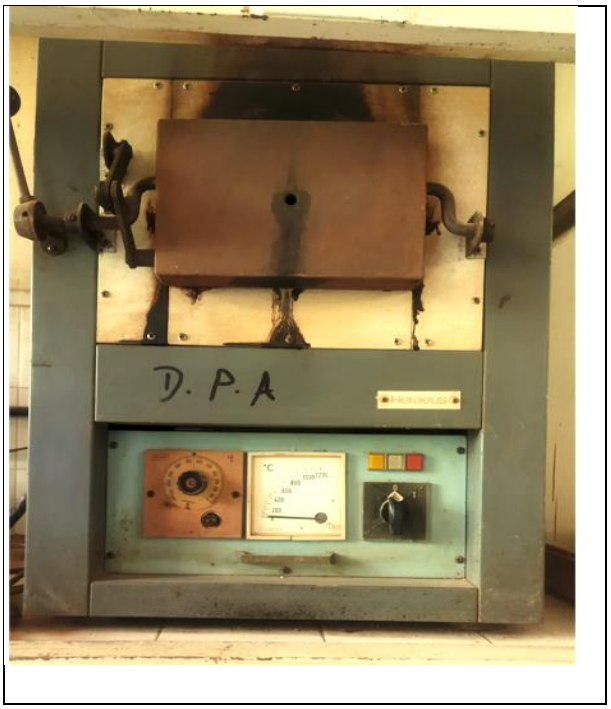


**Figure 3.18** A Furnace (Heraeus model)

### 3.4.5.3 Protein and nitrogen content test

Samples were weighed and put into tubes with a witness standard solution as a parallel additional tube. KJELDHAL standard tablets were added into each of the tubes with 10 mL concentrated $H_2SO_4$. All were put into the mineralizer (model VELP Scientifica DK 8) set at 420 $^{o}$ C for 30 minutes and left to cool down to room temperature overnight.

After mineralization, each sample was distilled via a distillation machine followed by titration.

$$\% \text{ Nitrogen} = \frac{(\mathbf{W_{sample} - W_{emplty}})\mathbf{x\ N\ x\ [H_2SO_4]}}{\mathbf{W_{sample}\ x\ 1000}} \text{ x } 100\% \qquad \textbf{Equation 3. 29}$$

%Protein = % Nitrogen x 6.25 (constant used mostly for beverage and foods) **Equation 3. 30**

**Figure 3.19** Mineralizer model VELP Scientifica DK 8

**Figure 3.20** Automatic distillation and titration machine

### 3.4.6 Fertilizer and intake

The fertilizer used was made up of dung and soil collected from a sheep rearing area as this kind of natural fertilizer is high rich in nitrogen as mentioned by many researchers such as Górecki & Górecki (2010)

**Figure 3.21** Fertilizer from small ruminant's dungs

### 3.4.7 Pests' control, Diseases and Damage

Apart from nets used as covering materials to reduce invaders, other phytosanitary products were used. Nonetheless, unforeseen circumstances caused damage to both structures and harvest products.

#### 3.4.7.1 Pests' control

For the sake of organic production, only organic pesticides were used as shown in the table below. Both industrial and natural plant based organic pesticides were tried on the field. Most of those products played a role of repellent since they create a repelling sent and taste driving away insects and other invaders. Yet, stubborn invaders such as rodents still find their way out.

### 3.4.8 Diseases and Damage

The damage and disease assessments were carried out by the analysis of the Agro Ecosystem (AAES) which allowed the observation of the symptoms of wilting, viral diseases and physical damage. The observations are made according to the requirements of the AAES.

## 3.5 Energy study

### 3.5.1 Estimated materials

To ensure energy autonomy of the greenhouse, solar photovoltaic energy was used. The estimation was as follow:

The greenhouse was to provide, largely, 6 extractors (75W each), 4 brewers (37W each) and two bulbs (50W each). Suppose devices will be functional for 15 hours using the energy stored in the batteries. Thus, the total energy that must be stored would be 582W x 15h = 8730Wh or 9000Wh. In addition, energy for night lighting using two 50W bulbs for 15 hours of lighting is 9750Wh considering that the batteries should not fall below 50% of their energy and a 12 V system. Therefore, this will require 6 batteries of 200 ah each.

Assuming that during the 8 hours of sunshine, the panels must be able to charge the batteries and at the same time operate the greenhouse. Then, the necessary energy would be the sum of the storage energy plus that of the operation of the greenhouse. The operating energy of the greenhouse is 5000Wh. This gives a total energy of 20000Wh. Assuming that the solar panels available on the steps have 50% efficiency; the number of panels thus rises to 20 panels of 250 W each. To ensure the energy autonomy of the greenhouse, we would need 6 batteries of 200 Ah each, of 20 panels of 250W each and the necessary accompaniments (cables, controllers, etc).

### 3.5.2 Used materials

For the sake of this research and due to the available financial resources, 4 batteries of 150 Ah each were used with 12 solar modules of 265 W each. Therefore, the storage capacity was 600 Ah or 7200 Wh while input power from panels was 3120 W peak. This set could allow using the greenhouse cooling system during the day but not its use during the night.

### 3.5.3 Electricity production estimate from the greenhouses

Due to the difficulty in acquiring ground field data from our installed PV system, PVGIS SARAH-2 data was used for estimating the off-grid power produced by the PV system using installed ground data. PVGIS SARAH-2 data is a solar radiation data from METEOSAT geostationary satellites covering Europa, Africa and Asia. The data available are long term averages calculated from hourly global and diffuse irradiance values.

**Table 3. 2** Provided inputs

| | | |
|---|---|---|
| **Location [Lat/Lon]:** | 13.000 | 2.000 |
| **Horizon:** | Calculated | |
| **Database used:** | PVGIS-SARAH2 | |
| **Discharge cutoff limit [%]:** | 20 | |
| **Consumption per day [Wh]:** | 4200 | |
| **Slope angle [Ã‚Â°]:** | 15 | |
| **Azimuth angle [Ã‚Â°]:** | 180 | |

## 3.6 Computational fluid dynamic analysis

This section explored the thermal behaviour of a photovoltaic cooling greenhouse under Sahel weather condition.

### 3.6.1 Experimental area and setup

This study was conducted using the 50 $m^2$ photovoltaic greenhouse installed for tomatoes production. With the help of the weather station, temperature, relative humidity, wind speed and solar irradiance data from inside and outside greenhouse were collected and analysed.

**Figure 3. 22** Experimental greenhouses

### 3.6.2 Numerical model and boundaries

Flow patterns and thermal behaviour of cooling photovoltaic greenhouse under natural convection was simulated using ANSYS fluent R2 2022 student version. The greenhouse was drawn using Space Claim 2022 with 2 m high crop row, 4 mm wall thickness and solar panels of 1650x995x40mm, which was then transferred to Workbench for CFD analysis before meshing.

The flow inside the greenhouse was assumed 3D, steady state, incompressible ideal gas and turbulent (Ferziger et al., 2020). The radiation was simulated by the Discrete Ordinates (DO) model as described in Chui and Raithby (1993) (Raithby & Chui, 1993). All boundary conditions as wall thickness, wind speed and temperature etc., were derived from actual materials datasheet (covering material, PV modules) used on the field and from weather station data installed. The external air data was directly taken from weather station output. The inlet air entered from 1.5 x 1m coolers blowing at variable rate depending on the upcoming wind velocity obtained from the weather station taking into account case scenarios and coolers wind filtering capacity as described in Djibrilla et al. (2021b) (Djibrilla et al., 2021b). The outlet direction was opposite to that of the inlet. Pressure drop boundary conditions were applied at the outlet. All side walls were assumed semi-transparent with mixed (radiative and convective). Solar modules were assumed opaque with mixed (radiative and convective) thermal conditions (Fatnassi et al., 2015).

The configuration was Pressure-based type solver with velocity formulation to be absolute under steady state adiabatic conditions. These conditions are using Reynolds Averaged Navier-Stokes (RANS) equations to resolve numerically the problem of energy distribution within the greenhouse through finite volume method. The specific source of fluid flow is directed by the viscosity loss term known as Darcy Law and an internal loss term. The energy distribution inside the greenhouse and its covering material is calculated by RANS equation (Fidaros et al., 2008).

RANS Equation: $\rho U_j \frac{\partial \Phi}{\partial x_j} = \frac{\partial}{\partial x_j}\left(\Gamma \frac{\partial \Phi}{\partial x_j}\right) + S^{\Phi}$ (Fidaros et al., 2008) **Equation 3. 31**

Where Φ stands for the three velocity components U, V, W, the temperature T (K), the spectral intensity I, the kinetic energy of turbulence k, the dissipation rate ε, the specific humidity w ($kg_{water}/kg_{moist\ air}$) and pressure P, and the parameters Γ and $S^{\Phi}$ represent the diffusion coefficient and source of term of Φ.

The SIMPLEC algorithm (Versteeg & Malalasekera, 1995) was used for pressure-velocity coupling leading to the formulation of mass conservation equation. The discretisation of the terms in the Reynolds Averaged Transport equation was materialized by the Second Order Upwind (SOU) scheme (Tamamidis & Assanis, 1993).

As described in Djibrilla et al. (2021a), wind at a specific speed crossing the evaporative cooling system gets its speed reduced by 21.113%. The latter represents input wind speed from the coolers. Input data from wind speed that are null were converted to a low reasonable value to avoid calculation error from the CFD system.

**Table 3. 3** Wind speed conversion data for simulation

| **Cases for event simulation** | **$v_{wind}$ from weather station (m/s)** | **$v_{wind}$ from coolers (m/s)** |
|---|---|---|
| **Low $T_{in}$** | 0 (considered as 0.1) | 0.02 |
| **High $T_{out}$** | 2.6 | 0.55 |
| **Low $T_{out}$** | 0 (considered as 0.1) | 0.02 |
| **High wind** | 11.5 | 2.43 |
| **High solar radiation** | 1.5 | 0.32 |

# CHAPTER FOUR – RESULTS AND DISCUSSION

## 4.1 Mechanical and materials analysis results

### 4.1.1 Selection of constructional materials

#### 4.1.1.1 Materials for setting up the frame or skeleton of the greenhouse

Using data of 2018 obtained from the International Crop Research Institute for Semi-Arid Tropics (ICRISAT) Sadore, a research center in the area, a maximum wind velocity of 13.7 m/s was input into the software. From the weight of the panels and the cooling materials, the force they exert on the structure was represented and applied as a load. All this input was processed through the software and optimization gave output presented in Table 4.1, which was used to construct the greenhouse frame. Besides, the map of the stress on the greenhouse (figure 4.3) showed no red area meaning that the framework could withstand the loads exerted on it. Hence, the design is acceptable.

Using the International Standard for Steel Building Materials AISC 14.0, a list of transverse sections of materials has been tested under the structural robot software to determine the optimal material section. The results of the simulation and calculations for the optimization of the materials were such that the vertical bars were suggested to be in round tube P2 except for the case of the intersection between the two compartments that have been put in P1.25 (see Table 4.1). The truss design resulted in simple 5 mm (L 2.5x2.5x0.1) angled iron against that of 20 mm (DL 2x2x0.125) if they were to be double at the external part of the truss.

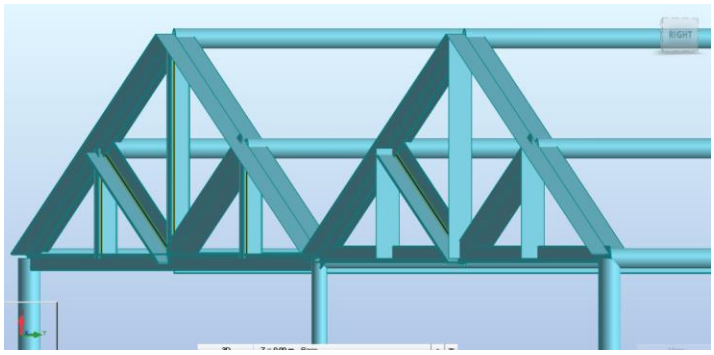

**Figure 4. 1** Side view of selected materials

ANSI/AISC 360-10 - Code Group Design ( ULS ) 1to5

Results | Messages

| Member | Section | Material | Lay | Laz | Ratio | Case |
|---|---|---|---|---|---|---|
| **Code group : 1 vertical middle bars** | | | | | | |
| 486 Simple bar_486 | P 1 | ACIER | 30.88 | 30.88 | 1.15 | 9 1.33G+1.42Q(expl.) +1.42WnX- |
| | P 1.25 | | 23.94 | 23.94 | 0.67 | |
| | P 1.5 | | 20.77 | 20.77 | 0.49 | |
| **Code group : 2 horizontall bars** | | | | | | |
| 488 Simple bar_488 | P 1.5 | ACIER | 314.73 | 314.73 | 0.37 | 8 1.33G+1.42Q(expl.) |
| | P 2 | | 251.07 | 251.07 | 0.22 | |
| **Code group : 3 truss single part** | | | | | | |
| 543 Simple bar_543 | L 2.5x2x0.375 | ACIER | 256.35 | 342.17 | 0.27 | 8 1.33G+1.42Q(expl.) +1.42WnY+ |
| | L 2.5x2.5x0.1 | | 255.46 | 255.46 | 0.51 | |
| | L 2.5x2.5x0.2 | | 258.14 | 258.14 | 0.37 | |
| **Code group : 4 truss double part** | | | | | | |
| 601 Simple bar_486 | DL 2x2x0.125 | ACIER | 20.94 | 16.07 | 0.40 | 9 1.33G+1.42Q(expl.) |
| | DL 2x2x0.187 | | 21.18 | 15.73 | 0.30 | |
| **Code group : 5 verticle side bars** | | | | | | |
| 543 Simple bar_543 | P 1.5 | ACIER | 314.73 | 314.73 | 0.36 | 8 1.33G+1.42Q(expl.) |
| | P 2 | | 251.07 | 251.07 | 0.22 | |

**Table 4. 1** Results from materials cross section optimization

The selected materials are galvanized steel round tubes for all the structure with the roof that will be angled iron to allow solar panels to sit upon. The round tubes are resistant to abrasion and corrosion, more resistant to the constraints of all kinds caused by external forces compared to other forms of tube section such as square tubes (Soni et al., 2005). They have low thermal conductivity compared to other metals.

| NOMINAL PIPE SIZE | OD | SCHEDULE DESIGNATIONS | | | WALL THICKNESS | | WEIGHT | | ID | |
|---|---|---|---|---|---|---|---|---|---|---|
| 1-1/2 | 1.900 | 5 | | 5S | 0.065 | 1.65 | 1.28 | 1.90 | 1.770 | 45.00 |
| 40 | 48.3 | 10 | | 10S | 0.109 | 2.77 | 2.09 | 3.11 | 1.682 | 42.76 |
| | | STD | 40 | 40S | 0.145 | 3.68 | 2.72 | 4.05 | 1.610 | 40.94 |
| | | XS | 80 | 80S | 0.200 | 5.08 | 3.63 | 5.41 | 1.500 | 38.14 |
| | | 160 | | | 0.281 | 7.14 | 4.86 | 7.25 | 1.338 | 34.02 |
| | | XX | | | 0.400 | 10.15 | 6.41 | 9.55 | 1.100 | 28.00 |
| 2 | 2.375 | 5 | | 5S | 0.065 | 1.65 | 1.61 | 2.39 | 2.245 | 57.00 |
| 50 | 60.3 | 10 | | 10S | 0.109 | 2.77 | 2.64 | 3.93 | 2.157 | 54.76 |
| | | STD | 40 | 40S | 0.154 | 3.91 | 3.66 | 5.44 | 2.067 | 52.48 |
| | | XS | 80 | 80S | 0.218 | 5.54 | 5.03 | 7.48 | 1.939 | 49.22 |
| | | 160 | | | 0.344 | 8.74 | 7.47 | 11.11 | 1.687 | 42.82 |
| | | XX | | | 0.436 | 11.07 | 9.04 | 13.44 | 1.503 | 38.16 |

**Figure 4. 2** (left) Portion of the Chart of round tubes available on the market as well as their characteristics (source: ((Tioga, 2013)); (Right) Portion of round tubes found on the market

#### 4.1.1.2 Analysis of charges on the structure

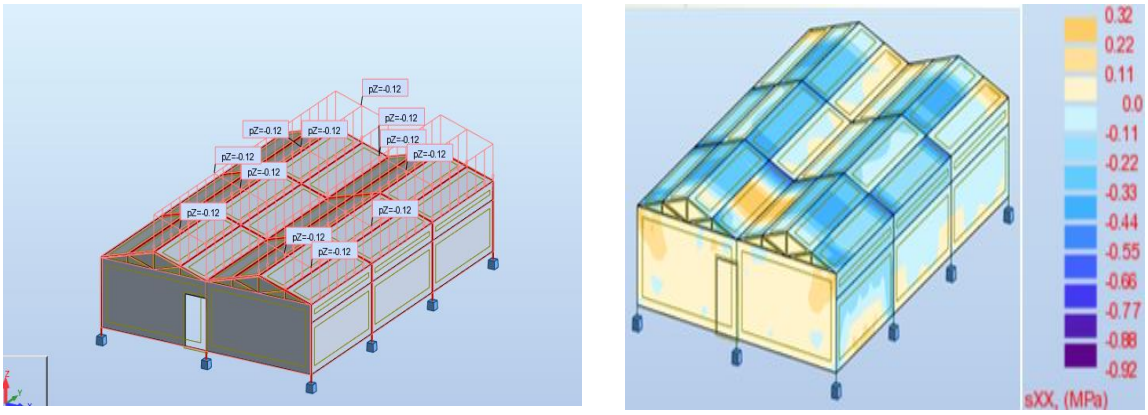


**Figure 4. 3** Results of charges simulation on the structure: loads from the top (left) and stress map (right)

The map of pressure stress from wind application, stress region varied from -0.12 kPa (dark purple) to 0.12 kPa (red). This shows that only faces in direct contact with the wind encounter pressure stress for a moment. Along the line, the stress is absorbed by the structure leading to stabilization. This is seen through the variation of colors from light blue to dark blue and purple.

### 4.1.2 Covering materials analysis

Materials for greenhouse covering were studied and the results are presented in figures above from figure 4.4 to 4.9 as well as table 4.2 and 4.3. Plane materials such as plastic Low Density Poly Ethylene (LDPE) films were compared to porous materials such as nets made from Jute bag and LDPE/PP.

**Table 4. 2** Light filtering capacity of some covering materials

| Light in intensity ($w/m^2$) | Solar panel cover | | Plastic black cover | | Fiber net cover | | Plastic Green cover | |
|---|---|---|---|---|---|---|---|---|
| | Light out ($w/m^2$) | Reduction | Light out ($w/m^2$) | Reduction | Light out ($w/m^2$) | Reduction | Light out ($w/m^2$) | Reduction |
| 100 | 1 | 99.00% | 1 | 99.00% | 8 | 92.00% | 53 | 47.00% |
| 150 | 1 | 99.33% | 1 | 99.33% | 9 | 94.00% | 88 | 41.33% |
| 200 | 1 | 99.50% | 1 | 99.50% | 19 | 90.50% | 119 | 40.50% |
| 250 | 1 | 99.60% | 1 | 99.60% | 20 | 92.00% | 145 | 42.00% |
| 300 | 1 | 99.67% | 1 | 99.67% | 22 | 92.67% | 178 | 40.67% |
| 400 | 1 | 99.75% | 1 | 99.75% | 30 | 92.50% | 225 | 43.75% |
| 500 | 1 | 99.80% | 1 | 99.80% | 36 | 92.80% | 280 | 44.00% |

**Table 4. 3** Light filtering capacity of some covering materials (continuation)

| Light in intensity ($w/m^2$) | Green Net cover | | Plastic blue cover | | Plastic white cover | |
|---|---|---|---|---|---|---|
| | Light out ($w/m^2$) | Reduction | Light out ($w/m^2$) | Reduction | Light out ($w/m^2$) | Reduction |
| 100 | 60 | 40.00% | 44 | 56.00% | 80 | 20.00% |
| 150 | 89 | 40.67% | 61 | 59.33% | 119 | 20.67% |
| 200 | 119 | 40.50% | 90 | 55.00% | 167 | 16.50% |
| 250 | 150 | 40.00% | 105 | 58.00% | 208 | 16.80% |
| 300 | 182 | 39.33% | 127 | 57.67% | 245 | 18.33% |
| 400 | 256 | 36.00% | 176 | 56.00% | 327 | 18.25% |
| 500 | 277 | 44.60% | 216 | 56.80% | 419 | 16.20% |

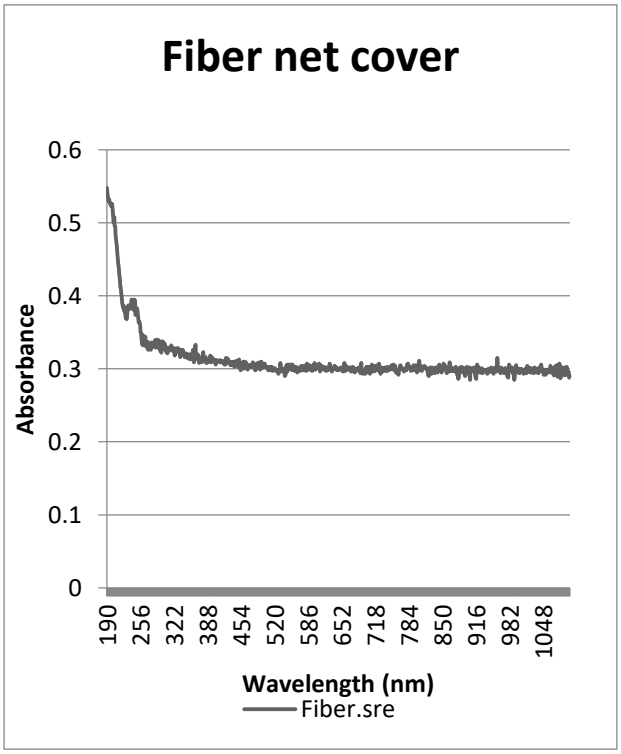


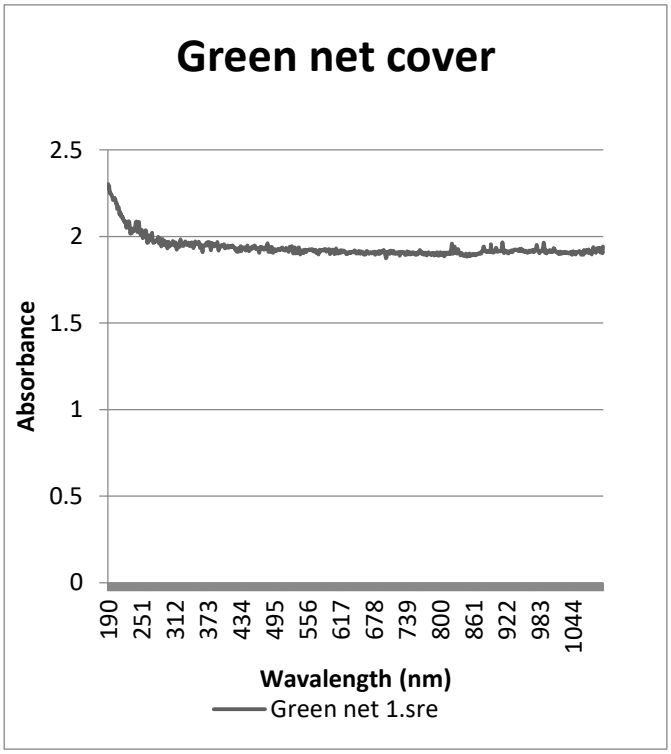


**Figure 4. 4** Spectrum of fiber net

**Figure 4. 5** Spectrum of green net

Clearly, Black plastic or Solar panels on top of the greenhouse roof do create a shadow effect since to do not allow any light passage as shown in table 4.1.

From the absorption spectra of figure 4.4 and 4.5, it could be seen that fiber net cover and green net cover do not show clear absorption peaks even though little range of absorption was appearing between 190 nm and 400 nm. The rest of information is not easy to explore. Then, referring to table 4.1 and 4.2, fiber net could reduce incident light intensity between 90.50% and

94.00%. From table 4.2, when exposed to light intensity between 100 and 500 w/m$^2$, green net could reduce the incident light intensity up to 44.60%. Fiber net is firm, hardly stretchable and small net size between 1-4 mm, made from jute bag. This could explain this light filtering capability compared to green net which is a stretchable plastic net with pores from 4-6 mm.

Compared to nets, planes transparent plastics presented a relatively lower light reduction capability except black plastic which was not transparent. While the black plastic absorption spectrum was flat with artifacts showing no clear absorption zone, the blue colored plastic cover showed three picks at 332 nm, 575 nm and 690 nm, the white transparent plastic absorbed from infrared to visible light region with no specific pick and the green plastic spectrum displayed picks at around 220 nm, a large absorption between 265 and 545 nm with another pick at 620 nm. Besides, from table 4.1 and 4.2, green plastic could reduce light intensity from 40.50% to 47.00%, blue plastic could reduce from 55.00% to 59.33% and white plastic could reduce from 16.50% to 20.67%.

Using white plastic could be the best option since it had a spectrum absorbing within a large ranger while reducing a certain amount of light intensity. Yet, the resistance of the available white LDPE plastic to outside weather was proven to be bad (Baneshi et al., 2020; Kittas & Baille, 1998). Fiber net from jute bag resisted most among these materials. Besides, the radiation passing through the fiber net in a very sunny area is also important for crops cultivation (Ureña-sánchez et al., 2012). Therefore, Jute bag fibers were used as a greenhouse covering material throughout this study (Baneshi et al., 2020; Kittas & Baille, 1998).

Figure 4.11 and 4.12 present two covering materials used: Green net cover and fiber net cover respectively. The green net cover was allowing too much solar irradiation and was melting at the point of contact between net and iron frames. Hence, Jute bag was the best alternative

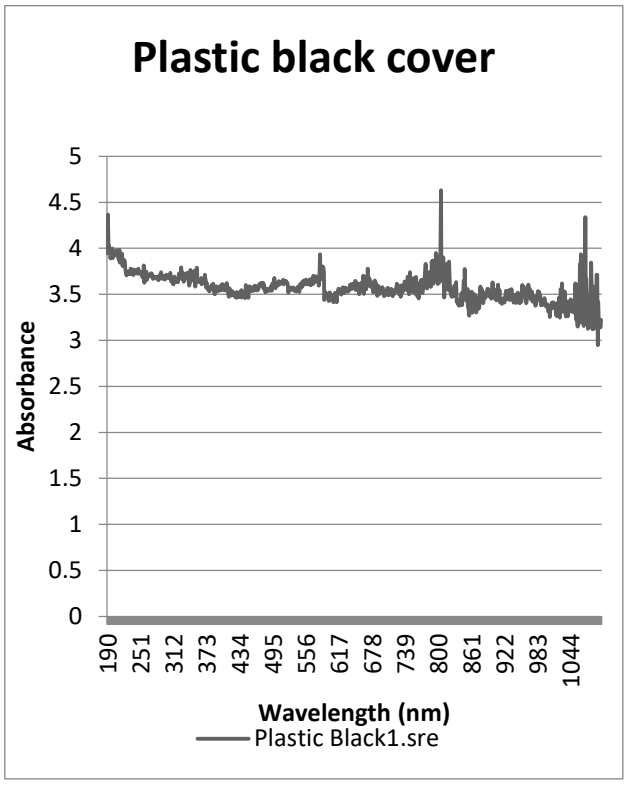


**Figure 4. 6** Spectrum of black plastic

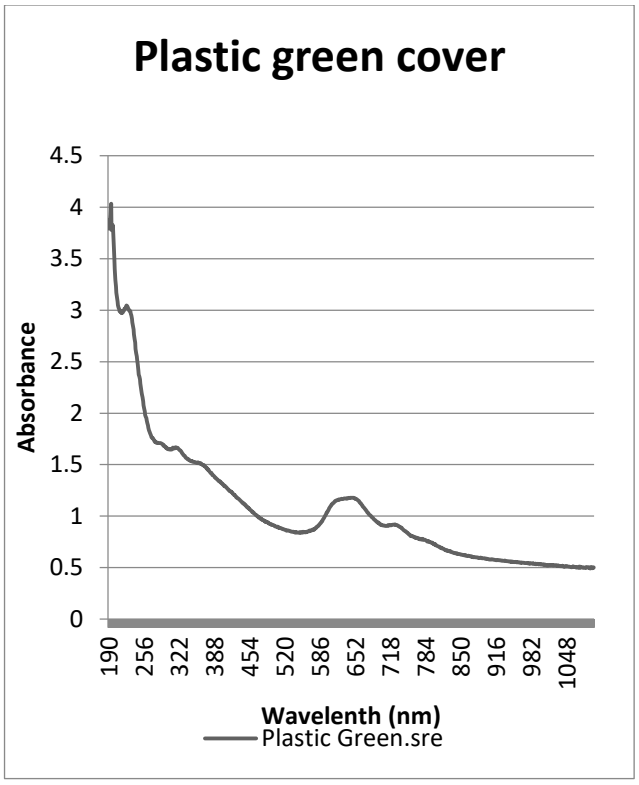


**Figure 4. 7** Spectrum of green plastic

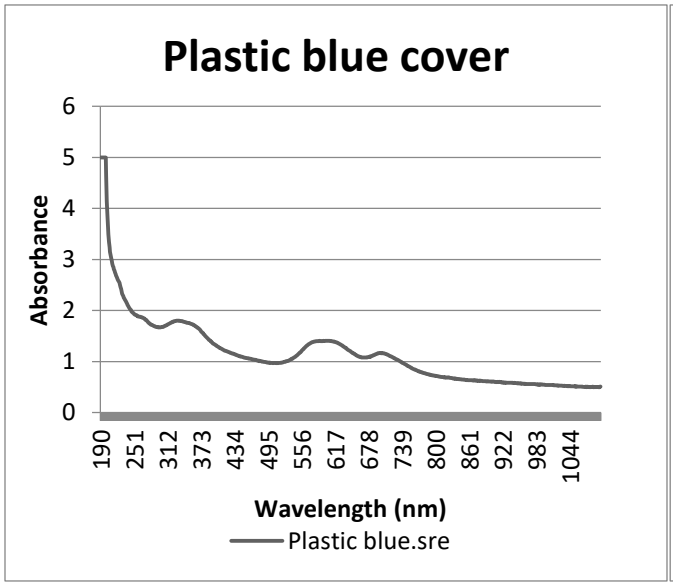


**Figure 4. 8** Spectrum of blue plastic

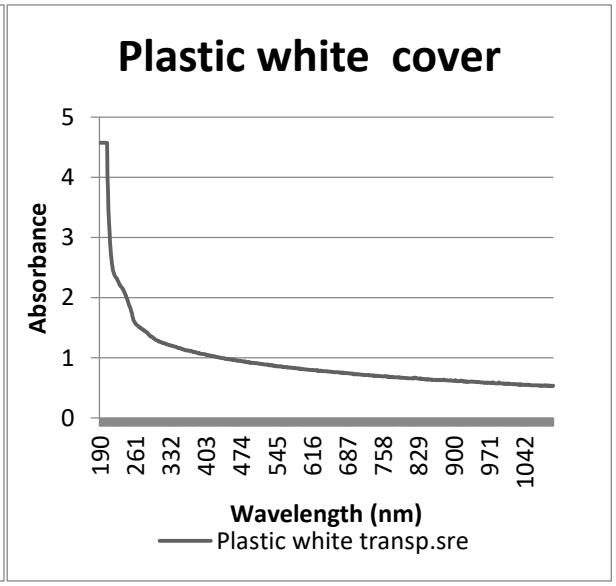


**Figure 4. 9** Spectrum of white plastic

**Figure 4. 10** Dji Greenhouse with green net cover

**Figure 4. 11** Dji Greenhouse with fiber net cover (jute bag cover)

**Figure 4. 12** Shading effect inside Dji Greenhouse covered by Fiber net

**Figure 4. 13** Shading effect inside CN Greenhouse covered by Fiber net

## 4.2 Development of greenhouse cooling technology

### 4.2.1 Overall analysis

Different cellulosic cooling pads locally made were characterized under two different fan speed 5.110 m/s and 5.522 m/s keeping the pad thickness constant (Ɛ=5 cm) throughout the experiment. Average values of the various thermodynamic data were used for the purpose of a comparative analysis.

In the Table 4.4 and table 4.5 are presented the various performances of the pads exposed to a frontal velocity of 5.110 m/s and 5.522 m/s respectively. Compared to the commercial Celdek pad used in conventional evaporative coolers, wood wool pad from the leaves stipulates of Hyphaene thebaica had saturation efficiency closer to that of Celdek and performed much better than the other local plant made pads. Indeed, with saturation efficiencies varying from 16.50% (Kuriya pad - *Ceiba pentandra* fibers) to 69.88% (wood wool pad) at lower fan speed and from 22.73% (Gamba pad - *Antropogon gayanus*) to 78.80% (wood wool pad) at higher fan speed, local materials' pad challenged the commercial Celdek pad which could reach as saturation efficiency of 70.02% at lower and 79.80% at higher frontal velocity. This comparison is better seen through the histograms presented in the figure 4.14. It is also observed that saturation efficiency increased with increasing frontal velocity as mentioned by Laknizi et al. (2018).

### 4.2.2 Effect of pad packing materials on outlet velocity

A cool wind is supposed to come fast enough to be better appreciated or to cool down an enclosure such as a room. Because all the local pads were made through packing, filling and rearrangement to attain a certain volume (in this case, L x H x Ɛ = 96.35 $cm^3$), this situation affects the velocity at which the outlet comfortable air should come out and could probably affect the efficiency and other thermodynamic properties (see table 4.4 and 4.5). The outlet winds ranged from 0.1 (over packed pads) to 0.657 m/s (Kaba pad – leaves of *Hyphaene thebaica*) and from 0.333 to 0.825 m/s (wood wool pad). Wood wool is in a coil form and arrangement, Kaba is straight while the rest are randomly packed (see figure 2.4). While the water is running, all disordered and unstable packing becomes more condensed to the extend to make obstruction to air flow. This situation reduces the outlet and could affect the efficiency and other thermodynamic parameters. In fact, the cooling efficiency of the cooling pad was reported to be affected by the flute size, the porosity and the water absorption capability of the pad; some physical characteristics similar to packing density of local pads (Barzegar et al., 2012).

**Table 4. 4** Thermal characteristics of various cooling pad at a lower fan speed (Djibrilla et al., 2021b)

| Pad type | Scientific names | Frontal Velocity v (m/s) | Mass flow rate ma (kg/s) | Average inlet dry bulb temperature $T_{db1}$ ($^oC$) | Average wet bulb temperature $T_{wb}$ ($^oC$) | Average outlet dry bulb temperature $T_{db2}$ ($^oC$) | Average saturation efficiency (%) | Average RH of inlet wind | Average RH of outlet wind | Outlet velocity $v_{out}$, m/s | Velocity decrease, %decr |
|---|---|---|---|---|---|---|---|---|---|---|---|
| Celdek pad | 'Trade name' | 5.110 | 0.0113 | 34.82 | 16.42 | 21.92 | 70.02% | 10.00% | 38.00% | 1.166 | 77.18% |
| Baata pad | *Ctenium elegans* | 5.110 | 0.0113 | 35.85 | 17.17 | 31.83 | 21.69% | 10.50% | 21.69% | 0.100 | 98.04% |
| Gamba pad | *Antropogon gayanus* | 5.110 | 0.0113 | 36.32 | 17.00 | 32.58 | 19.37% | 10.17% | 12.33% | 0.100 | 98.04% |
| Kaba pad | *Hyphaene thebaica* (leaves) | 5.110 | 0.0113 | 34.35 | 16.08 | 25.75 | 47.19% | 10.00% | 26.67% | 0.657 | 87.14% |
| Kaikai pad | *Pennisetum glaucum* (husk) | 5.110 | 0.0113 | 35.30 | 16.33 | 30.17 | 27.10% | 10.00% | 20.67% | 0.100 | 98.04% |
| Kuriya pad | *Ceiba pentandra* (fibers) | 5.110 | 0.0113 | 34.22 | 15.83 | 31.17 | 16.50% | 10.00% | 12.33% | 0.100 | 98.04% |
| Wood shavings pad | - | 5.110 | 0.0113 | 35.38 | 17.67 | 27.42 | 45.03% | 10.00% | 22.50% | 0.335 | 93.44% |
| Wood wool pad | *Hyphaene thebaica* (leaves stipulates) | 5.110 | 0.0113 | 35.65 | 16.92 | 22.58 | 69.88% | 10.00% | 37.17% | 0.448 | 91.23% |

**Table 4. 5** Thermal characteristics of various cooling pad at a higher fan speed (Djibrilla et al., 2021b)

| **Pad type** | **Scientific names** | **Frontal Velocity v (m/s)** | **Mass flow rate ma (kg/s)** | **Average inlet dry bulb temperature $T_{db1}$ (°C)** | **Average wet bulb temperature $T_{wb}$ (°C)** | **Average outlet dry bulb temperature $T_{db2}$ (°C)** | **Average saturation efficiency (%)** | **Average RH of inlet wind** | **Average RH of outlet wind** | **Outlet velocity $v_{out}$, m/s** | **Velocity decrease, %decr** |
|---|---|---|---|---|---|---|---|---|---|---|---|
| Celdek pad | 'Trade name' | 5.522 | 0.0122 | 34.5833 | 17.4167 | 20.9167 | 79.80% | 13.50% | 50.00% | 1.166 | 78.88% |
| Baata pad | *Ctenium elegans* | 5.522 | 0.0122 | 32.2833 | 14.7500 | 26.7500 | 31.54% | 10.33% | 15.00% | 0.659 | 88.07% |
| Gamba pad | *Antropogon gayanus* | 5.522 | 0.0122 | 35.2500 | 15.4167 | 30.7500 | 22.73% | 10.33% | 12.50% | 0.659 | 88.07% |
| Kaba pad | *Hyphaene thebaica* (leaves) | 5.522 | 0.0122 | 34.7500 | 16.5000 | 26.1667 | 47.01% | 10.00% | 24.17% | 0.803 | 85.46% |
| Kaikai pad | *Pennisetum glaucum* (husk) | 5.522 | 0.0122 | 36.6833 | 17.0000 | 30.8333 | 29.71% | 10.67% | 19.67% | 0.335 | 93.93% |
| Kuriya pad | *Ceiba pentandra* (fibers) | 5.522 | 0.0122 | 34.5500 | 18.0000 | 30.7500 | 23.18% | 10.00% | 25.17% | 0.333 | 93.97% |
| Wood shavings pad | - | 5.522 | 0.0122 | 33.6500 | 18.3333 | 21.8333 | 75.88% | 14.33% | 35.67% | 0.680 | 87.69% |
| Wood wool pad | *Hyphaene thebaica* (leaves stipulates) | 5.522 | 0.0122 | 35.6667 | 17.8333 | 21.8333 | 78.80% | 13.83% | 33.00% | 0.825 | 85.06% |

### 4.2.3 Effect of frontal velocity on saturation efficiency, cooling capacity and heat transfer coefficient

Figure 4.14, 4.15 and 4.16 show the saturation efficiency, cooling capacity and heat transfer coefficient of various pads. In fact, all these parameters increase with increasing frontal velocity. This is because these parameters are temperature driven which is an intrinsic property, not proportional or affected by the size of the material. From these histograms, it can be observed that at lower frontal velocity, Celdek, wood wool, Kaba and wood shavings pads had the four best efficiencies (70.02, 69.88, 47.19 and 45.03% respectively), cooling capacities q pad (0.1477, 0.1496, 0.0985 and 0.0912 kW respectively) and heat transfer coefficient $h_H$ (4.3400, 4.3150 and 1.6794 kW/m$^{2o}$C respectively). However, for higher frontal velocity, the same order in terms of performance is observed with, in this case, wood shavings pad having higher parameters. This sudden performance of wood shavings can be allocated to the fact that at a lower velocity, wind cannot penetrate the packing easily to be detected well by temperature and humidity sensors. Hence, more force is needed to penetrate this pad wall (see figure 4.20). Also, according to Barzegar et al. (2012) and Laknizi, et al. (2018), more time is needed for materials to absorb enough water allowing more heat and mass transfer (Barzegar et al., 2012; Laknizi et al., 2018).

### 4.2.4 Effect of frontal velocity on mass flow rate and permeability coefficient

At the same pad size and mass flow rate, the pads from Celdek, wood wool, Kaba, wood shavings and Kaikai (*Pennisetum glaucum*) transferred more mass of water vapour than the rest of local materials (see figure 4.17). The higher the frontal velocity, the higher the mass transfer coefficient $h_M$ except some anomalies observed in Gamba pad, Kaba and wood shavings. Besides, pad from *Ceiba pentandra* fibers (Kuriya pad) and *Antropogon gayanus* (Gamba pad) are the ones not performing well due to the impermeable shell protecting the various materials. These shells reduce the mass and heat transfer rate and affecting the other thermodynamic properties.

The permeability coefficient k pad is presented on figure 4.19. This parameter depends on the combination of the fluid and porous materials used. The higher this parameter is, the higher the rate of flow of fluid flow through a material. In this figure, it can be observed that all the materials with lowest performance (saturation efficiency and cooling capacity) had the highest permeability coefficient which is the cases of Baata, Gamba and Kuriya pads in this order. In fact, this is because, the materials do not allow a better moist air-cellulose mass and heat exchange.

### 4.2.5 Effect of relative humidity on pad performance

Figure 4.18 and 4.20 show the increase in relative humidity and the pressure drop across the pad. Materials with higher efficiencies, that exchanged more heat and which allowed better mass transfer create a higher increase in relative humidity and more pressure drop. We could observe the high stability of Celdek pad which has stable characteristics irrespective of the wind velocity contrary to Kuriya and wood wool. However, Materials presented a higher increase in relative humidity at a lower frontal velocity. Among the local material pads, wood wool pad could create

an increase of 271.67% at lower fan speed against 140.57% at higher speed whereas wood shavings could create a 149.40% increase. Here again, highly packed materials such as wood shavings perform well at higher speed whereas the opposite is observed in the case of well-performing pads such as wood wool and Celdek. Of course, the other thermodynamic parameters limit the extent to which a pad can increase the relative humidity.

From figures 4.18 and 4.19 we can see materials with lower permeability coefficient allow more time for water absorption and, hence, can create a higher increase in relative humidity.

The coefficients of performance of various pads are presented in the figure 4.21. The COP at lower frontal velocity is observed to be higher (range of 1.9064-6.1570 for lower and 1.7908-9.0074 for higher frontal velocity) than the one at higher COP and the same trend is observed with the relative humidity (figure 4.18). This shows that relative humidity affects the performance of a system as also observed by (Laknizi et al., 2018).

### 4.2.6 Cost effectiveness analysis

The financial analysis based on cost to efficiency ratio using CFA (XOF) and USD (United States Dollars-$) was presented in figures 4.22 and 4.23. The lower the ratio the better and the most recommended the pad material is in order to optimize cost and efficiency especially when thermal comfort is becoming a luxury. From figures 4.22 and 4.23, Celdek pad which is the most effective happen to be less recommended as compare to wood wool pad. This is because Celdek material cost is high since it is imported from overseas whereas wood wool is local, much cheaper and performs almost as well as Celdek pad.

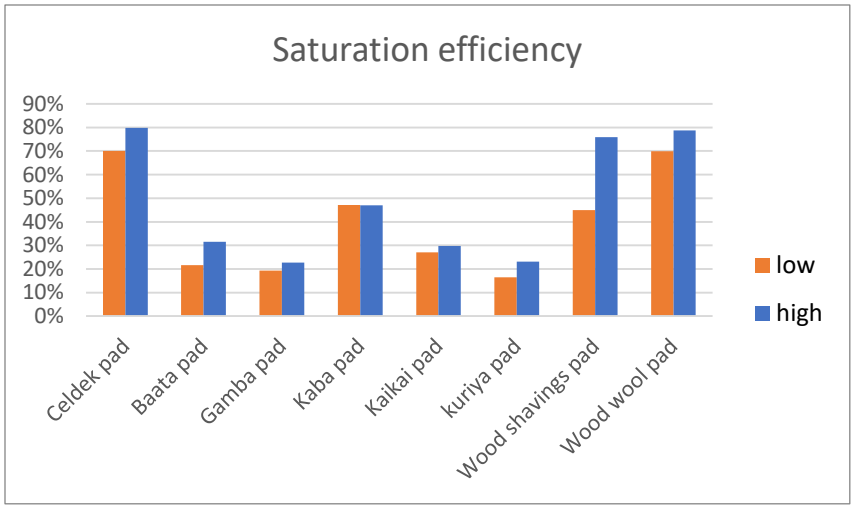


**Figure 4. 14** Saturation efficiency of various pads

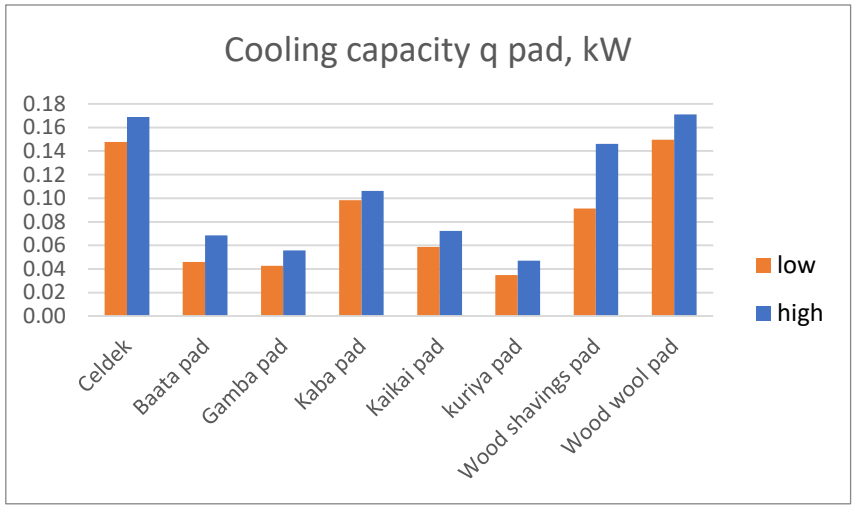


**Figure 4. 15** Cooling capacity of various pads

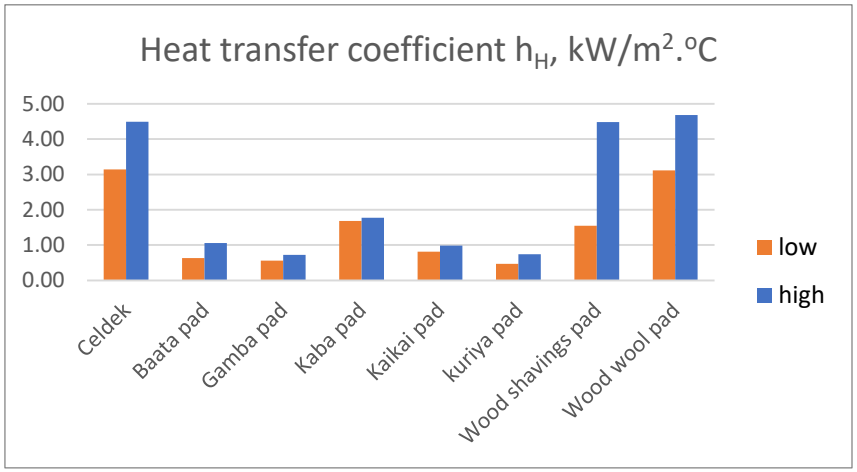


**Figure 4. 16** Heat transfer coefficient $h_H$, kW/m$^2$.$^o$C Cooling

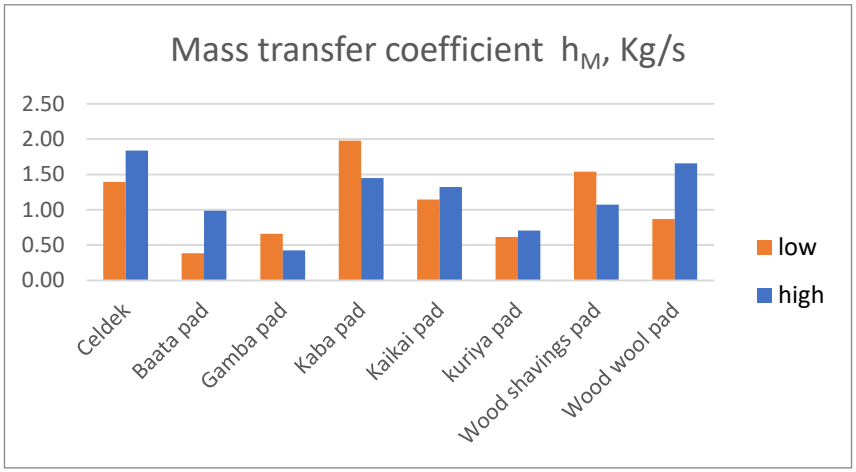


**Figure 4. 17** Mass transfer coefficient $h_M$, kg/s

Low= low frontal velocity; High= high frontal velocity

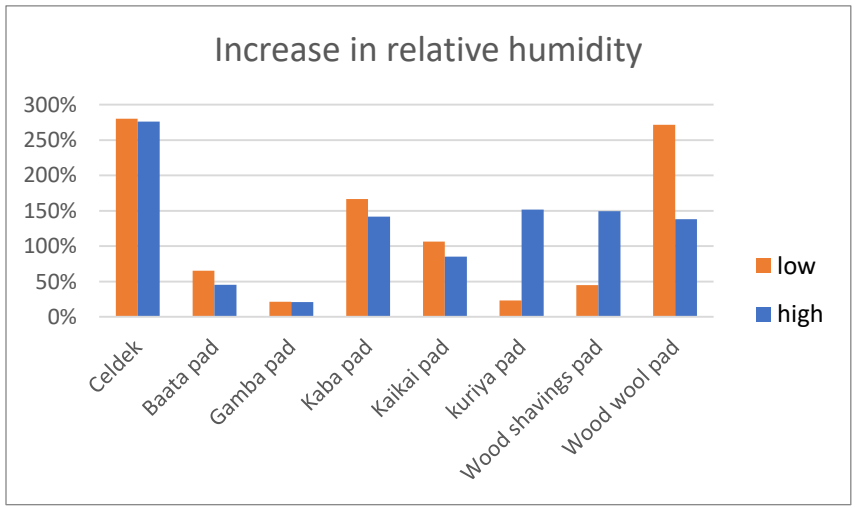


**Figure 4. 19** Permeability coefficient

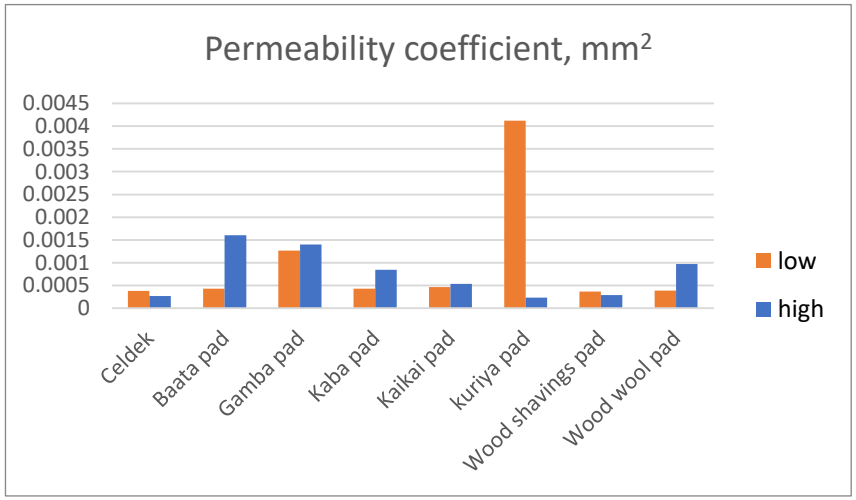


**Figure 4. 18** Increase in relative humidity

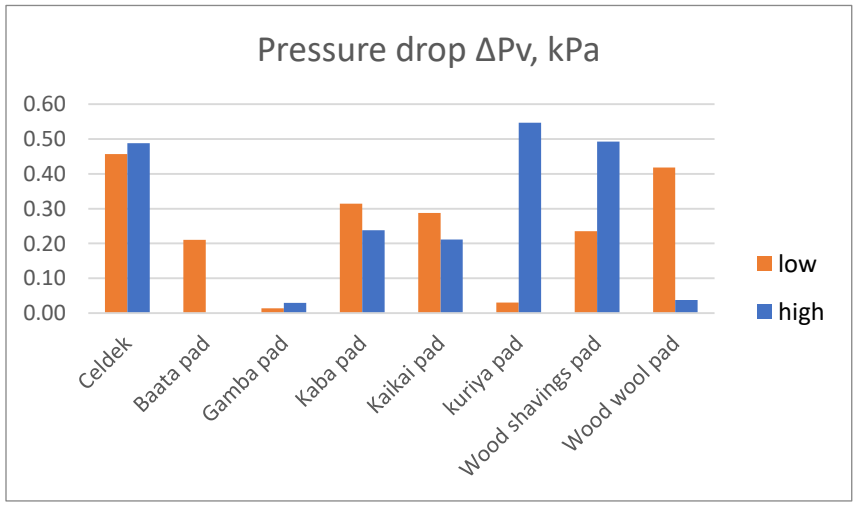


**Figure 4. 20** Pressure drop

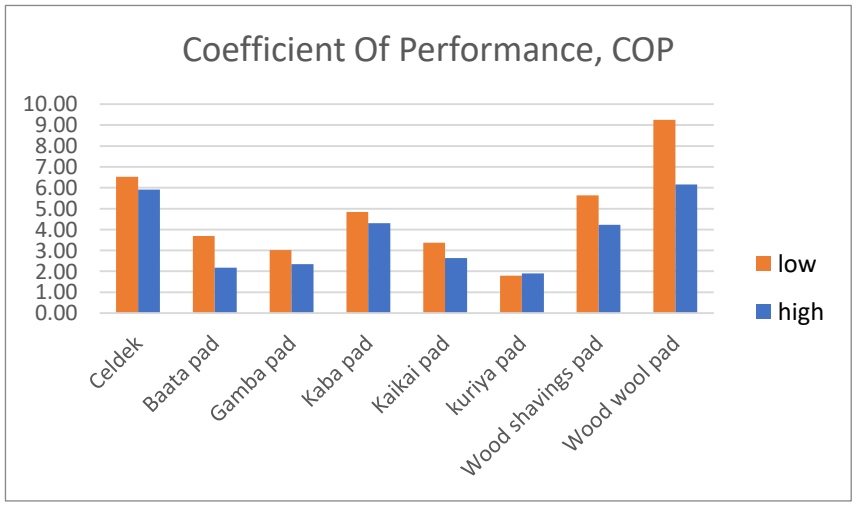


**Figure 4. 21** Coefficient of performance

Low= low frontal velocity; High= high frontal velocity

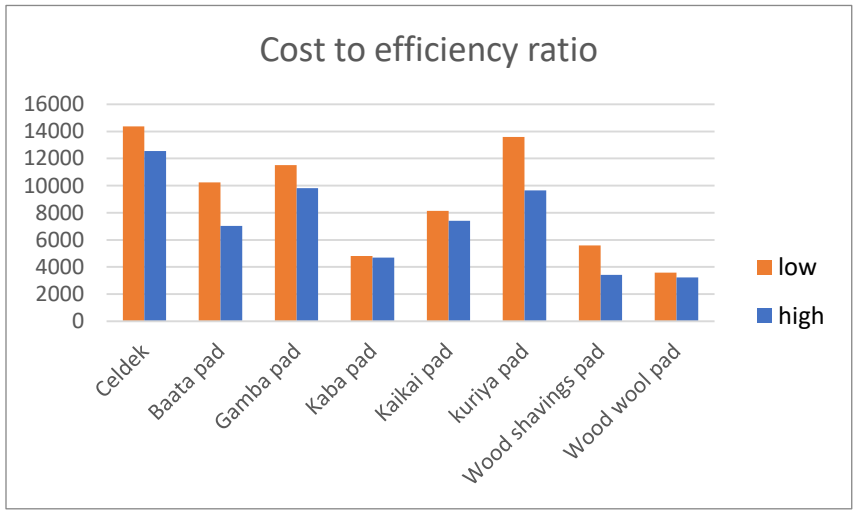


**Figure 4. 22** Cost to efficiency ratio CER based on CFA (XOF)

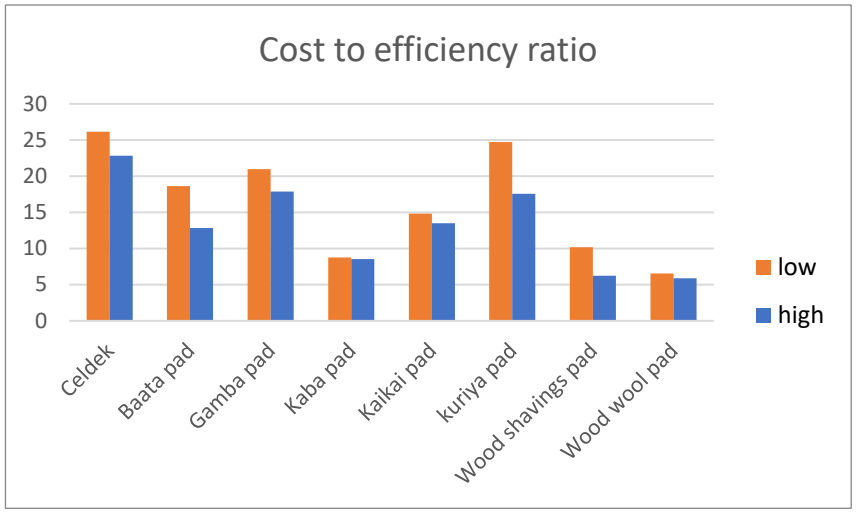


**Figure 4. 23** Cost to efficiency ratio CER based on USD

Low= low frontal velocity; High= high frontal velocity

### 4.2.7 Analysis between Celdek and Wood wool at higher frontal velocity

Table 4.6 and 4.7 present some physical and thermal properties of Celdek pad and wood wool pad *(Hyphaene thebaica*). On average data basis, Celdek pad and wood wool pad have similar performances. Wood wool could provide an outlet temperature of as low as 20.0$^{o}$C against 20.5$^{o}$C for Celdek even though the latter had a higher saturation efficiency (79.80%) and can provide a more humid air (50% Relative humidity). This higher relative humidity implies a higher water evaporation rate of 6581.736 L/h for Celdek pad. However, based on maximum values observed during the experiment, wood wool pad presented the highest saturation efficiency of 92.86% (see figure 4.27), highest cooling capacity of 0.1867 kW (figure 4.28), highest heat transfer coefficient of 7.3497 kW/m$^{2}$.$^{o}$C (figure 4.32), highest coefficient of performance of 9.9775 (figure 4.33) and the best (lowest) cost to efficiency ratio of 6.68076 (figure 4.36). Based on ASHRAE, a comfort zone should have a relative humidity between 19.8% and 79.5% (ASHRAE, 2013). In this experiment, wood wool could provide an outlet air with 33.33% relative humidity against 50% for Celdek on average basis. The mass transfer coefficient and the pressure drop across Celdek pad happened to be higher than that of wood wool pad. In fact, these two properties mostly are influenced by the size and the structure/ arrangement of the pad. As shown in table 4.6, Celdek pad is more organized with optimized size to perform well. On the other hand, wood wool pad is a filling of wood wool inside a certain structure. Individual wood wool fibers are packed in disordered and uncontrolled manner. That is what explains the non-smoothness of wood wool pad plots in the figure 4.30 (mass transfer coefficient graph) and figure 4.31 (water evaporation rate graph). However, less mass transfer could be an advantage because protecting against dirt, dust and parasites infiltration.

**Table 4. 6** Physical characteristics of Celdek and wood wool pad

| **Pad type** | **Scientific names** | **Frontal Velocity v (m/s)** | **Mass flow rate ma (kg/s)** | **Outlet velocity $v_{out}$, m/s** | **Flute thickness (mm)** | **Structure** | **Arrangement** | **Pad size, $cm^3$** | **Material's Weight (g)** | **Pad/packing density ($g/cm^3$)** |
|---|---|---|---|---|---|---|---|---|---|---|
| Celdek pad | 'Trade name' | 5.522 | 0.0122 | 1.166 | 1 | 1 cm between crest | order: 1 cm between crest | 9.635 | 351 | 36.4297 |
| Wood wool pad | *Hyphaene thebaica* (leaves stipulate) | 5.522 | 0.0122 | 0.825 | 1 | Coil | disorder: packing to filling | 9.635 | 180 | 18.6819 |

**Table 4. 7** Average temperature, efficiency and evaporation rate of Celdek and wood wool pad

| **Pad type** | **Average inlet dry bulb temperature $T_{db1}$ ($^oC$)** | **Average wet bulb temperature $T_{wb}$ ($^oC$)** | **Average outlet dry bulb temperature $T_{db2}$ ($^oC$)** | **Minimum outlet dry bulb temperature $T_{db2\ min}$ ($^oC$)** | **Average saturation efficiency (%)** | **Average RH of inlet wind** | **Average RH of outlet wind** | **Average water evaporation rate (L/h)** |
|---|---|---|---|---|---|---|---|---|
| Celdek pad | 34.58 | 17.42 | 20.92 | 20.50 | 79.80% | 13.50% | 50.00% | 6581.736 |
| Wood wool pad | 35.67 | 17.83 | 21.83 | 20.00 | 78.80% | 13.83% | 33.33% | 1984.414 |

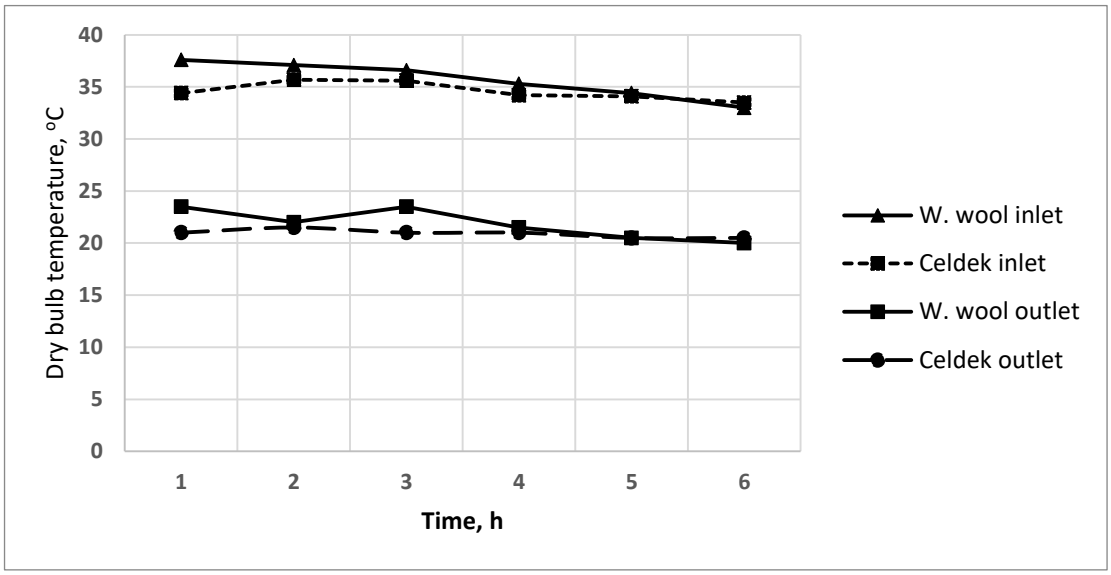


**Figure 4. 24** Dry bulb temperature at inlet and outlet for Celdek and wood wool pad at high frontal velocity

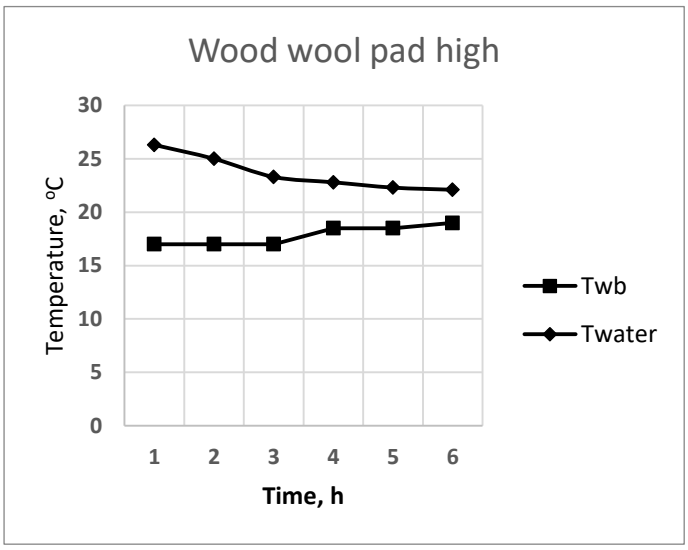


**Figure 4. 25** Wet bulb ($T_{wb}$) vs water temperature ($T_{water}$) for wood wool pad at high frontal velocity

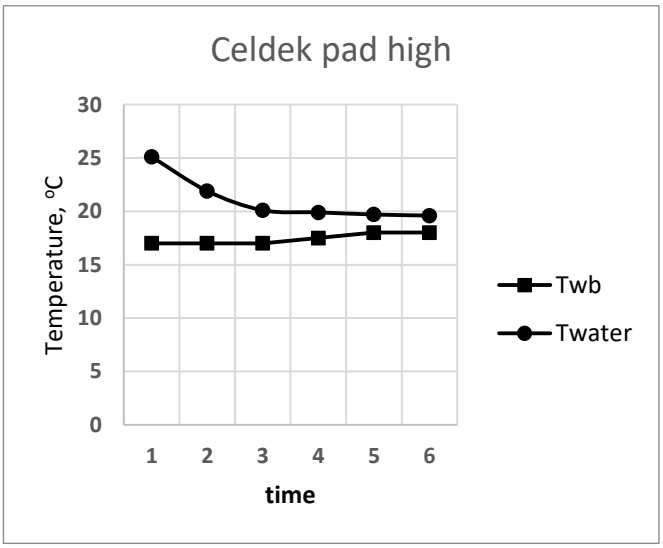


**Figure 4. 26** Wet bulb ($T_{wb}$) vs water temperature ($T_{water}$) for Celdek pad at high frontal velocity

Exposed to similar initial conditions of dry bulb temperature as shown on figure 4.24, Celdek pad and wood wool pad (*Hyphaene thebaica*) gave out similar outlet temperature with Celdek giving 20.92$^{o}$C on average against 21.83$^{o}$C for wood wool. Detailed experimental data are given from the figure 4.25 to figure 4.33 concerning saturation efficiency, cooling capacity, pressure drop, mass and heat transfer coefficients, water evaporation rate and coefficient of performance. Figure 4.25 and 4.26 present a plot of wet bulb and running water temperature with time at different frontal velocity, we observe that the water temperature is getting close to the wet bulb temperature in an asymptotic manner. At constant frontal velocity, with increasing time, the pads

become more wet and more efficient as shown in the figure 4.29. More mass is transferred (figure 4.30) creating more water to evaporate (figure 4.31). This drops the pressure drop across the pad and allows more heat exchange (figure 4.32) leading to a lower outlet temperature for better comfort. However, a variation of cooling capacity is observed in a form of a decreasing sinusoidal curve as showed in the figure 4.28 causing the pads to perform less with time (figure 4.33). This latter phenomenon could be assigned to the fact that with time, the pads become saturated with dirt since the water was directly recycled. Indeed, the water used was becoming cooler but dirtier since not cleaned throughout the process.

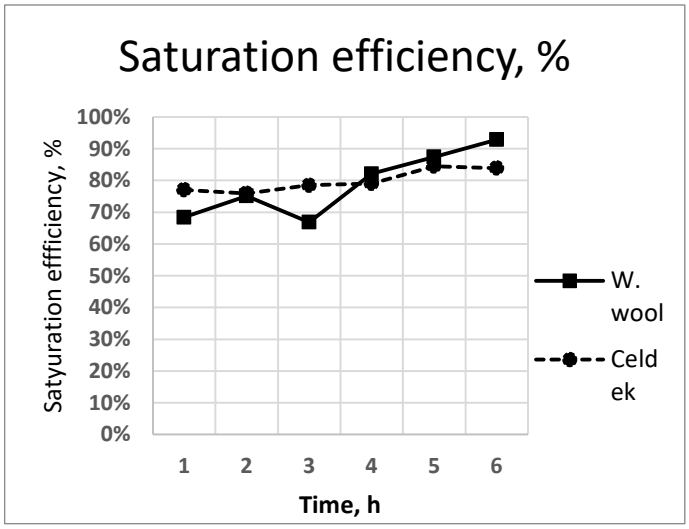


**Figure 4. 27** Saturation efficiency of Wood wool and Celdek pad (Djibrilla et al., 2021a)

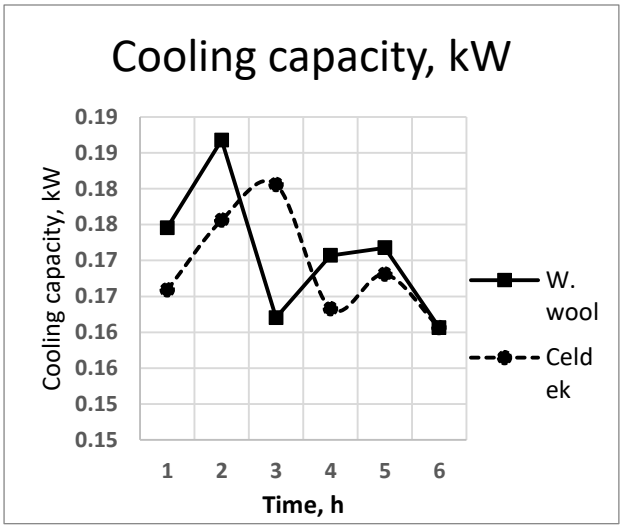


**Figure 4. 28** Cooling capacity of Wood wool and Celdek pad

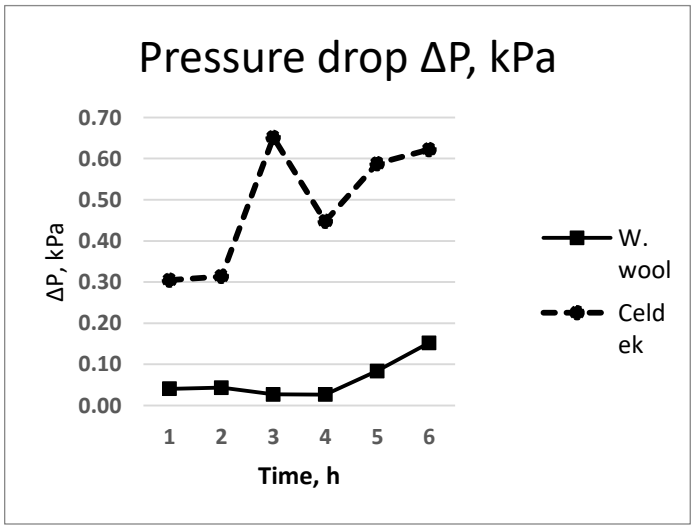


**Figure 4. 29** Pressure drop of Wood wool and Celdek pad

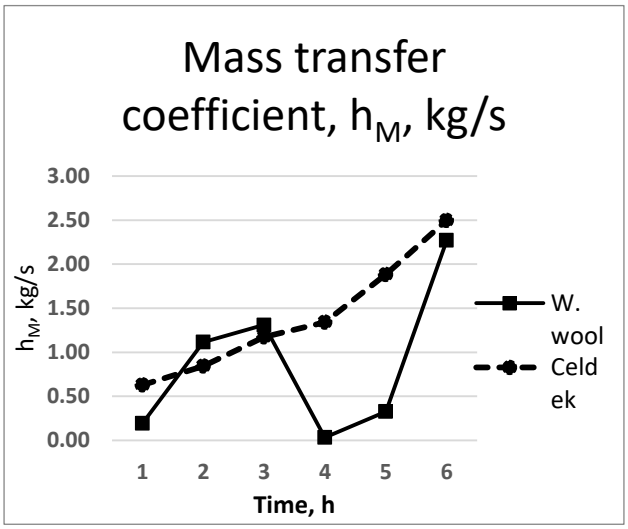


**Figure 4. 30** Mass transfer coefficient of Wood wool and Celdek pad

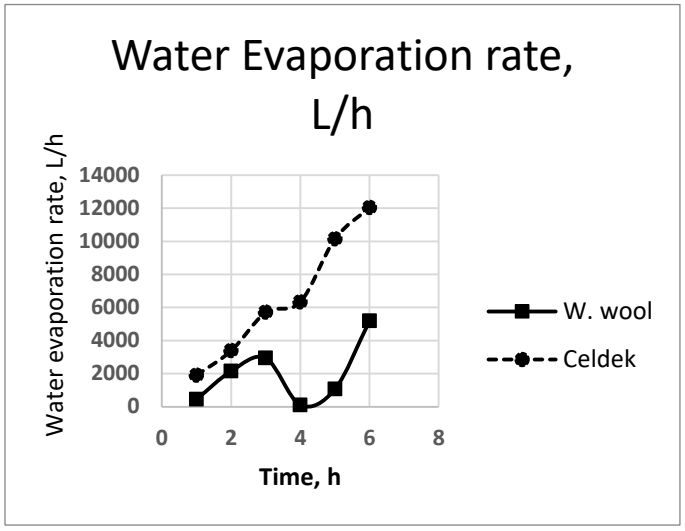


**Figure 4. 31** water evaporation rate of Wood wool and Celdek pad

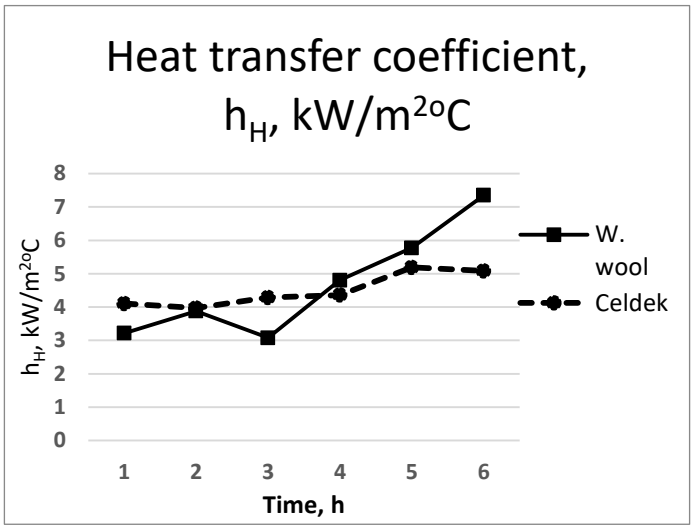


**Figure 4. 32** Heat transfer coefficient of Wood wool and Celdek pad

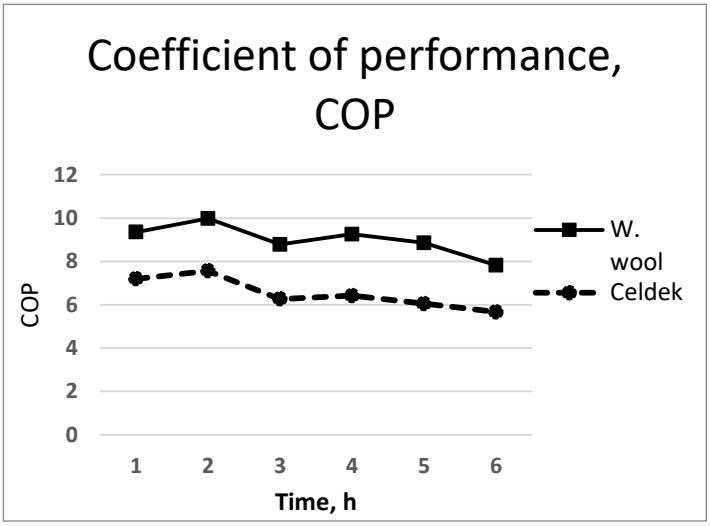


**Figure 4. 33** Coefficient of performance of Wood wool and Celdek pad (Djibrilla et al., 2021a)

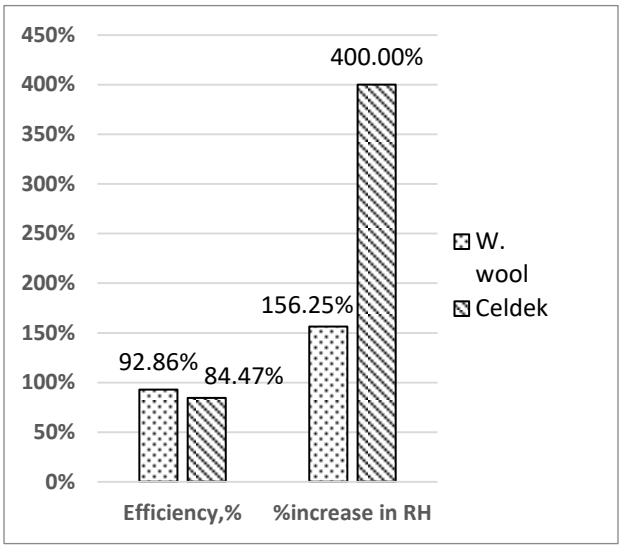


**Figure 4. 34** Maximum efficiency and relative humidity increase of Wood wool and Celdek pad

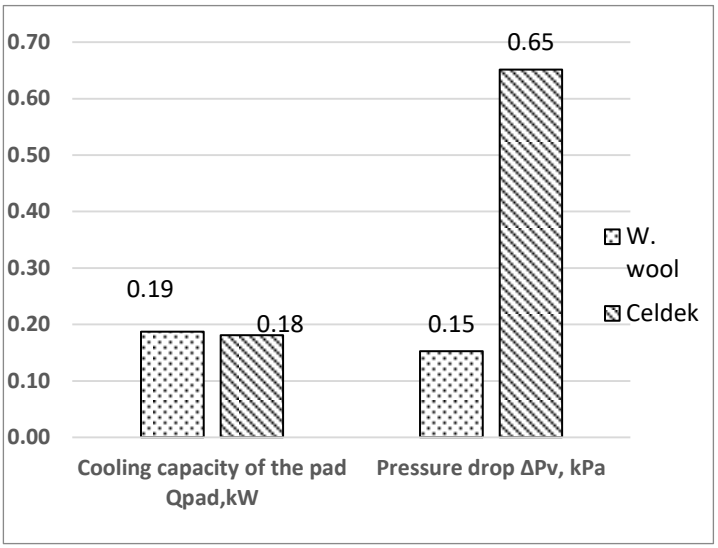


**Figure 4. 35** Maximum Cooling capacity and pressure drop of Wood wool and Celdek pad

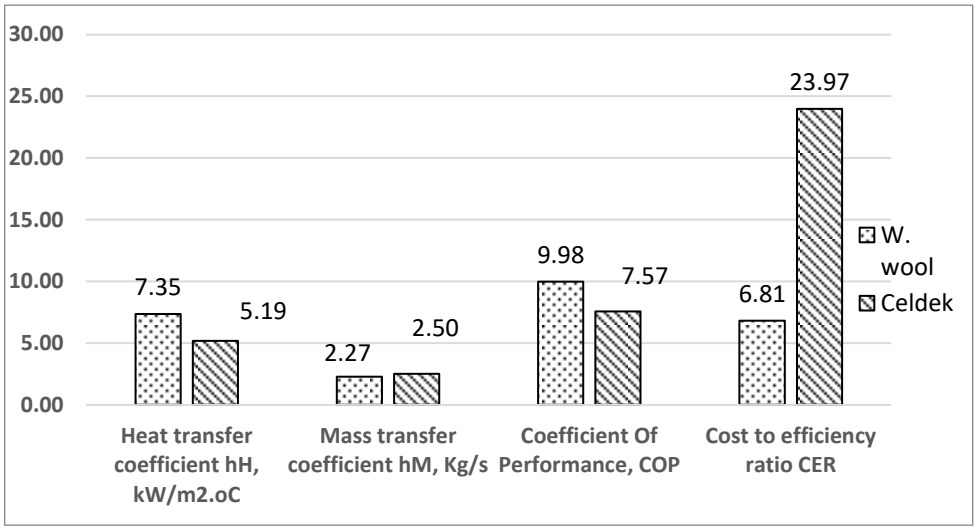


**Figure 4. 36** Maximum values of heat and mass transfer coefficients, coefficient of performance and cost to efficiency of Wood wool and Celdek pad

## 4.3 Open field crop cultivation under ambient conditions

### 4.3.1 Results of physico-chemical analysis of the cultivation soil

**Table 4. 8** Physical parameters of cultivation soil

| **Particles** | **Clay** | **Silt** | | **Sand** | | |
|---|---|---|---|---|---|---|
| Percentage (%) | 0.80 | Fine | Coarse | Fine | Medium | Coarse |
| | | 3.84 | 6.87 | 43.43 | 38.74 | 6.32 |

The granulometric analysis of the cultivation soil showed that the ground is sandy because the percentage of sand is greater than 70% according to the soil texture triangle (Ministère de l'Agriculture et de l'Elévage, 2019). This soil has low clay content (0.80%), 10.71% silt and most of it consists of sands with 88.49%. This sandy soil is very permeable to water and air from the because of its textural porosity resulting in good aeration, good soil drainage and good root development (Ministère de l'Agriculture et de l'Elévage, 2019). Thus, this soil is favorable for growing lettuce, potato, pepper, tomato and zucchini, from the grain size point of view since these plants grow easily on sandy soils (Ministère de l'Agriculture et de l'Elévage, 2019; Montemurro et al., 2013).
The results of the chemical analysis of the cultivation soil are contained in Table 4.9.

**Table 4. 9** Chemical parameters of cultivation soil

| **Parameters** | **pH** | **EC** | **Pt** | **Pas** | **Carbon** | **OM** | **Nitrogen** |
|---|---|---|---|---|---|---|---|
| Unit | 1/2.5 | µS $cm^{-1}$ | ppm | | % | | |
| Value | 6.35 | 183 | 11.24 | 6.27 | 0.20 | 0.34 | 0.02 |

| **Parameters** | **C/N** | **$Ca^{2+}$** | **$Mg^{2+}$** | **$Na^{+}$** | **$K^{+}$** | **S** | **CEC** | **S/T** |
|---|---|---|---|---|---|---|---|---|
| Unit | mass equivalent/100g | | | | | | | |
| Value | 9.50 | 5.32 | 3.27 | 0.08 | 0.11 | 8.78 | 10.25 | 0.86 |

EC: Electronic conductivity, Pt: Total phosphorus, Pas: Available phosphorus, OM: Organic matter, C/N: Carbon nitrogen ratio, S: Value of exchangeable bases, CEC: Cation exchange capacity, S/T: Saturation rate of the adsorbent complex.

These results characterize the salinity of this soil. Salinization is a major factor contributing to the loss of productivity of cultivation soils. The chemical analysis characterizing the salinity of the study site revealed a slightly acidic soil, which can make some chemical elements available due to an increase in their solubilization (Montemurro et al., 2013). The carbon-nitrogen (C/N) ratio of this soil was found to be 9.50 meaning that carbon composition of that soil is far superior

to that of nitrogen. However, we could observe a good mineralization of organic matter. Regarding the exchangeable cations, the rate of calcium ions was practically twice larger (5.32 mass equivalent (m eq)) than that of magnesium ions which was equal to 3.27 m eq/100g. The rate of divalent ions was higher than that of monovalent ions. The cation exchange capacity (CEC) was medium level with reference to the soil analysis guide from Montemurro et al. (2013). The soil's saturation rate of adsorbent complex (S/T) was 0.86 m eq/100g; hence, it could be deduced that this soil is almost saturated according to Simon (2009).

This salinity could be explained by the accumulation of salts brought by a water of poor quality (Montemurro et al., 2013; Simon, 2009). A consequence of this accumulation of salts leads to an inhibition of photosynthesis by reducing the quantities of chlorophylls which can affect the absorbance of light later on, hence, affecting the growth of the plant (Montemurro et al., 2013; Simon, 2009).

These physio-chemical characteristics results showed a certain poverty of the cultivation soil. Several methods of remediation exist in practice (Montemurro et al., 2013; Simon, 2009) among which the simplest method is an amendment through natural fertilizer (feces of cattle, sheep and goats) in order to balance its nutritional level.

Concerning the pH of the cultivation soil; a value of 7 showed its balanced aspect.

### 4.3.2 Agricultural and Field data analyses of various cultivated plants

Tables 4.10 to 4.25 present a summary of average crops' field data while figures 4.38 to 4.52 show plots of vapor pressure deficit against relative humidity and plots of harvest for lettuce, courgette, tomatoes, potatoes and green pepper respectively. In all the tables, temperatures of soil are lower than those of the leaves and the atmospheric air. The pH has been around 7 throughout the experiment. Data on plants growth were taken at fruiting stage because it's at that stage that most plants reach 80-100% of their growth capacity.

Harvest conversion formula Harvest1hect = $\frac{[(\text{Harvest}30m^2)\text{x } 10\,000]}{30}$

#### 4.3.2.1 Analysis on Lettuce crop: *Lactuca sativa* - Eden variety


**Figure 4. 37** Different growth stages of lettuce crop

**Table 4. 10** Lettuce crop field thermal data

| **Samples** | **Lettuce (variety Eden)** | | |
|---|---|---|---|
| **Stage** | **1** | **2** | **3** |
| **pH** | 7 | 7 | 7 |
| **$T_{leaf}$ ($^{o}$C)** | 32.33 | 23.83 | 24.33 |
| **$T_{soil}$ ($^{o}$C)** | 25.67 | 24.00 | 25.67 |
| **$T_{air}$ ($^{o}$C)** | 32.97 | 38.33 | 37.60 |
| **RH** | 43% | 10% | 10% |
| **Light (Lux) x100** | 698.00 | 841 | 697 |
| **Light (w/m$^2$)** | 550.91 | 663.77 | 550.12 |
| VPD (Pa) | 2685.5171 | 2279.2065 | 2395.3498 |

Considering three main growth stages: seedling stage (1), foliage stage (2) and bolting or head formation stage (3). At seedling stage, it was observed an average of two (2) leaves, eight (8) leaves at foliage stage and twelve (12) leaves at the bolting stage with formation of a head (see figure 4.38). This number of leaves influences photosynthesis, evapotranspiration rate and, hence, affecting the vapor pressure deficit. In fact, during the seedling stage, lettuce crop had few young leaves. This caused the VPD to be the highest of all stages (2.68 kPa) even though the leaves were exposed to a relatively cooler air temperature (32.97 $^{o}$C) and higher relative humidity (43%) compared to the other stages (38.33 $^{o}$C and 37.60 $^{o}$C at stage 2 and 3 respectively). The VPD dropped from 2.685 kPa (lifting stage) to 2.279 kPa at the foliage stage before climbing back to (2.395 kPa) at the bolting stage. This means during the second stage, lettuce crop had developed many young leaves allowing a more efficient photosynthesis hence reducing the stress of evapotranspiration whereas at the last stage where more old leaves were present, the crop needed to accelerate the evapotranspiration rate causing an increase in VPD.

**Table 4. 11** Lettuce crop field physical data

| **Variety Eden** | **Data From field** | **Data From literature/ datasheet** | **Reference** |
|---|---|---|---|
| **Number of days before 1st harvest** | 37 | 25-30 | |
| **Maximum Height of plants(cm)** | 14 | 20 | (TECHNISEM, 2019) |
| **Growth rate (max height/ideal height)** | 70.00% | | |

**Table 4. 12** Lettuce crop field production data

| **Variety Eden** | **Harvest Results over 30 $m^2$** | **Harvest Results converted to 1 Ha** | **Harvest Results From literature over 1 Ha** | **Reference** |
|---|---|---|---|---|
| **Number of fruits/leaves** | 378 | 126000 | | |
| **Weight of product (g)** | 31563 | 10521000 | 16500000 | (CRA-Dosso, 2018) |
| **Weight of spoilt product (g)** | 257 | 85666.6667 | | |
| **Actual Sales (CFA / XOF)** | 9050 | 3016666.67 | | |
| **Percentage healthy fruits** | 99.19% | 99.19% | | |

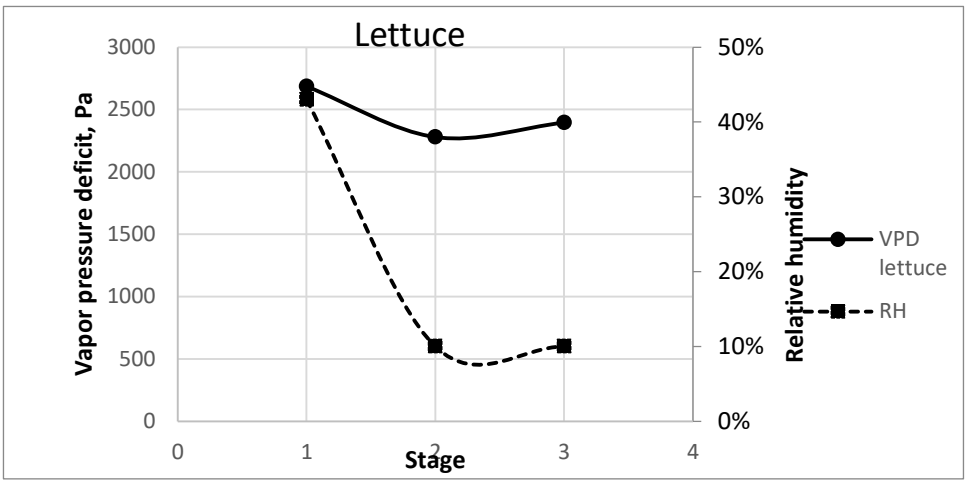


**Figure 4. 38** Vapor pressure deficit and relative humidity of lettuce at different growth stages

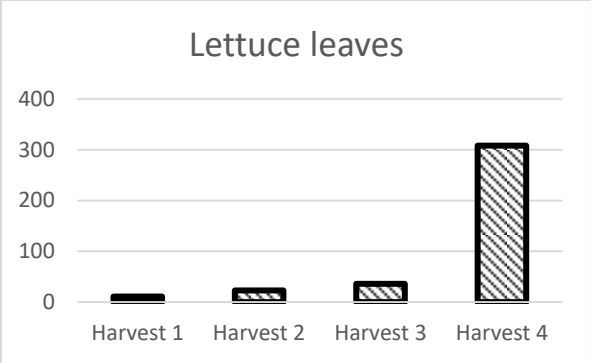


**Figure 4. 39** Plot of lettuce harvested leaves

The growth rate of the plant was monitored and compared to data from datasheet. This was shown in table 4.11 whereby the plant grew 70% of its ideal height (14 cm high against 20 cm from datasheet). Besides, we could start harvesting 37 days after plantation against a maximum of 30 days from datasheet.

A close look at the crop yield showed a percentage of good healthy and saint lettuce leaves of about 99.19% (see table 4.12). In fact, this was clearly seen in the products weight (31.563 kg over 30 $m^2$) against only 0.257 kg spoilt product. Projected to a hectare, 10.521 tons could be obtained. This result is acceptable, yet inferior to results obtained from local farmers in the region of Dosso (Niger) in 2018 which is 16.5 tons (CRA-Dosso, 2018). Most of those farmers used inorganic fertilizers to optimize their cultivation whereas ours is biologically pure with only organic natural fertilizers mainly cow dungs derived.

#### 4.3.2.2 Analysis on Courgette or Zucchini crop: *Curcubita pepo* - F1 color variety


**Figure 4. 40** Different growth stages of Courgette/zucchini crop

**Table 4. 13** Courgette crop field thermal data

| **Samples** | **Courgette (variety F1 Color)** | | |
|---|---|---|---|
| **Stage** | **1** | **2** | **3** |
| **pH** | 7 | 7 | 7 |
| **$T_{leaf}$ ($^{o}$C)** | 27.40 | 26.97 | 23.47 |
| **$T_{soil}$ ($^{o}$C)** | 28.33 | 26.67 | 25.00 |
| **$T_{air}$ ($^{o}$C)** | 37.60 | 41.23 | 35.60 |
| **RH** | 27% | 17% | 18% |
| **Light (Lux) x100** | 698 | 840 | 651 |
| VPD (Pa) | 1899.1147 | 2219.2586 | 1823.8427 |

Considering three main growth stages: advanced lifting stage (1), flowering stage (2) and fruiting stage (3). From table 4.13 and figure 4.41, it could be observed that Courgette plant had a higher VPD value at the flowering stage (2.219 kPa). This showed that a higher transpiration rate was needed for the plant to take more nutrients to produce. In average, the VPD turned between 1.823 and 1.899 kPa.

**Table 4. 14** Courgette crop field physical data

| **Variety F1 color** | **Data From field** | **Data From literature/ datasheet** | **Reference** |
|---|---|---|---|
| **Number of days before 1st harvest** | 41 | 45 | |
| **Maximum Height of plants(cm)** | 32 | 50 | (TECHNISEM, 2019) |
| **Growth rate (max height/ideal height)** | 64.00% | | |

**Table 4. 15** Courgette crop field production data

| **Variety F1 color** | **Harvest Results over 30 $m^2$** | **Harvest Results converted to 1 Ha** | **Harvest Results From literature over 1 Ha** | **Reference** |
|---|---|---|---|---|
| **Number of fruits/leaves** | 70 | 23333.3333 | NA | |
| **Weight of product (g)** | 12450 | 4150000 | NA | |
| **Weight of spoilt product (g)** | 1309 | 436333.333 | NA | |
| **Actual Sales (CFA / XOF)** | 6150 | 2050000 | NA | |
| **Percentage healthy fruits** | 89.49% | 89.49% | NA | |

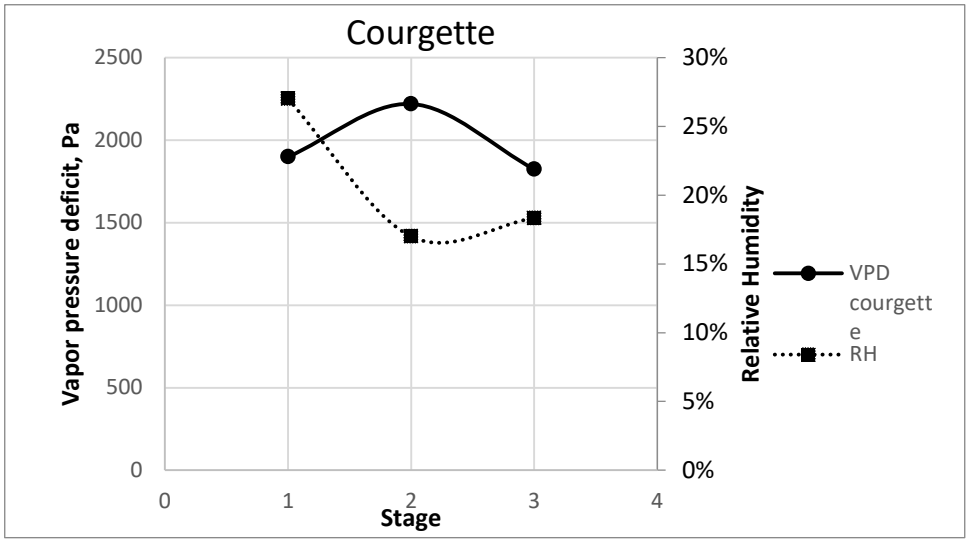


**Figure 4. 41** Vapor pressure deficit and relative humidity of Courgette at different growth stages

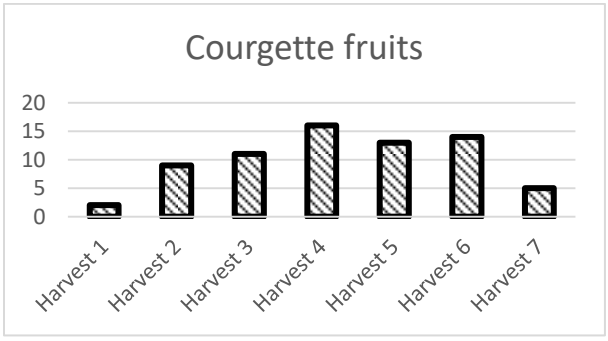


**Figure 4.42** Plot of courgette harvested fruits

The maximum height of the plant was 32 cm against 50 cm from datasheet which corresponds to a growth rate of 64%. It took 41 days before observing first fruits (see table 4.14) and from that day many harvests were done every day with an average of 10 fruits per day as shown in figure 4.43.

The cumulative harvest products, from seven harvests, amounted to 12.45 kg over the 30 $m^2$ land exploited with 89.49% of healthy fruits; Projected to 1 hectare, the production could amount to 4.15 tons of courgettes (see table 4.15). This result seems to be the first of its kind considering organic cultivation.

#### 4.3.2.3 *Analysis on Tomatoes crop: Solanum lycopersicum - F1 mongal variety*


**Figure 4. 43** Different growth stages of Tomatoes crop

**Table 4. 16** Tomatoes crop field thermal data

| **Samples** | **Tomatoes (variety Mongal)** | | |
|---|---|---|---|
| **Stage** | **1** | **2** | **3** |
| **pH** | 7 | 7 | 7 |
| **$T_{leaf}$ ($^{o}$C)** | 22.50 | 27.50 | 26.67 |
| **$T_{soil}$ ($^{o}$C)** | 25.67 | 31.00 | 29.33 |
| **$T_{air}$ ($^{o}$C)** | 25.17 | 43.00 | 44.47 |
| **RH** | 49% | 20% | 10% |
| **Light (Lux) x100** | 698 | 839 | 741 |
| VPD (Pa) | 1146.9958 | 1914.1732 | 2563.3866 |

Considering three main growth stages: advanced lifting stage (1), flowering stage (2) and fruiting stage (3). In figure 4.44 and table 4.16, VPD was increasing with advancement in stages from 1.146 kPa to 2.563 kPa. This increase was influence by the fact that fruit crops need more nutrients (Nitrogen, potassium, phosphorus, etc.) from the flowering to the fruiting stage in order to produce fruits. This need was more seen by the fact that the average leaves' temperature at flowering (27.50 $^{o}$C) was higher than at fruiting stage (26.67 $^{o}$C) even though the plant was exposed to a higher air temperature or ambient (44.47 $^{o}$C) in the latter stage.

**Table 4. 17** Tomatoes crop field physical data

| **Variety Mongal F1** | **Data From field** | **Data From literature/ datasheet** | **Reference** |
|---|---|---|---|
| **Number of days before 1st harvest** | 76 | 60-90 | |
| **Maximum Height of plants(cm)** | 65 | 100 | (TECHNISEM, 2019) |
| **Growth rate (max height/ideal height)** | 65.00% | | |

**Table 4. 18** Tomatoes crop field production data

| **Variety Mongal F1** | **Harvest Results over 30 m$^2$** | **Harvest Results converted to 1 Ha** | **Harvest Results From literature over 1 Ha** | **Reference** |
|---|---|---|---|---|
| **Number of fruits/leaves** | 761 | 253666.667 | NA | |
| **Weight of product (g)** | 33164 | 11054666.7 | 19700000 | (CRA-Maradi, 2017) |
| **Weight of spoilt product (g)** | 2180 | 726666.667 | NA | |
| **Actual Sales (CFA / XOF)** | 8750 | 2916666.67 | NA | |
| **Percentage healthy fruits** | 93.43% | 93.43% | NA | |

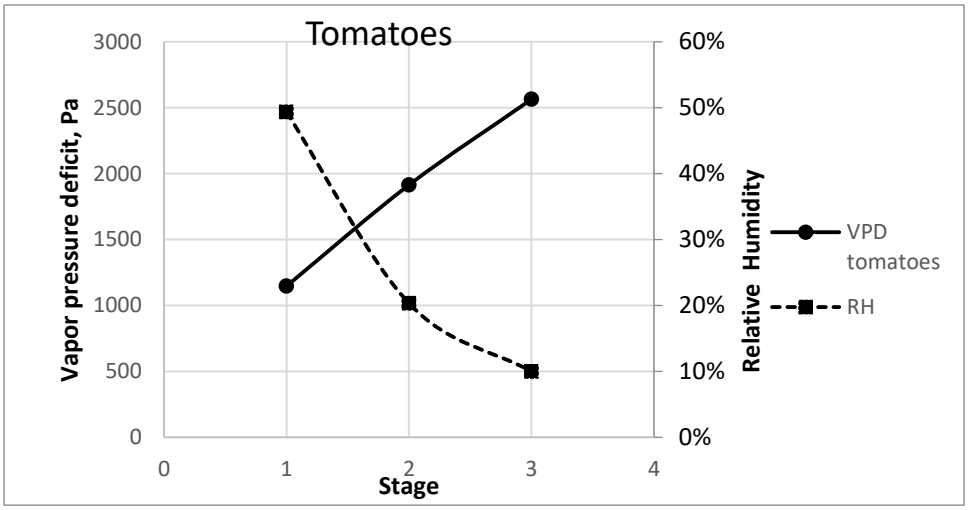


**Figure 4. 44** Vapor pressure deficit and relative humidity of tomatoes at different growth stages

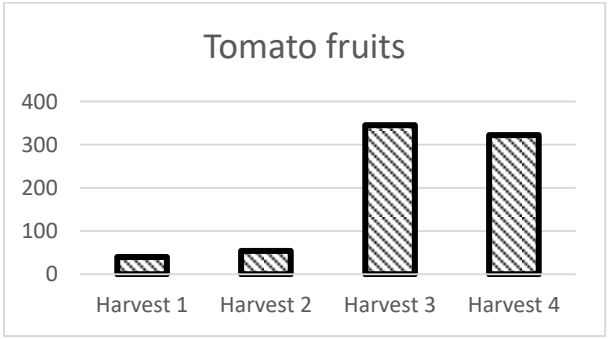


**Figure 4. 45** Plot of tomatoes harvested

The maximum height that could be observed was 65 cm against 100 cm from the datasheet of that variety. This corresponded to 65% growth rate compared to the plant's datasheet (see table 4.17). Moreover, it took 76 days before getting the first tomato fruit which was a good performance since it was within datasheet specifications (60-90 days). Figure 4.46 shows the harvest pattern per harvest days. In average, 190 tomatoes could be harvested each time.

The products, from four harvests, weighed 33.164 kg for the 30 $m^2$ exploited which could have reached 11.055 tons if done over 1 hectare. Most of the products (93.43%) were in good health meaning not spoilt. These harvest results from biological tomatoes cultivation (extrapolated to 11.055 t) were not far from results reported by Maradi Regional Chamber of Agriculture who announced 19.700 tons over 1 hectare from local farmers within the years 2016 and 2017 (CRA-Maradi, 2017). In fact, those farmers mostly use chemical fertilizers to boost their productivity which is not with no consequences overtime.

#### 4.3.2.4 Analysis on Potato crop: *Solanum tuberosum L.* - Pamela variety


**Figure 4. 46** Different growth stages of Potato crop

**Table 4. 19** Potatoes crop field thermal data

| **Samples** | **Potatoes (variety Pamela)** | | |
|---|---|---|---|
| **Stage** | **1** | **2** | **3** |
| **pH** | 7 | 7 | 7 |
| **$T_{leaf}$ ($^o$C)** | 29.67 | 25.17 | 28.17 |
| **$T_{soil}$ ($^o$C)** | 31.00 | 32.33 | 30.00 |
| **$T_{air}$ ($^o$C)** | 40.90 | 40.17 | 39.67 |
| **RH** | 14% | 10% | 20% |
| **Light (Lux) x100** | 727 | 839 | 719 |
| VPD (Pa) | 3078.7685 | 2454.7007 | 2367.1415 |

On Figure 4.48, it was observed that vapor pressure deficit of potatoes crop decreases from 3.078 kPa to 2.454 kPa and 2.367 kPa at last (see also table 4.19). As most tubers, potatoes crop drew a lot of nutrients at early development stage (vegetative stage) in order to have fruits (tubers) formed through intensive evapotranspiration. This phenomenon was, also, accelerated by ambient air temperature (T air) which was between 39.67 $^o$C and 40.90 $^{o\,0}$C as weather was hot.

**Table 4. 20** Potatoes crop field physical data

| **Variety Pamela** | **Data From field** | **Data From literature/ datasheet** | **Reference** |
|---|---|---|---|
| **Number of days before 1st harvest** | 37 | 25-30 | |
| **Maximum Height of plants(cm)** | 42 | 50 | (TECHNISEM, 2019) |
| **Growth rate (max height/ideal height)** | 84.00% | | |

**Table 4. 21** Potatoes crop field production data

| **Variety Pamela** | **Harvest Results over 30 $m^2$** | **Harvest Results converted to 1 Ha** | **Harvest Results From literature over 1 Ha** | **Reference** |
|---|---|---|---|---|
| **Number of fruits/leaves** | 372 | 124000 | NA | |
| **Weight of product (g)** | 18833 | 6277666.67 | 6240000 | (Moussa et al., 2020) |
| **Weight of spoilt product (g)** | 2054 | 684666.667 | NA | |
| **Actual Sales (CFA / XOF)** | 5650 | 1883333.33 | NA | |
| **Percentage healthy fruits** | 89.09% | 89.09% | NA | |

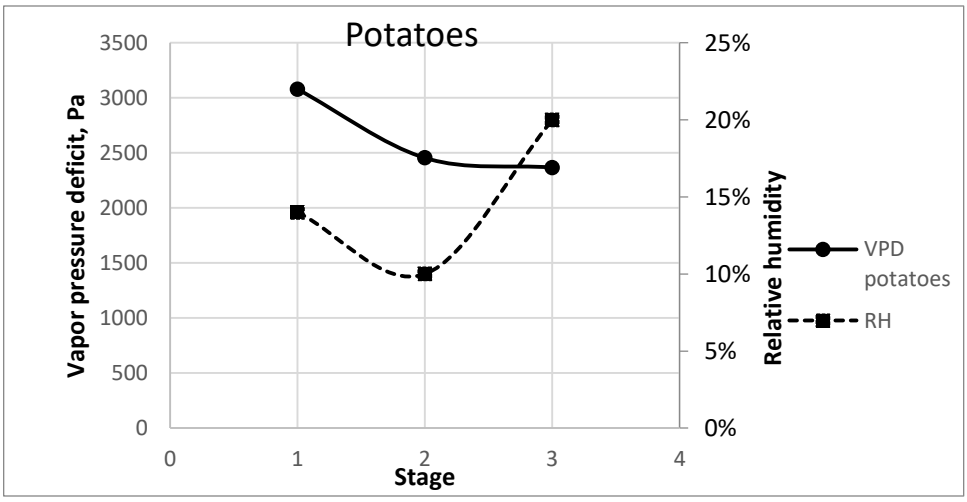


**Figure 4. 47** Vapor pressure deficit and relative humidity of potatoes at different growth stages

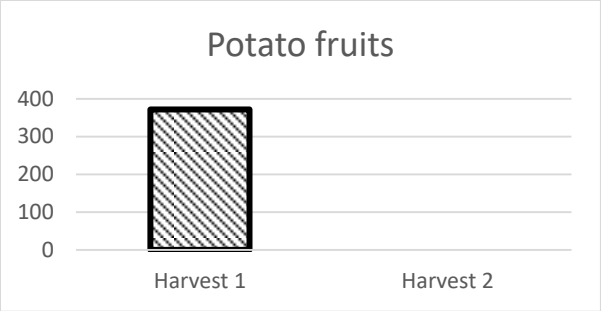


**Figure 4. 48** Plot of potatoes harvested

Although these elevated temperatures, potatoes plants could growth at a rate closer to datasheet specification (84% growth rate) with a maximum of 42 cm height per plant against 50 cm from literature. However, it took 37 days harvesting which is more time than specified (25-30 days).

The harvest, contrary to other cultivation, was done at once (Figure 4.49) which amounted to 18.833 kg of raw potatoes even though 10.91% were spoilt as shown in table 4.21. These results were done over 30 $m^2$ and could be extrapolated to reach 62.776 tons over 1 hectare. By doing a comparison at that scale, it could be seen that those results were like those obtained by an experiment conducted at the faculty of Agronomy-UAM in 2020. In fact, that latter research reported a harvest of 62.400 tons which was slightly below our result of 62.776 tons even though they used chemical fertilizer NPK 250-250-50 with variety Sahel F2E1 (Moussa et al., 2020). Moreover, the Regional Chamber of Agriculture of Tillabery (RECA-Tillabery) reported harvest results of year 2021 from Bonkoukou village to amount to 2.664 tons. This latter results from Bonkoukou village are much lower than our result probably due to many factors such as pour land (not rich in nutrient, no enough watering, etc.) (Maïga et al., 2021). In general, this experiment was satisfying with fruits up to standard through biological cultivation.

#### 4.3.2.5 Analysis on Sweet pepper crop: *Capsicum annuum* - Jason variety


**Figure 4. 49** Different growth stages of Sweet/green pepper crop

**Table 4. 22** Sweet pepper crop field thermal data

| **Samples** | **Sweet pepper (variety Jason)** | | |
|---|---|---|---|
| **Stage** | **1** | **2** | **3** |
| **pH** | 7 | 7 | 7 |
| **$T_{leaf}$ ($^{o}$C)** | 23.83 | 31.33 | 35.33 |
| **$T_{soil}$ ($^{o}$C)** | 26.33 | 29.33 | 36.67 |
| **$T_{air}$ ($^{o}$C)** | 37.90 | 39.53 | 51.33 |
| **RH** | 11% | 10% | 35% |
| **Light (Lux) x100** | 846 | 719 | 909 |
| VPD (Pa) | 2250.8942 | 3858.2454 | 1114.9960 |

Figure 4.51 and table 4.22 show crops evapotranspiration process expressed as Vapor Pressure Deficit (VPD). In fact, it could be observed from the above, an increase in VPD from 2.250 kPa at advanced lifting stage to 3.858 kPa at flowering stage which dropped to 1.114 kPa at the fruiting. This trend of VPD is similar to that from most fruit producing crops since more nutrient were needed to be sucked in by the plant through evapotranspiration process at flowering stage in order to prepare for fruit production.

**Table 4. 23** Sweet pepper crop field physical data

| **Variety Jason** | **Data From field** | **Data From literature/ datasheet** | **Reference** |
|---|---|---|---|
| **Number of days before 1st harvest** | 91 | 76 | |
| **Maximum Height of plants(cm)** | 33 | 50 | (TECHNISEM, 2019) |
| **Growth rate (max height/ideal height)** | 66.00% | | |

**Table 4. 24** Sweet pepper crop field production data

| **Variety Jason** | **Harvest Results over 30 $m^2$** | **Harvest Results converted to 1 Ha** | **Harvest Results From literature over 1 Ha** | **Reference** |
|---|---|---|---|---|
| **Number of fruits/leaves** | 184 | 61333.3333 | NA | |
| **Weight of product (g)** | 1926 | 642000 | 20000000 | (Mahamadou et al., 2016a, 2016b) |
| **Weight of spoilt product (g)** | 91 | 30333.3333 | NA | |
| **Actual Sales (CFA / XOF)** | 2200 | 733333.333 | NA | |
| **Percentage healthy fruits** | 95.28% | 95.28% | NA | |

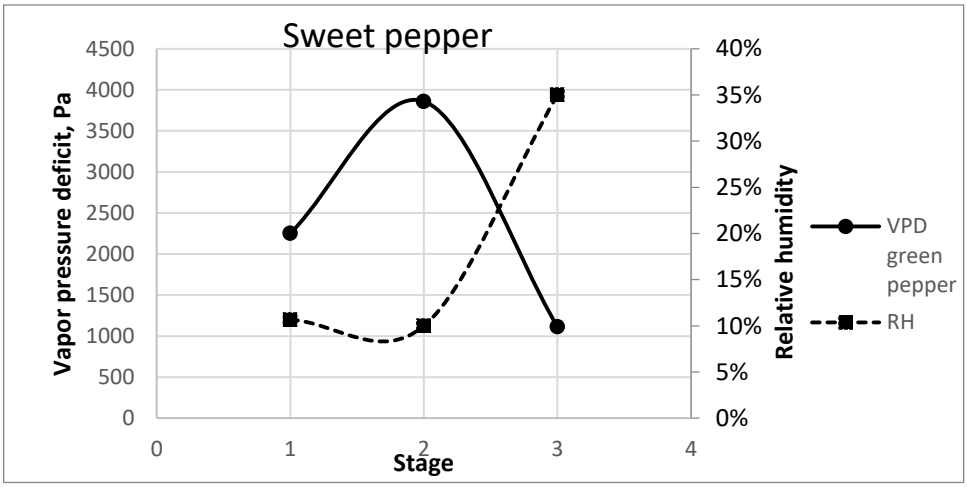


**Figure 4. 50** Vapor pressure deficit and relative humidity of Sweet pepper at different growth stages

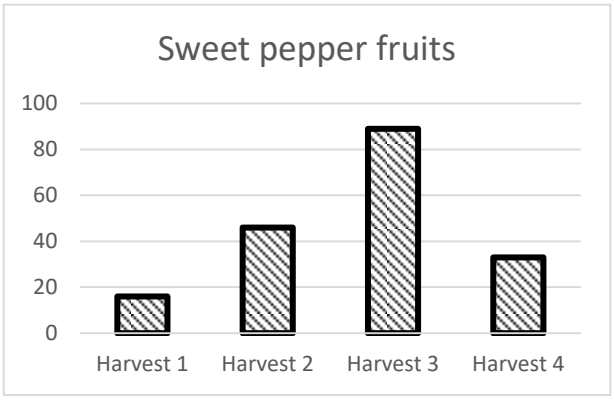


**Figure 4. 51** Plot of Sweet pepper harvested

The maximum height recorded from the crops was 33 cm corresponding to 66% growth rate compared to ideal datasheet height (50 cm) (see table 4.23). The harvest started only 91 days after transplantation which was 15 days more than the specified time provided by the crop's datasheet.

After the first harvest, an average of 46 green peppers could be obtained each time (see figure 10) which amounted to a cumulative amount of 1.926 kg after four harvest over 30 $m^2$ land exploited. If this result, presented in table 4.24, is extrapolated to a 1-hectare cultivation, it would be 0.642 tons against 20.00 tons reported by the Regional Chamber of Agriculture of Diffa (translated from French: RECA-Diffa) in 2016 with variety Yolo Wonder (Mahamadou et al., 2016a, 2016b). Our results were far inferior to that of RECA-Diffa for many reasons among which is the fact of our study was not exhaustive harvest, it was not using any boosting fertilizer and finally, it was not the same variety.

### 4.3.3 Photochemical analyses of plants' leaves extract

The radiation needs of plants during their growth could be estimated through absorption and transmittance spectra of photosynthetic pigments present in their leaves' extracts. In fact, those pigments help plants capture sun energy and convert it into chemical energy for their needs via photosynthesis. The presence of photosynthetic pigments could be confirmed by their individual characteristic peaks on a chromatogram.

#### 4.3.3.1 Optimization of solvent

With 5 g of vegetable leaves, volumes of 5, 10 and 20 mL of ethanol were used in order to find the appropriate volume for better recovery of photosynthetic pigments and it was shown uplifting results. On one hand, with 5 to 10 mL volume of ethanol, the extract obtained was insignificant and the expected greenish coloration was hardly observable. On the other hand, the quantity of the extract and the greenish coloring became very significant with a volume of 20 mL of ethanol. Traditionally a ratio (m:v) of 1:1 is used between the mass of the plant material and the volume of the solvent extracting. These results obtained showed that this report was not up to a good extraction. Using the volume of 20 mL, a ratio of 1:4, although resulting in 4 times more ethanol,

gave better extraction result. Besides, the nature of the filter paper plays an important role in filtration. Using small pore size filter paper such as filter paper N°1, filtration took more time. However, the use of a filter paper with bigger pore size or a cotton wool allowed rapid filtration with a better result. The latter type of filtering, in addition to allowing good filtration, is also cheaper and readily available. Usually, small pore size filter paper could promote the retention of some pigments which was a big drawback. At the end of this optimization, the best extraction conditions were a volume of 20 mL of ethanol and the use of the big pore size filter paper or cotton wool.

#### 4.3.3.2 Optimization of Eluent

Figure 4.52 shows the chromatograms of pigment identification photosynthetic extracts in different compositions in terms of petroleum ether and acetone eluent. The analysis of the chromatograms highlights five main kinds of pigments:

- Carotenes (yellow-orange): very little polar,
- Chlorophyll a (blue green): not very polar,
- Chlorophyll b (green-yellow): moderately polar,
- Xanthophyll (lutein) (yellow): polar,
- Pheophytin (grey).

With eluent 1 (see figure 4.52 (1)) whose composition was 40% petroleum ether and 60% acetone, after depositing the extract on the TLC plate and removing the latter from the test tube or elution container, no stain was observed on the plate at the level of its upper terminal. This means that no pigment could migrate. The molecules of the desired pigments, all polar, interacted strongly with those of the supporting plate. The fact that no elution was observed could also come from the pigments not much soluble in this eluent. When the proportions in the eluent passed to 50% petroleum ether and 50% of acetone (eluent 2) (see figure 4.52 (2)), the pigments appeared clearly. Yet, separation was not good because the pigments began to separate after passing the middle of the plate. The eluent was, therefore, very polar, which means that polar molecules are easily entrained. Passing to eluent 3 where petroleum ether and acetone are in proportion of 60% and 40% respectively (see figure 4.52 (3)), spots were observed on the plate. Therefore, this composition allowed a relative migration of the desired pigments. The fact that petroleum ether was in higher proportion than acetone, made the medium less polar favoring the migration of non-polar molecules and hardly entraining polar pigments. However, these spots obtained were not explicit to allow a possible identification of the pigments sought. Spots are observed on the TLC plate with eluent 4 (70% petroleum ether and 30% acetone) and eluent 6 (80% petroleum ether and 20% acetone) (see figure 4.52 (4) and (6) respectively). The separation of pigments was good, although chlorophyll b and lutein were not separated by a great distance. However, the separation of polar pigments was not very clear because the pigment spots were not recoverable due to that small distance which separated them. The results obtained with the

proportions of 75% petroleum ether and 25% acetone constituting the eluent 5 (see figure 4.52 (5)), were usable. The pigments were well separated by a distance allowing their recovery without any difficulty. Thus, the best composition of the eluent was reached.

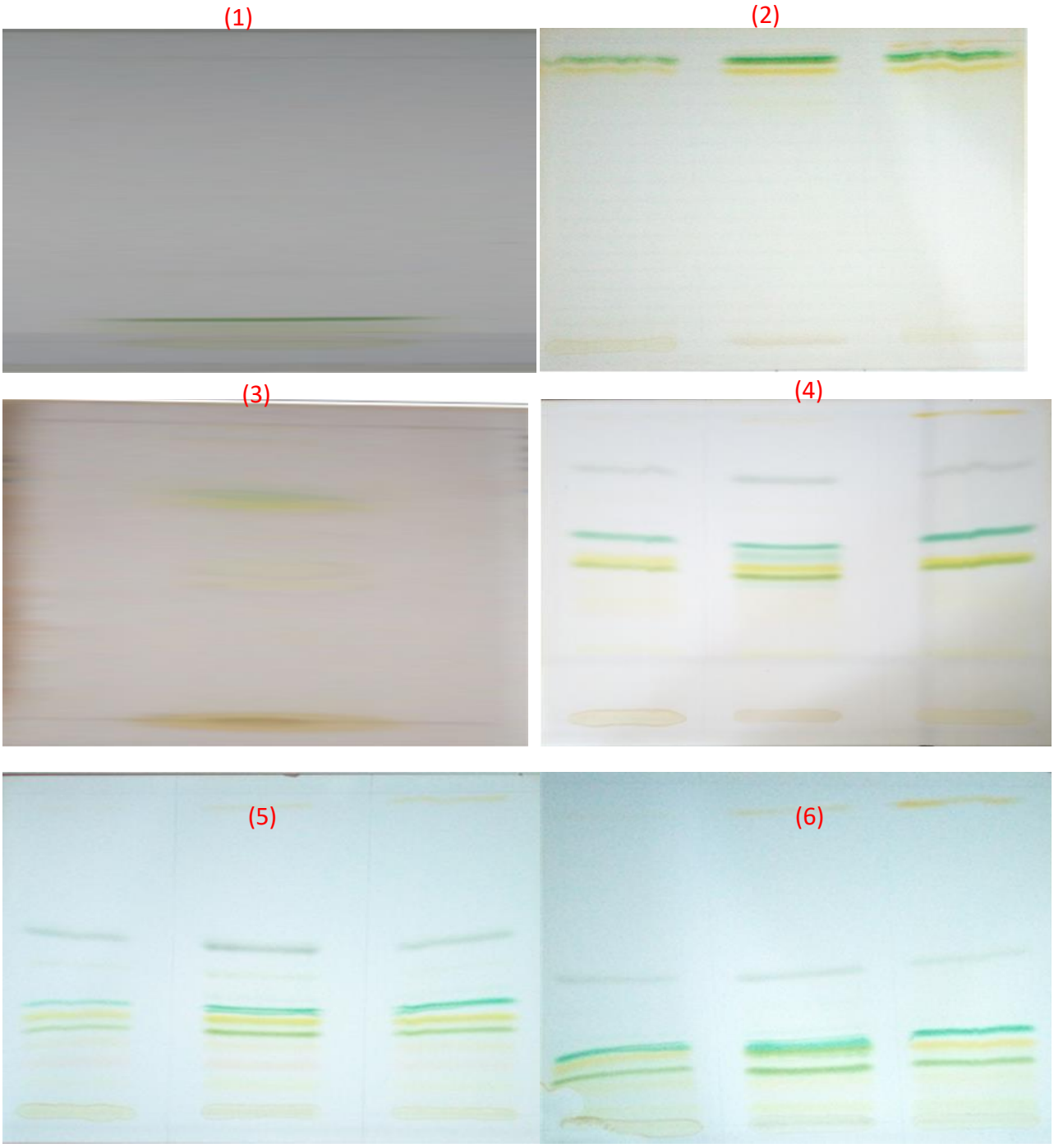


**Figure 4. 52** TLC of eluent

#### 4.3.3.3 Lettuce crop extract characterization

##### 4.3.3.3.1 Overall analysis

The photosynthetic pigments extracted from lettuce during its different growth stages are observed on the chromatograms presented in figure 4.53.

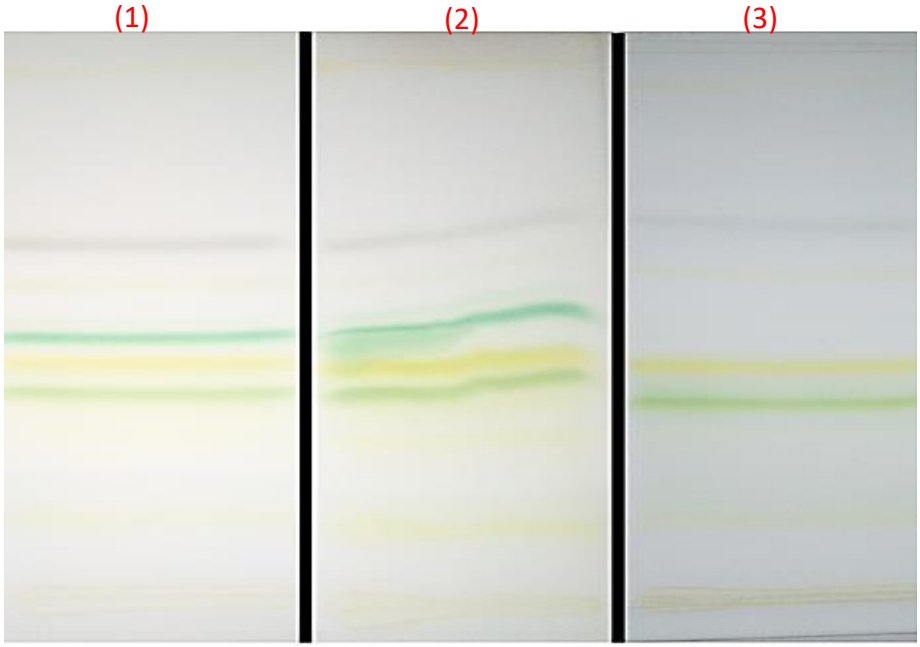


**Figure 4. 53** Chromatograph of growth stages of Lettuce crop 1, 2 and 3.

The migration of the pigments on the plate was made according to the polarity and the molecular weight. All desired photosynthetic pigments were shown through colored spots at different development stages of lettuce crop. Chronologically from top to down: α and β carotene, chlorophyll a, lutein (a xanthophyll) and chlorophyll b were observed clearly and almost identically in the first two stages of evolution. But to bolting or head formation stage (3) an absence of chlorophyll a is noted. This may be due to a change in photosynthetic activity at this stage or degradation during laboratory manipulations. On each chromatogram a spot gray was observed below carotenes' spot line. This stain might correspond to degraded chlorophylls also known as Pheophytin (Rai & Lee, 1964; Tomkins & Miller, 1993).

**Table 4. 25** Frontal ratios of different photosynthetic pigments of lettuce crop

| Pigments' color | Photosynthetic pigments | Stages of growth | | |
|---|---|---|---|---|
| | | Stage 1 | Stage 2 | Stage 3 |
| Yellowish Orange | Carotene α and β | 0.99 | 0.99 | 0.99 |
| Grey | Pheophytin (a breakdown product) | 0.66 | 0.66 | 0.66 |
| Blueish Green | Chlorophyll a | 0.50 | 0.50 | - |
| Yellowish Green | Lutein ( a xanthophyll) | 0.40 | 0.40 | 0.40 |
| Dark Green | Chlorophyll b | 0.37 | 0.37 | 0.37 |

Considering frontal ratios, it was observed that the completely non-polar carotenes migrated with the solvent front, resulting in a frontal ratio of 0.99 at each stage of growth, however that of chlorophyll a is 0.50 at all stages. In chlorophyll b, the frontal ratio is the same for the first two stages of evolution of the plant, but at the bolting stage it is 0.36. Lutein presented an identical frontal ratio at the level of the first two phases. The report of Pheophytin frontal ratio is the same at all stages.

#### 4.3.3.3.2 Spectral analysis of crude extract of lettuce leaves

Figure 4.54 presents the absorption spectra of the different extracts from lettuce at different growth stages. This figure shows the photochemical properties of a lettuce leaf between 190 and 1100 nm.

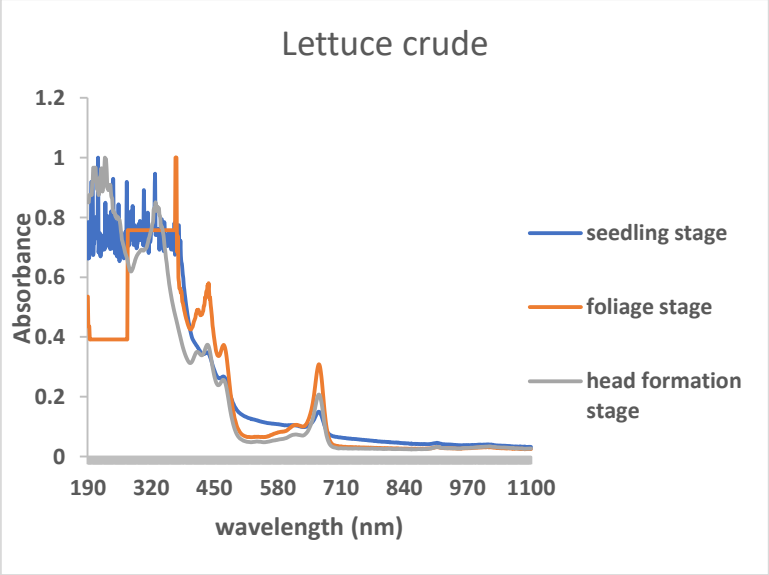


**Figure 4. 54** Graphs of absorbance of lettuce crop crude extract at different growth stages

In figure 4.54, two types of regions were observed: regions of strong absorption between 300 and 500 nm, and between 620 and 710 nm; and regions of low absorption between 500 and 620 nm, and between 710 and 1100 nm. In whole, four peaks were recorded in each spectrum, a peak at 664 nm which characterizes chlorophylls a and b, and three other peaks in the 400 to 500 nm range that characterize carotenoids and chlorophylls (414 nm, 435 nm and 466 nm). Those predominant pigments absorb in the same region in the blue and only the chlorophylls in the red.

Absorbance was greatest at the seedling stage. It increased at foliage stage and decreased at the bolting or head formation stage. This increase at the foliage stage could be to the fact that Lettuce needed to synthesize more of these pigments to develop much more leaves. Thereby, lettuce would require more sunlight.

#### 4.3.3.3.3 Spectral analysis of separated pigments of lettuce leaves

The various pure photosynthetic pigments obtained after thin layer chromatography followed a spectral analysis. Figure 4.55 to 4.59 combines all the absorbance spectra of the pigments found in lettuce leaves.

Absorbance was clear in the band from 400 to 500 nm. It decreased from stage at the first to the last growth stage of the plant. Carotene α and β were noticed to be more synthesized at the beginning and at the end of growth in lettuce (figure 4.55). The characteristic peak of carotenes is located at 460 nm wavelength. More light was absorbed by carotene pigments at foliage stage than at other stages.

At the head formation stage, chlorophyll-a was not detectable whereas its absorbance was greater at seedling and foliage stages with characteristic peaks around 414 nm and 666 nm (see figure 4.56).

On the chlorophyll-b graphs, it was observed an increase in absorbance from the seedling to the bolting stage. Peaks were detected at 433 nm, 463nm and 663 nm as shown in figure 4.58. As usual, the light requirement of lettuce for synthesis of chlorophyll-b is more important with advancement in the growth stages.

Spectral analysis of lutein (a xanthophyll) obtained from lettuce is presented the results in figure 4.57. Lutein absorbance decreased with advancement in the growth stages. Much more sunlight was absorbed at foliage stage since graph at that moment is above the ones at other growth stages with characteristic peaks observed at 440 nm and 465 nm, which are characteristic of lutein. Hence, lutein pigments needed more light during foliage growth stage.

Pheophytin is derived from the degradation of chlorophylls a and b; hence, its absorption spectra are as a result of these two synthetic pigments (figure 4.59). The spectral analysis of the pheophytin easily confirmed the presence of chlorophyll-a and b as the absorbance of the pheophytin in lettuce was greatest at the foliage stage. Three absorption peaks at 415, 435 and

664 nm were noted on the absorption spectra of pheophytin in lettuce. These peaks characterize pheophytin.

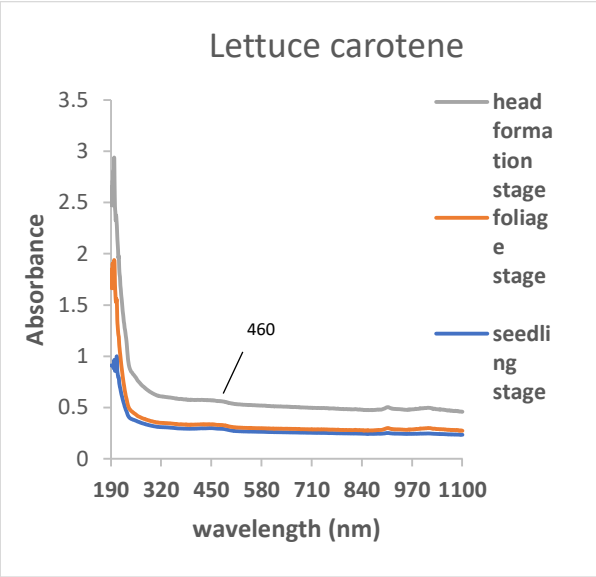


Figure 4. 55 α and β Carotene graphs from lettuce extract

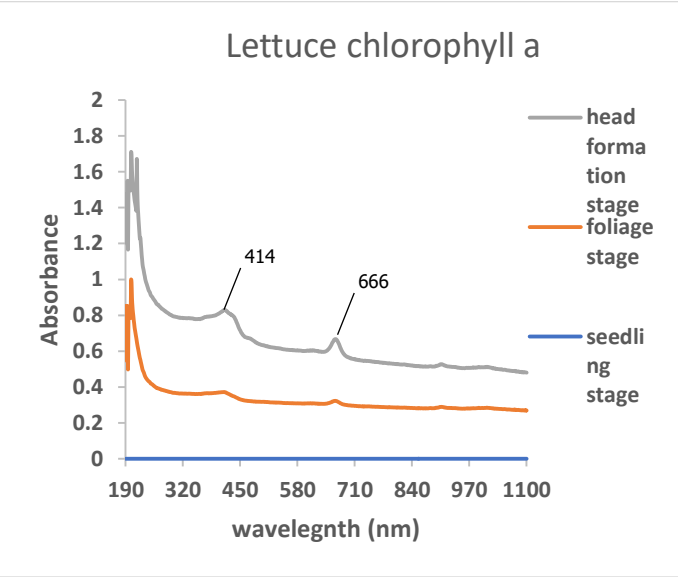


Figure 4. 56 chlorophyll a graphs from lettuce extract

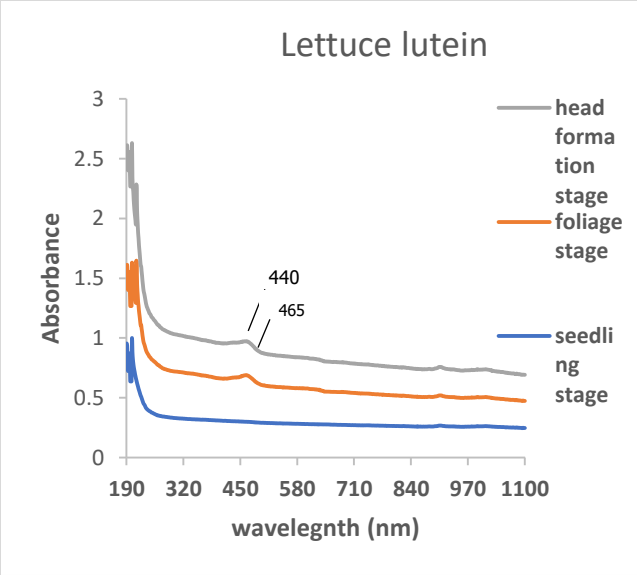


Figure 4. 57 lutein graphs from lettuce extract

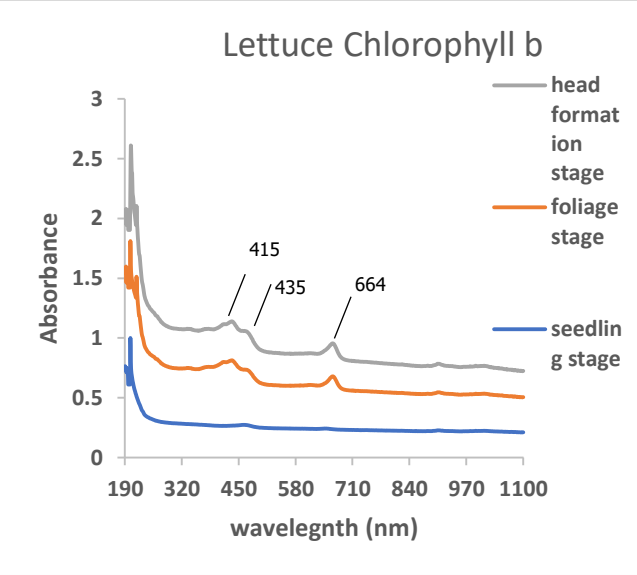


Figure 4. 58 chlorophyll b graphs from lettuce extract

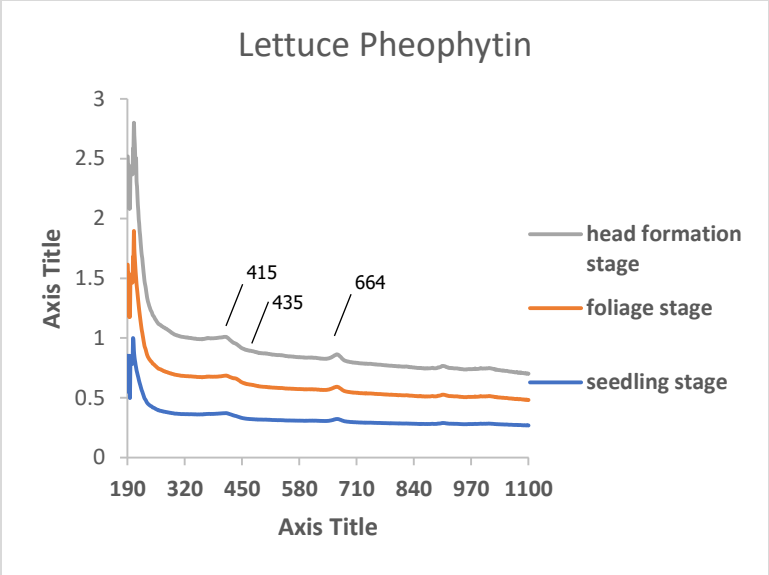


Figure 4. 59 Pheophytin graphs from lettuce extract

#### 4.3.3.4 Courgette or zucchini crop extract characterization

##### 4.3.3.4.1 Overall analysis

The analysis of the different extracts of the zucchini raised the following chromatography results shown in Figure 4.60.

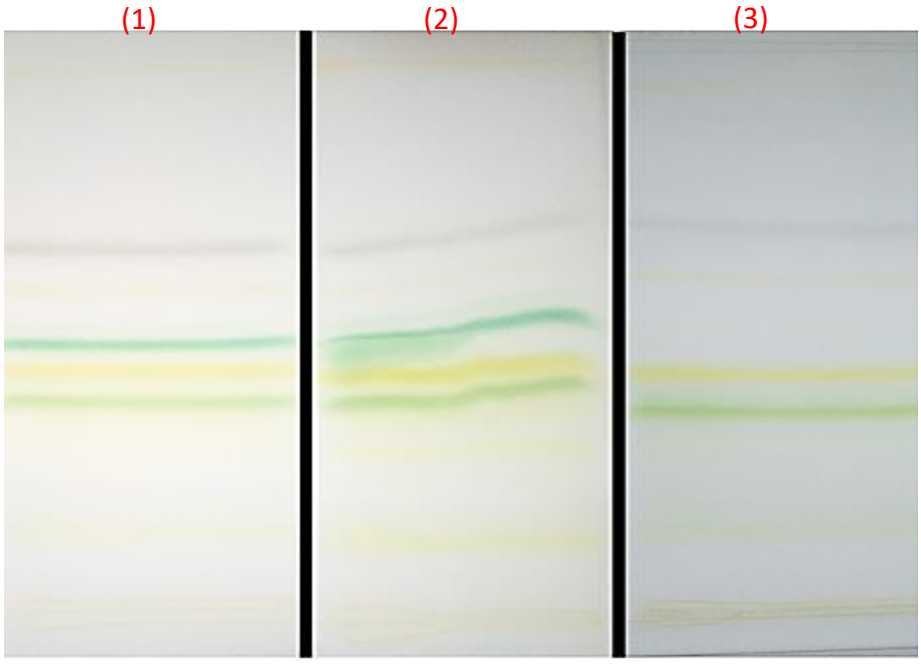


**Figure 4. 60** Chromatograph of growth stages of zucchini / courgette crop 1, 2 and 3

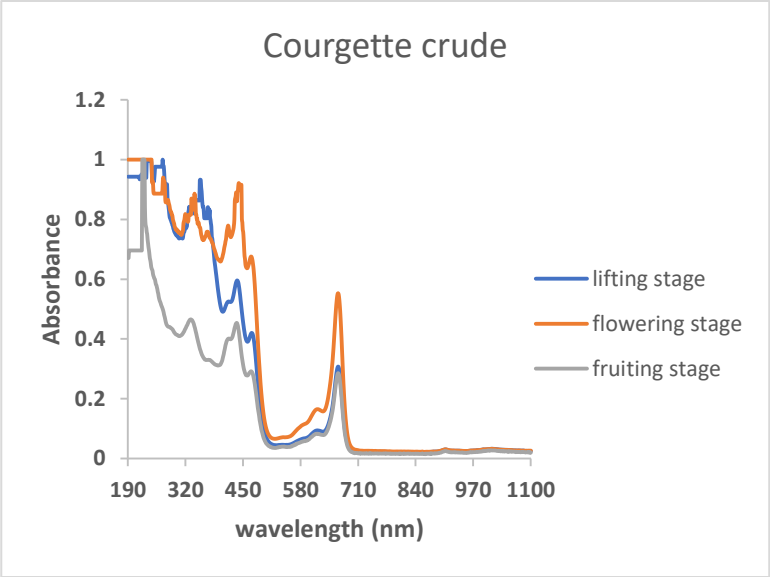


**Figure 4. 61** Growth stages chromatograms from crude extract of courgette crop leaves

Figure 4.60 and 4.61 show the different courgette chromatograms produced at each growth stage (early vegetative or lifting, flowering and fruiting). The different stains colored on these TLC plates corresponded respectively from top to bottom to: the α and β carotenes orange yellow in color which are actually very little polar which explains their migration first, chlorophyll a with a blue-green color which is not very polar, a yellow spot corresponding to the polar pigments called lutein (a xanthophyll) and finally, a pigment little polar green-yellow and the molecular weight, hence, the migration of xanthophyll before that of chlorophyll b. A gray spot located below carotene may be degraded chlorophyll (pheophytin). A yellow spot appeared between the gray spot and the chlorophyll a, perhaps a place of deposition of carotenes before their migration.

**Table 4. 26** Frontal ratio of different photosynthetic pigments of Tomato crop

| **Pigments' color** | **Photosynthetic pigments** | **Stages of growth** | | |
|---|---|---|---|---|
| | | **Stage 1** | **Stage 2** | **Stage 3** |
| Yellowish Orange | Carotene α and β | 0.98 | 0.99 | 0.98 |
| Grey | Pheophytin (a breakdown product) | 0.65 | 0.66 | 0.65 |
| Blueish Green | Chlorophyll a | 0.49 | 0.50 | 0.50 |
| Yellowish Green | Lutein ( a xanthophyll) | 0.40 | 0.39 | 0.40 |
| Dark Green | Chlorophyll b | 0.37 | 0.36 | 0.35 |

The carotenes had a frontal ratio (Rf) around 0.99 at the various growth stage of zucchini. However, chlorophyll a showed a ratio Rf of 0.49 at the first and last stage whereas during the flowering stage, a ratio of 0.50 could be observed. On one hand, a slight variation of frontal ratio was observed in the cases of pheophytin and lutein. On the other hand, chlorophyll b displayed a decreasing frontal ratio with the advancement if growth stages.

#### 4.3.3.4.2 Spectral analysis of crude extract of courgette leaves

On Figure 4.61 are presented the absorption spectra of courgette crop leaves' extracts collected at its various growth stages.

Five peaks appear on the absorption spectra of the crude extracts of the zucchini leaves during its growth. One of the peaks was located in the ultraviolet at 330 nm and the others within the visible light region (435, 466, 650 and 664 nm). The peak marked at 664 nm was the most intense and corresponded to the presence of chlorophyll-a. The low peak intensity at 650 nm was attributed to the presence of chlorophyll-b. The two peaks within the range 400 to 500 nm justify the presence of carotenoids and xanthophyll. The peak at 330 nm was probably due to flavonoids. From the lifting stage, absorbance increased till the flowering stage and from this stage it decreased until the last growth stage (fruiting) of zucchini. In fact, the level of photosynthetic pigments that were present in zucchini was more important at the flowering stage compared to the other stages. Visible radiation is most needed for the growth of courgette.

#### 4.3.3.4.3 Spectral analysis of separated pigments of courgette/zucchini leaves

In order to better understand the activity and light requirements of each photosynthetic pigment identified in zucchini, each of these pigments was analyzed under UV-vis spectroscopy and results are shown in Figure 4.62 to 4.66.

The absorbance of carotenes in zucchini decreased from the advanced lifting stage to flowering stage, then, grew from flowering stage to fruiting stage. A peak was noted at 460 nm in the range of 400 to 500 nm during the advanced lifting stage which was not distinguishable at the other stages. This characteristic peak of carotenes showed a high absorption of light by such pigment at that specific stage. In other words, α and β Carotenes were mostly synthesized at the beginning of zucchini growth.

In zucchini, the absorbance of chlorophyll-a is higher at the stage of flowering and less important at the fruiting and advanced lifting. The characteristic peaks of chlorophyll-a absorption were clearly visible at 414 and 666 nm. At the flowering stage, more chlorophyll-a was in activity for a better photosynthetic activity.

Light absorbed by chlorophyll-b in zucchini was greater in the flowering and fruiting stages compared to light absorbed at the lifting stage. The need of more light from the plant during flowering stage trigged more activity from chlorophyll-b. Chlorophyll-b spectrum displayed two characteristic peaks: one at 463 nm and another at 648 nm unique to this pigment.

Courgette lutein absorbed much more light at the flowering stage, a slightly lesser light at the fruiting stage and not much at the advanced lifting stage. Most of this absorbance was within 400 to 500 nm wavelength, with two lutein specific peaks at 445 and 475 nm.

As a degraded pigment of chlorophylls, pheophytin displayed absorption spectra with similar trend as its precursors. In fact, absorbance increased from advanced lifting stage to flowering stage and decreased from then on to fruiting stage. Two characteristic peaks were observed in the visible range, one at 414 nm and the other at 666 nm, these two peaks demonstrated the preponderance of the chlorophyll-a content over that of chlorophyll-b in zucchini.

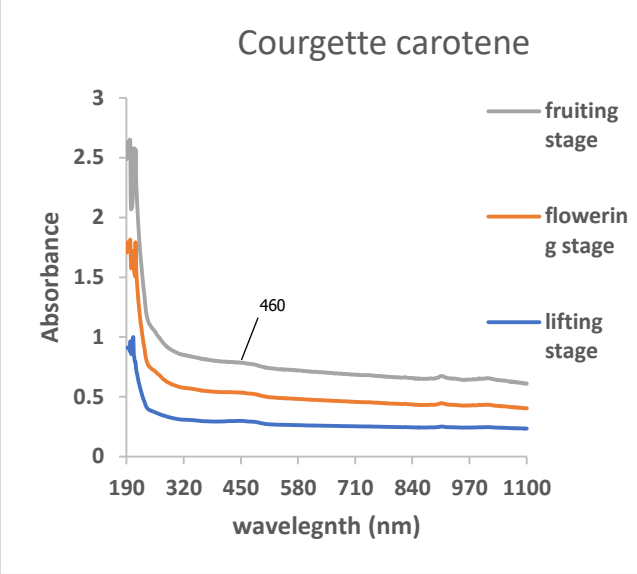


**Figure 4. 62** α and β Carotene graphs from courgette extract

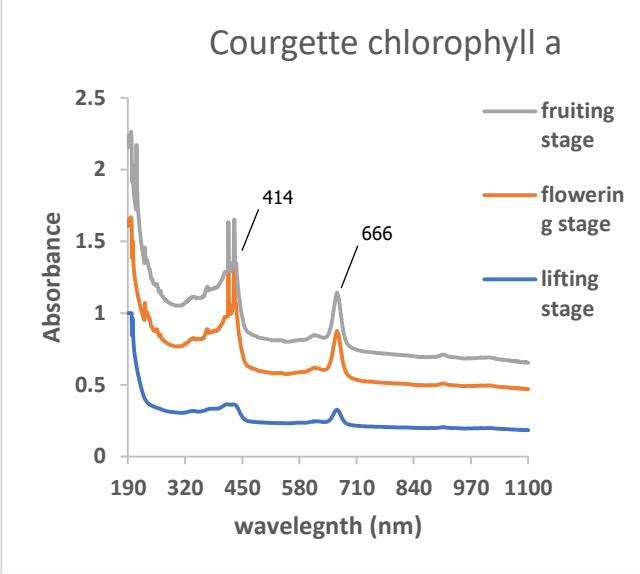


**Figure 4. 63** Chlorophyll a graphs from courgette extract

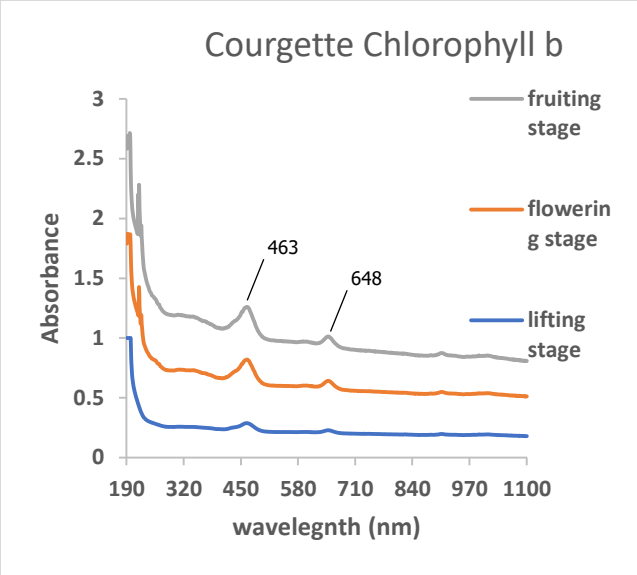


**Figure 4. 64** Chlorophyll b graphs from courgette extract

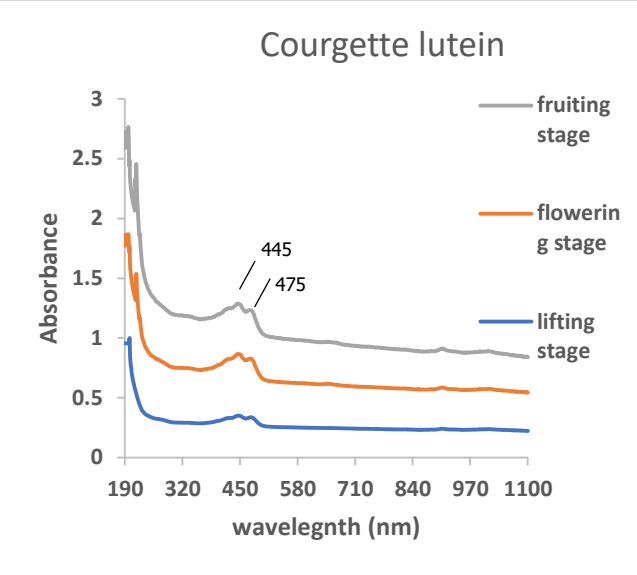


**Figure 4. 65** lutein graphs from courgette extract

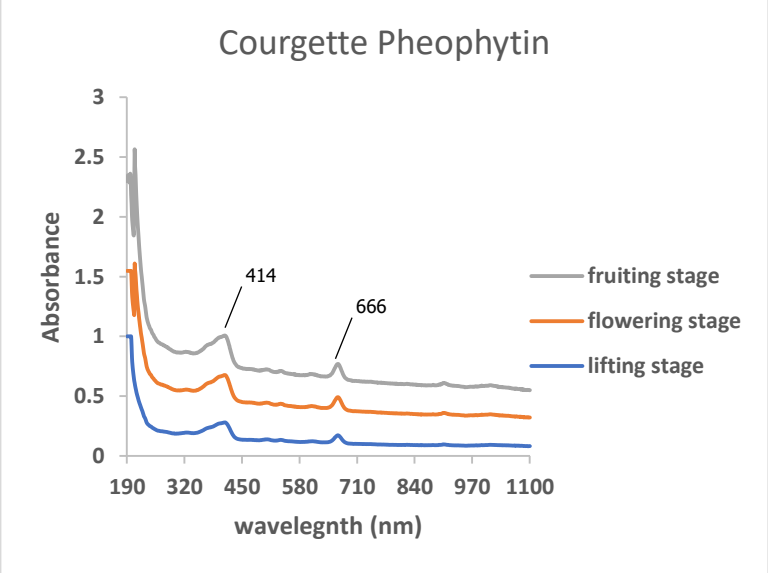


**Figure 4. 66** Pheophytin graphs from courgette extract

#### 4.3.3.5 Tomato crop extract characterization

##### 4.3.3.5.1 Overall analysis

The chromatograms of photosynthetic pigments extracted from tomato crop leaves during different growth stages

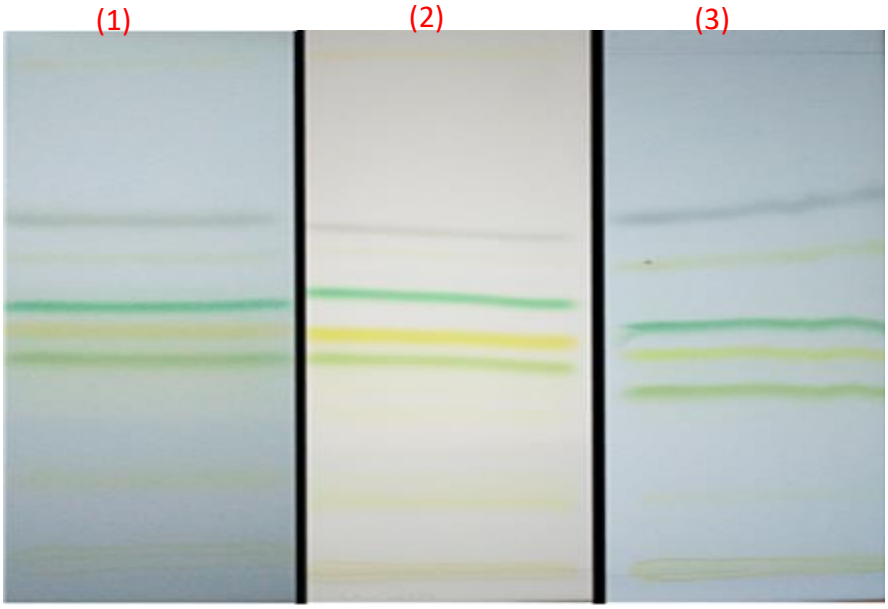


**Figure 4. 67** Chromatograph of growth stages of Tomato crop 1, 2 and 3**.**

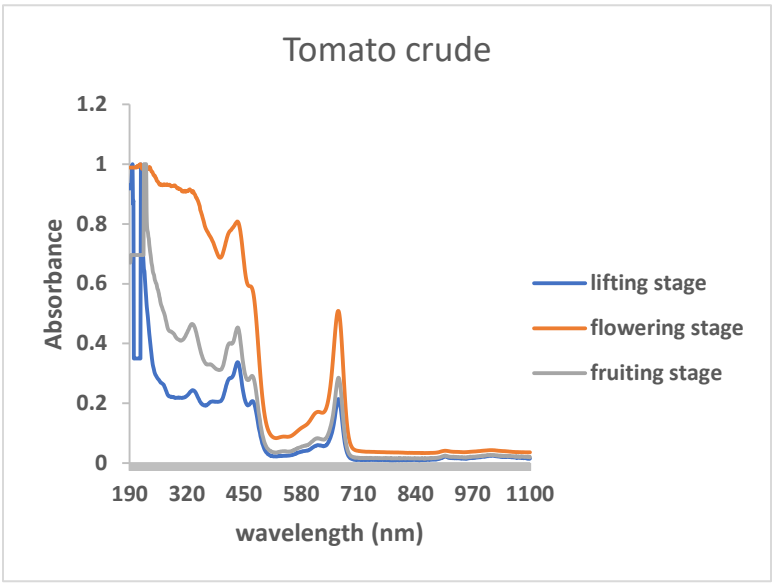


**Figure 4. 68** Growth stages chromatograms from crude extract of tomato crop leaves

Figure 4.67 presents the results of the chromatographic analysis of the extract of the tomato leaves at different stages of plant growth. This is how each plate was marked with spots that characterize the pigments sought. In addition, each plate presented from top to bottom: α and β carotenes, chlorophyll a, lutein and chlorophyll b. A gray spot is also marked on each plate below the carotenes; this may be due to degraded chlorophyll (pheophytin). The migration of pigments is made according to polarity and molecular weight.

**Table 4. 27** Frontal ratio of different photosynthetic pigments of Tomato crop

| **Pigments' color** | **Photosynthetic pigments** | **Stages of growth** | | |
|---|---|---|---|---|
| | | **Stage 1** | **Stage 2** | **Stage 3** |
| Yellowish Orange | Carotene α and β | 0.99 | 0.99 | 0.99 |
| Grey | Pheophytin (a breakdown product) | 0.66 | 0.66 | 0.67 |
| Blueish Green | Chlorophyll a | 0.50 | 0.50 | 0.51 |
| Yellowish Green | Lutein ( a xanthophyll) | 0.40 | 0.40 | 0.41 |
| Dark Green | Chlorophyll b | 0.37 | 0.37 | 0.38 |

The α and β carotenes migrated with the solvent front, which allows them to have a frontal ratio of 0.99 irrespective of growth stage of the tomato plant. However, at the level of chlorophyll a, the frontal ratio Rf = 0.50 was slightly different at fruiting stage. Besides, a slight variation in frontal ratio was observed in chlorophyll b as well as in lutein and pheophytin.

#### 4.3.3.5.2 Spectral analysis of crude extract of tomato leaves

The figures 4.68 represent the spectra absorption of tomato crop crude leaves' extracts during its growth. These spectra gave an overview of the different photosynthetic pigments present in tomato.

Spectra on figure 4.68 clearly showed that tomatoes crop leaves absorbed more light during flowering stage then, lesser amount of light at the fruiting stage and not much at the seedling stage. At this fact could be observed within the visible light region at 435, 466, 648 and 664 nm and one other peak at 330 nm which is in the ultra-violet region. These peaks gave more information about the presence of chlorophyll-a (664 nm), chlorophyll-b (648 nm), carotenoids (α and β carotenes) (400-500 nm) and flavonoids (330 nm). Those photosynthetic pigments are more synthesized during plant's full growth time or at the moments it needed more energy towards fruit creation. The demand in light increased from seedling to flowering stage and decreased from flowering to fruiting.

#### 4.3.3.5.3 Spectral analysis of separated pigments of tomato leaves

The spectral properties of these different photosynthetic pigments of tomato crop leaves extract isolated from thin layer chromatography are presented through the absorption spectra of Figure 4.69 – 4.73.

α and β Carotene absorption spectra showed no distinct peak tomato carotenes. This could be attributed to the fact that carotenes concentrations were very low, or a possible overlapping of the bands or a possible loss of the chromophore from the molecule. Nonetheless, we could observe a more absorption during flowering stage than other growth stages. Fruiting stage was the stage at which less carotene activity was noticed.

Two characteristic peaks of the chlorophyll-a pigment appeared: one at 414 nm and another at 666 nm. Content of chlorophyll-a in tomato crop was almost the same throughout its growth with a bit more during flowering stage.

Chlorophyll-b absorption spectra also displayed two characteristic peaks which were at 463 and 648 nm. Here too, more light was absorbed at the flowering stage than at the fruiting or lifting stage. In fact, Tomato crop synthesized more chlorophyll-b in the middle of its growth probably to prepare for fruit production.

The absorbance of tomato lutein (a xanthophyll) increased from advanced lifting stage to flowering stage then decreased from flowering stage to fruiting stage. The two peaks at wavelengths 445 nm and 475 nm highlighted the presence of lutein.

The absorbance of tomato crop leaves' pheophytin was highest at the flowering stage advanced. The characteristic peaks of pheophytin appeared at 412 and 665 nm at the advanced lifting stage and fruiting stage and at 440 nm at the fruiting stage.

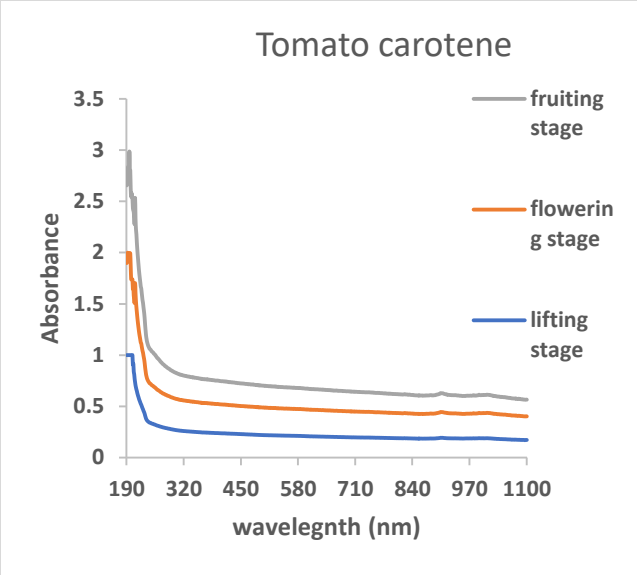


**Figure 4. 69** α and β Carotene graphs from tomato extract

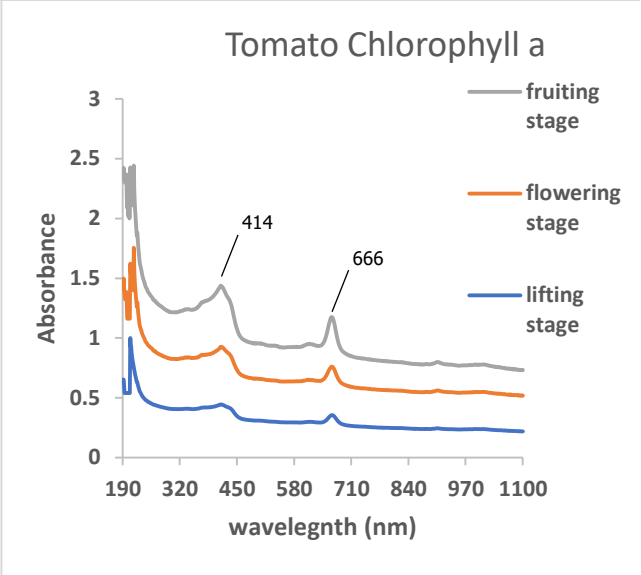


**Figure 4. 70** Chlorophyll a graphs from tomato extract

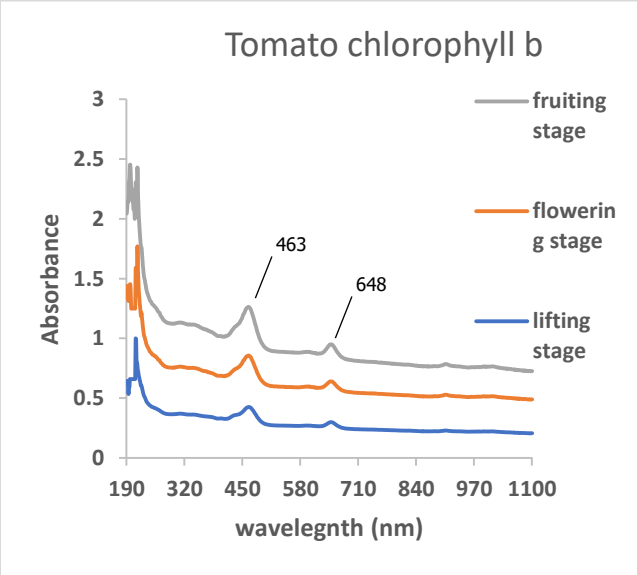


**Figure 4. 71** Chlorophyll b graphs from tomato extract

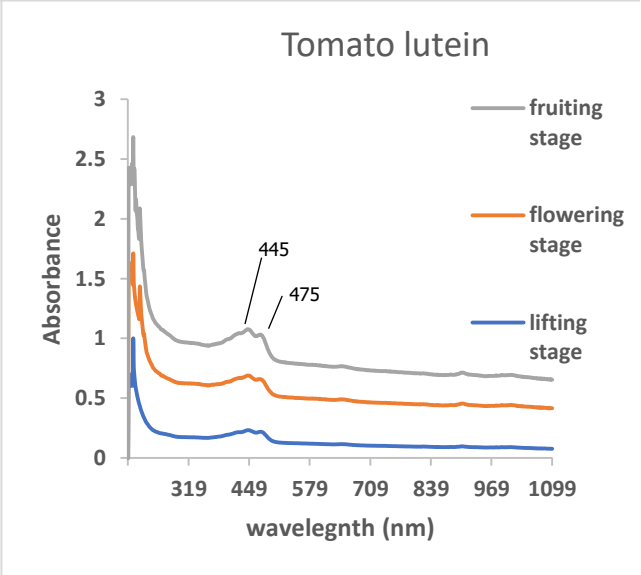


**Figure 4. 72** Lutein graphs from tomato extract

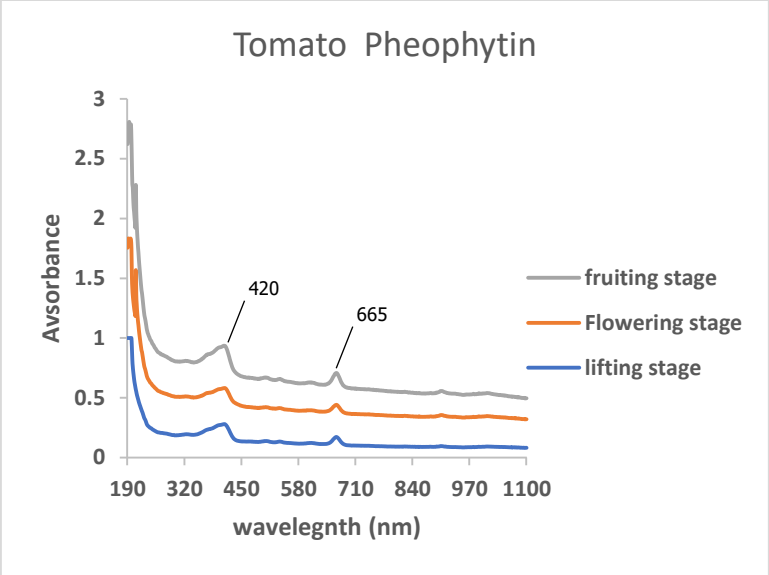


**Figure 4. 73** Pheophytin graphs from tomato extract

#### 4.3.3.6 Potato crop extract characterization

The chromatograms in Figure 4.74 show the different photosynthetic pigments properties of the potato crop according to its growth stages of evolution (vegetative, tuberization (tuber formation) and senescence).

(1) (2) (3)

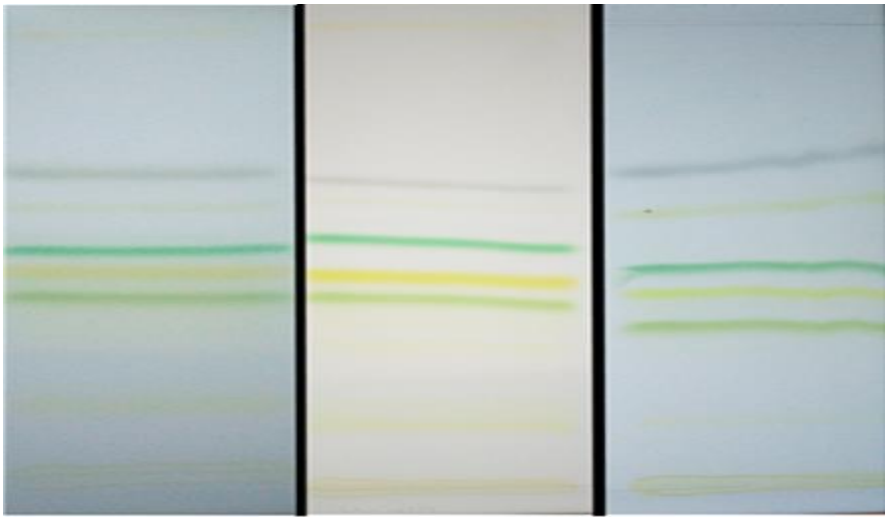

**Figure 4. 74** Chromatograph of growth stages of Potato crop 1, 2 and 3**.**

The colors of the chromatograms are of good intensity. The α and β carotene band corresponded to the first spot since carotenes are the least polar. Xanthophyll (lutein) appeared between chlorophyll a and chlorophyll b, due to the difference in molecular weight and polarity.

Chlorophyll b molecular weight is higher than that of lutein. The gray band located below the carotene was a degraded product of chlorophyll (pheophytin). Between the chlorophyll a and the gray spot, a yellow spot is observed; this spot may be due to a deposit of carotenes during their elution.

**Table 4. 28** Frontal ratio of different photosynthetic pigments of Potato crop

| **Pigments' color** | **Photosynthetic pigments** | **Stages of growth** | | |
|---|---|---|---|---|
| | | **Stage 1** | **Stage 2** | **Stage 3** |
| Yellowish Orange | Carotene α and β | 0.98 | 0.98 | 0.98 |
| Grey | Pheophytin (a breakdown product) | 0.65 | 0.66 | 0.65 |
| Blueish Green | Chlorophyll a | 0.50 | 0.50 | 0.51 |
| Yellowish Green | Lutein ( a xanthophyll) | 0.40 | 0.40 | 0.41 |
| Dark Green | Chlorophyll b | 0.37 | 0.37 | 0.38 |

The frontal ratio of carotenes (Rf = 0.98) was the same value for all growth stages. Chlorophyll a presented slightly different ratios at the various growth stages. The same trend was observed for chlorophyll b as well as the case of lutein and pheophytin (see figure 4.74).

#### 4.3.3.6.1 Spectral analysis of crude extract of potato leaves

Absorption spectra of the collected potato crop leaves' extracts at its different growth stages are presented in figure 4.75. These spectra reveal the optical properties of potato during its growth.

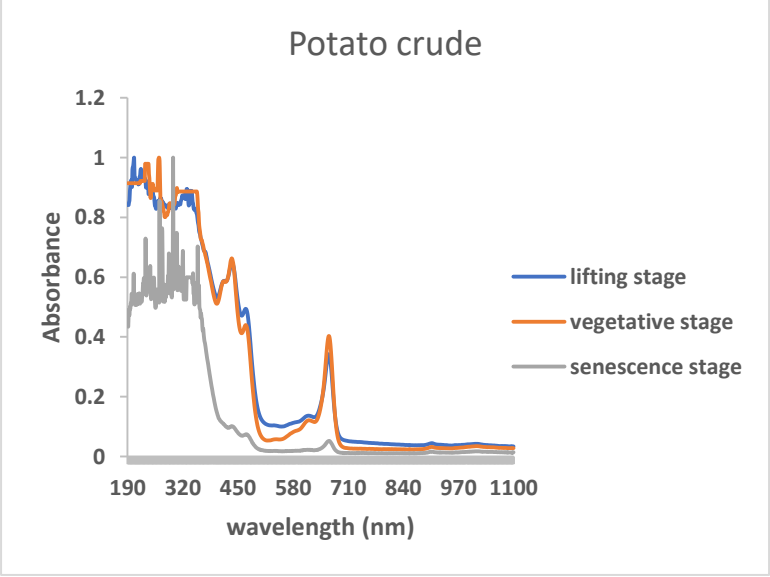


**Figure 4. 75** Graphs of absorbance of Potato crop crude extract at different growth stages

Figure 4.75 present the absorption spectra of potato crop leaves' extracts. Absorbance spectra presented three regions, the first between 200 and 400 nm which was characterized by artefacts unusable, the second region where all the peaks could be observed which was between 400 and 700 nm and a third region between 700 and 1100 nm where no absorbance was noticed. The peaks were five in number (413, 435, 470, 625, 665 nm) and all located in the visible light region. The three sharp peaks in the 400 to 500 nm range characterized carotenoids and chlorophylls. In whole, absorbance decreased in this order: lifting stage, vegetative or tuber formation stage and senescence stage. Thus, the number of photosynthetic pigments decreased drastically during potato growth stages. However, between 600 nm and 700 nm where the absorbance was most intense, the absorbance at vegetative stage was highest followed by the one at tuber formation or vegetative stage and at last the one at senescence stage. The plant absorbed less light in the senescence stage; maybe this was due to yellowing of the plant at that stage. A peak was observed around 650 nm, this peak characterized the presence of chlorophyll-b showing its second peak compared to that of chlorophyll-a observed around 625 nm.

The light requirement of the potato crop for the synthesis of photosynthetic pigments gradually decreased as the plant was growing. In fact, the essential radiation was found with the visible light region with a strong absorption around 665 nm.

#### 4.3.3.6.2 Spectral analysis of separated pigments of potato leaves

The different photosynthetic pigments obtained after thin layer chromatography were characterized through the absorption spectra shown on the figure 4.76 to 4.80.

The absorbance of potato crop's carotene (α and β carotenes) evolved upwards from lifting stage to senescence stage. The main absorbance band of carotenes was between 400 to 500 nm. No carotene absorbance peak appeared clearly within which mean that carotene content was low or almost non-existent in the potato leaves.

In potato crop leaves, the absorbance of chlorophyll-a was lower at the stage of senescence than at other growth stages. This may be due to the yellowing of the plant's leaves at this stage. Two absorbance peaks were noted over the entire study: one at 414 nm and another 666 nm. These peaks are specific to chlorophyll-a. The peak at 414 nm is more intense than that at 666 nm. This is probably due to the fact that at that stage starch produced by the crop through photosynthesis is accumulated in the tuber.

The absorption of chlorophyll-b evolved downward from the lifting stage to the stage of senescence of potato crop. This gradual drop in absorbance may be due to the need for chemical energy of the plant since chlorophyll-b transfers all the energy received to chlorophyll-a. Two peaks characteristic of chlorophyll-b were noted: one at 463 nm and the other at 648 nm.

The absorbance of lutein was greater at the lifting stage than vegetative and senescence stage. Specific peaks for lutein (a xanthophyll) absorbance were located around 445 nm and 475 nm.

Pheophytin is a degraded pigment of chlorophyll-a or b, spectra of absorption confirmed it. The absorbance of pheophytin in potato crop followed the same trend as in the cases of chlorophylls. Two peaks were noticed: one to 410 nm and another at 667 nm which both correspond to those of chlorophyll-a. This further implies that the content of chlorophyll-a is higher than that of chlorophyll-b in the potato crop throughout all of its growth stages.

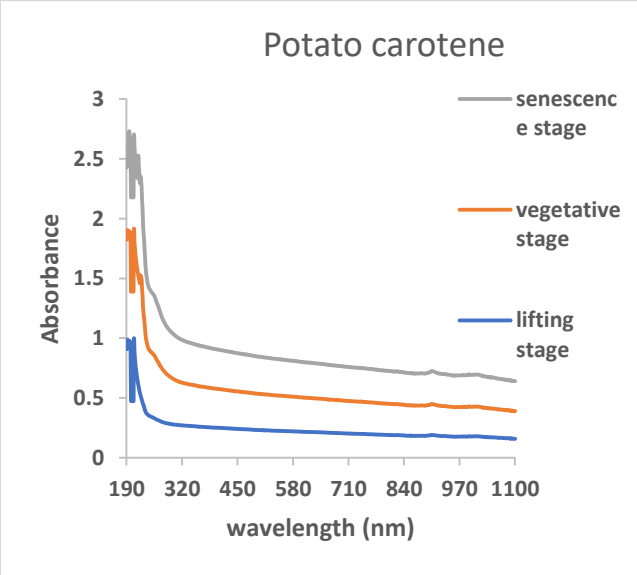


**Figure 4. 76** α and β Carotene graphs from potato extract

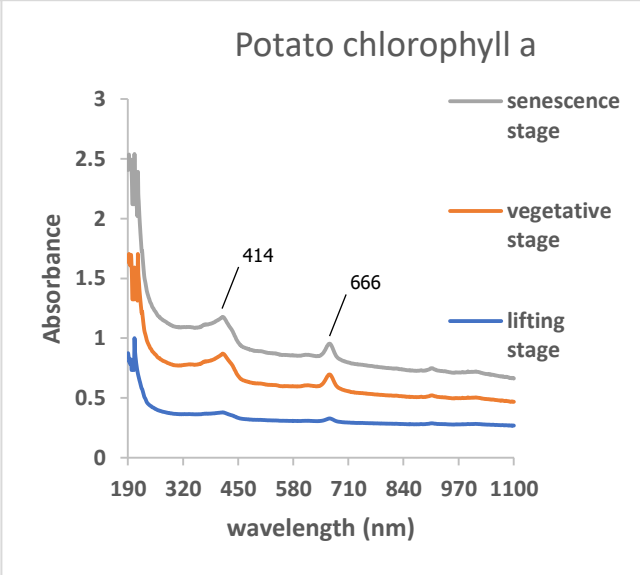


**Figure 4. 77** Chlorophyll a graphs from potato extract

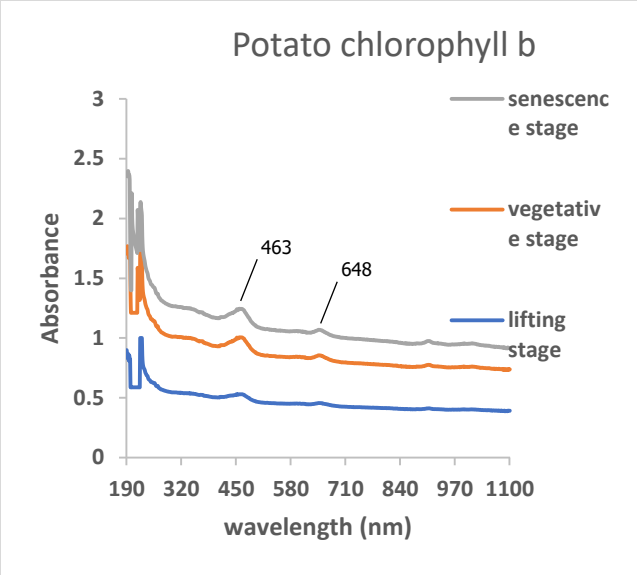


**Figure 4.** 78 Chlorophyll b graphs from potato extract

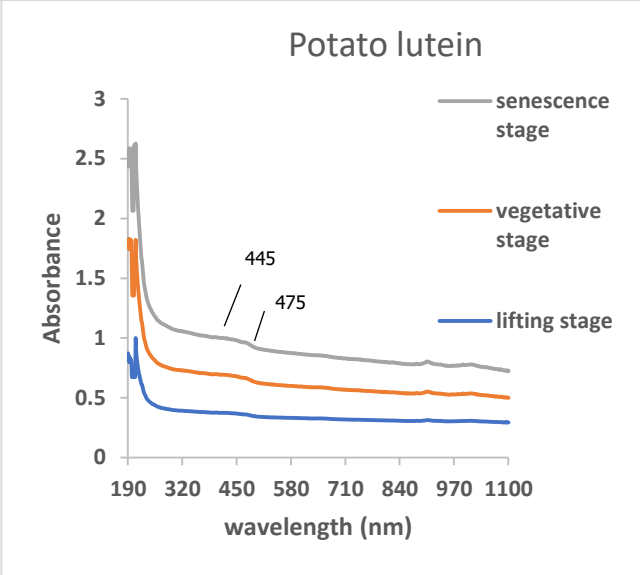


**Figure 4. 79** lutein graphs from potato extract

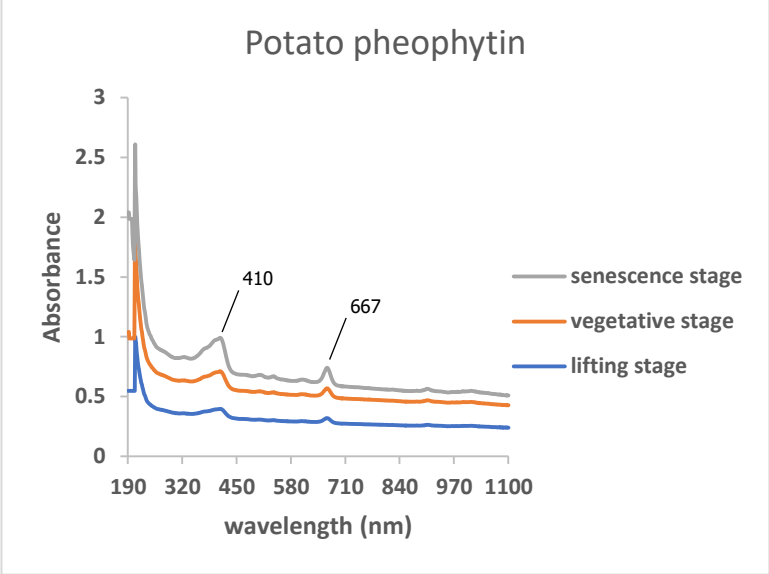


**Figure 4. 80** Pheophytin graphs from potato extract

#### 4.3.3.7 Sweet pepper crop extract characterization

##### 4.3.3.7.1 Overall analysis

The analysis of the different sweet pepper leaves extracts shows the chromatogram results following (Figure 4.81):

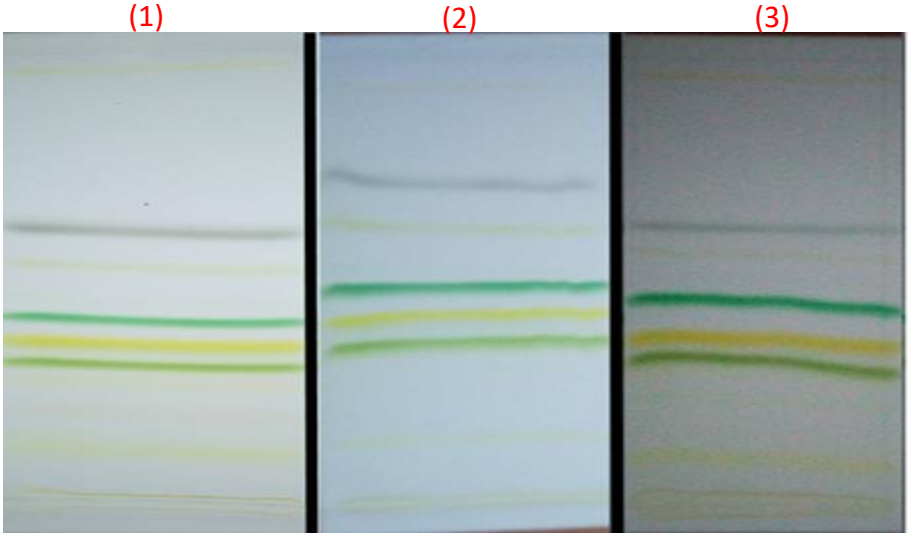


**Figure 4. 81** Chromatograph of growth stages of sweet pepper crop 1, 2 and 3

The chromatograms in Figure 4.81 present photosynthetic pigments of sweet pepper plant according to its growth stages. Thus, on each TLC plate was presented the following pigments from bottom to top order: chlorophyll b, lutein, chlorophyll a, pheophytin (gray stain) and α and β carotene. Pigment migration was made possible due to the difference in polarity and molecular weight. The less intense spots were places of deposit which was the beginning of interaction with silica layer.

**Table 4. 29** Frontal ratio of different photosynthetic pigments of Sweet pepper crop

| **Pigments' color** | **Photosynthetic pigments** | **Stages of growth** | | |
|---|---|---|---|---|
| | | **Stage 1** | **Stage 2** | **Stage 3** |
| Yellowish Orange | Carotene α and β | 0.99 | 0.99 | 0.99 |
| Grey | Pheophytin (a breakdown product) | 0.66 | 0.70 | 0.67 |
| Blueish Green | Chlorophyll a | 0.50 | 0.53 | 0.51 |
| Yellowish Green | Lutein ( a xanthophyll) | 0.40 | 0.42 | 0.41 |
| Dark Green | Chlorophyll b | 0.37 | 0.38 | 0.37 |

From this table 4.29, non-polar carotene (α and β) molecule migrated with the solvent front, hence, a frontal ratio of 0.99 at each phase. However, in the case of chlorophyll a, there was a variation from one stage to another. In chlorophyll b, the frontal ratio was the same at the first and at the last growth stage of the plant, whereas at the flowering stage it increased by 0.01 unit and became 0.38. Lutein exhibited a frontal ratio varying with the stage. This was the same case as in the pheophytin spot lines.

#### 4.3.3.7.2 Spectral analysis of crude extract of sweet pepper leaves

Figure 4.82 presents the absorbance spectra of the leaves' extracts from the sweet pepper crop during its growth (advanced lifting, flowering and fruiting stage).

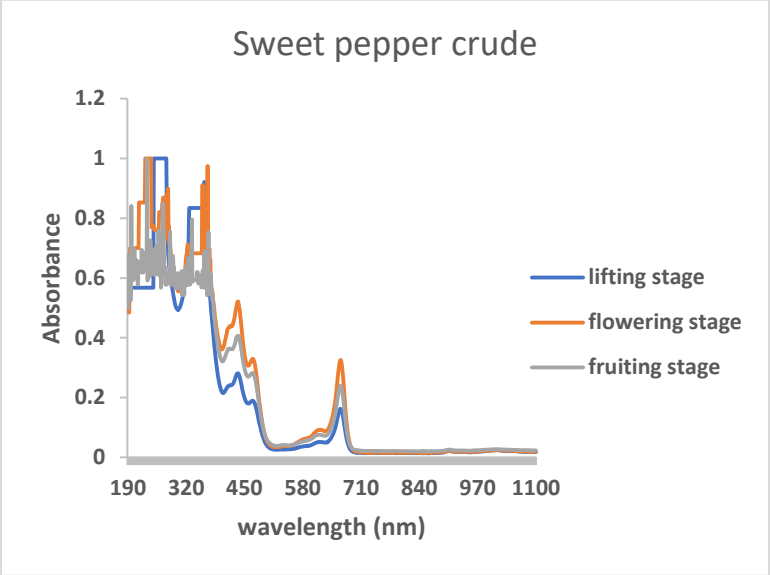


**Figure 4. 82** Graphs of absorbance of Sweet pepper crop crude extract at different growth stages

The absorption spectra in Figure 4.82 showed a strong absorbance within the interval 300 to 500 nm peaks at 415, 435 and 468 nm. These peaks were specific to pigments photosynthetic such as carotenes, chlorophylls and lutein (a xanthophyll). The second interval 600 and 700 nm showed a peak at 665 nm. These are characteristic peaks of chlorophylls. Absorbance was greater at the flowering stage and even less weak advanced lifting stage than at the fruiting stage. This means that Sweet pepper crop synthesized less xanthophyll at advanced lifting stage than at the other two stages. That implies a less need in light at that growth stage.

#### 4.3.3.7.3 Spectral analysis of separated pigments of Sweet pepper leaves

Figure 4.83 to 4.87 compiles absorption spectra of photosynthetic pigments found in Sweet pepper leaves extract after thin layer chromatography.

The absorbance band of α and β carotenes was mainly between 400 and 500 nm. The carotene absorbance peaks were not clearly visible probably due to their low quantity or activity in the

leaves. However, it could be observed that more light was absorbed at advanced lifting stage than at the other stages. Therefore, carotenes were less synthesized at the end of growth stage.

Concerning chlorophyll-a, two characteristic peaks on the absorption spectra: one at 414 nm and another at 665 nm. The absorbance of the chlorophyll-a in green pepper leaves increased throughout its growth from lifting to fruiting stage.

In chlorophyll-b spectra, two characteristic peaks were noted: one at 462 nm and another at 650 nm. This was where Chlorophyll-b made heavy use of light. Absorbance was low in the range of 700 to 1100 nm and from 500 to 600 nm and a little less strong below 400 nm. Overall, the absorbance decreased from the beginning to the end of the plant's growth.

Spectral analysis of lutein pigments in Sweet pepper leaves revealed high absorbance in the range from 400 to 500 nm, at each absorption spectrum. Three characteristic peaks were clearly noted: at 420 nm, at 446 nm and at 475nm. Absorption was higher during lifting and fruiting stages than at flowering stage. The light requirement of green pepper for synthesis of lutein was more important at the beginning than at other stages.

Pheophytin, a degraded pigment of chlorophylls, exhibited absorbance peaks specific to chlorophylls in the ranges of 400 to 500 nm and 600 to 700 nm. From 190 to 450 nm, absorbance was greater at the flowering stage than at the fruiting stage, for these stages displayed peaks at 410 nm and 437 nm which are characteristics of pheophytin precursors, chlorophylls-a and -b. From 450 to 1100 nm, the absorbance at the advanced lifting stage was slightly higher than that of the fruiting stage which was seen at 665 nm wavelength, chlorophyll-a characteristic peak.

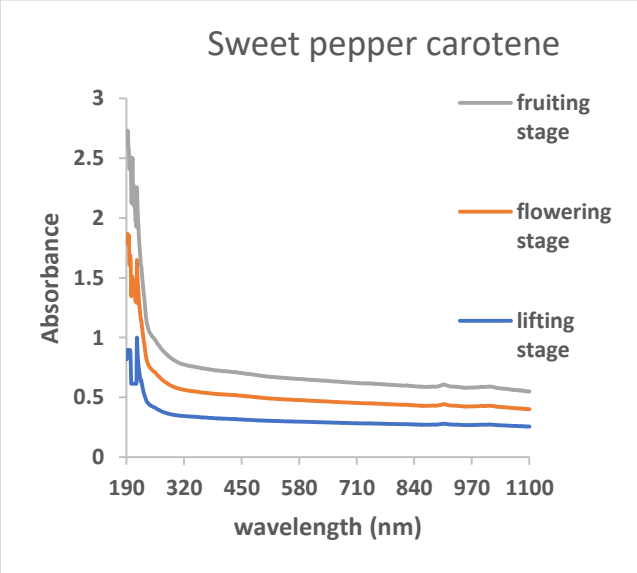


**Figure 4. 83** α and β Carotene graphs from sweet pepper extract

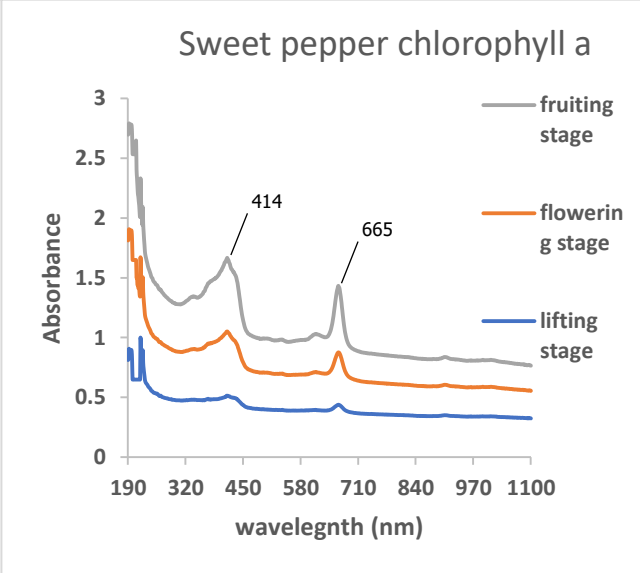


**Figure 4. 84** Chlorophyll a graphs from sweet pepper extract

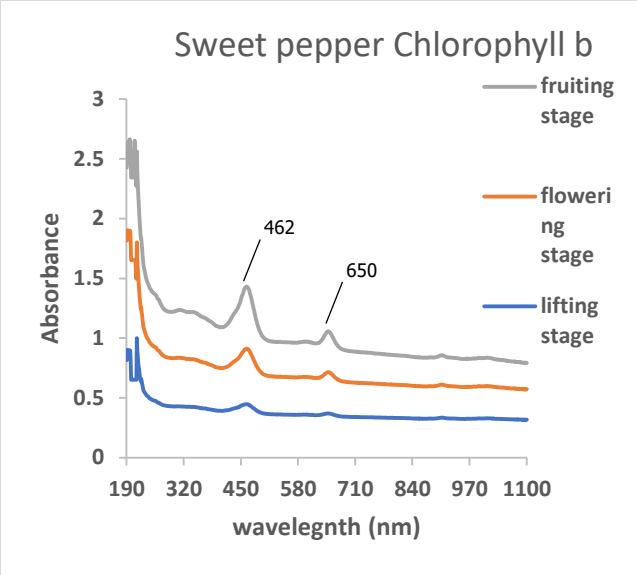


**Figure 4. 85** Chlorophyll b graphs from sweet pepper extract

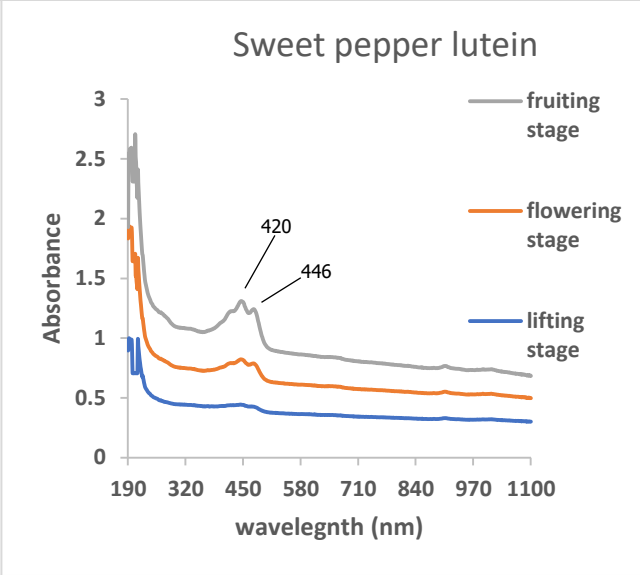


**Figure 4. 86** Lutein graphs from sweet pepper extract

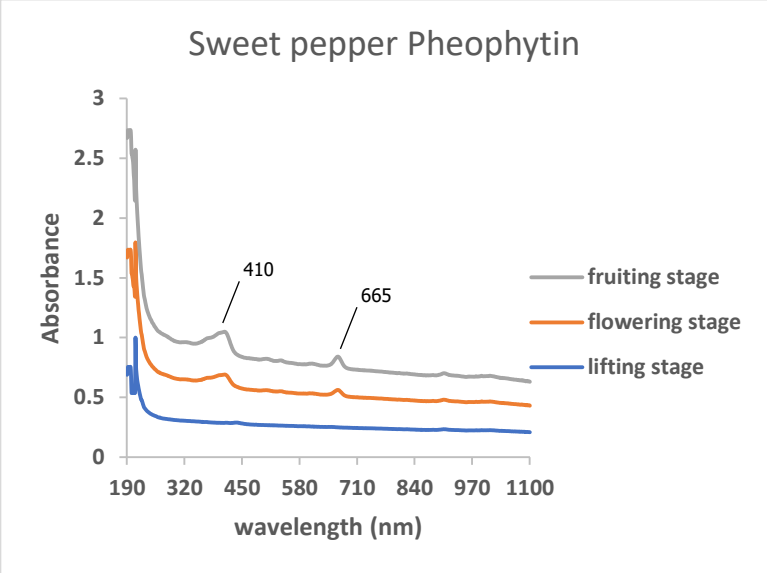


**Figure 4. 87** Pheophytin graphs from sweet pepper extract

## 4.4 Simultaneous crop cultivation under greenhouses and under ambient conditions greenhouse cooling technology

### 4.4.1 Physical and chemical constituents of soil and fertilizer used

Samples of soils were analysed. The samples were taken at 10 cm depth. Outside and greenhouse soils were taken from cultivation areas inside and outside the greenhouse after the various soils were arranged for cultivation.

**Table 4. 30.** Physical constituent of soil

| Reference | Granulometry (%) | | | | | |
|---|---|---|---|---|---|---|
| | **Clay** | **Silt fine** | **Silt coarse** | **Sand fine** | **Sand medium** | **Sand coarse** |
| | < 2µ | 2 µ à 20µ | 20 à 50µ | 50 à 200µ | 200 à 500µ | > 500µ |
| Outside | 0.62 | 2.14 | 14.28 | 31.25 | 48.07 | 3.64 |
| Greenhouse | 0.67 | 2.06 | 10.01 | 22.62 | 50.59 | 14.05 |

**Table 4. 31** Summarized Physical constituent of various soils

| Reference | Granulometry (%) | | |
|---|---|---|---|
| | **Clay Total** | **Silt total** | **Sand total** |
| Outside | 0.62 | 16.41 | 82.96 |
| Greenhouse | 0.67 | 12.07 | 87.25 |

The results from soil analysis are presented in the table 4.30 to 4.32. The samples presented a higher amount of sand 82.96% sand for outside soil and 87.25% sand for greenhouse soil. Silt content in all soils varied between 16.41% (for outside soil) 12.07% (for greenhouse soil) while clay content was below 1%. The high percentage of sand against little traces of silt make the soil have a sandy silk texture. Therefore, the soil is porous, very permeable to water and air, which leads to good aeration, good soil drainage and good root development.

**Table 4. 32** Chemical composition of various soils

| Reference | OM (%) | Carbon (%) | Nitrogen (%) | C/N (%) | Total Phosphorous (ppm) | Available Phosphorous (ppm) | pH |
|---|---|---|---|---|---|---|---|
| Outside | 1.10 | 0.64 | 0.06 | 10.60 | 54.4 | 6.4 | 7 |
| Greenhouse | 0.41 | 0.24 | 0.02 | 9.85 | 63.5 | 18.3 | 7 |

The chemical composition of the soils samples showed a high amount of phosphorous (63.5 ppm for greenhouse, 54.4 ppm for outside, 45.3 ppm for neutral)

**Table 4. 33** Small ruminant based fertilizer

| Reference | MM (%) | OM (%) | Carbon (%) | Nitrogen (%) | C/N (%) | Total Phosphorous (ppm) | Available Phosphorous (ppm) |
|---|---|---|---|---|---|---|---|
| Organic fertilizer | 28.40 | 71.60 | 29.93 | 2.03 | 14.78 | 335.5 | 34.1 |

MM = mineral matter; OM = organic matter; C/N = carbon to nitrogen ratio

Table 4.33 shows the composition of the organic fertilizer used in amending the soil. In fact, this fertilizer is derived from sheep dung. The analysis showed a high amount of phosphorous (335.5 ppm for total phosphorous, 34.1 ppm for available phosphorous). In fact, in replacement of cow dung, people in Niger usually use sheep dung to amend soils due to its availability as most Nigeriens rear sheep at home. Besides, many research proved that sheep dung based fertilizer is a good source of protein and keratin rich in Nitrogen, sulphur and Phosphorous (Górecki & Górecki, 2010).

### 4.4.2 Thermal analysis

The temperature pattern presented in figure 4.88 shows that outside temperature was much higher than that of the two greenhouses as expected (average of 36.04$^{o}$C for outside against 32.17 $^{o}$C and 30,71$^{o}$C for CN greenhouse (greenhouse with Celdek pad) and Dji Greenhouse (greenhouse with wood wool pad) respectively. Meanwhile, Wet bulb temperatures ranged from 17.50 $^{o}$C to 28$^{o}$C for greenhouses' microclimate and from 20.30 to 32.10$^{o}$C for outside environment (figure 4.89). The greenhouse made from imported coolers (CN GnH) had a higher temperature and humidity drop as shown in figure 4.89 and 4.90. That was obvious since these materials were also proven to be creating a relatively higher or more humid microclimate as mentioned in Djibrilla et al. (2021) which is the celdek based pad. Yet, the difference is little. In fact, from table 4.33, the lowest temperature during afternoon observed from CN greenhouse was 25.4 $^{o}$ C against 26.7 $^{o}$ C and average relative humidity was 68.88% against 62.15% for CN and Dji greenhouse respectively. Negative values in drops plots (figure 4.89 and 4.90) showed that at that instant, outside conditions were more comfortable. This occurred during a rain even where relative humidity is higher outside than inside greenhouses (see rain event from weather station data). More detailed are shown in figure 4.95, 4.96 and 4.97 where individual temperature and humidity are displayed. Furthermore, it was observed that water out of the cooling process

became cool since it took away some of the heat. The temperature of the Water recovered ranged from 19.50 $^{o}$ C to 21.50 $^{o}$ C (figure 4.94). Reusing that water for the next cooling process could improve cooling efficiency ( Djibrilla et al., 2021)

The light irradiances in the two greenhouses are similar with averages of 80.33 w/m$^2$ and 73.81 w/m$^2$ for CN GnH and Dji GnH respectively. More sunlight was detected in CN GnH because it was located at the east of the Dji GnH causing some shades for the latter. These averages were way lower than outside conditions which was 555.71 w/m$^2$. In fact, from table 4.1 and 4.2, the fiber used as greenhouse covering material has the ability to reduce incident light by up to 92.80%. The availability of light is known to be a limiting factor in the productivity of sheltered crops cultivation as experimented by Iraqi et al. (1997) and Vallières (2018) (Iraqi et al., 1997; Vallières, 2018).

Figure 4.86 show the $CO_2$ content in the two greenhouses against outside environment. As expected, the amount of $CO_2$ in the two greenhouses was higher than outside which were 912.10 ppm for CN GnH and 913.50 ppm for Dji GnH against 898.08 ppm for outside. Plants gathered in confined environment cause gases content within the microclimate to climb as the rule of greenhouse gases emission. Plants emit $CO_2$ during the evapotranspiration process.

Figure 4.87 present the vapor pressure deficit (VPD) pattern inside and outside the greenhouses. VPD of outside environment was higher than that of the two greenhouses with the CN GnH have the lowest pattern. Under normal circumstances Low vapor pressure deficits (VDP) are limiting factors in the productivity of sheltered crops since the absorption of nutrients from the growing medium is directly related to the flow of water through the plant directed by the evapotranspiration as quoted in Iraqi et al. (1997) and Vallières (2018). The actual values from the experiment were 508.88 Pa for CN GnH, 781.51 Pa for Dji GnH and 1270.51 Pa for Outside.

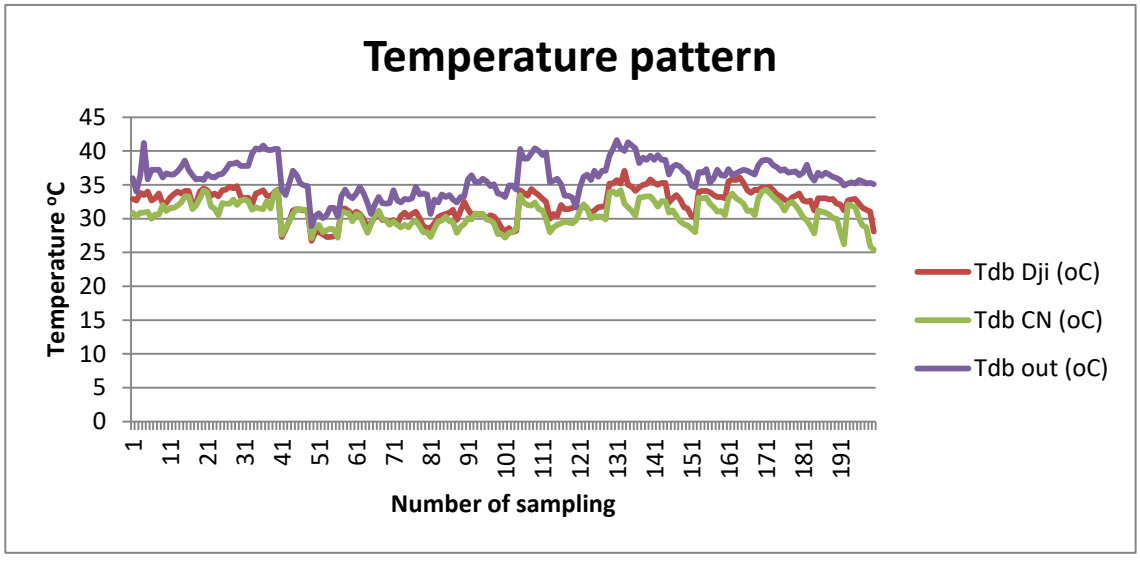


**Figure 4. 88** Dry bulb temperature graphs

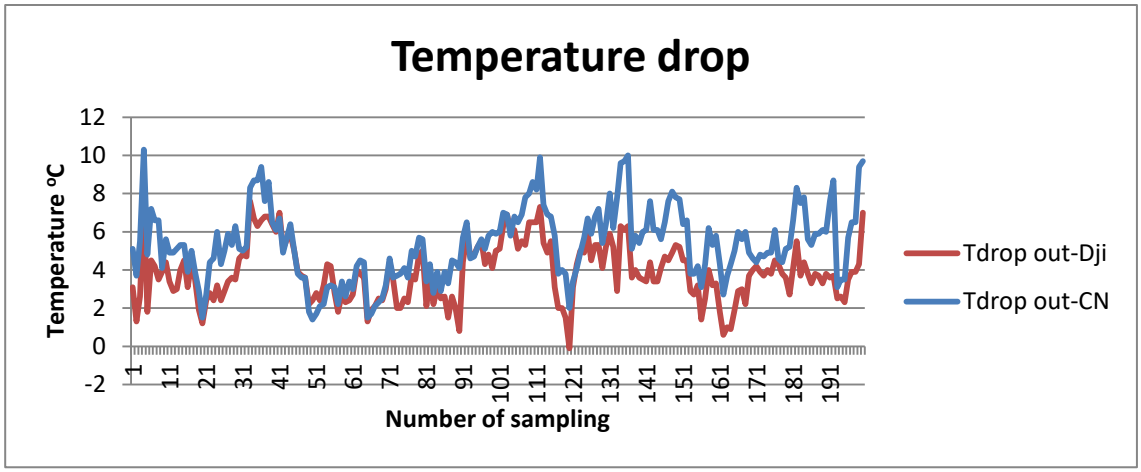


**Figure 4. 89** Greenhouse temperature drop relative to outside environment

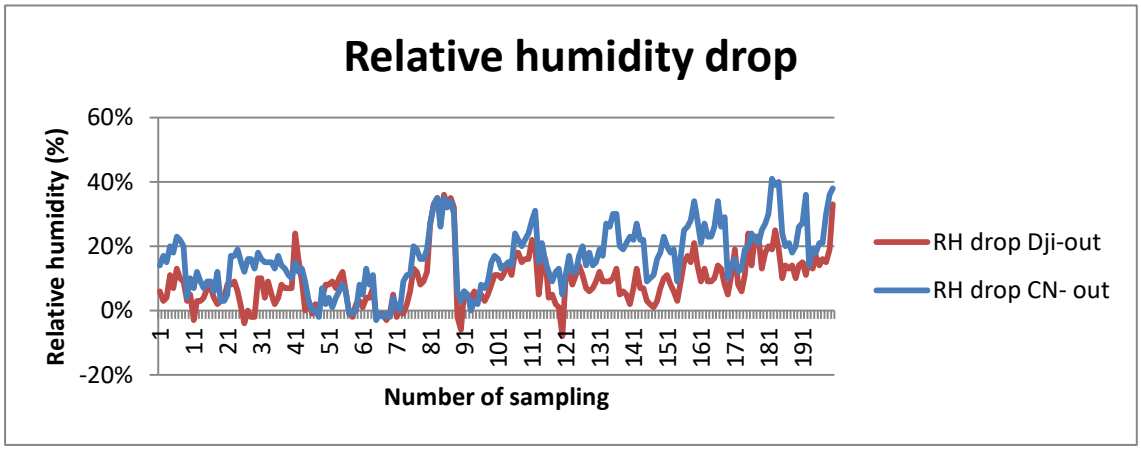


**Figure 4. 90** Greenhouse relative humidity drop relative to outside environment

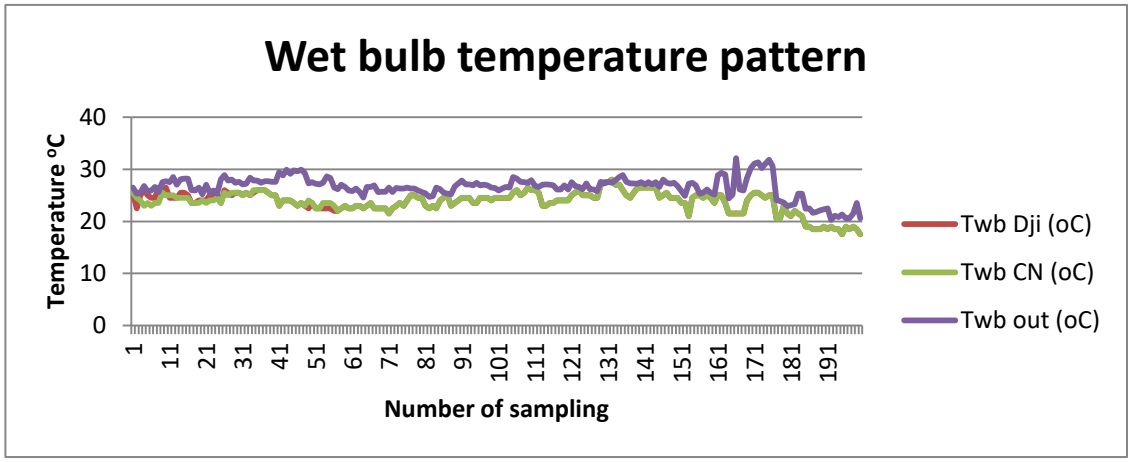


**Figure 4. 91** Wet bulb temperature graphs

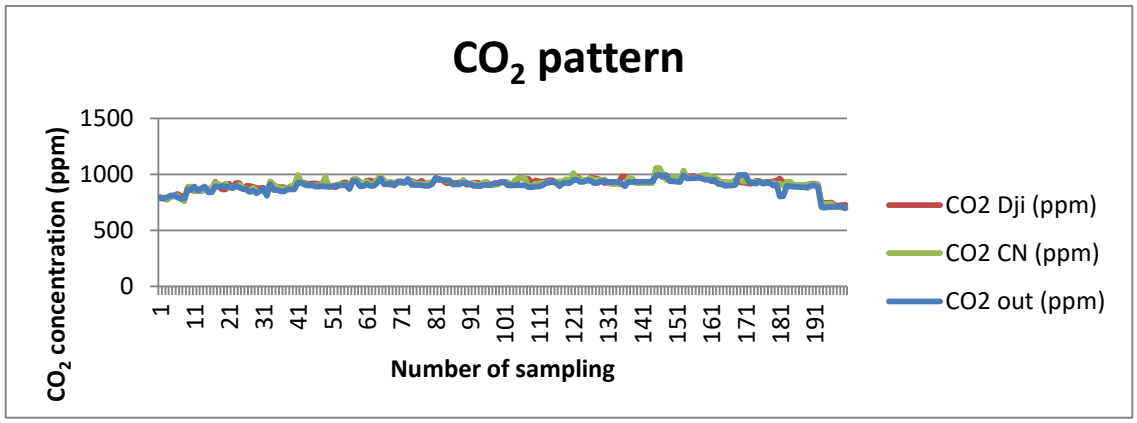


**Figure 4. 92** $CO_2$ graphs

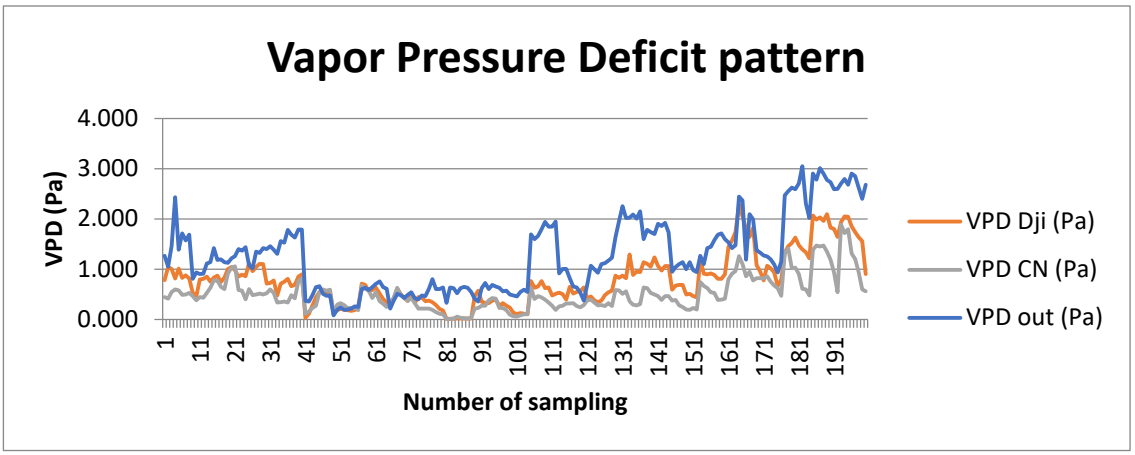


**Figure 4. 93** Vapor Pressure Deficit graphs

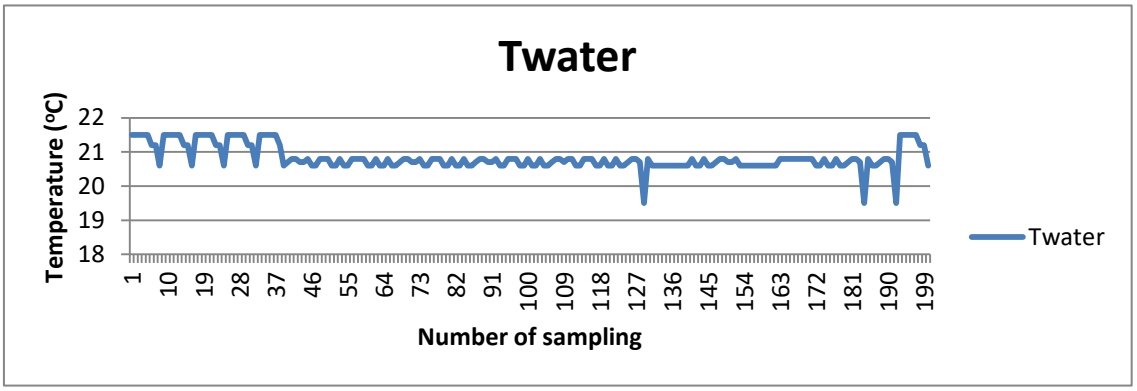


**Figure 4. 94** Recovered water graphs

**Table 4. 34** CN greenhouse summarized microclimate data

| | **Twb CN (°C)** | **Tdb CN (°C)** | **VPD CN (Pa)** | **$CO_2$ CN (ppm)** | **RH CN (%)** | **Irradiance w/m²** |
|---|---|---|---|---|---|---|
| Min | 17.50 | 25.40 | 8.19 | 698.00 | 29.00% | 8.80 |
| Max | 28.00 | 34.30 | 1882.38 | 1057.00 | 99.00% | 751.00 |
| Average | 23.73 | 30.71 | 508.88 | 912.10 | 68.88% | 80.33 |

**Table 4. 35** Dji greenhouse summarized microclimate data

| | **Twb Dji (°C)** | **Tdb Dji (°C)** | **VPD Dji (Pa)** | **$CO_2$ Dji (ppm)** | **RH Dji (%)** | **Irradiance w/m²** |
|---|---|---|---|---|---|---|
| Min | 17.50 | 26.70 | 11.04 | 721.00 | 27.00% | 8.60 |
| Max | 28.00 | 37.10 | 2283.59 | 1016.00 | 99.00% | 762.00 |
| Average | 23.77 | 32.17 | 781.51 | 913.50 | 62.15% | 73.81 |

**Table 4. 36** Outside environment summarized weather data

| | **Twb out (°C)** | **Tdb out (°C)** | **VPD out (Pa)** | **$CO_2$ out (ppm)** | **RH out (%)** | **Irradiance w/m²** |
|---|---|---|---|---|---|---|
| Min | 20.30 | 28.90 | 77.86 | 698.00 | 15.00% | 61.16 |
| Max | 32.10 | 41.60 | 3047.96 | 996.00 | 78.00% | 1097.00 |
| Average | 26.55 | 36.04 | 1270.51 | 898.08 | 52.83% | 555.71 |

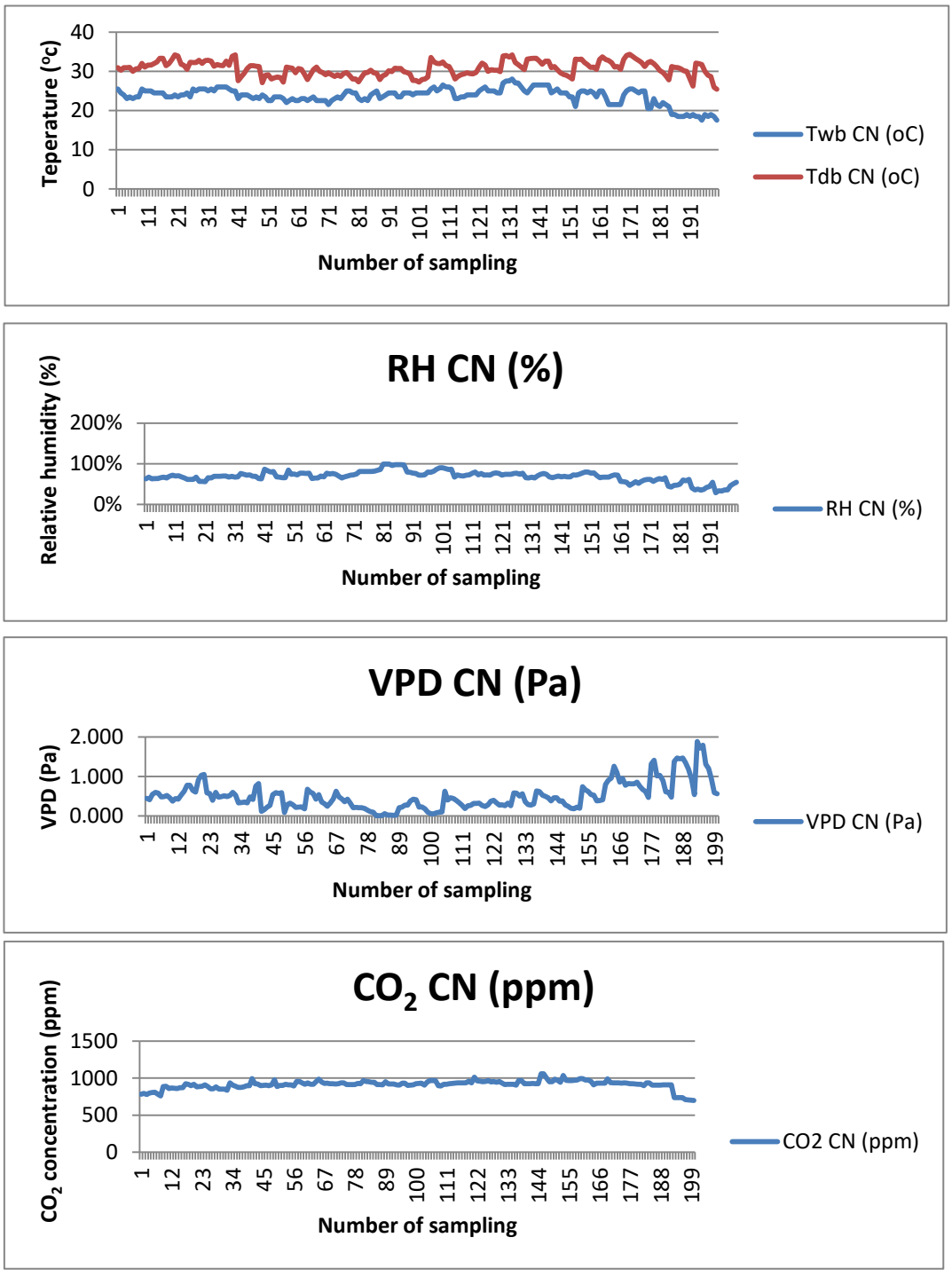


**Figure 4. 95** Temperature, relative humidity, vapour pressure deficit and $CO_2$ graphs for CN greenhouse

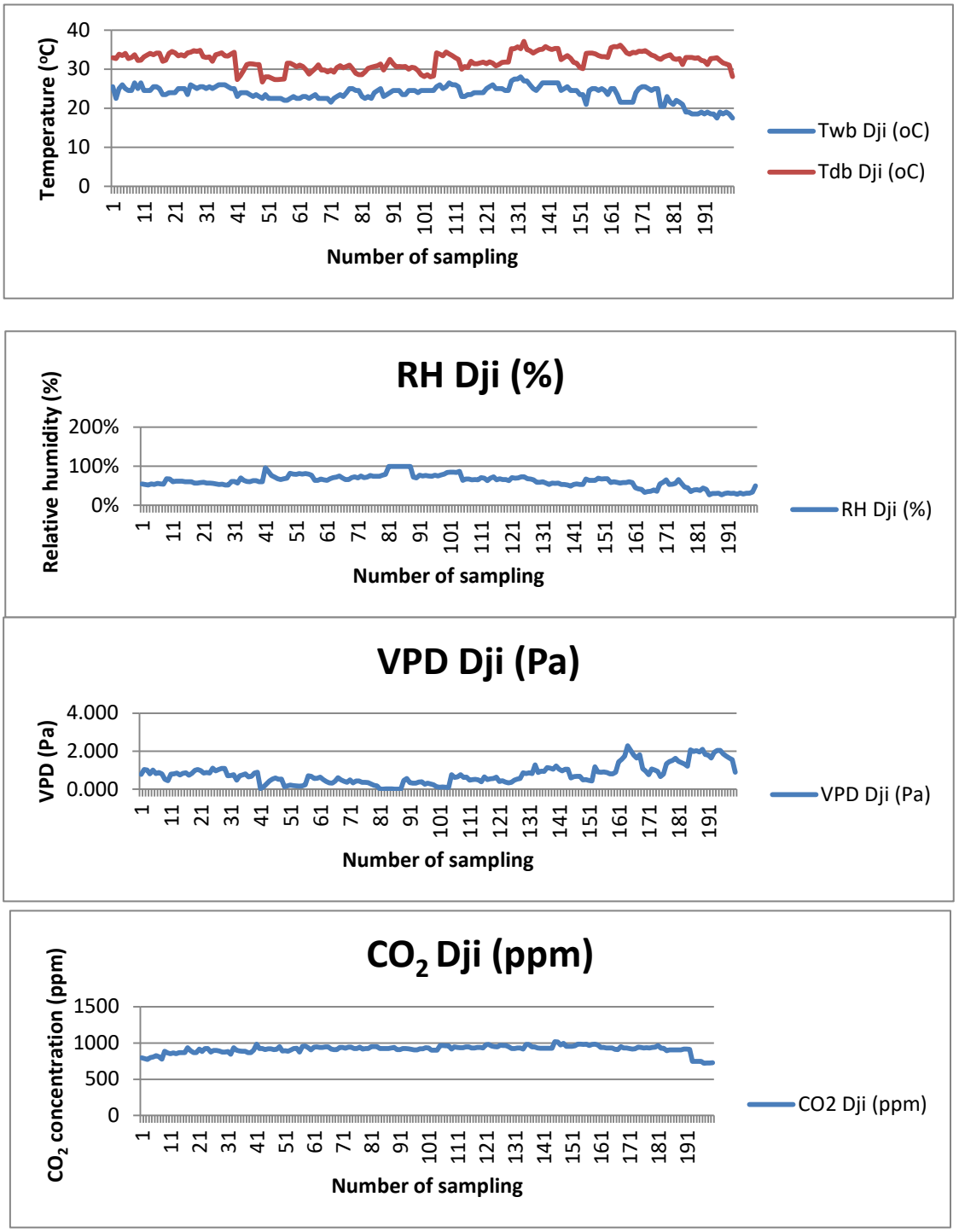


**Figure 4. 96** Temperature, relative humidity, vapour pressure deficit and $CO_2$ graphs for Dji greenhouse

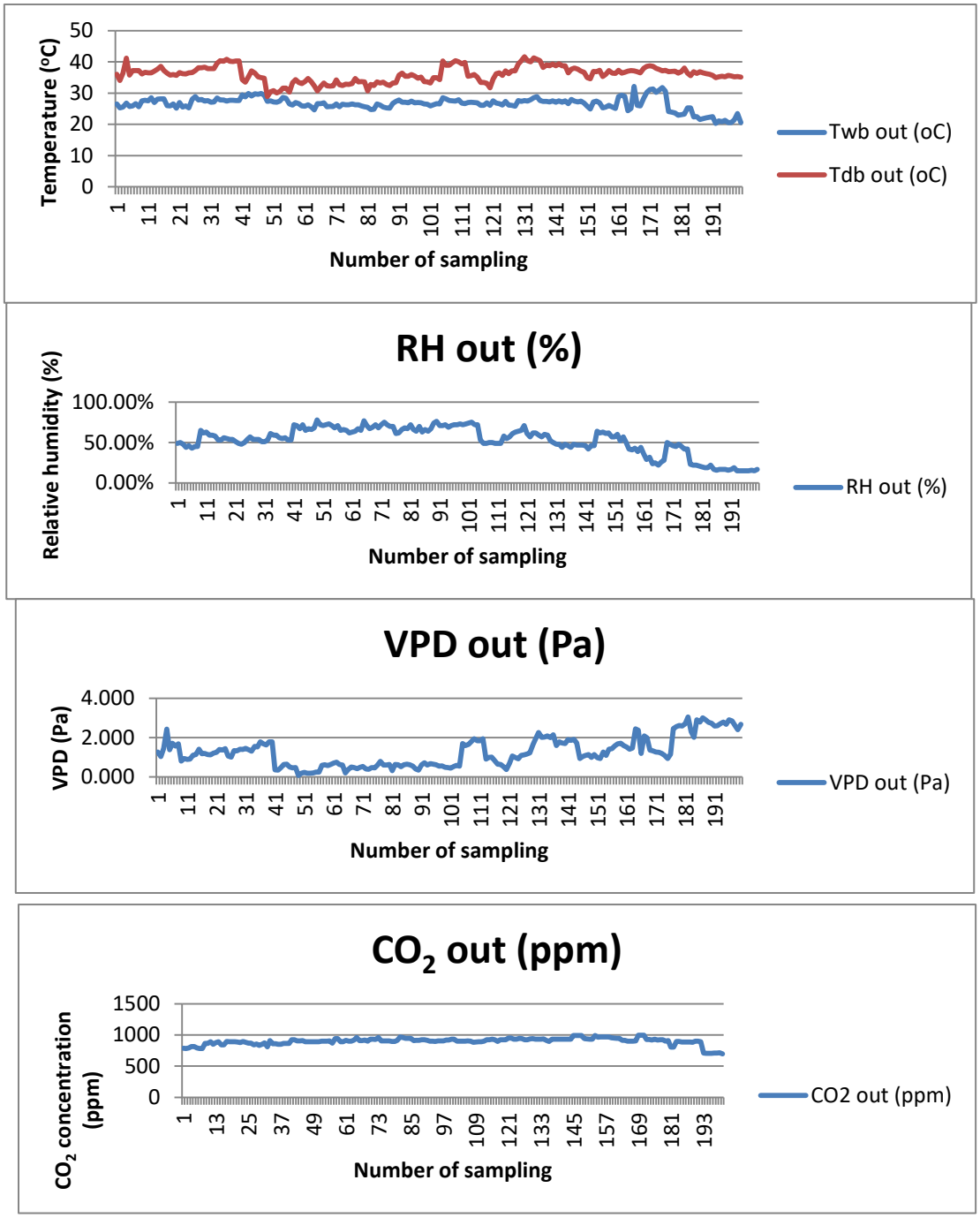


**Figure 4. 97** Temperature, relative humidity, vapour pressure deficit and $CO_2$ graphs for outside environment

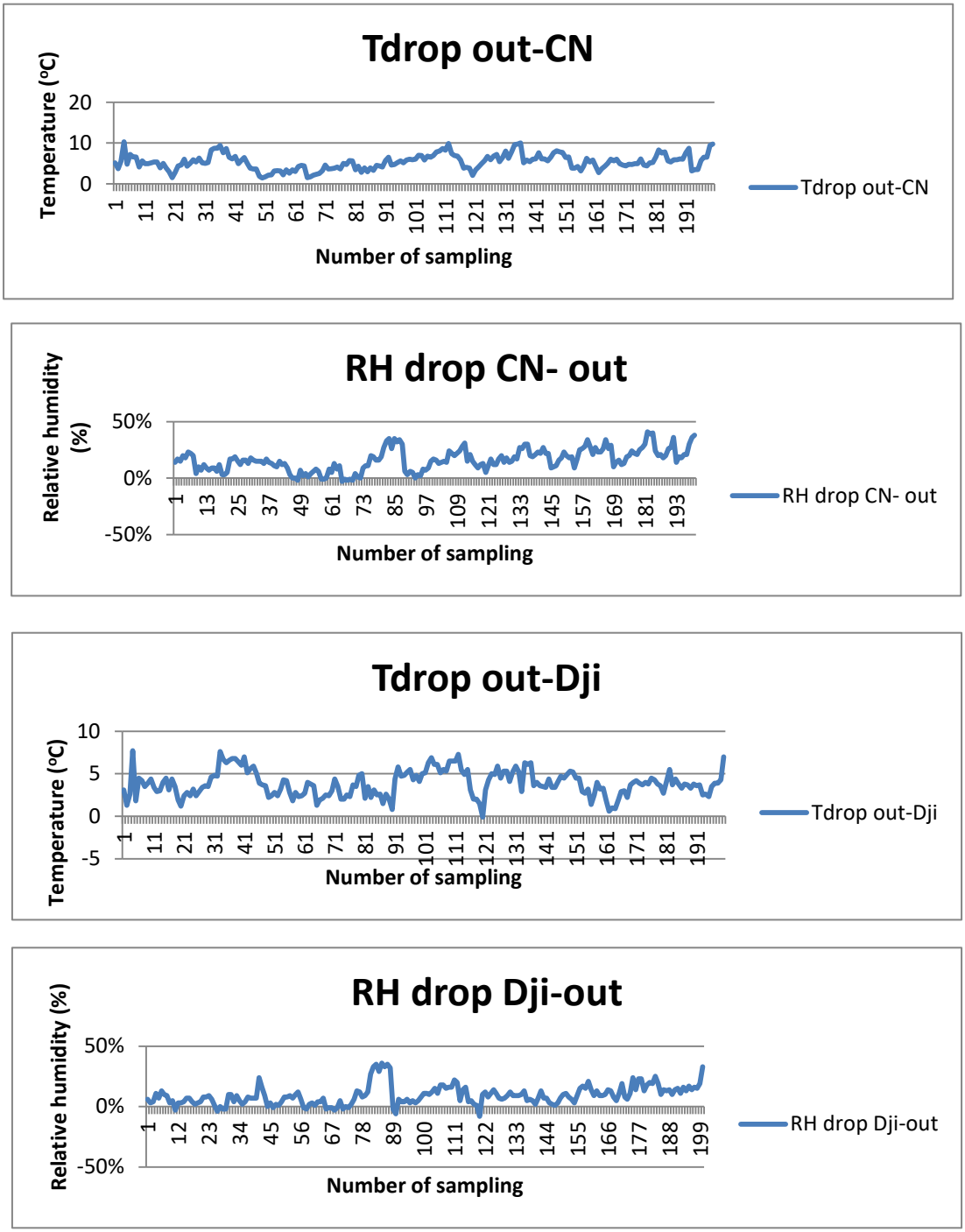


**Figure 4. 98** .Comparative drop in weather parameters between greenhouses and outside environment

### 4.4.3 Agricultural analysis

#### 4.4.3.1 Plant physical properties

The plants' physical data started the first (1) week after transplantation. With the aid of a measuring tape and a weighing scale, plants' height and fruit weight were recorded twice a week on Wednesdays and Saturdays from 30/07/2022 to 29/10/2022; in other terms, till constant heights were observed during harvesting period.

**Table 4. 37** Water and fertilizer used

| | Plot area | | | | | | Total |
|---|---|---|---|---|---|---|---|
| | **Line 1** | **Line 2** | **Line 3** | **Line 4** | **Line 5** | **Line 6** | |
| **Organic fertilizer before transplanting (g)** | 5220 | 5220 | 5220 | 5220 | 5220 | 5220 | 31320 |
| **Organic fertilizer after flowering stage (g)** | 870 | 870 | 870 | 870 | 870 | 870 | 5220 |
| **Water sprinkling before fruiting stage (L)** | 10 | 10 | 10 | 10 | 10 | 10 | 60 |
| **Water sprinkling after fruiting stage (L)** | 20 | 20 | 20 | 20 | 20 | 20 | 120 |

Table 4.37 shows the type of fertilizer used for this study. 31.32 kg of sheep or small ruminant based fertilizer was used over the exploited area (42.5 $m^2$) at the beginning before the transplantation of the nursery. 5.22 kg of the fertilizer was added at the flowering stage to prepare for the fruiting stage. Moreover, the amount of water used during the cultivation was about 60 liters before fruiting stage and that amount doubled to 120 L from the fruiting stage to harvesting stage. The amount was adjusted according to the demand of the plant and experience obtained from local farmers as well as recommendations from local seed providers.

Figure 4.99 to 4.104 present the physical aspects of plants studied during their growth stages. Due to good weather conditions created by greenhouse's microclimate, tomatoes crops grew higher and could reach a height of 190 cm for Dji GnH and 160 cm for CN GnH compared to a maximum of 80 cm high under ambient conditions. The combination of favorable light intensity (average = 71.83 $w/m^2$ (Dji GnH) and 80.33 $w/m^2$ (CN GnH)), relative humidity (average = 62.15% (Dji GnH) and 68.88% (CN GnH)) and temperature (average = 32.17 (Dji GnH) and 30.17 $^oC$ (CN GnH)) within the various microclimates allowed leaves to open up and reach an area of 50 $cm^2$ and 60 $cm^2$ for Dji GnH and CN GnH respectively against 15 $cm^2$ under outside condition. However, the number of leaves formed by various plants did not follow that trend. In fact, from Dji GnH, a maximum of 48 leaves (big composite leaves) was observed on a plant against 72 leaves (big composite leaves) in CN GnH and 58 leaves (small composite leaves) outside greenhouses.

A cut of various fruits showed that fruits from the greenhouses were more intense in color than the ones cultivated outside. This influences the nutritional values of harvest products (see figure 4.105).

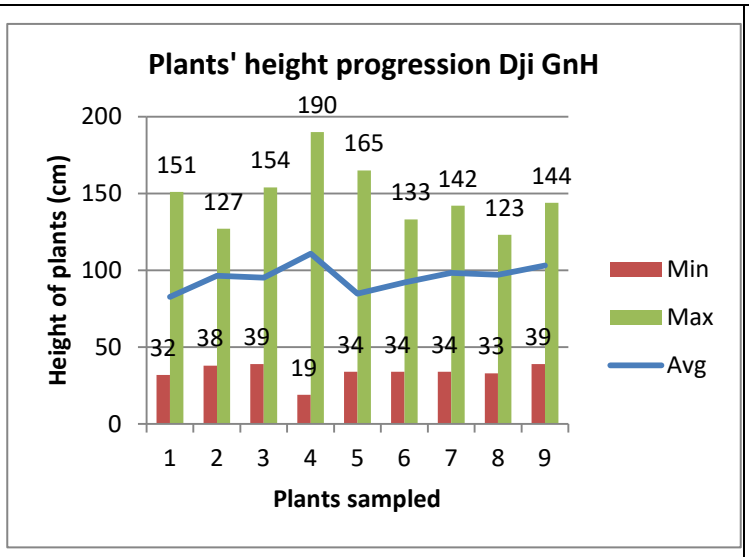


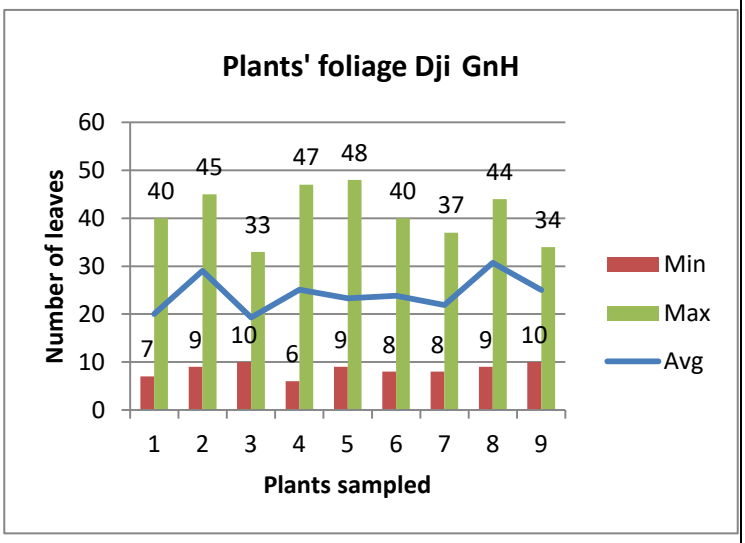


**Figure 4. 99**Plants' height and foliage progression in Dji GnH

**Table 4. 38** Dji GnH leaves size

| Leaves average size Dji GnH | | |
|---|---|---|
| Length (cm) | Width (cm) | Area ($cm^2$) |
| 10 | 5 | 50 |

**Figure 4. 100**.Fruit from Dji GnH

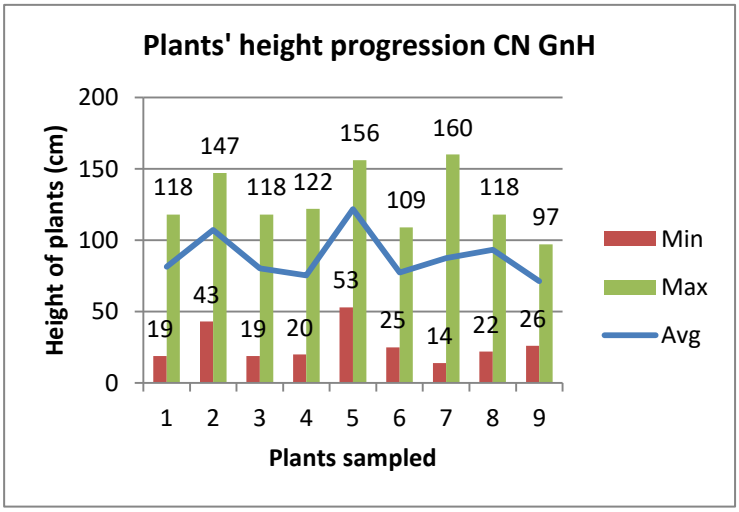


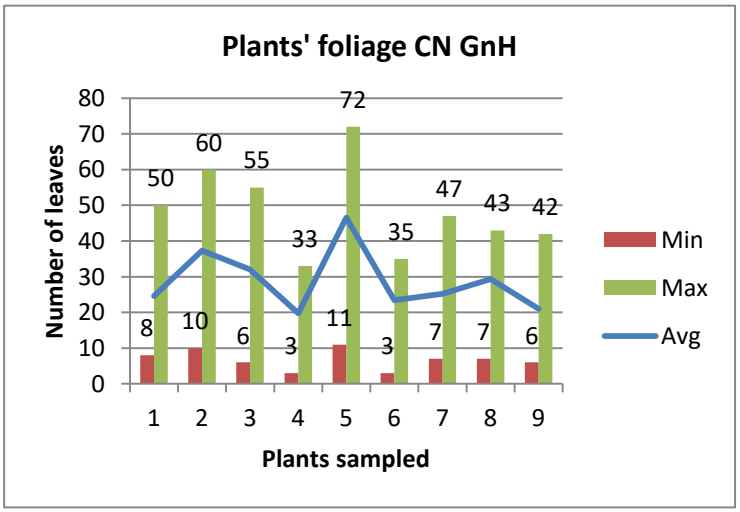


**Figure 4. 101** Plants' height and foliage progression in CN GnH

**Table 4. 39** CN GnH leaves size

| Leaves average size CN GnH | | |
|---|---|---|
| Length (cm) | Width (cm) | Area ($cm^2$) |
| 10 | 6 | 60 |

**Figure 4. 102** Fruit from CN GnH

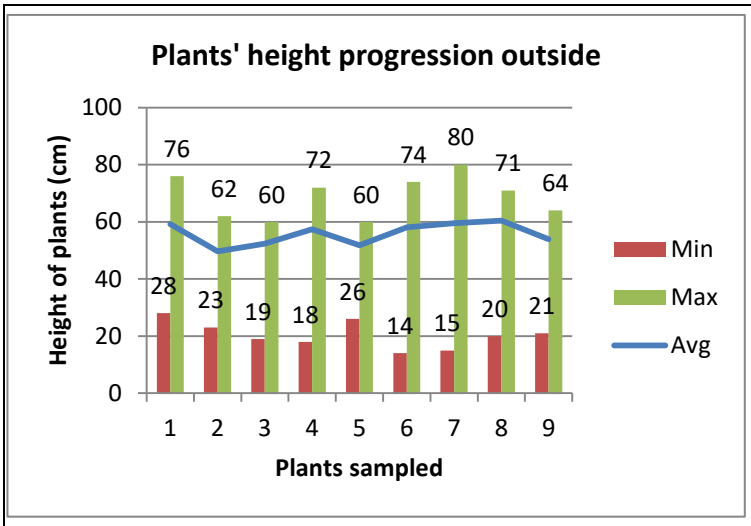


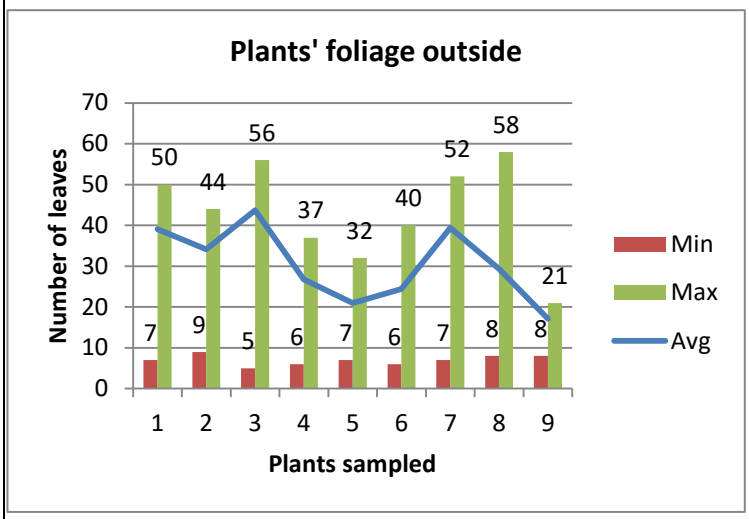


**Figure 4. 103** Plants' height and foliage progression outside GnH

**Table 4. 40** Outside GnH leaves size

| Leaves average size outside | | |
|---|---|---|
| Length (cm) | Width (cm) | Area ($cm^2$) |
| 6 | 2.5 | 15 |

**Figure 4. 104** Fruit from outside GnH

Fruits from outside | Fruits from greenhouses

**Figure 4. 105**.Fruit from outside (left) VS fruit from Greenhouses (right)

**Figure 4. 106**.Outside plantation

**Figure 4. 107**.Inside greenhouse plantation

#### 4.4.3.2 Harvest analysis

##### 4.4.3.2.1 Fruit production analysis

Fruit harvesting started about 48 days after transplantation under ambient conditions (outside and outside bonus) against 81 days under Dji and CN Greenhouse (Dji GnH and CN GnH). Light availability and low ventilation within the greenhouse were advanced to be the cause of this delay in fruiting stage within the greenhouse. (see table 4.41 to 4.44).. In fact, the experiment of Iraqi et al. (1997) and Vallières (2018) confirmed that the availability of light is known to be a limiting factor in the productivity of sheltered crops cultivation (Iraqi et al., 1997; Vallières, 2018). Furthermore, the greenhouse covering material filters sun radiations to some extend as shown in the spectrum of the covering material from figure 4.4. As mention by Carlini et al. (2012), certain radiations are necessary for plants' growth (Carlini et al., 2012) Besides, tomatoes plant needed a ventilation or aeration. Other reasons were that, all this could be linked to the variety which was for the Sahel harsh condition. Because of those unpredicted sources of delay, less fruit were produced within the greenhouse compare to outside conditions. In fact, expanded over a hectare, a production of 12.217 tons could be reached outside with the extra outside plot producing also up to 10.435 tons whereas inside greenhouse CN, 2.673 tons could be reached against only 0.15 tons inside Dji greenhouse (see tables from 4.46 to 4.49). The greenhouses produced much less than under outside conditions due to many reasons. One of the reasons was the fact that plantations were done during the rainy season making availability for rainwater, wind and sun radiations optimum for outside productivity. However, the variation of the outside temperature affected the leaves growth making them not growing well as shown the figures 4.106 and 4.107. Besides, attacks from plants enemies such as rodents, insect larvae and others affected fruit quality of outside production as shown in figures 4.42, 4.43, 4.44 and 4.45 where most greenhouse fruits were in good condition. Moreover, the use of a most suitable tomato variety for this rainy season also helped to get better results outside the greenhouse since it was a hybrid crop variety adapted for the Sahel, or harsh condition. A reduction of productivity was observed (see table 4.50). This was because the plants were left to continue to produce over two seasons instead of removing old and replanting new plants.

**Table 4. 41** Dji GnH harvest data

| Sampling times | Dji | | | | | | |
|---|---|---|---|---|---|---|---|
| | **TOTAL fruit yield (g)** | **TOTAL fruit unit** | **TOTAL Good** | **TOTAL Bad** | **Percentage Good fruit** | **Total number of plants** | **Yield per plant** |
| 1 | 0 | 0 | 0 | 0 | 0.00% | 238 | 0.00 |
| 2 | 0 | 0 | 0 | 0 | 0.00% | - | 0.00 |
| 3 | 0 | 0 | 0 | 0 | 0.00% | - | 0.00 |
| 4 | 0 | 0 | 0 | 0 | 0.00% | - | 0.00 |
| 5 | 0 | 0 | 0 | 0 | 0.00% | - | 0.00 |
| 6 | 0 | 0 | 0 | 0 | 0.00% | - | 0.00 |
| 7 | 0 | 0 | 0 | 0 | 0.00% | - | 0.00 |
| 8 | 0 | 0 | 0 | 0 | 0.00% | - | 0.00 |
| 9 | 0 | 0 | 0 | 0 | 0.00% | - | 0.00 |
| 10 | 0 | 0 | 0 | 0 | 0.00% | - | 0.00 |
| 11 | 0 | 0 | 0 | 0 | 0.00% | - | 0.00 |
| 12 | 0 | 0 | 0 | 0 | 0.00% | - | 0.00 |
| 13 | 0 | 0 | 0 | 0 | 0.00% | - | 0.00 |
| 14 | 36 | 2 | 36 | 0 | 100.00% | - | 0.00 |
| 15 | 36 | 2 | 36 | 0 | 100.00% | - | 0.15 |
| 16 | 0 | 0 | 0 | 0 | 0.00% | - | 0.00 |
| 17 | 0 | 0 | 0 | 0 | 0.00% | - | 0.00 |
| 18 | 0 | 0 | 0 | 0 | 0.00% | - | 0.00 |
| 19 | 0 | 0 | 0 | 0 | 0.00% | - | 0.00 |
| 20 | 36 | 1 | 36 | 0 | 100.00% | - | 0.00 |
| 21 | 0 | 0 | 0 | 0 | 0.00% | - | 0.00 |
| 22 | 0 | 0 | 0 | 0 | 0.00% | - | 0.00 |
| 23 | 108 | 3 | 108 | 0 | 100.00% | - | 0.45 |
| 24 | 459 | 12 | 459 | 0 | 100.00% | - | 1.93 |
| | | | | | | | |
| **TOTAL** | **639** | **18** | **639** | **0** | | | |

**Table 4. 42** CN GnH harvest data

| Sampling times | CN | | | | | | |
|---|---|---|---|---|---|---|---|
| | **TOTAL fruit yield (g)** | **TOTAL fruit unit** | **TOTAL Good** | **TOTAL Bad** | **Percentage Good fruit** | **Total number of plants** | **Yield per plant** |
| 1 | 0 | 0 | 0 | 0 | 0.00% | 191 | 0.00 |
| 2 | 0 | 0 | 0 | 0 | 0.00% | - | 0.00 |
| 3 | 0 | 0 | 0 | 0 | 0.00% | - | 0.00 |
| 4 | 0 | 0 | 0 | 0 | 0.00% | - | 0.00 |
| 5 | 0 | 0 | 0 | 0 | 0.00% | - | 0.00 |
| 6 | 0 | 0 | 0 | 0 | 0.00% | - | 0.00 |
| 7 | 0 | 0 | 0 | 0 | 0.00% | - | 0.00 |
| 8 | 61 | 3 | 33 | 28 | 54.10% | - | 0.32 |
| 9 | 601 | 12 | 601 | 0 | 100.00% | - | 3.15 |
| 10 | 1109 | 31 | 844 | 265 | 76.10% | - | 5.81 |
| 11 | 863 | 19 | 863 | 0 | 100.00% | - | 4.52 |
| 12 | 282 | 8 | 282 | 0 | 100.00% | - | 1.48 |
| 13 | 873 | 24 | 858 | 15 | 98.28% | - | 4.57 |
| 14 | 0 | 0 | 0 | 0 | 0.00% | - | 0.00 |
| 15 | 1944 | 45 | 1944 | 0 | 100.00% | - | 10.18 |
| 16 | 0 | 0 | 0 | 0 | 0.00% | - | 0.00 |
| 17 | 0 | 0 | 0 | 0 | 0.00% | - | 0.00 |
| 18 | 0 | 0 | 0 | 0 | 0.00% | - | 0.00 |
| 19 | 0 | 0 | 0 | 0 | 0.00% | - | 0.00 |
| 20 | 18 | 1 | 18 | 0 | 100.00% | - | 0.09 |
| 21 | 1610 | 49 | 1585 | 25 | 98.45% | - | 8.43 |
| 22 | 0 | 0 | 0 | 0 | 0.00% | - | 0.00 |
| 23 | 2705 | 95 | 2705 | 0 | 100.00% | | 14.16 |
| 24 | 1628 | 63 | 1628 | 0 | 100.00% | | 8.52 |
| | | | | | | | |
| **TOTAL** | **11694** | **350** | **11361** | **333** | | | |

**Table 4.43** Outside environment harvest data

| Sampling times | Outside | | | | | | |
|---|---|---|---|---|---|---|---|
| | **TOTAL fruit yield (g)** | **TOTAL fruit unit** | **TOTAL Good** | **TOTAL Bad** | **Percentage Good fruit** | **Total number of plants** | **Yield per plant** |
| 1 | 229 | 8 | 88 | 141 | 38.43% | 208 | 1.10 |
| 2 | 2361 | 50 | 1988 | 373 | 84.20% | - | 11.35 |
| 3 | 1688 | 36 | 1553 | 135 | 92.00% | - | 8.12 |
| 4 | 2756 | 66 | 2694 | 62 | 97.75% | - | 13.25 |
| 5 | 6406 | 156 | 6317 | 89 | 98.61% | - | 30.80 |
| 6 | 5701 | 143 | 5191 | 510 | 91.05% | - | 27.41 |
| 7 | 4119 | 104 | 3980 | 139 | 96.63% | - | 19.80 |
| 8 | 6283 | 173 | 5766 | 517 | 91.77% | - | 30.21 |
| 9 | 3234 | 87 | 3201 | 33 | 98.98% | - | 15.55 |
| 10 | 1307 | 39 | 1294 | 13 | 99.01% | - | 6.28 |
| 11 | 758 | 39 | 718 | 40 | 94.72% | - | 3.64 |
| 12 | 303 | 9 | 247 | 56 | 81.52% | - | 1.46 |
| 13 | 330 | 12 | 250 | 80 | 75.76% | - | 1.59 |
| 14 | 0 | 0 | 0 | 0 | 0.00% | - | 0.00 |
| 15 | 152 | 5 | 152 | 0 | 100.00% | - | 0.73 |
| 16 | 0 | 0 | 0 | 0 | 0.00% | - | 0.00 |
| 17 | 0 | 0 | 0 | 0 | 0.00% | - | 0.00 |
| 18 | 0 | 0 | 0 | 0 | 0.00% | - | 0.00 |
| 19 | 0 | 0 | 0 | 0 | 0.00% | - | 0.00 |
| 20 | 422 | 24 | 422 | 0 | 100.00% | - | 2.03 |
| 21 | 8573 | 349 | 8517 | 56 | 99.35% | - | 41.22 |
| 22 | 0 | 0 | 0 | 0 | 0.00% | - | 0.00 |
| 23 | 6498 | 298 | 6484 | 14 | 99.78% | - | 31.24 |
| 24 | 3115 | 135 | 3062 | 53 | 98.30% | - | 14.98 |
| | | | | | | | |
| **TOTAL** | **35475** | **922** | **33287** | **2188** | | | |

**Table 4.44** Outside bonus harvest data

| Sampling times | Outside bonus | | | | | | |
|---|---|---|---|---|---|---|---|
| | **TOTAL fruit yield (g)** | **TOTAL fruit unit** | **TOTAL Good** | **TOTAL Bad** | **Percentage Good fruit** | **Total number of plants** | **Yield per plant** |
| 1 | 41 | 1 | 0 | 41 | 0.00% | 254 | 0.16 |
| 2 | 254 | 7 | 163 | 91 | 64.17% | - | 1.00 |
| 3 | 403 | 11 | 375 | 28 | 93.05% | - | 1.59 |
| 4 | 1232 | 66 | 1161 | 71 | 94.24% | - | 4.85 |
| 5 | 3813 | 107 | 3634 | 179 | 95.31% | - | 15.01 |
| 6 | 3575 | 107 | 3403 | 172 | 95.19% | - | 14.07 |
| 7 | 3144 | 88 | 2856 | 288 | 90.84% | - | 12.38 |
| 8 | 9833 | 264 | 9389 | 444 | 95.48% | - | 38.71 |
| 9 | 4699 | 141 | 4471 | 228 | 95.15% | - | 18.50 |
| 10 | 3240 | 93 | 3172 | 68 | 97.90% | - | 12.76 |
| 11 | 2924 | 81 | 2762 | 162 | 94.46% | - | 11.51 |
| 12 | 1688 | 56 | 1439 | 249 | 85.25% | - | 6.65 |
| 13 | 3430 | 100 | 2882 | 548 | 84.02% | - | 13.50 |
| 14 | 0 | 0 | 0 | 0 | 0.00% | - | 0.00 |
| 15 | 1173 | 39 | 1082 | 91 | 92.24% | - | 4.62 |
| 16 | 0 | 0 | 0 | 0 | 0.00% | - | 0.00 |
| 17 | 0 | 0 | 0 | 0 | 0.00% | - | 0.00 |
| 18 | 0 | 0 | 0 | 0 | 0.00% | - | 0.00 |
| 19 | 0 | 0 | 0 | 0 | 0.00% | - | 0.00 |
| 20 | 100 | 6 | 73 | 27 | 73.00% | - | 0.39 |
| 21 | 2880 | 118 | 2870 | 10 | 99.65% | - | 11.34 |
| 22 | 0 | 0 | 0 | 0 | 0.00% | - | 0.00 |
| 23 | 3138 | 148 | 3138 | 0 | 100.00% | - | 12.35 |
| 24 | 1479 | 76 | 1479 | 0 | 100.00% | - | 5.82 |
| | | | | | | | |
| **TOTAL** | **38276** | **1122** | **35707** | **2569** | | **254** | **150.69** |

**Table 4.45** Plots partition

| | Plot area | | | | | | Total plants |
|---|---|---|---|---|---|---|---|
| | **Line 1** | **Line 2** | **Line 3** | **Line 4** | **Line 5** | **Line 6** | |
| **Dji GnH** | 37 | 36 | 38 | 47 | 40 | 40 | 238 |
| **CN GnH** | 31 | 32 | 31 | 33 | 32 | 32 | 191 |
| **Outside** | 34 | 34 | 35 | 34 | 36 | 35 | 208 |
| **Outside Bonus** | 41 | 43 | 42 | 43 | 42 | 43 | 254 |

**Table 4.46** Cultivation timeline

| | **Date** | **Days** | **Date** | **Days** | **Date** | **Days** | **Date** | **Days** |
|---|---|---|---|---|---|---|---|---|
| | **Transplantation** | | **1st flowering** | | **1st fruit** | | **1st harvest** | |
| **Dji GnH** | 21/7/2022 | 0 | 24/8/2022 | 34 | 9/10/2022 | 81 | 9/11/2022 | 111 |
| **CN GnH** | 21/7/2022 | 0 | 20/8/2022 | 30 | 10/9/2022 | 51 | 9/10/2022 | 81 |
| **Outside** | 21/7/2022 | 0 | 10/8/2022 | 20 | 17/8/2022 | 27 | 7/9/2022 | 48 |
| **Outside Bonus** | 21/7/2022 | 0 | 3/8/2022 | 13 | 10/8/2022 | 20 | 6/9/2022 | 47 |

**Table 4.47** Accumulated harvest data 1

| | **Weight (g)** | **Weight (kg)** | **Cost per kg** | **Predicted Sales (CFA)** | **Actual Sales (CFA)** | **Loss through gifts, transportation and bad sales** |
|---|---|---|---|---|---|---|
| **Total Dji** | 639 | 0.639 | 500 | 320 | | |
| **Total CN** | 11361 | 11.361 | 500 | 5681 | | |
| **Total outside** | 51924 | 51.924 | 500 | 25962 | | |
| **TOTAL 1** | 63924 | 63.924 | | 31962 | | 31962 |
| **Total outside bonus** | 44349 | 44.349 | 500 | 22175 | | |
| | | | | | | |
| **TOTAL 2** | 108273 | 108.273 | | 54137 | 36500 | 17637 |

**Table 4.48** Accumulated harvest data 2

| | **Actual Area used ($m^2$) 8,5x5m** | **Production per m2 ($g/m^2$)** | **Expansion over a hectare (10000 $m^2$)** | **Total plants** | **Production per plant (g/plant)** |
|---|---|---|---|---|---|
| **Total Dji** | 42.5 | 15.04 | 150352.9412 | 238 | 2.68487395 |
| **Total CN** | 42.5 | 267.32 | 2673176 | 191 | 59.48167539 |
| **Total outside** | 42.5 | 1221.74 | 12217412 | 208 | 249.6346154 |
| **TOTAL 1** | 128 | 1504 | 15040941 | 637 | 312 |
| **Total outside bonus** | 42.5 | 1043.51 | 10435059 | 254 | 174.6023622 |
| | | | | | |
| **TOTAL 2** | 170 | 2548 | 25476000 | 891 | 486 |

**Table 4.49** Production per campaign

| | **1st production** | | | **2nd production** | | |
|---|---|---|---|---|---|---|
| | **Weight (g)** | **Weight (kg)** | | **Weight (g)** | **Weight (kg)** | |
| | | Area of 42.5 $m^3$ | Area of 1 Ha | | Area of 42.5 $m^3$ | Area of 1 Ha |
| Total Dji | 36 | 0.036 | 8.47058824 | 603 | 0.603 | 141.882353 |
| Total CN | 5425 | 5.425 | 1276.47059 | 5936 | 5.936 | 1396.70588 |
| Total outside | 33439 | 33.439 | 7868 | 18485 | 18.485 | 4349.41176 |
| **TOTAL 1** | **38900** | **38.900** | **9152.941** | **25024** | **25.024** | **5888.000** |
| Total outside bonus | 36789 | 36.789 | 8656.23529 | 7560 | 7.56 | 1778.82353 |
| | | | | | | |
| **TOTAL 2** | **75689** | **75.689** | **17809.1765** | **32584** | **32.584** | **7666.82353** |

#### 4.4.3.2.2 Fruit quality analysis

The fruits produced under greenhouse appeared intense in color, deep red, and fleshier than those from outside environment as shown in figure 4.100, 4.102, 4.104 and 4.105. On one hand, under outside conditions, tomatoes turn from green to yellow and to light red or red color when ripe. On the other side, under greenhouse microclimate, tomatoes were turning from green to red then deep or intense red color when ripe. This is explained by the fact that the excessive sunshine

outside influences certain pigments present in the fruit. Photosynthetic pigments such as flavonoids, carotene and anthocyanin can easily be deteriorated under high exposure to intense sunshine (Pharmawati & Wrasiati, 2020; Saldaña et al., 2020). Besides, Fruits from the greenhouses were of higher quality and much fresh looking than fruits from outside environment. That is because fruit quality relies on the optimization of fruit-water relation in response to environmental stress as indicated by Guichard *et al.* (2005). The fruit-water balance is the result of sap influxes through the phloem and xylem tissue of the pedicel, and water efflux by transpiration (Guichard et al., 2005).

### 4.4.4 Nutritional value analysis

#### 4.4.4.1 Dry Matter content

**Table 4.50** Dry Matter content based on fresh samples

| Sample of fresh tomatoes | Tests number | Weight of Empty pot ($W_{empty}$) (g) | Weight of Sample ($W_{sample}$) (g) | Weight of Pot + sample ($W_f$) (g) | % Dry Matter (%DM) | % Humidity (%H) |
|---|---|---|---|---|---|---|
| CN GnH Tomato fruits | 1 | 45.049 | 26.26 | 46.605 | 5.9254% | 94.0746% |
| | 2 | 45.677 | 27.664 | 47.314 | 5.9174% | 94.0826% |
| Outside Tomato fruits | 3 | 45.16 | 20.092 | 46.465 | 6.4951% | 93.5049% |
| | 4 | 44.991 | 20.245 | 46.271 | 6.3225% | 93.6775% |

**Table 4.51** Dry Matter content based on dried samples

| Sample from tomatoes crop | | Weight of Empty pot ($W_{empty}$) (g) | Weight of Sample ($W_{sample}$) (g) | Weight of Pot + sample ($W_f$) (g) | % Dry Matter (%DM) | % Humidity (%H) |
|---|---|---|---|---|---|---|
| CN GnH | Fruits | 44.331 | 2.006 | 46.074 | 86.889% | 13.111% |
| | Leaves | 42.664 | 2.006 | 44.556 | 94.317% | 5.683% |
| | Stems | 46.036 | 2.006 | 47.943 | 95.065% | 4.935% |
| Dji GnH | Fruits | 44.331 | 2.006 | 46.074 | 86.889% | 13.111% |
| | Leaves | 43.223 | 2.002 | 45.117 | 94.605% | 5.395% |
| | Stems | 43.714 | 2.004 | 45.625 | 95.359% | 4.641% |
| Outside GnH 1 | Fruits | 46.13 | 2.003 | 47.905 | 88.617% | 11.383% |
| | Leaves | 44.301 | 2.008 | 46.197 | 94.422% | 5.578% |
| | Stems | 45.935 | 2.001 | 47.821 | 94.253% | 5.747% |
| Outside GnH 2 | Fruits | 46.13 | 2.003 | 47.905 | 88.617% | 11.383% |
| | Leaves | 46.379 | 2.007 | 48.27 | 94.220% | 5.780% |
| | Stems | 43.905 | 2.005 | 45.792 | 94.115% | 5.885% |

Table 4.45 and 4.46 presented results of dry matter test from tomatoes fruits. Fruits from inside greenhouse had an average dry matter of 5.9214% whereas fruits from outside had 6.4088%. Both results were within the range of 5%-8% as indicated in Guichard *et al.* (2005). This difference is usually dependent on genotype and environment. The water content of those fruits being between 92%–95%, assured that those fruits were mature. On dry basis, the same trend was followed whereby fruits from inside greenhouses (CN GnH and Dji GnH) were having higher moisture content (13.111% for inside against 11.383% for outside). The other parts of crops had other trend depending on many parameters.

#### 4.4.4.2 Mineral matter content

**Table 4.52** Mineral Matter content

| **Sample from tomatoes crop** | | **Weight of Empty pot ($W_{empty}$) (g)** | **Weight of Sample ($W_{sample}$) (g)** | **Weight of Pot + sample ($W_f$) (g)** | **% Mineral Matter (%MM)** |
|---|---|---|---|---|---|
| CN GnH | Fruits | 59.999 | 1.003 | 60.088 | 8.873% |
| | Leaves | 67.354 | 1.000 | 67.577 | 22.300% |
| | Stems | 58.075 | 1.005 | 58.232 | 15.622% |
| Dji GnH | Fruits | 59.999 | 1.003 | 60.088 | 8.873% |
| | Leaves | 50.491 | 1.002 | 50.694 | 20.259% |
| | Stems | 48.143 | 1.002 | 48.301 | 15.768% |
| Outside GnH 1 | Fruits | 69.492 | 1.001 | 69.569 | 7.692% |
| | Leaves | 55.295 | 1.005 | 55.438 | 14.229% |
| | Stems | 35.827 | 1.003 | 35.978 | 15.055% |
| Outside GnH 2 | Fruits | 69.492 | 1.001 | 69.569 | 7.692% |
| | Leaves | 33.423 | 1.002 | 33.607 | 18.363% |
| | Stems | 19.573 | 1.004 | 19.701 | 12.749% |

Table 4.47 presents mineral matter content from crops cultivated inside and outside the greenhouses. In fact, from all parts and all areas, fruits had the least mineral matter content compared to other parts of the crops followed by stems. Leaves had accumulated amount of mineral matter which explains the reason why highest percentage of mineral matter was found in leaves. However, from a group of crops cultivated outside, leaves had a bit less mineral matter than stems (14.229% against 15.055% respectively).

#### 4.4.4.3 Protein and nitrogen content

**Table 4.53** Protein and nitrogen content

| Sample from tomatoes crop | | Weight of Sample ($W_{sample}$) (g) | Nitrogen content, % | Protein content, % |
|---|---|---|---|---|
| CN GnH | Fruits | 0.200 | 4.757 | 29.728 |
| | Leaves | 0.200 | 3.467 | 21.667 |
| | Stems | 0.200 | 1.885 | 11.782 |
| Dji GnH | Fruits | 0.200 | 4.757 | 29.728 |
| | Leaves | 0.200 | 3.944 | 24.649 |
| | Stems | 0.200 | 2.238 | 13.989 |
| Outside GnH 1 | Fruits | 0.200 | 2.264 | 14.153 |
| | Leaves | 0.200 | 3.361 | 21.008 |
| | Stems | 0.200 | 1.415 | 8.846 |
| Outside GnH 2 | Fruits | 0.200 | 2.264 | 14.153 |
| | Leaves | 0.200 | 3.408 | 21.302 |
| | Stems | 0.200 | 2.022 | 12.639 |

Table 4.48 presented protein and nitrogen content on various samples analyzed. Fruits from inside greenhouse had higher content of nitrogen and protein than those from outside greenhouse (4.757% Nitrogen and 29.728% Protein against 2.264 % Nitrogen14.153% Protein) surely because of sun exposure which influences nitrogenous compounds. In other term, inside greenhouse fruit had 2.493% more Nitrogen and 15.575% more protein than outside environment fruit. This is also confirmed through the fruits' colors observed previously with inside greenhouse fruit being more intense in red color. Leaves from inside greenhouse crops had high nitrogen and protein content compared to leaves from outside greenhouse with those from Dji GnH. Although, CN GnH produced more fruits than Dji GnH, it was observed that Dji GnH crops had better nutrient content in terms of nitrogen and protein. This could be caused by the fact that crops inside Dji GnH still had that much nutrient since it did almost not used it for fruit production. In fact, the absorption of nutrients from the growing medium is directly related to the flow of water through the plant directed by the evapotranspiration as quoted in Iraqi et al. (1997) and Vallières (2018).

## 4.5 Diseases and Damage

Apart from nets used as covering materials to reduce invaders attack, other phytosanitary products were also used. Nonetheless, unforeseen circumstances caused damage to both structures and harvest products.

### 4.5.1 Diseases

#### 4.5.1.1 Withering

The symptoms of withering have been observed on most crops, particularly the tomato, zucchini and potato that presented a slowdown and then a growth stop of the aerial parts (Figure 4.108). It was noted that withering could also be caused by luck of water during hours which the plant needed it especially during hot weather time. However, if it was caused by a bacteria, then the bacteria responsible is usually *Ralstonia solanacearum* as mentioned in Simon (2009). Between 14 and 32 Days After Transplanting (DAT), 4 tomato plants, 5 plants of potato and 2 zucchini withered. The first indications that young shoots have presented have been the collapse and withering of the lower leaves with the loss of green colour, followed by withering and death of the plant. This may be the case with a withering of the Fusarium that accessed the plants thanks to the moisture of the ground. It is transmitted through the ground and passes roots upwards into the water driving system of the stem. The blockage of the water conductive ships would be the main reason for withering. The invasion occurs by wounds of roots that grow in infested soil. Long-distance propagation is done by seeds and transplants. Afterwards, the magnitude of the disease has weakened on all crops after the application of aqueous extracts. Green pepper and lettuce presented no symptom of withering at that date. The cases of withering observed would be due to a bacteriosis or a fungal, virulent and colonizing xylem disease.

**Figure 4.108** Cases of withering

#### 4.5.1.2 Stunting

All plants are likely to contract a potentially dangerous pathology due to phytovirus. Most crops have not presented viral symptoms. However, typical stunting symptoms have been observed in tomato crops especially on around 61 days after transplanting (Figure 4.109). The plants have presented malformations of leaves especially on young shoots that end up falling with a reduction of the leaf surface, a general weakening or even a stop of growth because of the decrease in photosynthetic activity. This stunting phenomena was also reported by Simon (2009) to be the Tomato Yellow Leaf Curl Virus (TYLCV).

**Figure 4.109** Case of stunting

#### 4.5.1.3 Root-knot nematodes

Root-knot nematodes (see figure 4.110) are among the soil pests that cause significant problems on a wide range of hosts: Solanaceae, Cucurbataceae and others market crops are usually attacked by species of meloidogyne spp family (such as Meloidogyne incognita or southern root-nematode, a plant parasite).

**Figure 4.110** Root-knot nematodes

#### 4.5.1.4 Unusual attack

Some unusual attacks were detected characterized by an appearance of dark bluish points on the fruits of tomatoes caused either by stings of some insects known to be flower lover insects or a bacterial attack such as *xanthomonas camppestris* (see Figure 4.111). Joly (1967) showed that this dark bluish black colour on tomatoes fruits with rotten-like appearance attack could be provoked by a bacteria known as Alternaria family such as *A. tenuis*, *A. chartarum*, *A. tennuissima* and *A. consortialis* (Joly, 1967).

**Figure 4.111** Attack by collectors insect

### 4.5.2 Physical Damage

A few physical damage was observed on all different parts of the cultures (root, stems, leaves, fruits). The main identified pests are mainly the squirrel and the Gambia's rat (*Cricetomys gambianus*) which are large granivorous rodents and frugivorous. These rodents are responsible for most of the damage that affected the harvests (Figure 4.112), especially that of the potato and pepper. His crop bio-aggressors represent a major constraint on the intensification of agricultural production in the area. They manifested themselves by deterrents of tubers, shear of young seedlings, throttle perforations and fruit snacks. The methods of struggles used have been physical such as the cleaning of the parcels, the destruction of the burrows, the beaten or hunting with club and the use of local fence called *Zana* (in straw) for the protection of the plots.

Cricetomys gambianus

Sciurus niger

**Figure 4.112** A big rat caught and a squirrel

#### 4.5.2.1 Invaders damage

##### 4.5.2.1.1 Rodent attack

In many cases, rodents attack ripe fruits or those that are ready to harvest and sell. Squirrel and rats usually cause this kind of damage to fruits leading to losses in products (see figure 4.113 and 4.114).

**Figure 4. 113** Rodent attack on green pepper (left) and zucchini (right)

**Figure 4. 114** Rats holes in potato farm; rodent attack on tomato

##### 4.5.2.1.2 Tomato fruit borer

One of the most important insect pests of tomatoes is the tomato fruit borer (*Helicoverpa armigera; Lepidoptera: Noctuidae*) (Simon, 2009). This species is known for the galleries they dig into the fruit. This makes it very difficult to fight if it has already taken hold. The larvae of its caterpillar (Figure 4.115) were observed on tomato during the flowering stage (32 Days after transplanting), and then it passed unnoticed after organic treatment with neem leaves until the onset of fruit maturity. The young caterpillar is inconspicuous with variable colour (greenish, yellowish, pinkish or brownish).The young larvae attack the succulent parts: leaves, flowers, buds, flower buds, fruits and facilitate the development of fungi. The damage it has caused is

mainly dropping and early ripening or deformation of fruit by digging holes in the fruit attacked, developing pathogenic agents (molds) and thus causing rotting of the fruits (Figure 4.115). The protection actions were mainly uprooting and destructing attacked fruits, spraying with aqueous extracts and organic pesticides, monitoring general of the possible arrival of caterpillars, weeding and destruction of plant residues all around the plot.

Caterpillar: *Helicoverpa armigera*

*Helicoverpa armigera* in tomato

Tomato fruit borer

*Helicoverpa armigera*

*Spodoptera sp. (Lepidoptera Noctuidae)*

*Lepidoptera Sphingidae*

**Figure 4. 115** Crawling insect invaders

*Mylabre flexuosa*

*Dysdercus volkerii*

*Hyménoptera*

Grasshopper

*Lepidoptera Pieridae*

**Figure 4.116** Flying insect invaders

Most of larvae were from eggs laid by flying insect invaders who entered the greenhouse while people were entering as they are all around the plots because of the favourable rainy season environment (figure 4.115 and 4.116).

**4.5.2.1.3** Maggot on zucchini crop

Many feet of the zucchini presented the symptoms of attack of the maggots from the first fruits to 27 days after transplanting. Pitted fruits rot (Figure 4.117) and in section show the presence of yellowish maggots. They usually deform the fruit interior throughout small galleries. The areas around the brown spawning hole soften and sometimes softened completely. These symptoms were similar to those of Vertebratus dacus, which is the largest of the species of white flies in the Sahel and who attack the cucurbitaceae (cucumber, zucchini, melon, and watermelon), tomato, papaya and mango (Ministère de l'Agriculture & PromAP, 2019; RECA, 2015). It is a polyvoltine species that leads a larval life in the leak and cause progressive damage with the development of taps(Ministère de l'Agriculture & PromAP, 2019; RECA, 2015). At the appearance of stung fruits, these have been removed and destroyed so that the ones that are there inside do not give new flies.

**Figure 4.117** Maggots attack on zucchini

### 4.5.3 Indirect threats

These threats affect the daily work by attacking the worker himself ending up affecting the overall productivity. Some of the indirect threats were snakes, scorpions, religious mentis Chameleon and other bush lizards as shown in figure 4.118. There are also predators to insect pests.

Snake

Scorpions

Religious mantis

Chameleon

Bush lizards

**Figure 4. 118** Indirect threats

## 4.6 Energy production analysis

The performance of off-grid PV system installed on a greenhouse roof at Dalwai department (Location: Latitude 13.000, Longitude: 2.000) was estimated using PVGIS data (PVGIS-SARAH-2 database). As input, different scenarios including the real case and projected cases were simulated using as baseline, a consumption of 4200 Wh per day, a discharge cutoff limit for battery of 20%, a slope angle of PV module of 15° and an azimuth angle of 180° (south oriented solar panels). SARAH-2 database is a credible source of data that has been used by many researchers for data validation especially solar data (Erim et al., 2023; Remedio et al., 2019; Sawadogo et al., 2021).

Considering the interval of the period of study to be from July to February, two seasons were observed: from July to October, the rainy season, and from October to February, the dry and cold season.

### 4.6.1 Real case scenario

#### 4.6.1.1 Irradiation and temperature from satellite data

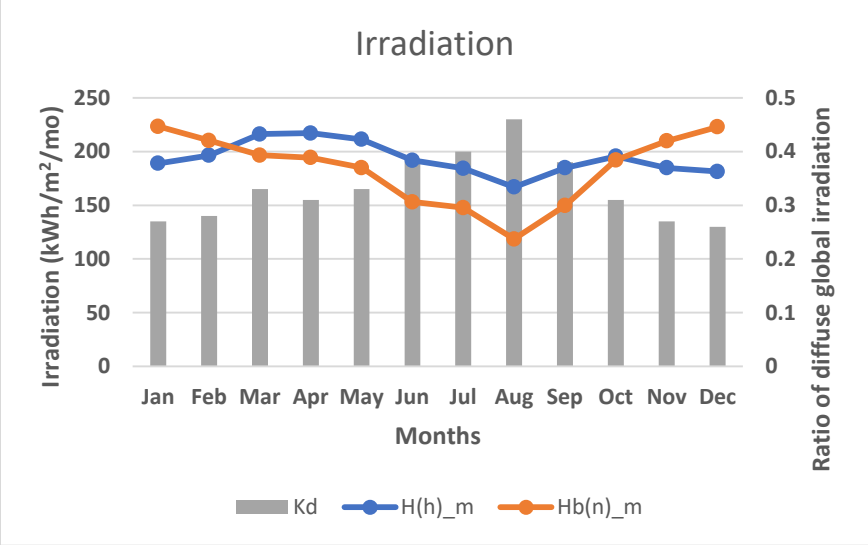


**Figure 4. 119** Irradiation profile

H(h)_m: Irradiation on horizontal plane (kWh/ $m^2$/day ).

Hb(n)_m: Monthly beam (direct) irradiation on a plane always normal to sun rays (kWh/$m^2$/day).

Kd: Ratio of diffuse to global irradiation.

On the figure 4.108 are presented irradiation on horizontal plane H(h_m) and monthly beam (direct) irradiation on a plane always normal to sun rays (Hb(n)_m).

Over the period of study more of irradiation is hitting the plane normal to sun rays from July to October and less is hitting the plane normal to sun rays from October to February. This phenomenon was due to cloud movement in the sky as the sky was quite open during the first interval and quite occupied by clouds during the second interval. October was the month during which sun rays came both from a horizontal plane and from plane normal to sun rays (figure 4.119). In January, most of the sun radiations were coming from a plane normal always normal to sun rays (223.48 kWh/m$^2$/day). Figure 4.120 presents the monthly average values of daily temperature. The hottest month of the year was reported to be April with 34.7°C but the hottest month during our period of trial was October with 29.2$^o$C as average monthly temperature.

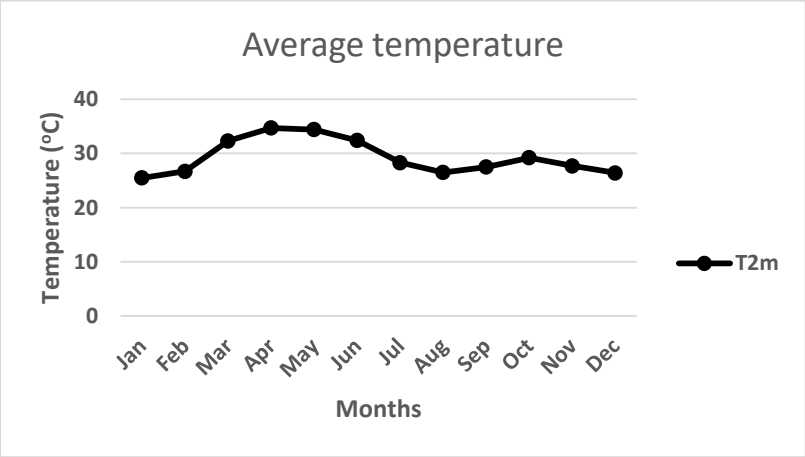


**Figure 4. 120** Temperature profile

#### 4.6.1.2 Power production estimate expressed as a monthly average performance

Power production estimate was done based on PV system installed on the roof of the greenhouse.

**Table 4.54** Energy estimate

| **Month** | **E_d** (Wh/day) | **E_lost_d** (Wh/day) | **E** (Wh/day) |
|---|---|---|---|
| January | 4194 | 6030.79 | 10225 |
| February | 4200.02 | 7916.29 | 12116 |
| March | 4196.2 | 9446.49 | 13643 |
| April | 4200.01 | 10576.49 | 14777 |
| May | 4200.65 | 10215.93 | 14417 |
| June | 4201.02 | 9731.13 | 13932 |
| July | 4198.81 | 8604.8 | 12804 |
| August | 4200.26 | 7673.37 | 11874 |
| September | 4197.8 | 8094.01 | 12292 |
| October | 4198.97 | 7573.14 | 11772 |
| November | 4199.24 | 6158.64 | 10358 |
| December | 4201.07 | 5403.31 | 9604 |

E represents the monthly energy available from the PV modules (Wh/day).

E_d represents the monthly average of daily energy production per day (Wh/day) and E_loss_d, the monthly average energy not captured per day (Wh/day). These were calculated due to full battery.

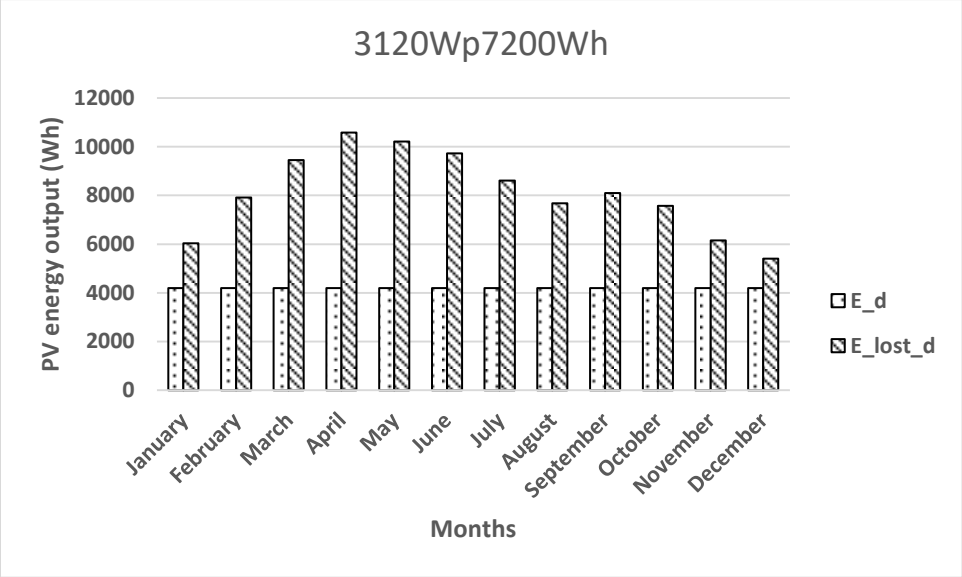


**Figure 4. 121** Power production estimate for field PV system

Most energy consumed was around 4200 Wh due to the load made up of equipment such as fans used for cooling the greenhouse. The highest value of energy loss in the year was 10 576.49 Wh/day in April, whereas the highest energy loss during the trial's period was in July (8604.8 Wh/day) followed by September (8094.01 Wh/day) then February (7916.29 Wh/day), which means more batteries were needed to store that energy or it could have been channeled for other uses (figure 4.121). This represents a huge loss since it is 2.04 to 1.88 times (compared to July and February) to more than the energy consumed per day. In fact, looking at figures 4.122 and 4.123, we realize that the batteries are mostly full at 96% (average battery full value) throughout the month. Moreover, from figure 5, it was clear that batteries are charged between 92 and 100% during 41% of the days of the month. This confirms that there are more solar modules than batteries necessary.

#### 4.6.1.3 Battery performance estimate expressed as a percentage of days

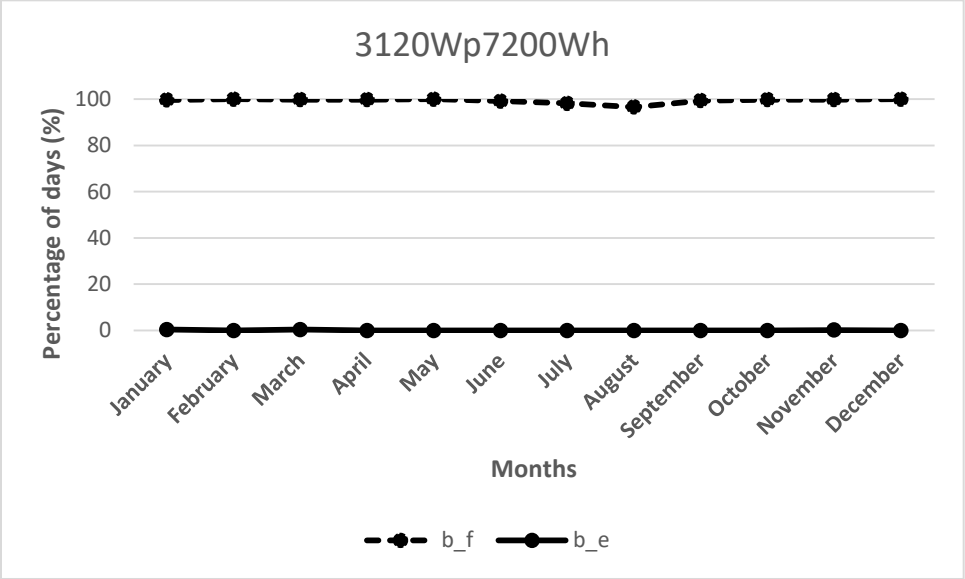


**Figure 4. 122** Battery performance estimate for field PV system

b_f represents the Percentage of days when battery became full (%) while b_e is the Percentage of days when battery became empty (%).

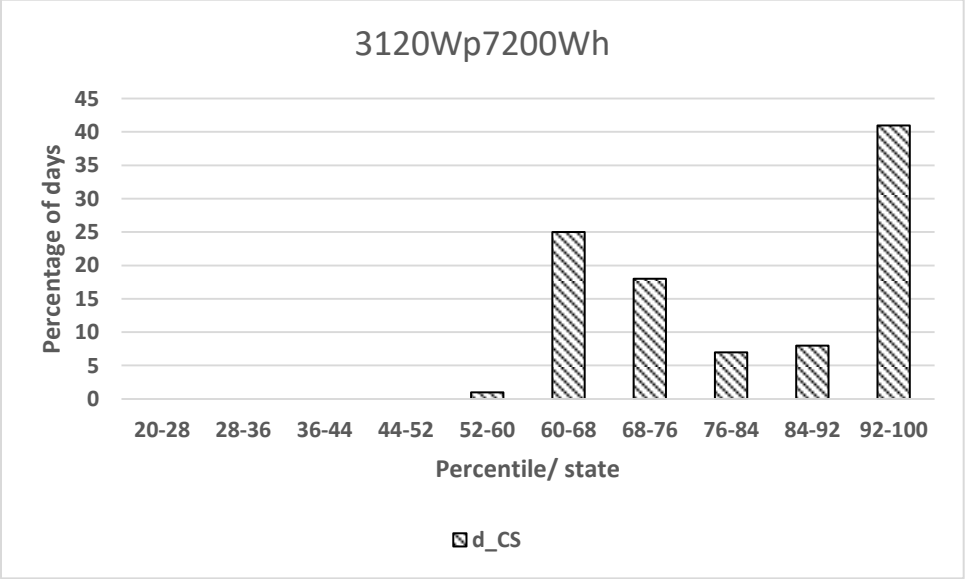


**Figure 4. 123** Probability of battery charge state at the end of the day for field PV system

Cs represents the Charge state at the end of each day (%).

### 4.6.2 Comparison of electricity production of real case scenario against projected scenarios

**Table 4.55** Cases for electricity production estimation

| Cases | Modules Wp | Number of modules | PV installed Wp | Battery Ah | Number of batteries | Working time h | Battery capacity Wh | Load (Wh) | Effects |
|---|---|---|---|---|---|---|---|---|---|
| 1 | 260 | 6 | 1560 | 150 | 4 | 12 | 7200 | 4200 | Less PV |
| 2 | 260 | 12 | 3120 | 150 | 2 | 12 | 3600 | 4200 | Less Battery |
| 3 | 260 | 12 | 3120 | 150 | 4 | 12 | 7200 | 4200 | Real case |
| 4 | 260 | 12 | 3120 | 150 | 4 | 12 | 7200 | 8400 | More load |
| 5 | 260 | 12 | 3120 | 150 | 4 | 24 | 14400 | 4200 | More working time |
| 6 | 260 | 16 | 4160 | 150 | 4 | 12 | 7200 | 4200 | Neutral |
| 7 | 260 | 16 | 4160 | 150 | 4 | 12 | 7200 | 8400 | More load |
| 8 | 260 | 16 | 4160 | 150 | 4 | 24 | 14400 | 4200 | More working time |
| 9 | 260 | 16 | 4160 | 150 | 4 | 24 | 14400 | 8400 | More load and working time |

Cases from 1 to 5 represent real case with projections of varying parameter such as solar modules, batteries, load or working time.
Cases from 6 to 9 represent projected cases for scenarios where the greenhouse roof would be fully covered by solar panels, with variation of certain parameters.

#### 4.6.2.1 Power production estimate in scenarios 1 to 5

**Table 4.56** Production estimate for case scenarios from Case 1 to 5

| Months | Case 1 E_d_1560-7200 (Wh/day) | Case 2 E_d_3120-3600 (Wh/day) | Case 3 E_d_3120-7200 (Wh/day) | Case 4 E_d_3120-7201b (Wh/day) | Case 5 E_d_3120-14400 (Wh/day) |
|---|---|---|---|---|---|
| January | 4163.85 | 4183.67 | 4194 | 8265.09 | 4198.44 |
| February | 4201.69 | 4199.72 | 4200.02 | 8389.85 | 4200.02 |
| March | 4191.73 | 4190.28 | 4196.2 | 8353.86 | 4199.14 |
| April | 4203.77 | 4197.82 | 4200.01 | 8364.34 | 4200.01 |
| May | 4200.89 | 4198.21 | 4200.65 | 8341.37 | 4200.65 |
| June | 4199.25 | 4196.2 | 4201.02 | 8268.74 | 4201.02 |
| July | 4173.72 | 4188.58 | 4198.81 | 8157.55 | 4198.81 |
| August | 4223.53 | 4183.19 | 4200.26 | 8071.02 | 4200.26 |
| September | 4194.26 | 4194.01 | 4197.8 | 8227.7 | 4197.8 |
| October | 4203.63 | 4193.87 | 4198.97 | 8362.26 | 4198.97 |
| November | 4193.61 | 4191.42 | 4199.24 | 8321.71 | 4199.94 |
| December | 4199.32 | 4199.54 | 4201.07 | 8322 | 4201.07 |
| | | | | | |
| Average | 4195.77083 | 4193.0425 | 4199.00417 | 8287.12417 | 4199.6775 |

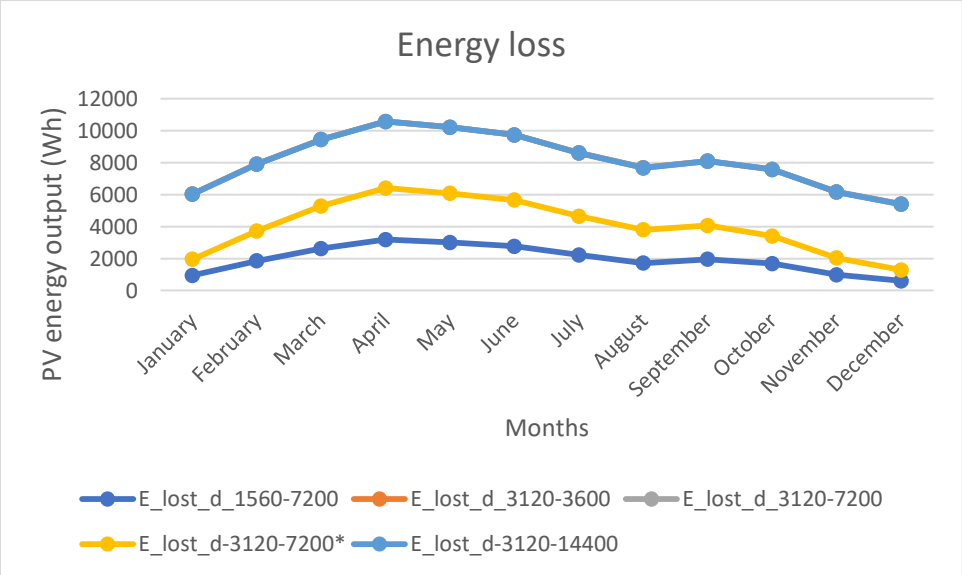


**Figure 4. 124** Energy not harnessed for various case scenarios from Case 1 to 5

The production estimate presented in Table 4.57 shows that compared to case 3 which was the real field case, reducing the number of solar modules (case 1) lowered the energy harnessed by solar modules, considering the same consumption rate of 4200 Wh/day. The direct consequence of that was the reduction of energy loss (figure 4.124 to 4.125). On the other hand, reducing the batteries (Case 2) did not much affect the energy production. Adding more load (Case 4) helped

to find equilibrium between production and losses since as soon as produced the energy was consumed. In most cases, the batteries were full by the end of the day with the lowest case scenarios of full battery being in August (figure 4.126). Because of the augmentation of the load (from 4200 to 8400 Wh/day), case 4 was the only case whereby high values of a probability of having days with battery empty was registered (up to 100% in December). Finally, the probability of encountering a battery charge state of 92-100% was high varying from 31 to 100% of days (figure 4.127).

#### 4.6.2.2 Battery performance estimate in scenarios 1 to 5

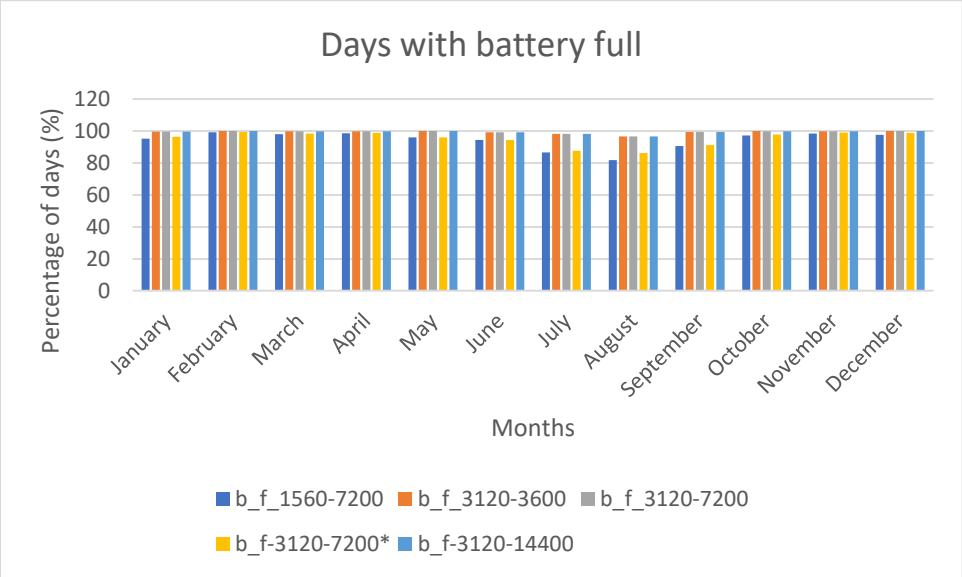


**Figure 4. 125** Days with battery full estimate for various case scenarios from Case 1 to 5

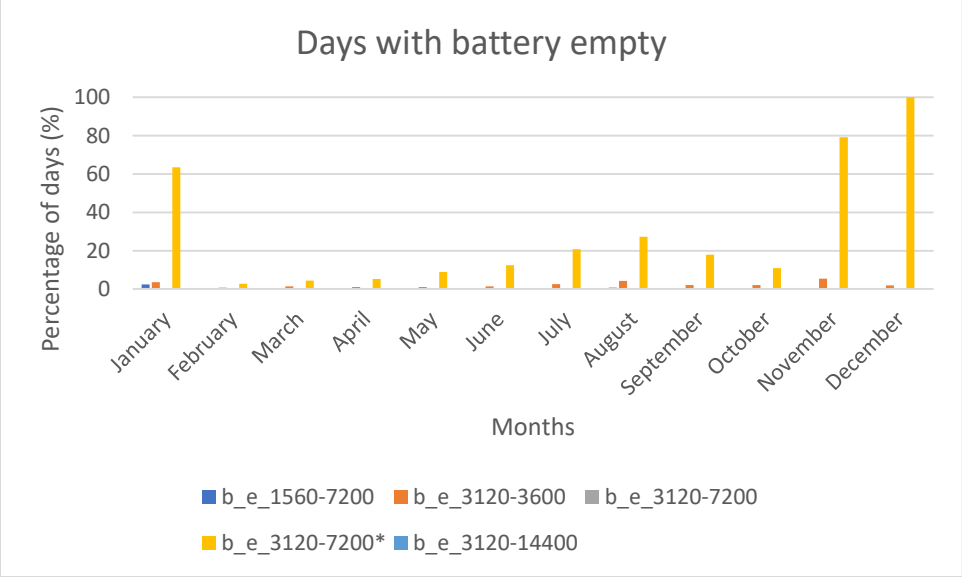


**Figure 4. 126** Days with battery empty estimate for various case scenarios from Case 1 to 5

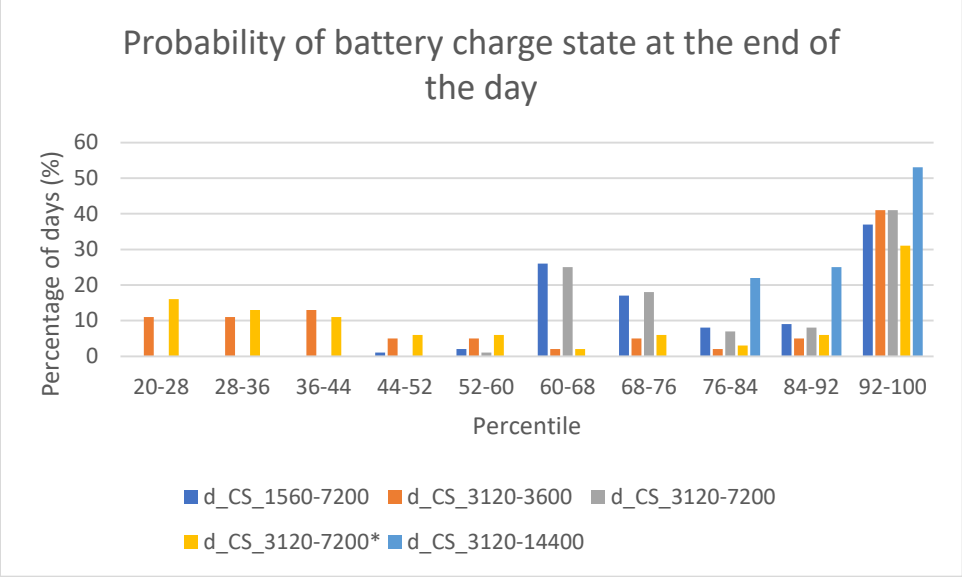


**Figure 4. 127** Probability of battery charge state at the end of the day for various case scenarios from Case 1 to 5

### 4.6.3 Projected electricity production estimate for cases of greenhouse fully covered with solar module: Cases of Agri-PV concepts

Projections were done for cases where the entire roof of the greenhouse was covered by solar modules, and this represented case 6 characterized by 4160 Wp from PV modules, 7200 Wh battery capacity on 12 h working time and a load of 4200 Wp/day. On that, many other scenarios were studies such as where load was doubled (Case 7), working time was doubled (case 8), and where load and working time were both doubled (case 9). All power produced averaged around 4199 Wh for 4200 Wh load and 8390 Wh for 8400 Wh load.

The energy loss due to battery full had two groups of curves depending as to the system being subjected to 4200 Wh (case 6 and 8) or 8400 Wh (case 7 and 9) load irrespective of the PV number installed. The highest loss was registered in April with a value as high as 15501.8 Wh (case 6 and 8) and 11302.65 Wh (case 7 and 9) (figure 4.128). Less energy was lost for the cases with 8400 Wh because the working time was extended like increasing batteries scenarios. In fact, in figure 4.129, it could be seen that there were less days during which batteries were full in other terms more days with battery empty (figure 4.130). Looking at figure 4.129, from case 6 being the reference, increasing only solar modules does not affect days with battery full, but rather increasing load as in case 7 reduces this parameter of days with battery full. Case 7 had the highest value of days with battery empty since the load was increased, yet the PV input was kept intact.

#### 4.6.3.1 Power production estimate in different scenarios

**Table 4.57** Production estimate for case scenarios from Case 6 to 9

| Months | Case 6 E_d_4160-7200 (Wh/day) | Case 7 E_d_4160-7200b (Wh/day) | Case 8 E_d_4160-14400 (Wh/day) | Case 9 E_d_4160-14400b (Wh/day) |
|---|---|---|---|---|
| January | 4193.46 | 8333.42 | 4197.71 | 8361.03 |
| February | 4200 | 8395.3 | 4200 | 8402.01 |
| March | 4196.48 | 8376.95 | 4199.23 | 8391.81 |
| April | 4200.2 | 8381.95 | 4200.2 | 8399.35 |
| May | 4200.5 | 8381.4 | 4200.5 | 8401.48 |
| June | 4201.17 | 8344.62 | 4201.17 | 8401.67 |
| July | 4199.16 | 8301.94 | 4199.16 | 8379.26 |
| August | 4199.7 | 8243.68 | 4199.7 | 8419.72 |
| September | 4199.71 | 8334.02 | 4199.71 | 8388.37 |
| October | 4197.49 | 8381.44 | 4197.49 | 8404.26 |
| November | 4199.94 | 8371.63 | 4199.94 | 8397.11 |
| December | 4201.44 | 8391.08 | 4201.44 | 8395.87 |
| | | | | |
| Average | 4199.10417 | 8353.11917 | 4199.6875 | 8395.16167 |

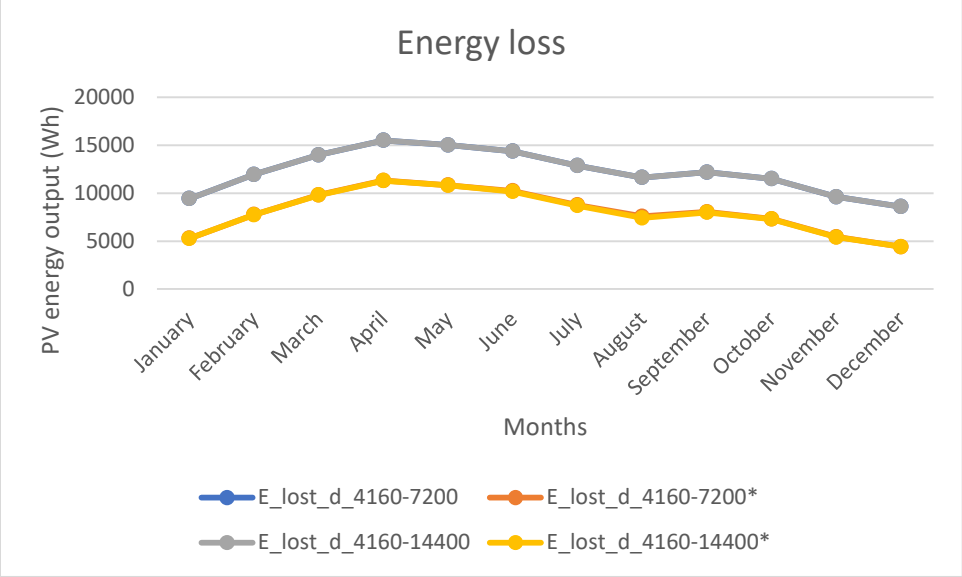


**Figure 4. 128** Energy not harnessed for various case scenarios from case 6 to 9

#### 4.6.3.2 Battery performance estimate in different scenarios

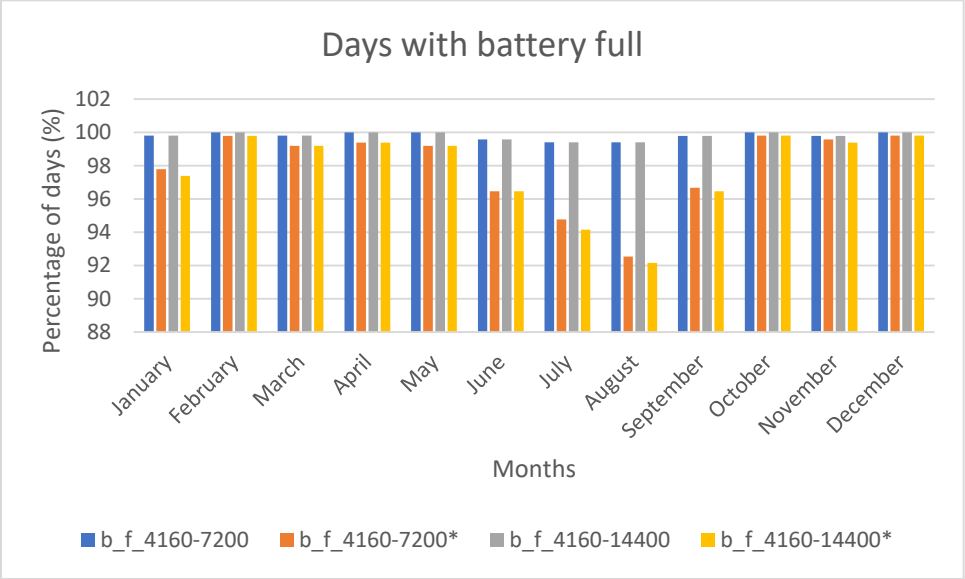


**Figure 4. 129** Days with battery full estimate for various case scenarios from case 6 to 9

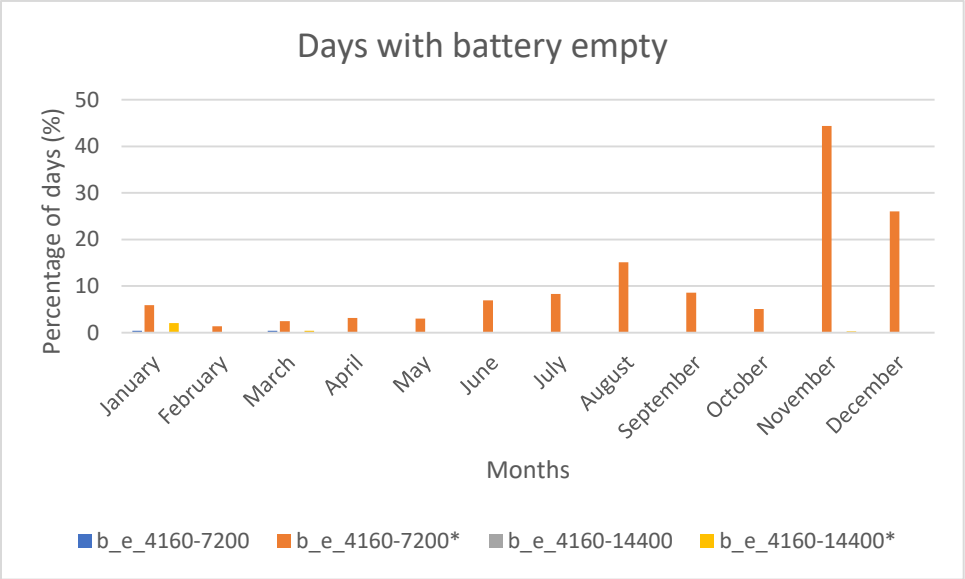


**Figure 4. 130** Days with battery empty estimate for various case scenarios from case 6 to 9

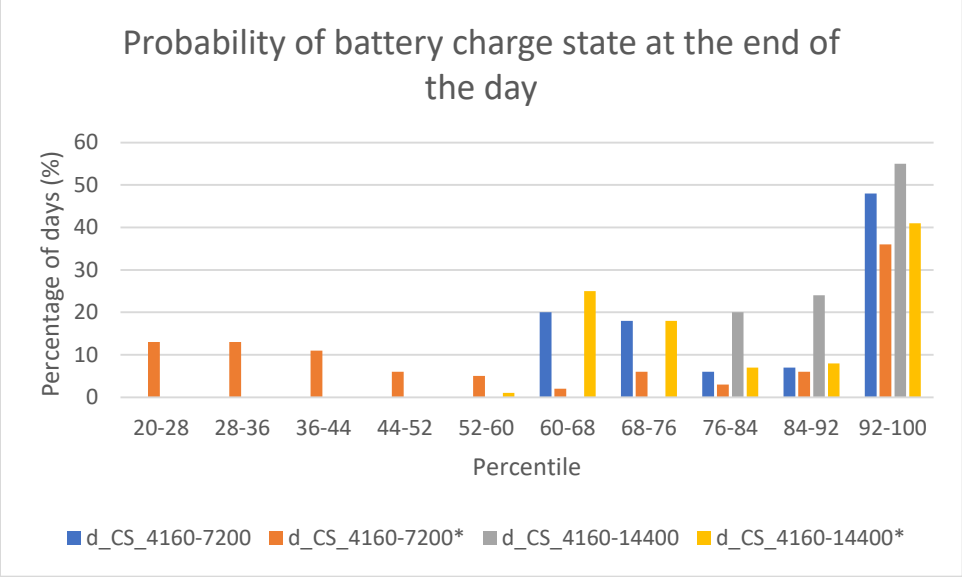


**Figure 4. 131** Probability of battery charge state at the end of the day for various case scenarios from case 6 to 9

Figure 4.131 presents the probability of finding the battery at different power stages during the days of the month. In fact, the case with more working time had the highest percentage of days during which the battery stayed charge between 92 and 100. Case 7 was highly presenting days during which battery charge level was less than 52 and 60% full.

From that analysis, it was derived that the PV system sizing was undersized for 24h usage for cooling and oversized in terms of solar modules for 12h usage. The waste or unused energy could be used to store energy in another form such as potential energy or to produce hydrogen for fuel cell backup system since in all sizing presented, the batteries remained full for many hours.

## 4.7 Computation fluid dynamics (CFD) analysis using weather station data

### 4.7.1 Thermal and flow pattern of the greenhouse microclimate under natural convection

#### 4.7.1.1 Weather station data

Table 4.58 summarizes data collected from weather station into maximum, minimum, average and median value as well as most repeated value. Relationship between these values is presented in figure 4.132 and 4.133.

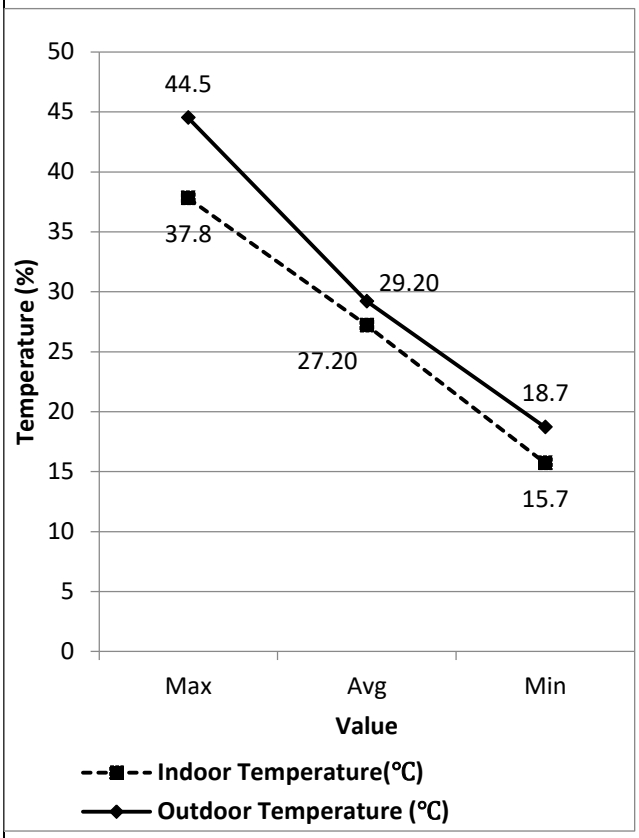


**Figure 4. 132**. Indoor vs outdoor temperature

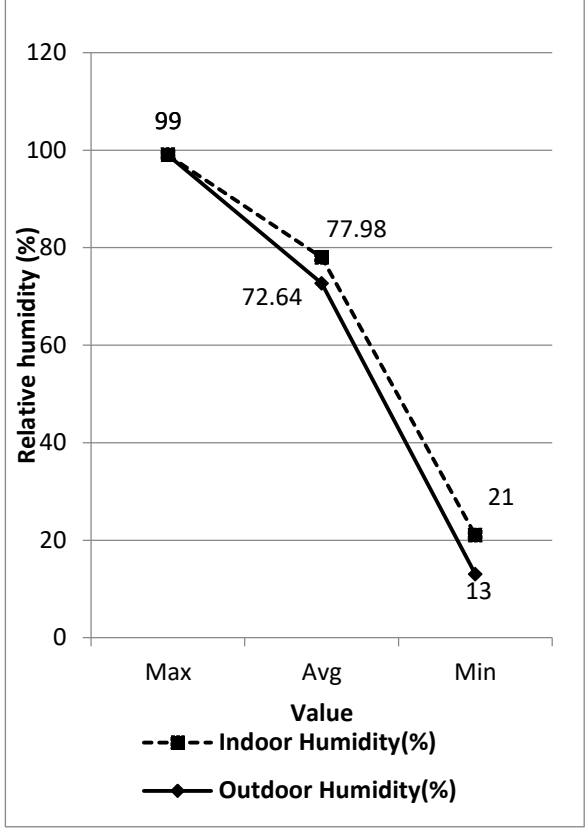


**Figure 4. 133** Indoor vs outdoor relative humidity

The cooling of the greenhouse made the temperature of the greenhouse microclimate to be lower than outside with a difference of 6.7$^{o}$C between highest values and 3$^{o}$C between lowest values. Relative humidity was at its highest (99%) for both inside and outside greenhouse due to a rain event. However, the average and lowest values of relative humidity differed by 5.33% and 8% respectively. This shows that the microclimate reduces stresses of plants due to dry environment. The RH conservation is better seen though Table 4.133 whereby middle value of 81% RH inside against 76% outside was obtained.

**Table 4.58** Summarized weather data

| | $T_{in}$ (°C) | $RH_{in}$ (%) | $RH_{out}$ (%) | Dew Point (°C) | $T_{out}$ (°C) | $v_{wind}$ (m/s) | Wind Direction (°) | Solar Rad (w/m$^2$) | Event rain (mm) |
|---|---|---|---|---|---|---|---|---|---|
| **Maximum** | 37.8 | 99 | 99 | 26.3 | 44.5 | 11.5 | 359 | 1355.6 | 36.3 |
| **Average** | 27.24 | 77.98 | 72.61 | 22.98 | 31.69 | 1.41 | 204.15 | 216.51 | 1.57 |
| **Minimum** | 15.7 | 21 | 13 | 2.8 | 18.7 | 0 | 0 | 0 | 0 |
| **Median** | 26.6 | 81 | 76 | 22.6 | 28.9 | 1.1 | 213 | 1.2 | 0 |
| **Most repeated value** | 25 | 99 | 99 | 23.4 | 25.3 | 0 | 223 | 0 | 0 |

$T_{in}$ is Indoor Temperature, $T_{out}$ is Outdoor Temperature, $RH_{in}$ is inside greenhouse relative humidity, $RH_{out}$ is outdoor relative humidity and $v_{wind}$ is wind velocity.

The most occurring wind comes from azimuth 223$^o$ or the southern-west direction and the maximum wind speed was 11.5 m/s (table 4.59) with a sudden wind burst known as gust speed having a maximum of 13.3 m/s (table 4.60). Solar radiations could reach an intensity of 1355.6 w/m$^2$ while the maximum rain fall event was 36.3 mm (table 4.59).

Tables 4.60 and 4.61 give details on climatic conditions for the various event scenarios. Depending on the case scenario occurring in daytime or in the night, solar radiation effect was turned on or off. High wind speed and low temperature events occurred in the night while high solar radiation and high temperature events occurred during the day.

### 4.7.1.2 CFD analysis under natural convection

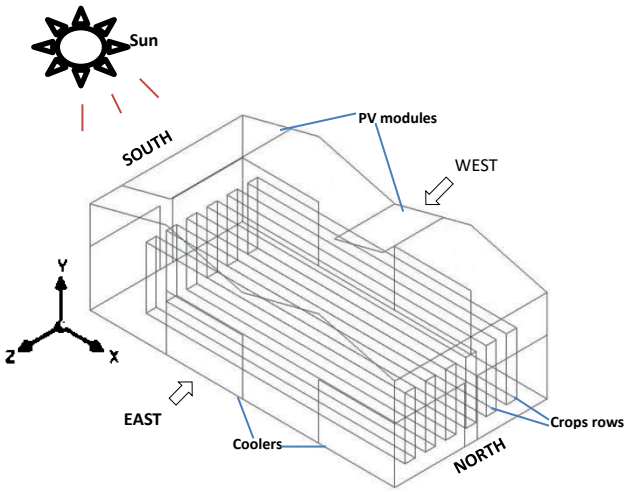


**Figure 4. 134** Greenhouse under natural convection (Djibrilla et al., 2024)

**Table 4.59** Temperature, relative humidity and wind data

| Cases for event simulation | $T_{in}$ (°C) | $RH_{in}$ (%) | $RH_{out}$ (%) | Dew Point(°C) | $T_{out}$ (°C) | $v_{wind}$ (m/s) | Gust (m/s) | Wind Direction (°) |
|---|---|---|---|---|---|---|---|---|
| **Low $T_{in}$ and $T_{out}$** | 15.7 | 72 | 44 | 6.2 | 18.7 | 0 | 0 | 349 |
| **High $T_{out}$** | 36.1 | 54 | 49 | 24.3 | 44.5 | 2.6 | 3.6 | 267 |
| **High wind** | 24.9 | 97 | 86 | 22.7 | 25.2 | 11.5 | 13.3 | 127 |
| **High solar radiation** | 29.4 | 86 | 71 | 23.8 | 34.3 | 1.5 | 1.5 | 170 |

**Table 4.60**. Solar radiation and rain event data

| Cases for event simulation | Solar Radiation ($w/m^2$) | Daily Rain (mm) | Weekly Rain (mm) | Monthly Rain (mm) | Yearly Rain (mm) |
|---|---|---|---|---|---|
| **Low $T_{in}$ and $T_{out}$** | 0 | 0 | 0 | 31.5 | 179.7 |
| **High $T_{out}$** | 471.1 | 0 | 0 | 15.8 | 125.6 |
| **High wind** | 0 | 0 | 38.1 | 0 | 109.8 |
| **High solar radiation** | 1355.6 | 0 | 1 | 9.4 | 119.2 |

Simulations were done according to various case scenarios. Results of the simulations were viewed on planes YZ (X= 1.6m or 4.6m) and XY (Z= -1m).

At high wind speed occurring during the night (figure 4.135) and coming from the south-east ($127^o$), temperature spread rapidly and evenly within the greenhouse except at the extreme top or roof. Heat accumulation at the roof was also noticed by Saberian & Sajadiye (2019). This spread is shown well by the velocity profile (up to 3.083 m/s) causing high pressure difference inside (-0.8386 Pa to 5.216 Pa). This case of high speed made the density almost constant throughout the interior (1.184 $kg/m^3$). Velocity of air stream is key for heat propagation (Campen, 2005).

High wind speed event (Djibrilla et al., 2024)

Along XY plane

Along YZ plane

Temperature

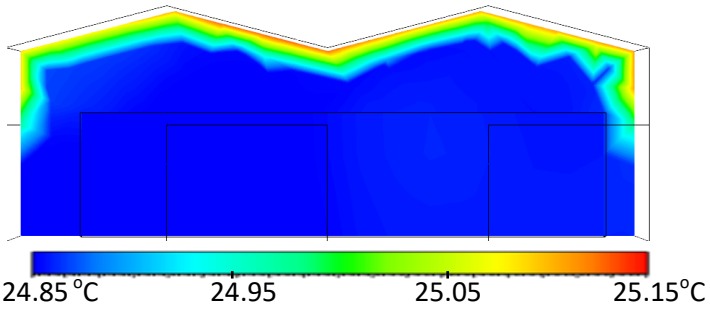


Density

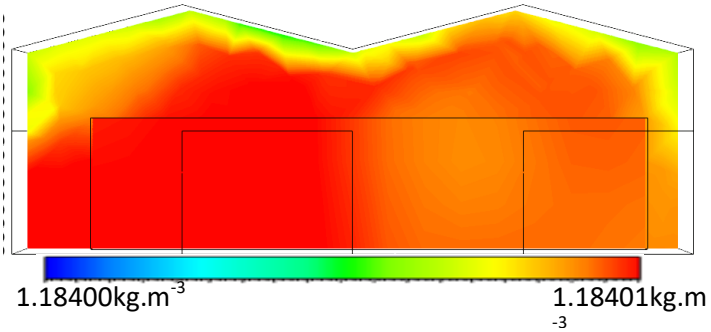


Pressure

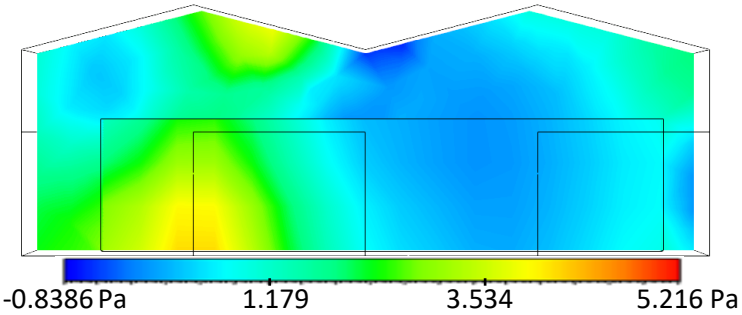


Velocity

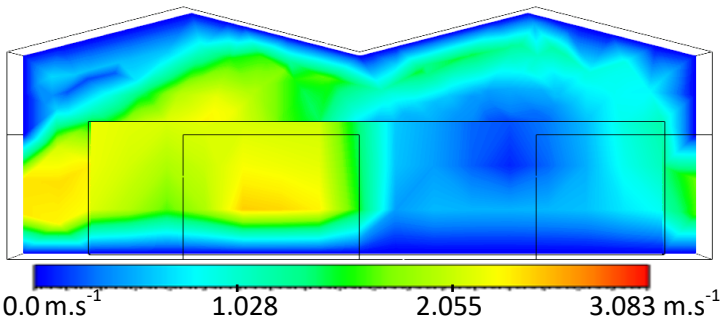


**Figure 4. 135** Temperature, density, pressure and velocity contours at high wind speed event

The case scenario of high sun radiation event occurred during a day with wind coming from the south-east ($170^{o}$). Temperature was at its lowest value right from the cooling wall inlet ($26.85^{o}C$) and at the highest value or at hotter point at the upper edge of the greenhouse and a part of the ground via radiation. Temperature rapidly increased due to heat transferred by photons from the sunshine. The far edge away from the blower happened to be cooler and air got denser there with less pressure. It is probably because this corner place is away from sun rays though accumulating humid cooler air as being closer to the exit. The covering material which is filtering near infrared radiation played a role in keeping the temperature constant within the greenhouse as indicated by Kumar et al. (2009). Besides, the temperature results obtained at night were lower than those obtained in the days as also noticed by Ahmed et al. (2010) when using evaporative cooling pads.

High sun radiation event (Djibrilla et al., 2024)

Along XY plane

Along YZ plane

Temperature

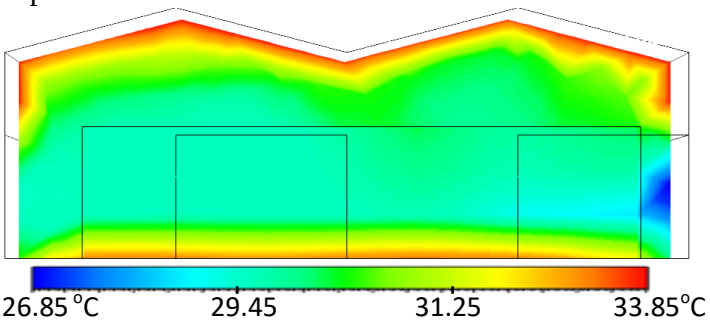


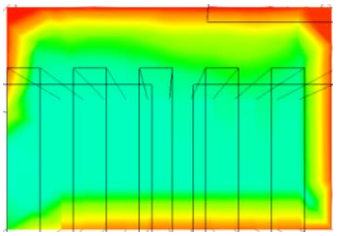

Density

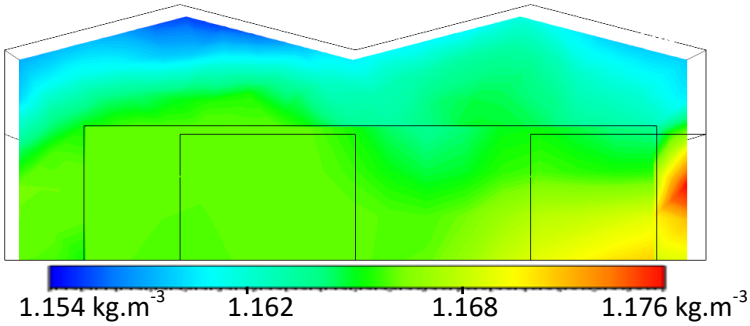


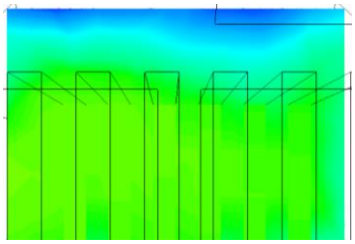

Pressure

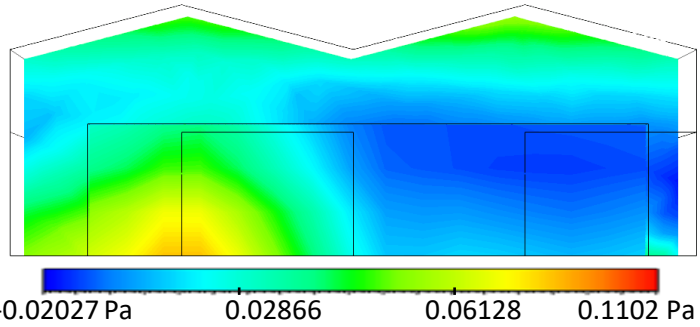


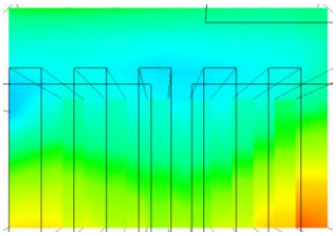

Velocity

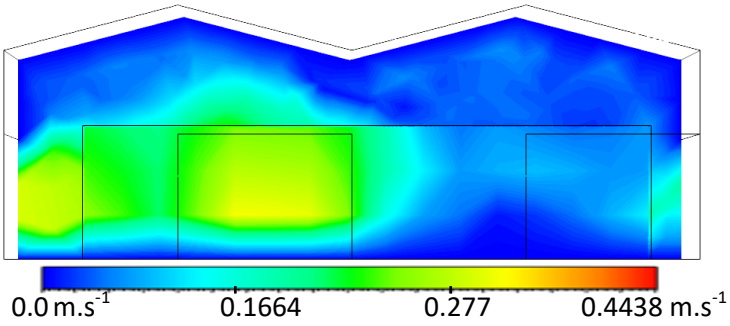


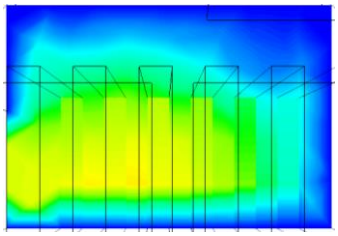

**Figure 4. 136** Temperature, density, pressure and velocity contours at high sun radiation event

The low temperature scenario occurred at latter part of the night towards dawn whereby wind speed was very low and even not well detected by the weather station sensor. At that moment, the temperature nearby the inlet cooler was 15.7$^{o}$C. Pressure was low and constant along the canopy height. The atmosphere was less dense except at the inlet.

Low temperature event (Djibrilla et al., 2024)

Along XY plane

Along YZ plane

Temperature

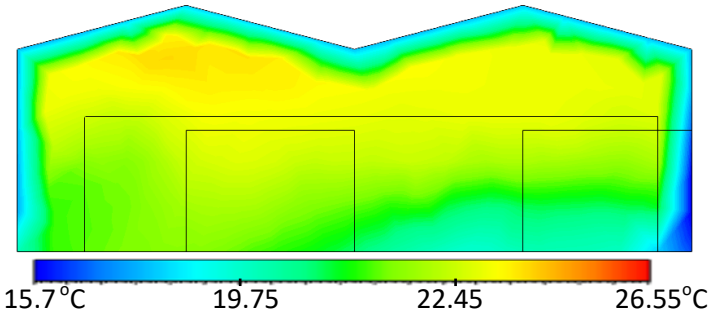


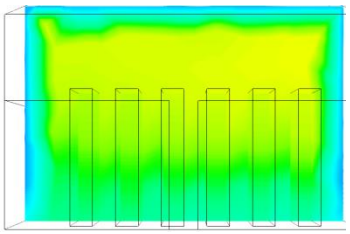

Density

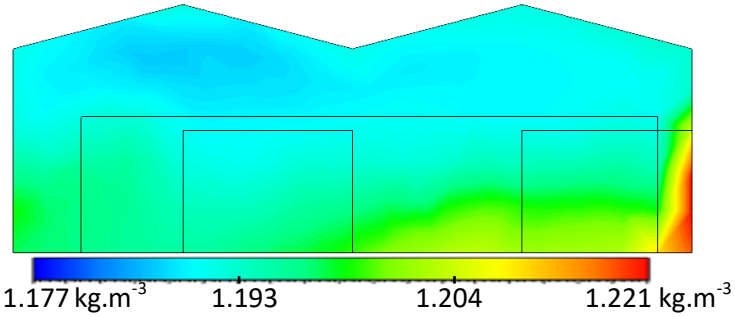


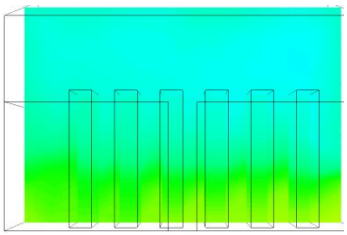

Pressure

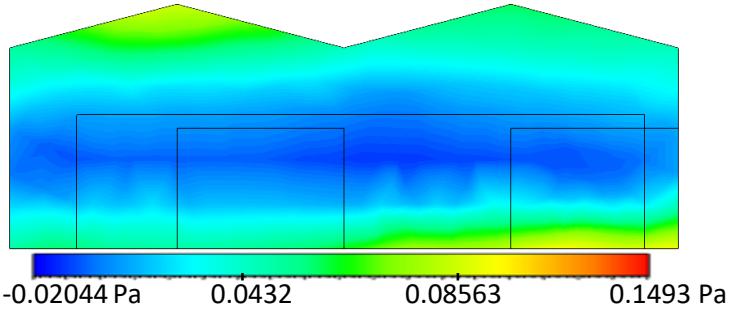


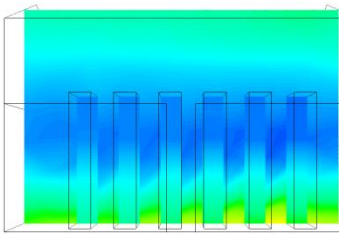

Velocity

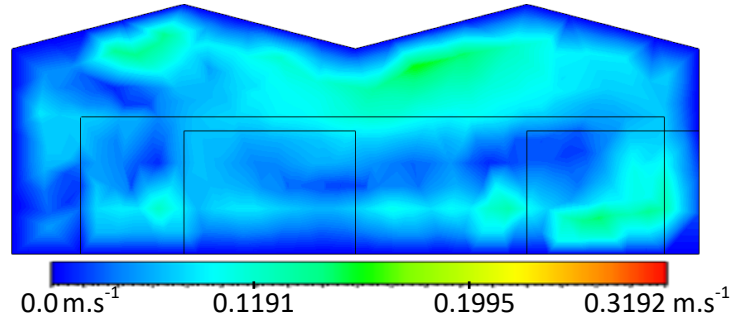


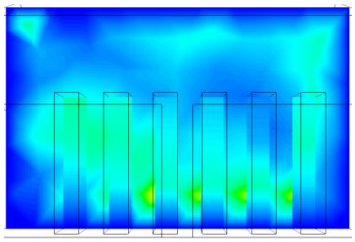

**Figure 4. 137** Temperature, density, pressure and velocity contours at low temperature event

In figure 4.137, hot air entered and spread throughout the greenhouse. This event occurred when coolers were down for maintenance after cultivation and the outside weather conditions were hot as well. The accumulated heat accompanied with heat radiated by the soil made the ground hot with some point reaching temperature beyond 60$^{o}$C. However, most temperature was between 36.05 $^{o}$C and 47.85$^{o}$C. As suggested by Kumar et al. (2009), during hot season ventilation with ventilation area between 15-30% at the ridge of the greenhouse could reduce the temperature for a while as well as the use of cladding material with ability to reflect near infrared radiation.

High temperature event (Djibrilla et al., 2024)

Along XY plane

Along YZ plane

Temperature

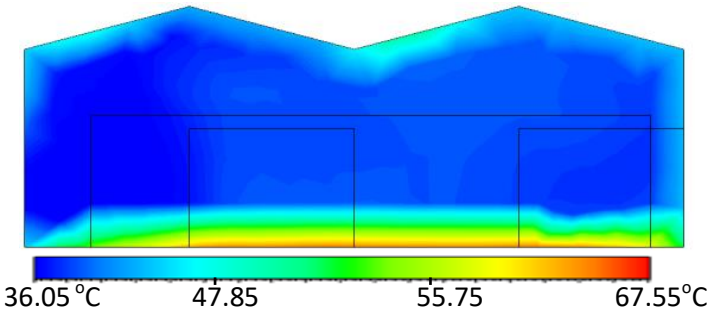


Density

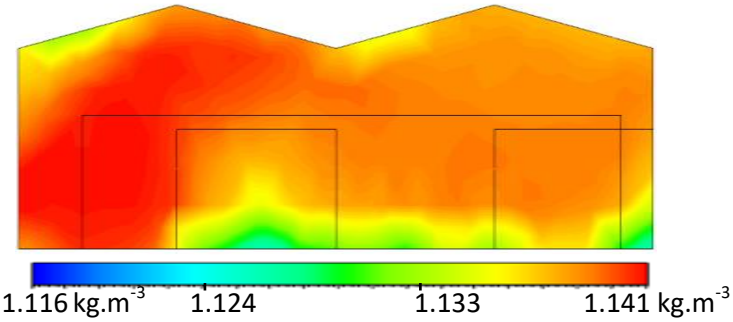


Pressure

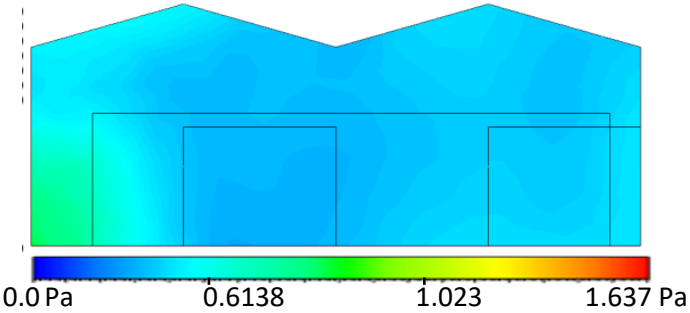


Velocity

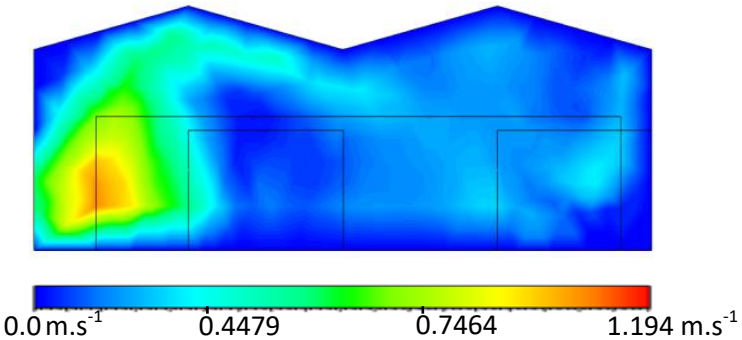


**Figure 4. 138** Temperature, density, pressure and velocity contours at high temperature event

### 4.7.2 Thermal and flow pattern of the greenhouse microclimate under forced convection

#### 4.7.2.1 Comparative thermodynamic data of coolers for the cooling system

**Table 4.61** Thermodynamic parameters of studied pads (Djibrilla et al., 2021a).

| Parameters | Cooling pads | |
|---|---|---|
| | **Hyphaene fibers** | **Celdek** |
| Average saturation efficiency | 78.80% | 79.80% |
| Average mass flow rate, kg/s | 0.012 | 0.012 |
| Average cooling capacity, kJ/s | 0.172 | 0.170 |
| Average heat transfer coefficient, $kW/m^{2c}C$ | 4.699 | 4.518 |
| Average Mass transfer coefficient, kg/s | 0.875 | 1.395 |
| Average Coefficient Of Performance | 9.036 | 6.557 |
| Cost to Efficiency Ratio | 5.25 | 20.73 |
| Minimum temperature from the coolers, T ($^oC$) | 20.00 | 20.50 |
| Average temperature from the coolers, T ($^oC$) | 21.83 | 20.92 |
| Average relative humidity of wind from coolers, RH (%) | 33.33% | 50.00% |

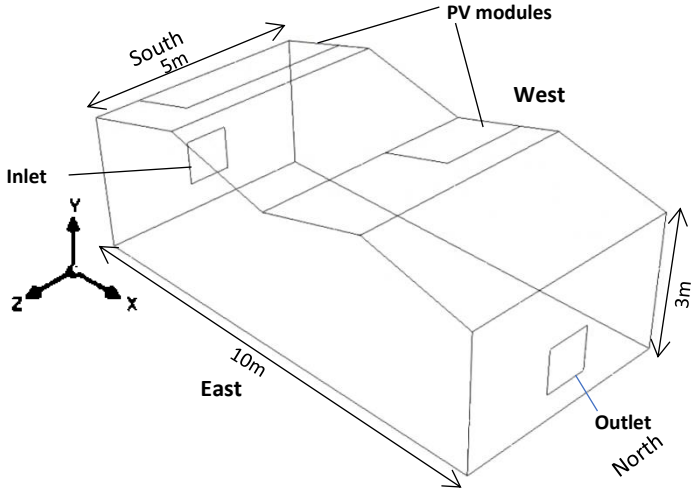


**Figure 4. 139** Greenhouse under natural convection

#### 4.7.2.2 CFD analysis under forced convection

The results of the simulation are presented in the figures below. Results of the simulations were viewed on planes ZX (Y= 0.75m) and XY (Z= -2.5m)

Due to the differences in physical parameters, the air blown from of Celdek (1.166 m/s) and Hyphaene fibers (0.825 m/s) pads did not have the same trend (figure 4.140). As moving far away from the inlet, velocity magnitude dropped and got constantly low at about 6.5 m away (Figure 4.141). The air velocity affects many other parameters such as temperature, density, pressure and others. This was proven by Campen (2005) who found that a low air flow rate is disadvantageous in a greenhouse of length around 12 m making cooling not easy. Hence, additional ventilation is necessary to secure cool environment.

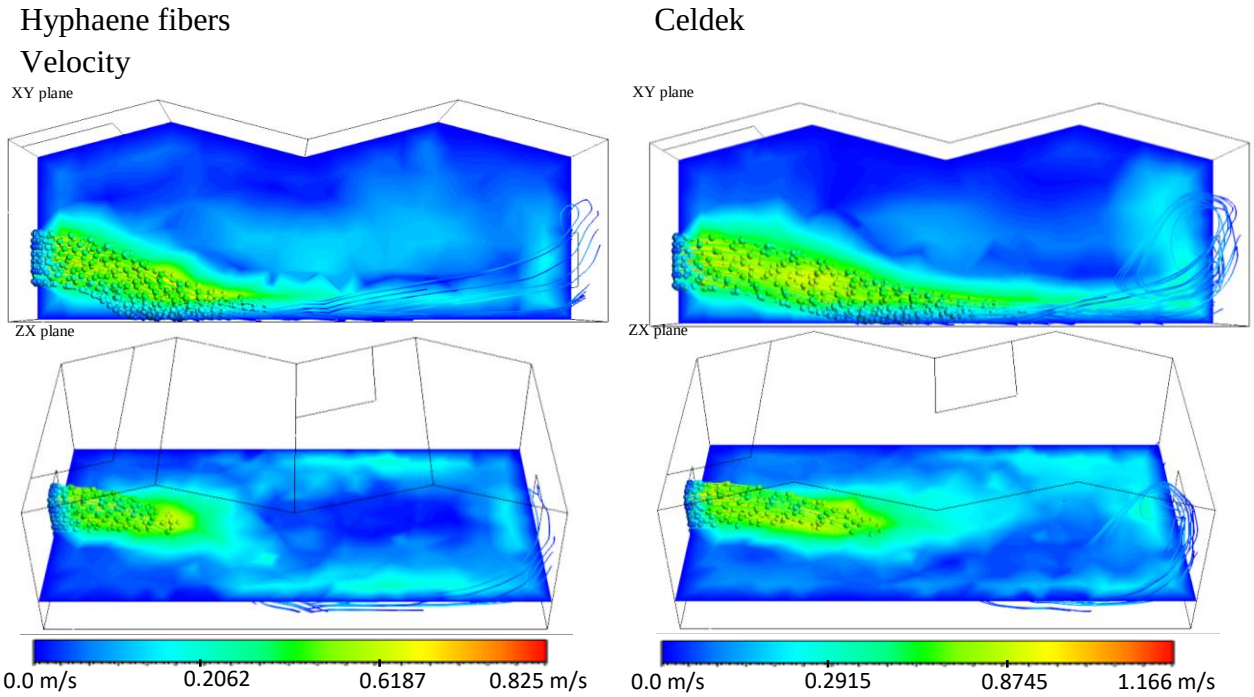


**Figure 4. 140** Velocity contours

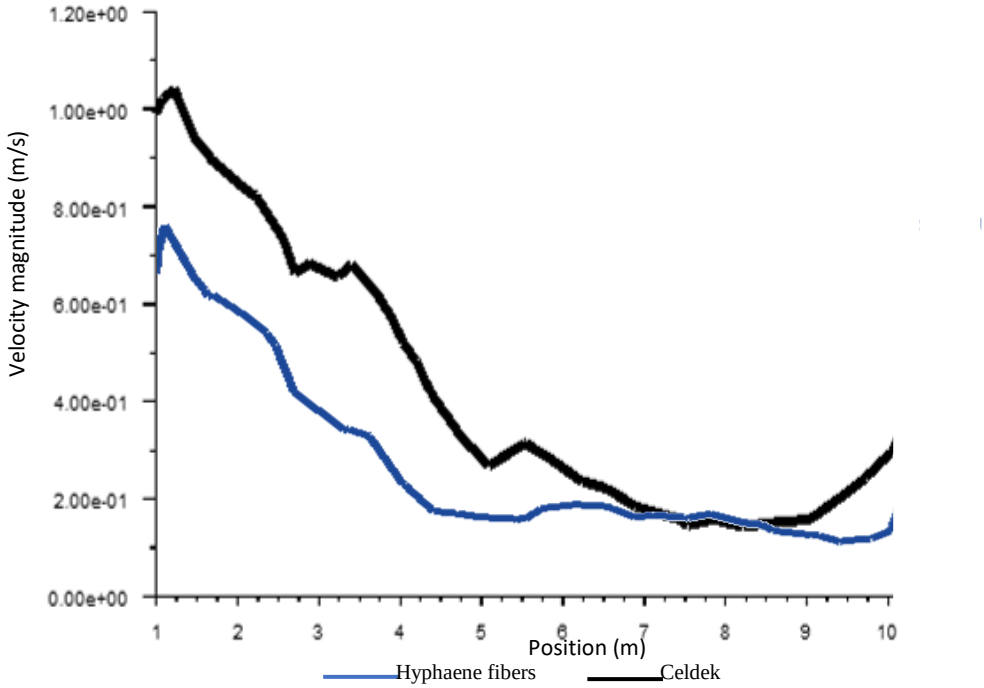


**Figure 4. 141** Plot of velocity magnitude from inlet to outlet

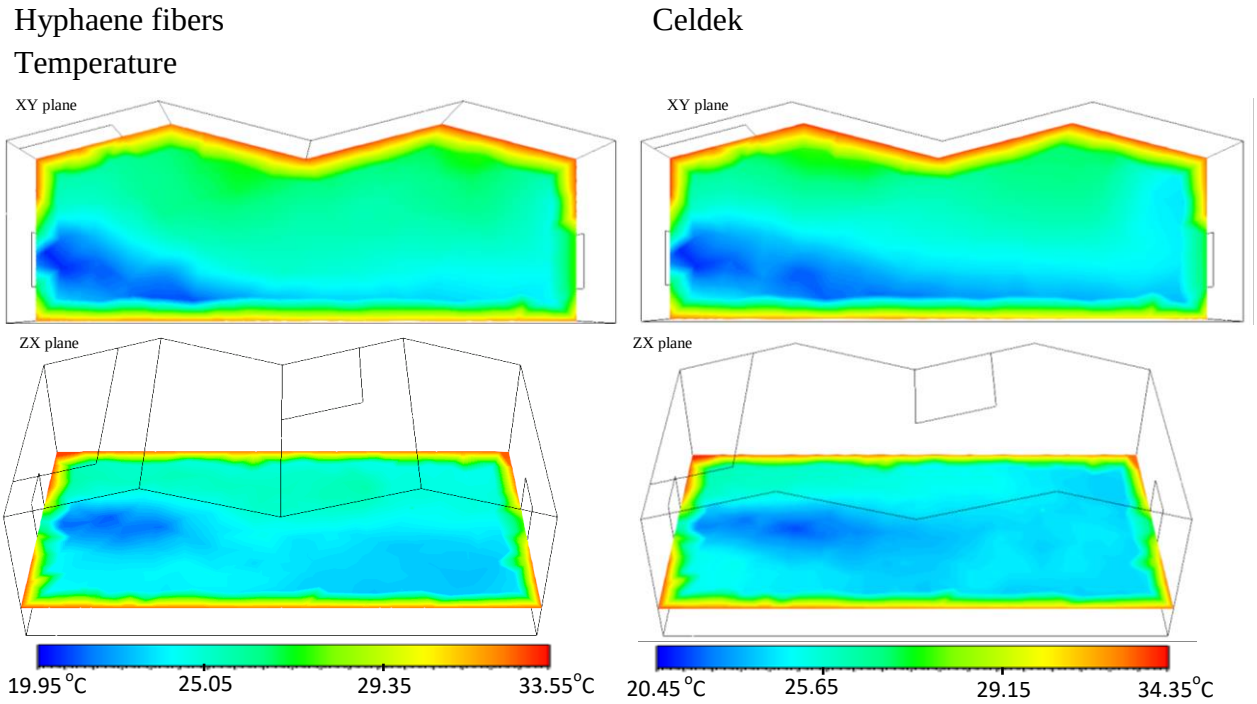


**Figure 4. 142** Temperature contours

In fact, the temperature contours, as influenced by velocity of air stream, showed that cool air of below 24°C could be spread up to 5 m from Celdek pad against 3.75 m from Hyphaene fiber pad. Yet, both air streams along the line parallel to the inlet-outlet line were kept below 25°C. However, on the top and side extremities, temperature could reach 33.55°C (Hyphaene fibers pad) and 34.55°C (Celdek pad). Between the middle of the greenhouse and the extreme top of the greenhouse, a difference of about 6.35°C (Hyphaene fiber case) and 6.95°C (Celdek case) was noticed. Similar results were obtained by Saberian & Sajadiye (2019) who noticed heat accumulation at the roof with a variation of up to 8°C between the floor and the roof.

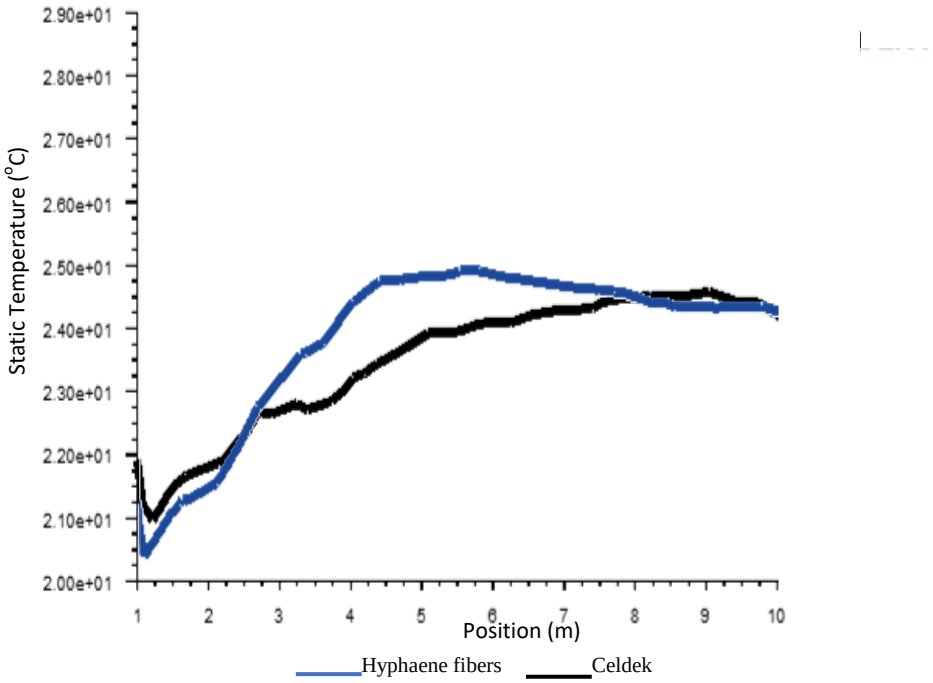


**Figure 4. 143** Plot of static temperature from inlet to outlet

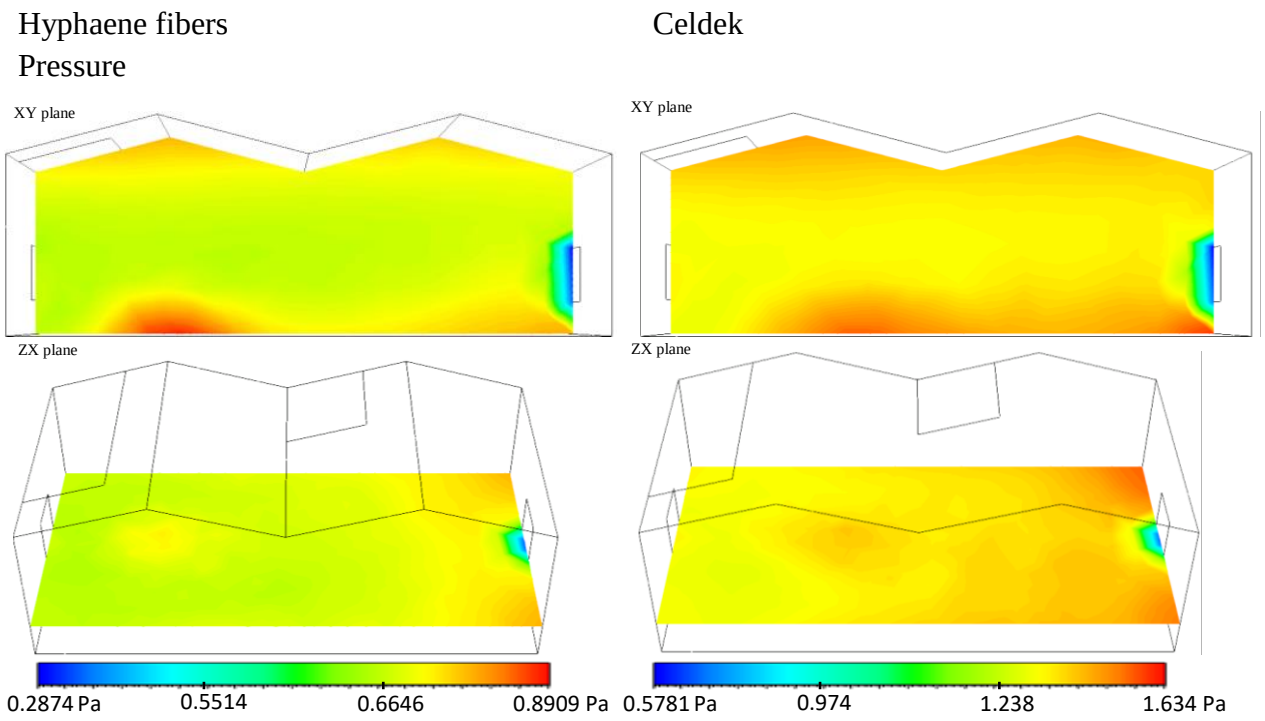


**Figure 4. 144** Pressure contours

Pressure was relatively constant in both cases even though the static pressure value of Celdek pad (1.42 Pa) was about the double to that of Hyphaene fibers pad (0.71 Pa). This was due to the velocity of the inlet air being practically the double as well. Pressure magnitudes were more noticed in Celdek pad cases, again, due to higher air stream velocity. Less pressure was noticed at the exit from the structure.

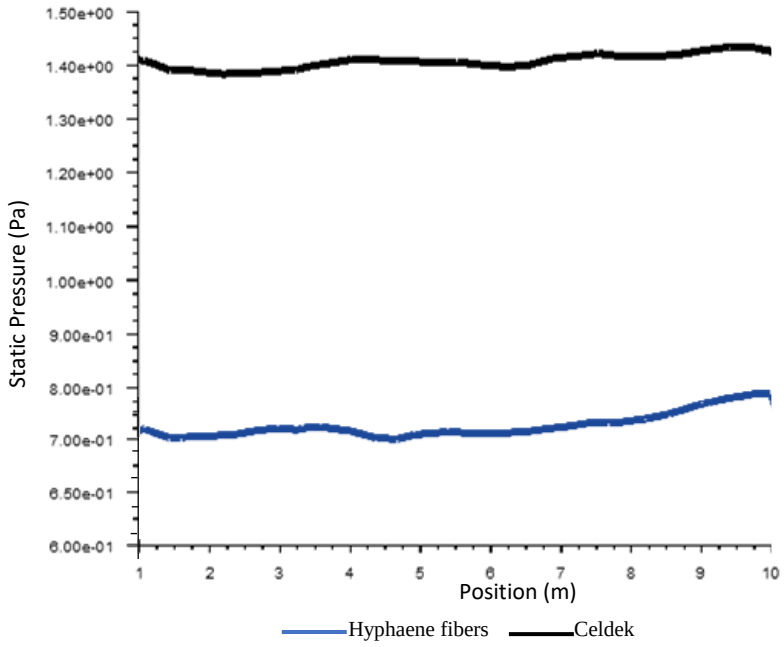


**Figure 4. 145** Plot of static pressure from inlet to outlet

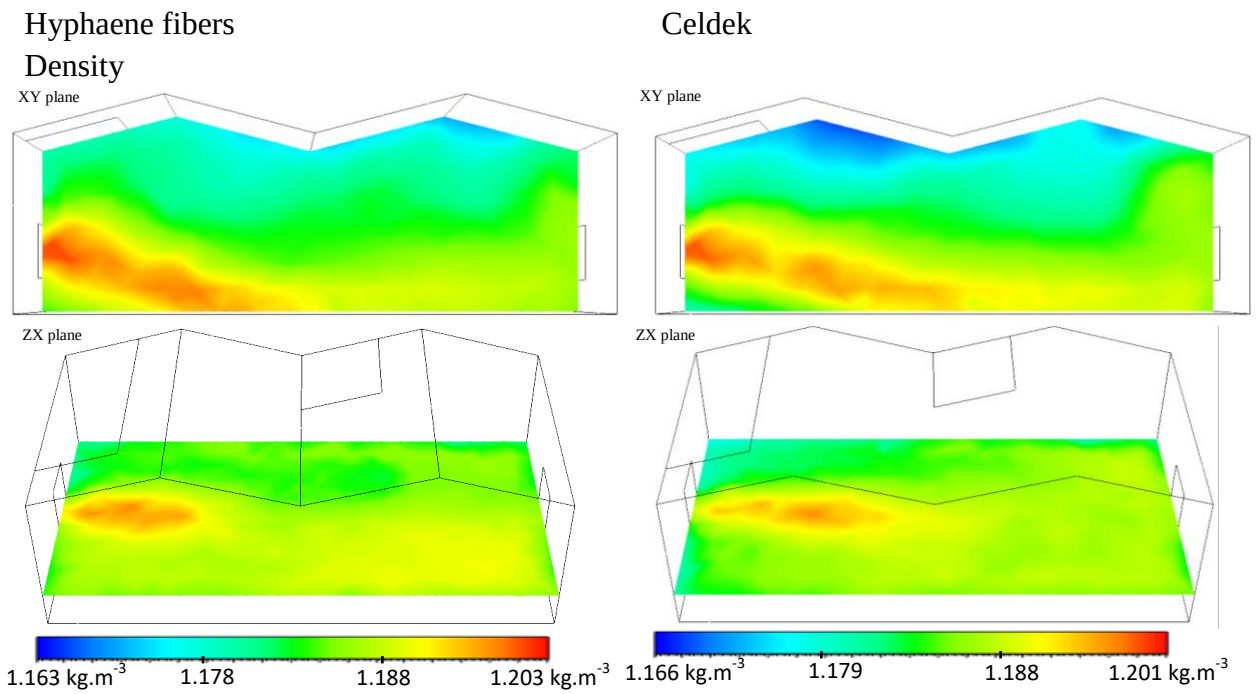


**Figure 4. 146** Density contours

Density was at its highest value (1.2 kg/m$^3$) at the outlet of the cooler and at its lowest value (1.16 kg/m$^3$) around the roof (see figure 4.146). Following the air stream line, density was low at about 5.6 m and 9 m away from the inlet for Hyphaene fiber and Celdek pads respectively (figure 4.147). The molecular viscosity (figure 4.148) was inversely proportional to the density. The higher the density, the lower the molecular viscosity is and the more difficult it is for molecules to flow. Molecular viscosity is the kinematic viscosity at the molecule level. It represents the frictions between molecules in the fluid. A variation in molecular viscosity was observed between 1.829 x $10^{-5}$ kg/m.s to 1.837 x $10^{-5}$ kg/m.s.

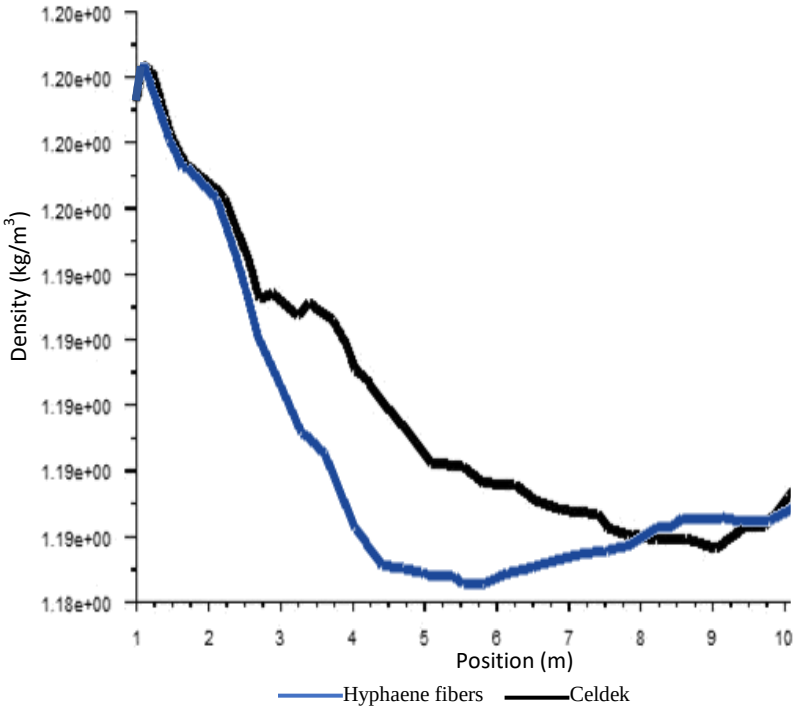


**Figure 4. 147** Plot of density from inlet to outlet

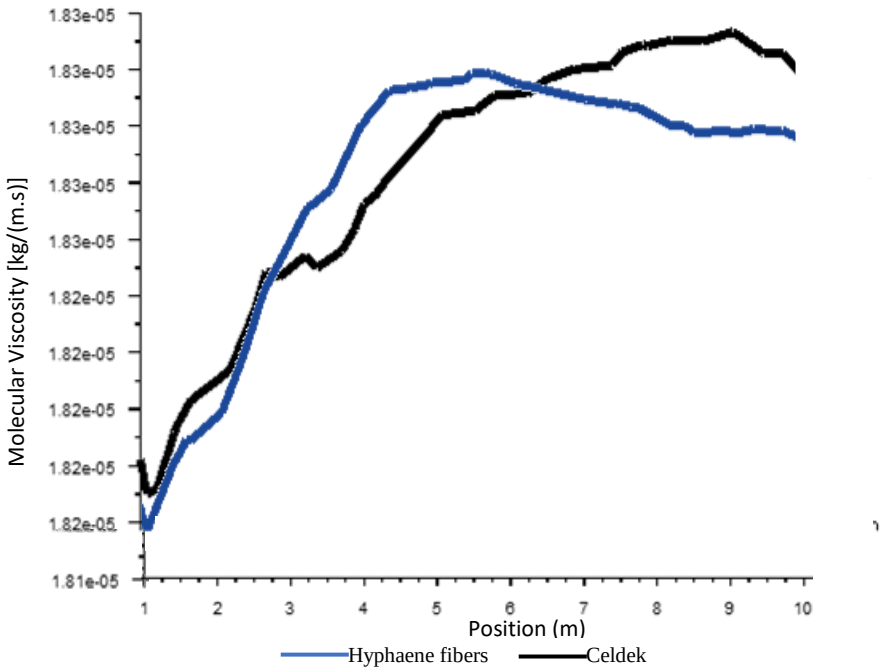


**Figure 4. 148** Plot of molecular viscosity from inlet to outlet

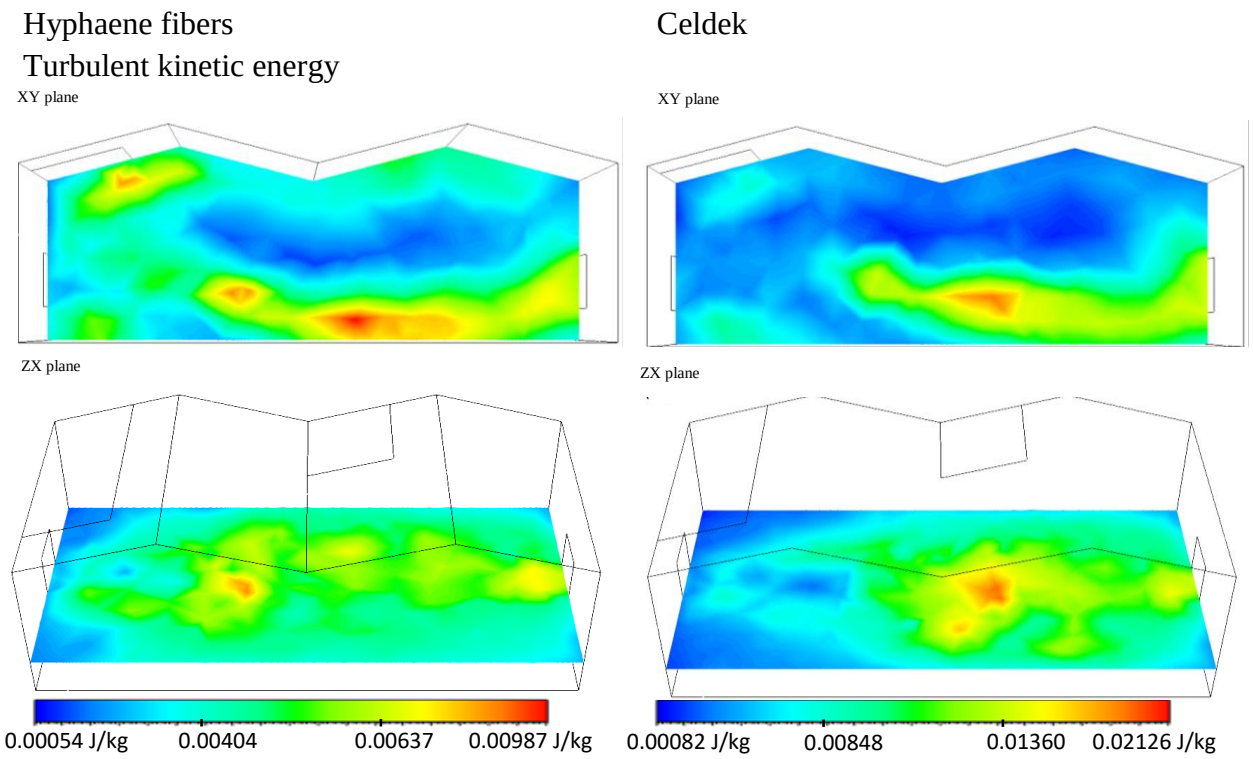


**Figure 4. 149** Turbulent kinetic energy contours

Representing the mean kinetic energy per unit mass, the turbulent kinetic energy through presented contours showed higher turbulence at an interval of 2 to 6 m (0.00404 - 0.00987 J/ kg) and 4 to 9 m (0.00848 – 0.02126 J/ kg) away from the heat source or the inlet for Hyphaene fibers and Celdek pad respectively. The turbulent in the case of Hyphaene fiber is felt a the top of the first compartment and at the bottom of the second compartment while due to the velocity increase, turbulence is predominant at the bottom of the second compartment in the case of Celdek. This is cause by the buoyancy force and the force due to air flow resulting in heat accumulation. The same case was noticed by Campen (2005).

The rate at which turbulent kinetic energy is converted into thermal internal energy per unit volume and time is known as the specific dissipation rate. Both contours showed higher dissipation rate at the inlet up to 2 m away from the blower. A value of $32.78s^{-1}$ was from Celdek pad air stream due to its higher velocity against 16.47 $s^{-1}$ obtained from Hyphaene fibers pad. Dissipation got higher again at the bottom of the second compartment for the Hyphaene fiber case where turbulence occurred most and it is the same situation for the case of Celdek pad.

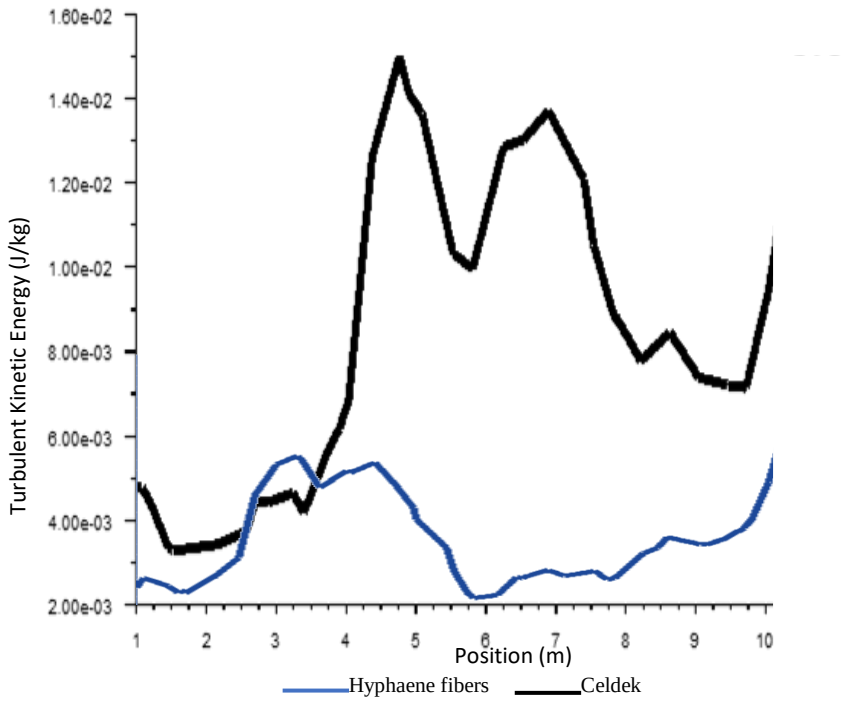


**Figure 4. 150** Plot of turbulent kinetic energy from inlet to outlet

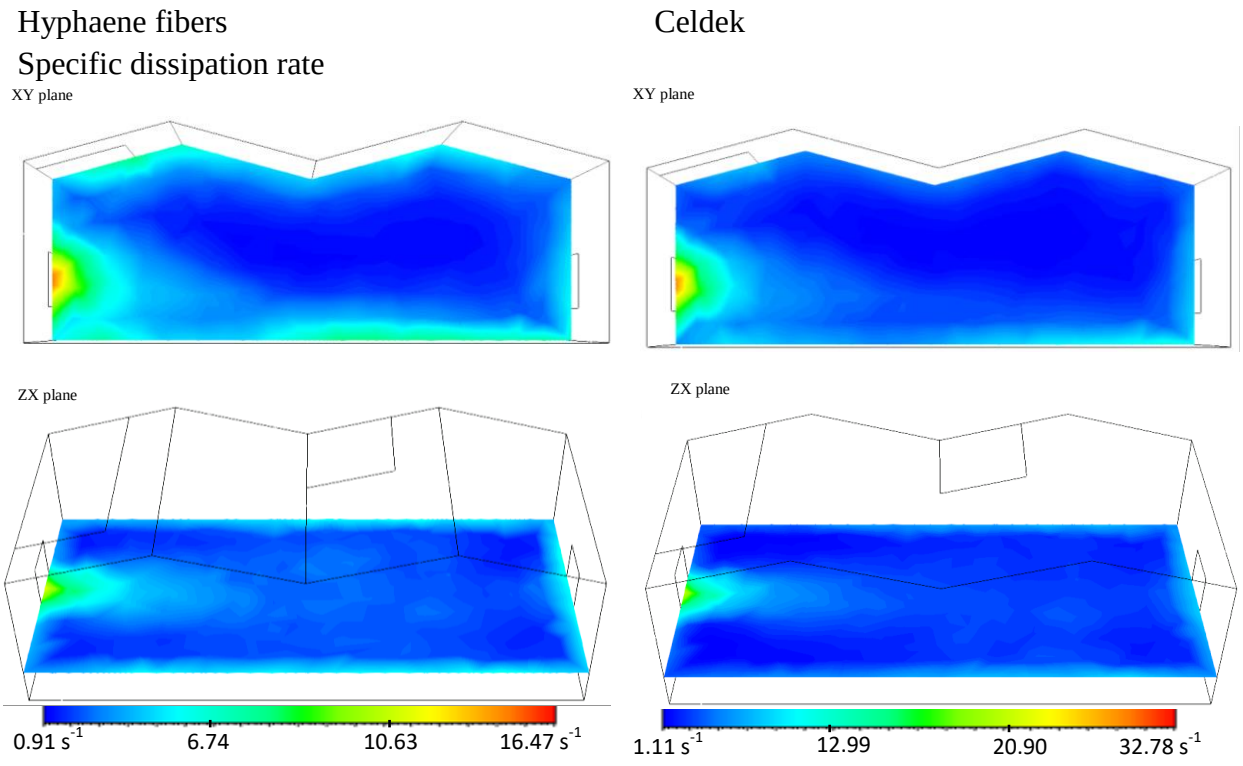


**Figure 4. 151** Specific dissipation rate contours

# 5 CONCLUSION AND RECOMMENDATIONS

## 5.1 Conclusion

Photovoltaic cooling greenhouse was successfully designed using Robot Structural software and constructed on the field using local materials such as locally made cooling pad whose performance was compared to the one using Celdek cooling pads.

The experiment on local cellulosic material as alternative cooling pad materials has been successful. Cooling pad from the fibers of the stipulates of Hyphaene thebaica emerged to be the most performing pad with thermodynamic characteristics challenging those of the commercial Celdek pad and having the best cost-to-efficiency ratio (9.97). The CFD analysis, using ANSYS software, of the thermal behavior of the PV greenhouse microsystem under forced convection via application of evaporative cooler from Hyphaene thebaica fibers pad showed that temperature could be kept around 24$^{o}$C in an environment when outside temperature was between 35 $^{o}$C and 40$^{o}$C. This can make the environment conducive for farming vegetables, rearing animals or even for human comfort zone. Due to the ecofriendly nature of Hyphaene fiber evaporative cooler, it is one of the best adaptive solutions and an opportunity to mitigating the disastrous effects of global warming.

Preliminary crop cultivation under ambient conditions was done. Data obtained on physical, thermal and production characteristics of those cultivated crops showed reasonable performances compared to literature. In most cases, biologically grown crops were showing productivity close to that under chemical fertilizers but were facing environmental inconveniences such as bad weather and invaders threat. From this experiment, photosynthetic pigments (carotenes, xanthophylls, chlorophyll a, chlorophyll b) were successfully extracted in optimum extraction conditions such as a ratio (m:v) of 1:4 between the mass of plant material and a solvent, ethanol, for good filtration at an optimum volume. Individual photosynthetic pigments were distinctly identified and easily recovered with great purity through their colors and frontal relationships through thin layer chromatography characterization method with the best eluent composition (75% petroleum ether and 25% acetone). All these photosynthetic pigments were present in vegetables studied: lettuce (*Lactuca sativa* - Eden variety), zucchini or courgette (*Curcubita pepo* - F1 color variety), tomato (*Solanum lycopersicum* - F1 mongal variety), potato (*Solanum tuberosum L.* - Pamela variety) and green pepper (*Capsicum annuum* - Jason variety). This investigation allowed to know the optimum conditions to duplicate for greenhouse crops cultivation and conditions needed at various growth stages.

The simultaneous experiment carried out inside and outside greenhouse showed that plants inside greenhouse grew much better than outside, yet, due to the season favorable and made for that variety, outside plants produced more fruits than inside. However, the number of spoilt, rotten or damaged fruits outside was much more important than the number of fruits inside the greenhouse with the latter quality, richness in crude fiber, energy and protein, being relatively higher.

Furthermore, very little production was observed in one of the greenhouses which must be investigated by experts in the domain in order to understand better this phenomenon.

Energy used for the cooling, mostly during the day, was in excess due to high sun days, yet not enough to power the system for 24h. Optimization could make the system more cost effective.

### 5.2 Recommendations

Study could be conducted using another covering or cladding material such as High-Density PE plastic specialized for greenhouse in order to compare performance with Jute bag covering material. An automated drip irrigation system should be installed to optimize water usage. A better adapted variety of tomato or selected crop should be used for greenhouse. A redefinition of organic crop cultivation should be done such that using organic fertilizer all out except at the stage of combating stubborn pests because some organic pesticides aren't powerful enough. This could lead to 50% to 90% organic farming which will maximize profit. For the energy optimization, more batteries should be used in order to cover for full day and night usage.

# 6 REFERENCES

Ahmed, E. M., Abaas, O., & Ahmed, M. (2010). Performance evaluation of three different types of local evaporative cooling pads in greenhouses in Sudan. *Saudi Journal of Biological Sciences, 18*(1), 45–51. https://doi.org/10.1016/j.sjbs.2010.09.005

Alvarado, S. A., & Klein, F. L. (1970). Property tables and charts: Table a – 9. In *Thermophysical Properties of Matter* (Vol. 3, pp. 939–956).

Amitrano, C., Rouphael, Y., Pannico, A., De Pascale, S., & De Micco, V. (2021). Reducing the evaporative demand improves photosynthesis and water use efficiency of indoor cultivated lettuce. *Agronomy*, *11*(7). https://doi.org/10.3390/agronomy11071396

Arbel, A., Barak, M., & Shklyar, A. (2003). Combination of Forced Ventilation and Fogging Systems for Cooling Greenhouses. *Biosystems Engineering*, *84*(1), 45–55. https://doi.org/10.1016/S1537-5110(02)00216-7

Arbel, A., Yekutieli, O., & Barak, M. (1999). Performance of a Fog System for Cooling Greenhouses. *J. Agric. Engng Res.*, *72*, 129–136.

ASHRAE. (1992). *Psychrometric Chart No. 1* (p. 1). Center for applied thermodynamics studies.

ASHRAE. (2013). *ASHRAE Handbook Fundamentals (SI)* (pp. 9.11-9.14). ASHRAE.

Aziz, A., Mainil, R. I., Mainil, A. K., & Listiono, H. (2017). Effect of water temperature and air stream velocity on performance of direct evaporative air cooler for thermal comfort Effect of Water Temperature and Air Stream Velocity on Performance of Direct Evaporative Air Cooler for Thermal Comfort. *AIP Conference Proceedings*, *030024*(2017), 1–6. https://doi.org/10.1063/1.4968277

Bakker, J. C., Zwart, H. F. De, & Campen, J. B. (2006). Greenhouse Cooling and Heat Recovery using Fine Wire Heat Exchangers in a Closed Pot Plant Greenhouse : Design of an Energy Producing Greenhouse. In B. J. Bailey (Ed.), *Plant Research International*. Acta Horticulturae.

Baneshi, M., Gonome, H., & Maruyama, S. (2020). Wide-range spectral measurement of radiative properties of commercial greenhouse covering plastics and their impacts into the energy management in a greenhouse. *Energy*, *210*, 118535. https://doi.org/10.1016/j.energy.2020.118535

Barzegar, M., Layeghi, M., Ebrahimi, G., Hamzeh, Y., & Khorasani, M. (2012). Experimental evaluation of the performances of cellulosic pads made out of Kraft and NSSC corrugated papers as evaporative media. *Energy Conversion and Management*, *54*(1), 24–29. https://doi.org/10.1016/j.enconman.2011.09.016

Bruno, F. (2009). Technical background research on evaporative air conditioners and feasibility of rating their water consumption. In *WATER RATING* (Issue September 2009). copyright@agriculture.gov.au.

Campen, J. B. (2005). Greenhouse Design Applying CFD for Indonesian Conditions. *Agrotechnology & Food Innovations*, *691*(ISHS 2005), 419–424.

Carlini, M., Honorati, T., & Castellucci, S. (2012). Photovoltaic Greenhouses : Comparison of Optical and Thermal Behaviour for Energy Savings. *Mathematical Problems in Engineering*, *2012*(Article ID 743764), 10. https://doi.org/10.1155/2012/743764

Chijioke, O. V. (2017). Review on Evaporative Cooling Systems By Review on Evaporative Cooling Systems. *Greener Journal of Science, Engineering and Technology Research*, *7*(1), 1–20. https://doi.org/http://doi.org/10.15580/GJSETR.2017.1.031817038

Cossu, M., Murgia, L., Ledda, L., Deligios, P. A., Sirigu, A., Chessa, F., & Pazzona, A. (2014). Solar radiation distribution inside a greenhouse with south-oriented photovoltaic roofs and effects on crop productivity. *APPLIED ENERGY*, *133*(2014), 89–100. https://doi.org/10.1016/j.apenergy.2014.07.070

CRA-Dosso. (2018). Fiche technico-économique pour la culture de la laitue Région de Dosso. *Chambren Régionale d'Agriculturende Dosso*, *February (*(1), 1–4.

CRA-Maradi. (2017, August). Fiche technico-économique pour la culture de la tomate. *Chambre Régionale d'Agriculture de Maradi*, *August (20*(1), 1–4.

Cuce, E., Harjunowibowo, D., & Mert, P. (2016). Renewable and sustainable energy saving strategies for greenhouse systems : A comprehensive review. *Renewable and Sustainable Energy Reviews*, *64*(2016), 34–59. https://doi.org/10.1016/j.rser.2016.05.077

Dajuma, A., Yahaya, S., Touré, S., Diedhiou, A., & Adamou, R. (2016). Sensitivity of Solar Photovoltaic Panel Efficiency to Weather and Dust over West Africa : Comparative Experimental Study between Niamey ( Niger ) and Abidjan ( Côte d ' Ivoire ). *Scientific Research Publishing*, *2016*(5), 123–147. https://doi.org/10.4236/cweee.2016.54012

Djibrilla, A. S. M., Abdoulkader, A. H., Illyassou, K. M., Aissetou, D. Y., & Rabani, A. (2021a). Investigation of Evaporative Cooling Pad Material from Hyphaene Thebaica Fibers. *Journal of Engineering Research and Reports*, *21*(9), 64–75. https://doi.org/10.9734/JERR/2021/v21i917491

Djibrilla, A. S. M., Abdoulkader, A. H., Illyassou, K. M., Aissetou, Y., & Rabani, A. (2021b). Performance of Evaporative Cooling Pads Made from Different Plant Materials of Sub-Saharan Area ( NIGER ). *LC International Journal of STEM*, *02*(04), 38–49. https://doi.org/10.5281/zenodo.0000000

Djibrilla, A. S. M., Rabani, A., Illyassou, K. M., Abdoulkader, A. H., & Aissetou, D. Y. (2024). CFD Analysis of Photovoltaic Greenhouse Cooling System Through Natural Convection as a Nature-Based Solution to a Sustainable Agriculture in Niger, Sahel Region. In W. Leal Filho, G. J. Nagy, & D. Ayal (Eds.), *Handbook of Nature-Based Solutions to Mitigation and Adaptation to Climate Change* (Springer C, p. 18). Springer Nature Switzerland AG 2024. https://doi.org/https://doi.org/10.1007/978-3-030-98067-2_141-1

Elsner, B. Von, Briassoulis, D., Waaijenberg, D., Mistriotis, A., Zabeltitz, C. Von, & Gratraud, J. (2000). *Review of Structural and Functional Characteristics of Greenhouses in European Union Countries , Part II : Typical Designs*. 111–126. https://doi.org/10.1006/jaer.1999.0512

Erim, M., Udo, S. O., Ewona, I. O., Chukwujindu, S., Ogbulezie, J. C., & Okechukwu, S. (2023). Potential impacts of climate change on global solar radiation and PV output using the CMIP6 model in West Africa. *Cleaner Engineering and Technology*, *13*(November 2022), 100630. https://doi.org/10.1016/j.clet.2023.100630

Fatnassi, H., Poncet, C., Bazzano, M. M., Brun, R., & Bertin, N. (2015). A numerical simulation of the photovoltaic greenhouse microclimate. *Solar Energy*, *120*, 575–584. https://doi.org/10.1016/j.solener.2015.07.019

Ferziger, J. H., Peric, M., & Street, R. L. (2020). *Computational Methods for Fluid Dynamics* (4th ed.). Springer Cham. https://doi.org/https://doi.org/10.1007/978-3-319-99691-6

Fidaros, D., Baxevanou, C., Bartzanas, T., & Kittas, C. (2008). Flow characteristics and temperature patterns in a fan ventilated greenhouse. *Acta Horticulturae*, *797*(June 2014), 123–130. https://doi.org/10.17660/actahortic.2008.797.15

Fuchs, M., Dayan, E., & Presnov, E. (2006). Evaporative cooling of a ventilated greenhouse rose crop. *Evaporative Cooling of a Ventilated Greenhouse Rose Crop*, *138*(2006), 203–215. https://doi.org/10.1016/j.agrformet.2006.05.002

Ghosal, M. K., Tiwari, G. N., & Srivastava, N. S. L. (2004). *Thermal modeling of a greenhouse with an integrated earth to air heat exchanger : an experimental validation*. *36*, 219–227. https://doi.org/10.1016/j.enbuild.2003.10.006

Górecki, R. S., & Górecki, M. T. (2010). Utilization of waste wool as substrate amendment in pot cultivation of tomato, sweet pepper, and eggplant. *Polish Journal of Environmental Studies*, *19*(5), 1083–1087.

Guichard, S., Gary, C., Leonardi, C., & Bertin, N. (2005). Analysis of growth and water relations of tomato fruits in relation to air vapor pressure deficit and plant fruit load. *Journal of Plant Growth Regulation*, *24*(3), 201–213. https://doi.org/10.1007/s00344-005-0040-z

Gupta, M. J., & Chandra, P. (2002). Effect of greenhouse design parameters on conservation of energy for greenhouse environmental control. *ENERGY*, *27*(2002), 777–794.

Harjunowibowo, D., DING, Y., OMER, S., & RIFFAT, S. (2018). RECENT ACTIVE TECHNOLOGIES OF GREENHOUSE SYSTEMS –. *Bulgarian Journal of Agricultural Science*, *24*(1), 158–170.

Hassanien, R. H. E., Li, M., & Lin, W. D. (2016). Advanced applications of solar energy in agricultural greenhouses. *Renewable and Sustainable Energy Reviews*, *54*(2016), 989–1001. https://doi.org/10.1016/j.rser.2015.10.095

Hemming, S., Kempkes, F., Braak, N. Van Der, Dueck, T., & Marissen, N. (2006). *Greenhouse Cooling by NIR-reflection*. 97–106.

Impron, I., Hemming, S., & Bot, G. P. A. (2007). *Simple greenhouse climate model as a design tool for greenhouses in tropical lowland*. *98*, 79–89. https://doi.org/10.1016/j.biosystemseng.2007.03.028

International Association for the Properties of Water and Steam (IAPWS). (1995). Property Tables of Water. *Formulation for the Thermodynamic Properties of Ordinary Water Substance for General and Scientific Use*. https://www.cambridge.org/br/files/9813/6697/5550/Appendix_B.pdf

Iraqi, D., Gauthier, L., Dorais, M., & Gosselin, A. (1997). Influence du déficit de pression de vapeur et de la photopériode sur la croissance , la productivité et la composition minérale de la tomate de serre. *Canadian Journal of Plant Science*, *77*, 267–272.

Jain, D., & Tiwari, G. N. (2002). Modeling and optimal design of evaporative cooling system in controlled environment greenhouse. *Energy Conversion and Management*, *43*(2002), 2235–2250.

Joly, P. (1967). Les pourritures noires des agrumes provoquées par les Alternaria. *Fruits*, *22*(2), 89–95.

Kandji, S. T., Verchot, L., & Mackensen, J. (2006). *Climate Change and Variability in the Sahel Region : Impacts and Adaptation Strategies in the Agricultural Sector* (Issue 2006).

Khobragade, N. N., & Kongre, S. C. (2016). Experimental Performance of Different Evaporative Cooling Pad Material of Direct Evaporative Cooler in Hot and Dry Region. *INTERNATIONAL JOURNAL OF INNOVATIVE TECHNOLOGY AND RESEARCH*, *4*(3), 2920–2923. http://www.ijitr.com

Kittas, C., & Baille, A. (1998). Determination of the Spectral Properties of Several Greenhouse Cover Materials and Evaluation of Specific Parameters Related to Plant Response. *J. Agric. Engng Res.*, *71*(1998), 193–202.

Kläring, H.-P., Schwarz, D., & Heissner, A. (1997). Control of nutrient solution concentration in tomato crop using models of photosynthesis and transpiration. *Acta Horticulturae*, *450*, 329–334.

Kumar, K. S., Tiwari, K. N., & Jha, M. K. (2009). Design and technology for greenhouse cooling in tropical and subtropical regions : A review. *Energy and Buildings*, *41*(2009), 1269–1275. https://doi.org/10.1016/j.enbuild.2009.08.003

Laknizi, A., Mahdaoui, M., Abdellah, A. Ben, Anoune, K., Bakhouya, M., & Ezbakhe, H. (2018). Performance analysis and optimal parameters of a direct evaporative pad cooling system under the climate conditions of Morocco. *Case Studies in Thermal Engineering*, *S2214-157X*(18), 1–22. https://doi.org/10.1016/j.csite.2018.11.013

Laknizi, A., Mahdaoui, M., & Ben, A. (2019). Case Studies in Thermal Engineering Performance analysis and optimal parameters of a direct evaporative pad cooling system under the climate conditions of Morocco. *Case Studies in Thermal Engineering*, *13*(April 2018), 1–11. https://doi.org/10.1016/j.csite.2018.11.013

López, J., Way, D. A., & Sadok, W. (2021). Systemic effects of rising atmospheric vapor pressure deficit on plant physiology and productivity. *Global Change Biology*, *27*(9), 1704–1720. https://doi.org/10.1111/gcb.15548

Lu, N., Nukaya, T., Kamimura, T., Zhang, D., Kurimoto, I., Takagaki, M., Maruo, T., Kozai, T., & Yamori, W. (2015). Control of vapor pressure deficit (VPD) in greenhouse enhanced tomato growth and productivity during the winter season. *Scientia Horticulturae*, *197*, 17–23. https://doi.org/10.1016/j.scienta.2015.11.001

Mahamadou, A., Korodji, D., Maman, A., Magal, G., Oumarou, I. I., & Delmas, P. (2016a). Résultats du conseil de gestion à l'exploitation agricole pour la culture du poivron / campagne 2015 – 2016. *Chambre Régionale d'Agriculture de Diffa*, *1*(1), 1–11.

Mahamadou, A., Korodji, D., Maman, A., Magal, G., Oumarou, I. I., & Delmas, P. (2016b). Résultats du conseil de gestion à l'exploitation agricole pour la culture du poivron / campagne 2015 – 2016. *Chambre Régionale d'Agriculture de Diffa*, *1*(2), 1–7.

Maïga, I. G. D., Serki, I. H., & Zakey, Y. (2021). Fiche technico-économique pour la culture de la pomme de terre Région de Tillabéri. *Chambre Régionale d'Agriculture de Tillaberi*, *January (2*(1), 1–4.

Manuwa, S. I., & Odey, S. O. (2012). Evaluation of Pads and Geometrical Shapes for Constructing Evaporative Cooling System. *Modern Applied Science*, *6*(6), 45–53. https://doi.org/10.5539/mas.v6n6p45

McAdam, S. A. M., & Brodribb, T. J. (2015). The evolution of mechanisms driving the stomatal response to vapor pressure deficit. *Plant Physiology*, *167*(3), 833–843. https://doi.org/10.1104/pp.114.252940

Ministère de l'Agriculture et de l'Elévage. (2019). *Rapport définitif de l'enquête sur les productions horticoles 2018/2019*.

Ministère de l'Agriculture, & PromAP. (2019). Module: Tomate. In *FORMATION DES PRESTATAIRES PUBLICS ET PRIVES DE LA PETITE IRRIGATION Techniques de production des cultures irriguées (Horticole, céréalières, fruitières, etc.)* (p. 31).

Modolon, T. A., Boff, P., Boff, M. I. C., & Miquelluti, D. J. (2012). Homeopathic and high dilution preparations for pest management to tomato crop under organic production system. *Horticultura Brasileira*, *30*(1), 51–57.

Monteith, J. L., & Mike H. Unsworth. (2013). *Principles of Environmental Physics Plants , Animals , and the Atmosphere* (fourth). Elsevier Ltd.

Montemurro, F., Fiore, A., Campanelli, G., Tittarelli, F., Ledda, L., & Canali, S. (2013). Organic fertilization, green manure, and vetch mulch to improve organic zucchini yield and quality. *HortScience*, *48*(8), 1027–1033. https://doi.org/10.21273/hortsci.48.8.1027

Moussa, B., SOUMANA, B., & BALLA, A. (2020). *Titre : Projet de Recherche- Action pour l ' Amélioration de la Filière de Pomme de Terre au Niger ( PRAAF / PT ).*

OECD. (2022). Environmental Fragibility in the Sahel. In *OECD Publishing* (Issue September).

Pal, L., Joyce, M. K., & Fleming, P. D. (2006). A simple method for calculation of the permeability coefficient of porous media. *Tappi Journal*, *5*(9), 10–16.

Pettigrew, W. T., Hesketh, J. D., Peters, D. B., & Woolley, J. T. (1990). A vapor pressure deficit effect on crop canopy photosynthesis. *Photosynthesis Research*, *24*(1), 27–34. https://doi.org/10.1007/BF00032641

Pharmawati, M., & Wrasiati, L. P. (2020). S phytochemical screening and ftir spectroscopy on crude extract from Enhalus acoroides leaves. *Malaysian Journal of Analytical Sciences*, *24*(1), 70–77.

Rai, H., & Lee, G. F. (1964). Separation of Planktonic Algal Pigments by Thin Layer Chromatography. *Analytical Chemistry*, *36*(11), 2208–2209. https://doi.org/10.1021/ac60217a062

Raithby, G. D., & Chui, E. H. (1993). A Finite-Volume Method for Predicting a Radiant Heat Transfer in Enclosures with Participating Media. *Transactions of ASME Journal of Heat Transfer*, *112*, 415–423.

Ray, J. D., Gesch, R. W., Sinclair, T. R., & Hartwell Allen, L. (2002). The effect of vapor pressure deficit on maize transpiration response to a drying soil. *Plant and Soil*, *239*(1), 113–121. https://doi.org/10.1023/A:1014947422468

RECA. (2015). *Gestion intégrée des principaux ravageurs et maladies de des cultures maraîchères au Niger Document technique : la protection de la tomate*. http://www.reca-niger.org/spip.php?article579

Remedio, A. R., Teichmann, C., Buntemeyer, L., Sieck, K., Weber, T., Rechid, D., Hoffmann, P., Nam, C., & Kotova, L. (2019). Evaluation of New CORDEX Simulations Using an Updated Köppen – Trewartha Climate Classification. *Atmosphere*, *10*(726), 1–25. https://doi.org/10.3390/atmos10110726

Saberian, A., & Sajadiye, S. M. (2019). The effect of dynamic solar heat load on the greenhouse microclimate using CFD simulation. *Renewable Energy*, *138*, 722–737. https://doi.org/10.1016/j.renene.2019.01.108

Saldaña, M., Valenzuela, S. A., Moor, S. R., Metola, P., & Anslyn, E. V. (2020). K-5 Thin-Layer Chromatography: Three-Dimensional Analysis of Pigments from Plant Materials Using an Interlocking Building-Block Photography Box. *Journal of Chemical Education*, *97*(12), 4414–4419. https://doi.org/10.1021/acs.jchemed.0c00625

Sanda, M. D. A., Badu, M., Awudza, J. A. M., & Boadi, N. O. (2021). Development of TiO 2 - based dye-sensitized solar cells using natural dyes extracted from some plant-based materials. *Chemistry International*, *7*(1), 9–20.

Sawadogo, W., Simões, M., Aissatou, R., & Rosmeri, F. (2021). Current and future potential of solar and wind energy over Africa using the RegCM4 CORDEX - CORE ensemble. *Climate Dynamics*, *57*(5), 1647–1672. https://doi.org/10.1007/s00382-020-05377-1

Simon, S. (2009). *Guide de la tomate hors sol à La Réunion* (CIRAD (ed.)). CIRAD.

Soni, P., Salokhe, V. M., & Tantau, H. J. (2005). Effect of Screen Mesh Size on Vertical Temperature Distribution in Naturally Ventilated Tropical Greenhouses. *Biosystems*

*Engineering*, *92*(4), 469–482. https://doi.org/10.1016/j.biosystemseng.2005.08.005

Tamamidis, P., & Assanis, D. N. (1993). Evaluation of various high order accuracy schemes with and without flux limiters. *Intnational Journal for Numerical Methods in Fluids*.

TECHNISEM. (2019). *Fiche Technique* (p. 1). Technisem. https://technisem.com/infos-techniques/

Tioga. (2013). *Tioga: Pipe Dimensions and Weights*. http://tiogapipe.com/assets/files/pipe-chart.pdf

Tomkins, S. P., & Miller, M. B. (1993). A rapid extraction and fast separation of leaf pigments using thin layer chromatography. *Science and Plants for Schools (SAPS) Programme*, 1–4.

Ureña-sánchez, R., Callejón-ferre, Á. J., Pérez-alonso, J., & Carreño-ortega, Á. (2012). Greenhouse tomato production with electricity generation by roof-mounted flexible solar panels. *Scienctia Agricola*, *69*(4), 233–239.

Vallières, M. (2018). *Comparaison de méthodes de refroidissement et de déshumidification pour une production en serre de tomates biologiques*. Universite LAVAL.

Versteeg, H. K., & Malalasekera, W. (1995). An introduction to Computational Fluid Dynamics. In *The finite volume method* (longman, pp. 102–206). Longman Scientific & Technical.

Wang, C., Nan, B., Wang, T., Bai, Y., & Li, Y. (2021). Wind pressure acting on greenhouses: A review. *International Journal of Agricultural and Biological Engineering*, *14*(2), 1–8. https://doi.org/10.25165/J.IJABE.20211402.5261

# 7 APPENDIX

**Table 7. 1** Field data collection sheet for the Analysis of the Agro Ecosystem (AAES)

AAES n°..... Type de parcelle :..... Date :..... Heure :..... Température :.....°c

| Données à collecter | Plant 1 | Plant 2 | Plant 3 | Plant 4 | Plant 5 | | | | | | |
|---|---|---|---|---|---|---|---|---|---|---|---|
| **Données entomologiques** | | | | | | | | | | | **Totaux** |
| **A. Ravageurs** | | | | | | | | | | | |
| 1. | | | | | | | | | | | |
| 2. | | | | | | | | | | | |
| 3. | | | | | | | | | | | |
| 4. | | | | | | | | | | | |
| 5. | | | | | | | | | | | |
| 6. | | | | | | | | | | | |
| 7. | | | | | | | | | | | |
| **B. Ennemis naturels** | | | | | | | | | | | |
| 1. | | | | | | | | | | | |
| 2. | | | | | | | | | | | |
| 3. | | | | | | | | | | | |
| 4. | | | | | | | | | | | |
| 5. | | | | | | | | | | | |
| 6. | | | | | | | | | | | |
| 7. | | | | | | | | | | | |
| **Données agronomiques** | P1 | P2 | P3 | P4 | P5 | P6 | P7 | P8 | P9 | P10 | **Moyennes** |
| Taille du plant (cm) | | | | | | | | | | | |
| Nbre de ramifications | | | | | | | | | | | |
| Nbre de feuilles | | | | | | | | | | | |
| Nbre de boutons floraux | | | | | | | | | | | |
| Nbre de fleurs | | | | | | | | | | | |
| Nbre de fruits formés | | | | | | | | | | | |
| Nbre de fruits murs | | | | | | | | | | | |

**Observations** :

.....

.....

.....

Village :……

Site :……

Parcelle :……

Température : ……°C

AAES

N°……

Date :……

Heure :……

**Informations générales**

- La culture : ……..
- La variété : ……..
- Date de repiquage :……
- Nombre de jours après repiquage (JAR) ……..
- Stade de développement :……

Conditions du sol :……..

**Donnée agronomiques**

- Hauteur moyenne (cm) :……
- Nombre moyen de ramifications :…
- Nombre moyen de feuilles :……
- Nbre moyen de boutons floraux :…
- Nbre moyen de fleurs :……
- Nbre de fruits formés :……
- Nbre de fruits attaqué :……..

**Ravageurs**

Total =

DESSIN DE LA PLANTE DE_____

**Ennemis naturels**

Total =

| Observations | Causes possibles | Recommandations |
|---|---|---|
| | | |

**Table 7. 2** Summary of the light requirements of different photosynthetic pigments of the speculations studied and of the leaves of the latter.

| **Plants/crops** | **Stages** | **α and β Carotene (400-500 nm)** | **Chlorophyll-a (400-500 nm and 600-700 nm)** | **Chlorophyll-b (400-500 nm and 600-700 nm)** | **Lutein (400-500 nm)** | **Pheophytin (400-500 nm and 600-700 nm)** |
|---|---|---|---|---|---|---|
| **Lettuce** | Seedling | High | Medium | Low | Medium | High |
| | Foliage | Low | High | High | High | Medium |
| | Bolting/head formation | Medium | High | Medium | Medium | Medium |
| **Courgette / Zucchini** | Advanced lifting | High | Medium | Low | Low | Low |
| | Flowering | Low | High | High | High | High |
| | Fruiting | Medium | Low | Medium | Medium | Medium |
| **Tomato** | Advanced lifting | Medium | Medium | Medium | Low | Medium |
| | Flowering | High | High | High | High | High |
| | Fruiting | Medium | High | Medium | Medium | High |
| **Potato** | Lifting/early vegetative | Low | Medium | High | High | High |
| | Advanced vegetative or Tuber formation | Medium | High | High | Medium | Medium |
| | Senescence | High | Low | Medium | Medium | Low |
| **Sweet / Bell pepper** | Advanced lifting | High | Medium | High | Medium | Low |
| | Flowering | Medium | Medium | Medium | Low | High |
| | Fruiting | Medium | High | Medium | High | Medium |